Testing the Validity of the Randall–Sundrum Model with Flavor Physics, and a Higgs Decay

Dissertation
zur Erlangung des Grades
"Doktor
der Naturwissenschaften"

am Fachbereich Physik, Mathematik und Informatik

der Johannes Gutenberg–Universität Mainz
in Mainz

Kristiane Sylvia Novotny

geb. in Bad Kreuznach
Mainz, den 12.12.2017
Erste von Rechtschreibfehlern überarbeitete Version.

1.Berichterstatter:
2.Berichterstatter:
Tag der mündlichen Prüfung: 23.04.2018

Kristiane Novotny,
Testing the Validity of the Randall–Sundrum Model with Flavor Physics and a Higgs Decay,
Dissertation zur Erlangung des Grades "Doktor der Naturwissenschaften" am Fachbereich 08 – Physik, Mathematik und Informatik der Johannes Gutenberg–Universität Mainz-Mainz **D77**

Abstract

The Standard Model of particle physics describes nature in a very elegant and accurate way, but still there are some open questions such as the hierarchy problem and the flavor problem. One of the most promising candidates for physics beyond the Standard model is the Randall Sundrum model, which addresses many of these questions and predicts Kaluza Klein excitations. Incorporating the Standard model and extending it with an extra dimension, the Randall Sundrum model is a very elegant and natural way for a resolution of the Standard model shortcomings, because it explains both the hierarchy problem and the flavor hierarchies by localization of the Standard model fields along the extra dimension.
The aim of this thesis is to test the Randall Sundrum model's validity *via* Higgs physics, and flavor physics. First, the loop–induced decay of the Higgs boson into two photons is investigated. We show that this decay is sensitive to new physics. New particles beyond the Standard model appear in the loop and lead to contributions to this decay. Thus, the 5D propagators are derived for the calculation of the loop–induced decay of the Higgs boson into two photons. It is found that the amplitude of the diagram with fermion propagators depends on the Higgs–localisation in the Randall Sundrum model.
The Randall Sundrum model is extended by a gauge–singlet 5D scalar particle and its couplings to fermions give rise to flavor changing neutral currents. This was inspired by the 2015 measurements at ATLAS and CMS, which suggested an excess in the diphoton channel. Although this particular excess turned out to be a statistical fluctuation, the general appearance of a new flavor changing neutral current inducing scalar particle is intriguing. Following this hypothesis, the Randall Sundrum model is extended based on a former work, in which the contributions of the couplings of fermions to flavor–changing gauge bosons and their role in rare Standard model decays were investigated. The focus in this thesis is on neutral meson mixing. It turns out that there is a relative deviation to the Standard model values of $\mathcal{O}\left(10^{-5}\right)$ in case of Δm_{B_d}, of $\mathcal{O}\left(10^{-8}\right)$ in case of Δm_{B_s}, of $\mathcal{O}\left(10^{-4}\right)$ in case of Δm_K, and of $\mathcal{O}\left(10^{-14}\right)$ in case of $\mathcal{B}r\left(b \to s\mu^+\mu^-\right)$.
Possible contributions to the electric dipole moment of the neutron and deuteron are studied, as well. In case of the neutron electric dipole moment, a relative deviation of the Standard model values of $\mathcal{O}\left(10^{-3}\right)$ is found. While the deuteron electric dipole moment is in the Standard model calculated to be $2.8{\cdot}10^{-31} e\,\mathrm{cm}$, contributions to the deuteron electric dipole moment in the Randall Sundrum are predicted to be up to 10^5 times larger than the Standard model value of the calculation.

Zusammenfassung

Das Standard Modell der Teilchenphysik beschreibt die Natur in einer eleganten und sehr genauen Art und Weise. Allerdings gibt es immer noch offene Fragestellungen, wie z.B. das Hierarchieproblem. Einer der vielversprechendsten Kandidaten für ein neues Physikmodell ist das Randall Sundrum Modell, das sich mit vielen dieser offenen Fragen beschäftigt und neue Teilchen vorhergesagt. Dafür wird das Standard Modell wird mit einer Extradimension erweitert. In dieser eleganten und natürlichen Weise erklärt das Randall Sundrum Modell sowohl das Hierarchieproblem als auch das Flavor Hierarchieproblem durch eine Lokalisierung der Teilchen entlang der Extradimension.
Das Ziel dieser Dissertation ist ein Gültigkeitstest des Randall Sundrum Modell mit einem Higgszerfall und der Flavorphysik. Zuerst wird im Randall Sundrum Modell im der loop–induzierte Zerfall des Higgsbosons in zwei Photonen betrachtet. Wir zeigen, dass dieser Zerfall sensitiv auf Beiträge neuer Physik ist. Neue Teilchen außerhalb des Standard Modell erscheinen im Loop der Diagramme und geben Beiträge zum Zerfall. Für diesen loop–induzierten Zerfall werden die 5D Propagatoren hergeleitet. Die Amplituden von Diagrammen mit Fermionpropagatoren hängen von der Higgslokalisation im Randall Sundrum Modell ab.
Die Gültigkeit des Randall Sundrum Modells wird untersucht nach einer Erweiterung mit einem skalaren 5D Teilchen, dessen Kopplungen an Fermionen Flavorveränderungen verursacht. Diese Hypothese geht auf eine vermeintliche Struktur im Diphotonkanal der in 2015 genommenen Daten von ATLAS und CMS zurück. Diese Erweiterung durch ein skalares Teilchens ist sehr interessant, obwohl es sich bei der vermeintlichen Struktur in den Daten für eine statistische Fluktuation handelte. Auf dieser Hypothese aufbauend wurde das Randall Sundrum Modell erweitert, eine frühere Arbeit dieser Arbeitsgruppe wiederholt worden. Die damalige Arbeit untersuchte Beiträge von Kopplungen zwischen Fermionen und geladenen sowie ungeladenen Eichbosonen zu seltenen Standard Modell Zerfällen. Die vorliegende Dissertation befasst sich mit neutralen Mesonmischungen. Die relative Abweichung zu den SM Werten beträgt $\mathcal{O}\left(10^{-5}\right)$ im Fall von Δm_{B_d}, $\mathcal{O}\left(10^{-8}\right)$ im Fall von Δm_{B_s}, $\mathcal{O}\left(10^{-4}\right)$ im Fall von Δm_K und $\mathcal{O}\left(10^{-14}\right)$ im Fall von $\mathcal{B}r\left(b \to s\mu^+\mu^-\right)$. Darüber hinaus werden Beiträge dieser Kopplung sowohl zum elektrischen Dipolmoment des Neutrons als auch zum elektrischen Dipolmoment des Deuterons untersucht. Im Fall des elektrischen Dipolmoments des Neutrons wurde eine relative Abweichung zum Standard Modell Wert von $\mathcal{O}\left(10^{-3}\right)$ gefunden, während im Fall des elektrischen Dipolmoments des Deuterons eine relative Abweichung zum Wert der Standard Modell Rechnung um einen Faktor bis zu 10^5 gefunden worden ist.

Contents

Preface

The first chapter of this thesis is dedicated to the Standard Model, the theory in particle physics that combines three of the four fundamental forces. These forces are the electromagnetic force, the weak force and the strong force. Until today, the SM is successfully proven by experiments. After the discovery of the Higgs boson in 2014 at the LHC by ATLAS and CMS, the Standard Model of particle physics (SM) is considered to be complete. This thesis adopts the SM as the foundation of the theory that is examined. The SM is assumed to be valid up to the electroweak scale, which is in the range of the vacuum expectation value of the Higgs field. So far, physics experiments could not find any hint for physics beyond the electroweak scale. In the age of the LHC, it is nowadays possible to probe physics up to a higher energy range. At the electroweak scale, gravitational forces are treated as small perturbations that can be neglected. The closer one comes in range of the Planck scale, the perturbative approach will break down, because then the growth of the effective coupling of the graviton is proportional to E/M_{Pl}. The electroweak scale is much smaller than the Planck scale $M_{\mathrm{Pl}} = \sqrt{\hbar c/G} \approx 1.22 \cdot 10^9\,\mathrm{GeV}$[1]. For the correct description of elementary particles, gravitational forces are not negligible anymore at the Planck scale. The huge energy gap between the electroweak scale and the Planck scale lead physicists to find an explanation for this phenomenon and other phenomena that exist in nature, but can not described by the SM. This search lead to the development of theories that are referred to as *beyond the SM* (BSM) models, in which the SM is a low energy description for a more fundamental theory. One of these BSM is the Randall Sundrum (RS) model that explains the difference of the fermion masses (hierarchy problem), and quark mixings. It also offers an explanation for the suppression of flavor changing neutral currents. The main characteristic of the RS model is the extension of the SM by a warped extra–dimension. The incorporation of the SM into the RS model is shown in Ch. 2, in which both similarities and differences of the RS model compared to the SM are highlighted. The particles in the RS model are excitations of the SM particles and are referred to as Kaluza Klein (KK) particles. These particles were not yet detected at the LHC, because they might be too heavy to be produced at the LHC or because they might not exist. Furthermore, the RS model permits a variable imbedding of the Higgs boson that is discussed in Sec. 2.2. Besides the exact implementing of the SM into the RS model, which is referred to as the *minimal* RS model that incorporates the SM gauge group into the bulk, there is also another setup of this model with an enlarged gauge group. The latter setup is referred to as the *custodial* RS model and is discussed in Sec. 2.5, because the corrections to the T parameter become finite. The RS model can be also probed *via* indirect measurements of rare decays at the LHC or deviations from the expected SM value.
The RS model is then probed in Ch. 4–Ch. 5. The decay of a Higgs boson into two

[1] Natural units, *i.e.* $\hbar = c = 1$ are used in this thesis, except for the comparison of contributions to the neutron EDM and deuteron EDM in Ch. 5. In the equation appear the reduced Planck constant $\hbar$, the speed of light c and the gravitational constant G.

photons *via* a fermion loop is investigated in Ch. 4. In both the fermion loop of the triangle diagram and the gauge boson loop diagrams that describe the decay of a Higgs boson into two photons could be virtual RS fermions as well as virtual RS gauge bosons that could give sizable contributions. These contributions should not deviate compared to the SM value for the scattering amplitude of this process. A possible deviation and its meaning for the validity of the RS model is then discussed in Sec. 4.6. The probe of the validity of the RS model *via* the decay $h \to \gamma\gamma$ is done with the help of the propagators in the 5D picture for the corresponding particles derived in Ch. 3. The boson propagators originally have been derived in [106]. In 2016, there was a discussion of a possible diphoton excess in LHC data [211, 212]. This excess could not be confirmed in subsequent analyses with higher statistics, but it rose the question of new scalar particles that can not only probe the SM, but the RS model and other BSM. If deviations from the SM predictions for the values are there, the largest deviations are expected in flavor observables. This possibility of an additional scalar that has no analogue in the SM, *i.e.* it is considered as a pure BSM particle, and its impact to the current measurements is investigated in Ch. 5. This scalar is allowed to induce a flavor change. The results of this investigation are compared with the present experimental bounds. As a possible BSM particle, the contributions stemming from the scalar have to fit into the current values of the experimental data.

1 Introduction

1.1 Standard Model of particle physics (SM)

A mathematical description for three of the four fundamental forces that are the electromagnetic force, the weak force and the strong force is provided by the Standard model of particle physics (SM). A brief explanation of the SM as the mathematical description of particle physics is provided in Sec. 1.1, followed by the treatment of the SM as an effective field theory in Sec. 1.2. The hierarchy problem that is a question, which the SM is unable to address, is investigated in greater detail in Sec. 1.3.1. This discussion leads then to a solution that is found in theories that are referred to as *beyond the SM* (BSM) models.
Based on books and articles [1–6] and theses in this group [127–130], a review of the discrepancies of the SM is given as well as a suggestion of their resolution is offered, leading to the motivation of the model used throughout this thesis. Established in the early 1960s by Glashow, Weinberg and Salam [7–9], the SM offers the best explanation of today's physics, although it only explains a part that does not include gravity. The SM describes all experimentally found particles and with the Higgs discovery [10, 11] the last missing particle to complete the SM was found. As the SM forms the basis of the BSM model discussed in this thesis, a brief overview is given and details are discussed in Ch. 2, in which the differences between the SM and the developments in the RS model are discussed and compared. The SM unifies the electromagnetic and the weak interaction as was shown by Glashow, Weinberg, and Salam [7–9]. Renormalizability of the theory was proven by 't Hooft and Veltman [12] shortly after the discovery of the J/Ψ particle [13, 14] and the charm quark *via* the GIM mechanism [15].
QCD is the theory of strong interactions [16]. Quarks are the matter fields of QCD as a quantum theory [1–6]. Gross, Wilczek and Politzer showed that non–abelian gauge theories posses asymptotic freedom, which means that the quarks decouple for very large energies [18–20] and confinement are the two most important properties of QCD. The concept of confinement means the yet unproven hypothesis that an observation of free quarks is not possible [6, 21–24]. With these foundations the SM became a very well–proven theory with the discoveries of the weak gauge bosons [25–27], the top quark [28, 29] and the Higgs boson [10, 11]. The gauge group of the SM reads

$$G_{\mathrm{SM}} = SU(3)_c \times SU(2)_L \times U(1)_Y \,. \tag{1.1}$$

Here, the group $SU(3)_c$ represents the strong interaction and describing QCD, whereas the $SU(2)_L \times U(1)_Y$ describes the weak interaction. Furthermore, Y is the hypercharge that relates the electric charge with the third component of the isospin. The SM Lagrangian has the following contributions.

$$\begin{aligned} \mathcal{L}_{\mathrm{SM}} = \mathcal{L}_{\mathrm{Gauge}} + \mathcal{L}_{\mathrm{Fermion}} + \mathcal{L}_{\mathrm{Higgs}} + \mathcal{L}_{\mathrm{Yukawa}} \\ + \mathcal{L}_{\mathrm{Fadeev-Popov}} + \mathcal{L}_{\mathrm{Gauge-Fixing}}. \end{aligned} \tag{1.2}$$

The first part, $\mathcal{L}_{\text{Gauge}}$, describes the forces acting between the particles that are mediated *via* so–called *gauge bosons*. In analogy to the electromagnetic field strength tensor, $\mathcal{L}_{\text{Gauge}}$ takes the form of

$$\mathcal{L}_{\text{Gauge}} = -\frac{1}{4} G^a_{\mu\nu} G^{a,\mu\nu} - \frac{1}{4} W^i_{\mu\nu} W^{i,\mu\nu} - \frac{1}{4} B_{\mu\nu} B^{\mu\nu} \tag{1.3}$$

and contains the field strength tensor of the $SU(3)$ color, $G^a_{\mu\nu} = \partial_\mu G^a_\nu - \partial_\nu G^a_\mu + g_s f^{abc} G^b_\mu G^c_\nu$. The $SU(3)$ is the gauge group of QCD [30]. The gauge bosons called *gluon*s and can couple to each other through the $SU(3)$ structure constant f^{abc} with the coupling strength g_s. Furthermore, $\mathcal{L}_{\text{Gauge}}$ contains the field strength tensors of the $SU(2)_L$, $W^i_{\mu\nu} = \partial_\mu W^i_\nu - \partial_\nu W^i_\mu + g\epsilon^{ijk} W^j_\mu W^k_\nu$ and the field strength tensor $B_{\mu\nu} = \partial_\mu B_\nu - \partial_\nu B_\mu$ for the $U(1)$ group. Proper quantization is ensured by both the gauge-fixing term $\mathcal{L}_{\text{Gauge-Fixing}}$ [31–33] as well as the Fadeev-Popov term $\mathcal{L}_{\text{Fadeev-Popov}}$ [34], respectively, that are not discussed in further detail as both terms are not relevant for this thesis.

The term $\mathcal{L}_{\text{Fermion}}$ describes the so–called fermions, which are spin 1/2 fields. So far, the SM looks like a chiral theory with the projection operators $P_{L,R} = \frac{1}{2}(1 \mp \gamma_5)$ that project out left–handed and right–handed components. With the help of these operators, the handedness of fermions can be distinguished and consequently, fermions transform according to their handedness under the SM gauge group Eq. (1.1) differently. Left–handed fields transform under the $SU(2)_L$ group as doublets Q^i_L, while right–handed fields u_R, d_R, e_R transform as singlets under $SU(2)_L$, where u denotes up–type quarks, d denotes down–type quarks and e denotes leptons. Neutrinos are charged under the SM gauge group. The fermions in general are collected in the kinetic term of the SM Lagrangian,

$$\mathcal{L}_{\text{Fermion}} = \bar{Q}^i_L i \not{D} Q^i_L + \bar{L}^i_L i \not{D} L^i_L + \bar{u}^i_R i \not{D} u^i_R + \bar{d}^i_R i \not{D} d^i_R + \bar{e}^i_R i \not{D} e^i_R \tag{1.4}$$

with $\not{D} = \gamma^\mu D_\mu$ and the covariant derivative

$$D_\mu = \partial_\mu - i g_s G^a_\mu \frac{t^a}{2} - i g W^i_\mu \frac{\sigma^i}{2} - i g' B_\mu Y, \tag{1.5}$$

including the gauge couplings g_s, g and g' of the gauge groups $SU(3)_c$, $SU(2)_L$ and $U(1)_Y$ as well as the Pauli matrices σ^i, the generators of the $SU(2)_L$, the hypercharge Y and the generators of $SU(3)_c$, the Gell–Mann matrices t^a.

Up to this point, all fields are massless as the SM does not contain an explicit mass term, because its existence would lead to a violation of gauge invariance. The introduction of masses is provided by the so–called *Higgs mechanism* [35–38] that spontaneously breaks symmetry leaving the SM Lagrangian $\mathcal{L}_{\text{SM}}$ invariant. The electroweak gauge group is broken down to $U(1)_{\text{EM}}$, which means the symmetry $SU(2)_L \times U(1)_Y \to U(1)_{\text{EM}}$ is broken at the electroweak scale. This is similar to the symmetry breaking in QCD and in solid state physics, which leads to a preferred orientation to the spin. Historically, the Higgs mechanism was introduced for the latter. Therefore, the scalar doublet

$$\Phi(x) = \begin{pmatrix} -i\varphi^+(x) \\ \frac{1}{\sqrt{2}}\left[v + h(x) + i\varphi_3(x)\right] \end{pmatrix} \tag{1.6}$$

is introduced and transforms as $\left(1, 2, \frac{1}{2}\right)$ under the SM gauge group. This can be seen in the Higgs Lagrangian

$$\mathcal{L}_{\text{Higgs}} = \left(D_\mu \Phi\right)^\dagger \left(D_\nu \Phi\right) + \mu^2 \Phi^\dagger \Phi - \lambda \left(\Phi^\dagger \Phi\right)^2 . \tag{1.7}$$

The stability of the electroweak vacuum requires a lower bound manifesting in $\lambda > 0$ as well as a squared positive mass $\mu^2 > 0$. With these conditions, the ground state $\langle 0|\Phi^2|0\rangle$ breaks electroweak symmetry *via* $SU\left(2\right)_L \times U\left(1\right)_Y \rightarrow U\left(1\right)_{\text{EM}}$. The field Φ can be parametrized *via* Eq. (1.6) with a vacuum expectation value (VEV) $\langle 0|\Phi^2|0\rangle = v^2 = \mu^2/2$ that minimizes the potential. Furthermore, three Goldstone bosons $\varphi^\pm$ and φ^3 are generated *via* symmetry breaking. These are the longitudinal degrees of freedom of the massive gauge bosons and the Higgs field h, together with its corresponding mass $m_h = \sqrt{2\lambda v}$ [39]. The mass terms of the gauge bosons stem from the kinetic part of the Higgs Lagrangian, whereas the mass terms for fermions are obtained from the Yukawa part of Eq. (1.9)

$$\mathcal{L}_{\text{Yukawa}} = -\bar{Q}_L^i \Phi Y_d^{ij} d_R^j - \bar{Q}_L^i i\sigma^2 \Phi^\dagger Y_u^{ij} u_R^j - \bar{L}_L^i \Phi Y_e^{ij} e_R^j + \text{ h.c.}. \tag{1.8}$$

The Yukawa matrices $Y_{u,d,e}$ are 3×3 matrices in the generation space and are in general non–diagonal in the interaction basis. The Yukawa interactions are diagonalized *via* bi–unitary transformations of the mass eigenstates that are given by $\text{diag}\left(m_u, m_c, m_t\right) = \frac{v}{\sqrt{2}} U_u^\dagger Y_u W_u$, for which U_u and W_u are matrices that diagonalize Y. Fermion mass eigenstates are then expressed *via* $f_L \rightarrow U_f f_L$ and $f_R \rightarrow W_f f_R$, and $f = u, d, e$.
It should be noted that interactions of both leptons and quarks with neutral gauge bosons are invariant at tree–level, because flavor changing neutral currents (FCNCs) are forbidden at this level. Interactions of fermions and $W^\pm$ bosons are given *via* $g/\sqrt{2}\bar{u}_L \gamma^\mu W_\mu^+ V_{\text{CKM}} d_L + \text{h.c.}$ in the mass eigenstate basis with the CKM matrix [40, 41] $V_{\text{CKM}} = U_u^\dagger U_d$. The CKM matrix is unitary and contains rotation angles as well as one weak phase that is responsible for CP violation.

1.1.1 Flavor symmetry and custodial symmetry

If the Yukawa interaction is ignored, the SM is invariant under a $U\left(3\right)_{Q_L} \times U\left(3\right)_{u_R} \times U\left(3\right)_{d_R} \times U\left(3\right)_{L_L} \times U\left(3\right)_{e_R}$ symmetry containing 45 generators in the fundamental representation. After including the Yukawa interaction, the symmetry group breaks down to $U\left(1\right)_B \times U\left(1\right)_{L_e} \times U\left(1\right)_{L_\mu} \times U\left(1\right)_{L_\tau}$. B represents the Baryon number conservation and $L_{e,\mu,\tau}$ denotes the Lepton number conservation. As quantum numbers, only the difference $B - L$ is conserved [45–47], because neutrino oscillations occur [48]. One should note that these numbers are not imposed in the SM and therefore this symmetry is considered as an *accidental* symmetry following from the particle content of the SM, the gauge principle, and the renormalization condition. With the introduction of the Yukawa interaction there are 4 generators less, and $45 - 4 = 41$ generators of the broken theory remain. These generators as well as the resulting symmetry transformations are used to obtain 13 physical parameters from the $54 - 41$ real parameters of the Yukawa matrices Y_u, Y_d and Y_e in the SM, which are 6 quark masses, 3 lepton masses, 3 mixing angles, and 1 CP violating phase [43, 44].
Another interesting point of the SM in the limit of a vanishing electroweak coupling

$g' \to 0$, is that the Higgs Lagrangian Eq. (1.7) is invariant under a global $SO(4)$ symmetry. This symmetry is isomorph to a $SU(2)_L \times SU(2)_R$ symmetry, in which $SU(2)_L$ represents the global gauge symmetry. The VEV breaks $SU(2)_L \times SU(2)_R$ down to a $SU(2)_{L+R}$ symmetry and the gauge bosons transform as a triplet under the $SU(2)_{L+R}$ symmetry with equal masses, *i.e.* $m_W = m_Z$. Furthermore, in this limit, the ρ-parameter $\rho = \frac{m_W^2}{m_Z^2 c_{\theta_W}^2} = 1$ contains the cosine of the Weinberg angle defined by the ratio of the masses of the electroweak gauge bosons $c_{\theta_W}^2 = \frac{m_W^2}{m_Z^2}$. The ρ-parameter receives only small radiative corrections in the limit $g' \to 0$. In possible scenarios for physics beyond the SM this relation has to be fulfilled [49, 50]. Hence, the SM and its possible extension contains a *custodial* mechanism [51] to protect the ρ parameter. The electroweak T parameter measures deviations from the ρ parameter in the SM [52, 53] and will be discussed in Sec. 2.6.

1.2 Standard model of particle physics as an effective field theory

Another consideration of the SM is its as a low–energy description, *i.e.* as an effective field theory (EFT), of a more fundamental theory. In this approach, the SM Lagrangian is expanded in terms of higher dimensional operators that are both Lorentz invariant and gauge-invariant. This approach is satisfied if there exists a huge energy gap between the electroweak scale and the new physics scale. The new physics scale is defined as the scale where non–SM particles occur and interact with the SM particles. This assumption is experimentally justified as there does not exist any hint at the LHC for particles heavier than the top quark. Consequently the non-existence of new particles can be interpreted as the existence of a huge energy gap between the electroweak scale and the new physics scale. The energy gap can be described by the cutoff scale Λ that can be considered of an order similar to the Planck scale in the case of the SM.
From the point of view that there exists a huge gap between the energy scales, the SM is regarded as an effective field theory (EFT), which is described by the Wilson coefficients $\mathcal{C}_{(0,2)}, \mathcal{C}^{(i)}_{(4,5,6..)}$ containing the physics content and the operators $\mathcal{Q}^{(i)}_{(4,5,6,...)}$. Here, the subscripts indicate the dimension. Furthermore, the Wilson coefficients are scaled by the cutoff energy Λ with respect to the dimensionality of the operators $\mathcal{Q}^{(i)}$, yielding the overall dimension four effective SM Lagrangian

$$\mathcal{L}_{\text{Eff}} = \mathcal{C}_0\Lambda^4 + \mathcal{C}_2\Lambda^2\Phi^\dagger\Phi + \sum_i \mathcal{C}_4^{(i)}\mathcal{O}_4^{(i)} + \sum_i \frac{\mathcal{C}_5^{(i)}}{\Lambda}\mathcal{O}_5^{(i)} + \sum_i \frac{\mathcal{C}_6^{(i)}}{\Lambda^2}\mathcal{O}_6^{(i)} + ... \tag{1.9}$$

In general, the operators $\mathcal{O}_n^{(i)} \sim (E/\Lambda)^{n-4}$ appearing in Eq. (1.9) depend on the energy scale $E \ll \Lambda$ of the process and can be divided into three parts: the so–called *relevant* operators are expressed through a dimension dependence $n < 4$, while operators with a dimension $n = 4$ are called *marginal*, and the others are referred to as *irrelevant*. The division in three parts can be thought of the operator's relevance for the theory's low–energy description, because relevant operators are in general forbidden by a symmetry, marginal operators contain the renormalizable description, and irrelevant operators contain information about the fundamental theory [1]. The renormalizable SM Lagrangian $\mathcal{L}_{\text{SM}}$ contains both the Higgs operator, indicated by the term which is proportional to

the Wilson coefficient $\mathcal{C}_2$ as well as all other marginal operators of Eq. (1.9). After integrating out the heavy particles of the more fundamental theory and the additional degrees of freedom, the Wilson coefficients of relevant operators contain contributions of the underlying theory. In total, there are 59 dimension–six operators which preserve both baryon and lepton number conservation and that carry a flavor structure [54], although there are also other classifications, *e.g.* [55]. Only one dimension–five operator exists that is referred to as the Weinberg operator. The Weinberg operator gives rise to Majorana mass terms for the left-handed neutrinos after electroweak symmetry breaking (EWSB) [56].
A closer look to Eq. (1.9) reveals some interesting facts: the first term contributes to the energy density of the vacuum of space, which is another description of dark energy [57–59], in form of the cosmological constant. About 68.5% of the energy in the available universe is dark energy [60]. Following this fact, the bound on the Wilson coefficient $\mathcal{C}_0$ results in $\mathcal{C}_0 \sim \left(10^{-12}\,\mathrm{GeV}\right)^4/\Lambda^4$. If the scale Λ is about the same scale as the Planck scale, the Wilson coefficient $\mathcal{C}_0 \sim 10^{-120}$ creates difficulties with a cosmological constant. The Higgs mechanism would then be coupled to gravity. This would contribute to the cosmological constant and its value would be extremely large in contrast to experiments [3]. The only relevant term in the SM Lagrangian is the second term that contains the Wilson coefficient $\mathcal{C}_2$. As described in Sec. 1.1, the gauge groups $SU(2)_L \times U(1)_Y$ are broken at the electroweak scale, so $\mathcal{C}_2$ should be proportional to $\mathrm{M}_{\mathrm{EW}}^2/\Lambda^2$. This means, in the limit $\Lambda \sim M_{\mathrm{Pl}}$ the so–called hierarchy problem emerges why quarks have different masses. This is discussed in further detail in the next section Sec. 1.3.1. Although the SM offers a very good explanation of particle physics, it offers neither a description of gravity nor cosmology. Furthermore, there are more detailed problems such as the flavor puzzle and others, which will not be further discussed in this thesis. The interested reader is referred to [61–69].
Embedding the SM into an underlying BSM theory means also that the SM gauge group Eq. (1.1) has to be embedded in the gauge group of the BSM theory. Some groups were considered in the past, which meet these requirements, *e.g.* $SU(5)$ and others, see [70]. Consequently, the quantum numbers of the particles might change, as well, depending on the underlying gauge group, for instance for a protection of a possible proton decay [71].

1.3 Challenges for the SM

1.3.1 Hierarchy problem

The Higgs mass operator in Eq. (1.9), $\mathcal{O}_2 = \Phi^\dagger\Phi$ is the only relevant operator as described before ($\dim \mathcal{O}_2 = 4$). Using the effective field theory approach, the Wilson coefficient is expressed *via* the dimensionless Wilson coefficient $c_2 = \mu^2/\Lambda^2$, where Λ is the energy scale, in which the SM remains valid. Assuming the validity of the SM until the Planck scale, *i.e.* $\Lambda \sim M_{\mathrm{Pl}}$, the Wilson coefficient gets very small $c_2 \sim 10^{-34} \ll \mathcal{O}(1)$ if $\mu \sim 100\mathrm{GeV}$ is considered to be the electroweak scale. A natural value of c_2 would be 1 from the EFT point of view, because the Higgs mass operator is not protected by a symmetry. This difference in the expectation of the Wilson coefficient is considered *unnatural*, but it is not a physical criterion for any inconsistency of the SM. Furthermore, the meaning of *natural* might be somewhat misleading as there are various definitions

of *naturalness*, *c.f.* [72–74]. On the one hand a hierarchy in the bare parameters in the Lagrangian is allowed, and on the other hand it is demanded that radiative corrections of those bare parameters are not much larger compared to them. This is referred to as technical naturalness [75]. Therefore, radiative corrections to the Higgs mass operator can be an example for a one loop diagram with virtual top quarks in the loop. Such a diagram gets UV divergent if the virtual top quarks are exchanged. After the Wick rotation, the momenta are now in the euclidean space, and a regularization with a cutoff Λ is performed. The corresponding corrections read

$$\delta m_h^2 = \frac{3N_c^2}{4\pi^2} y_t^2 \left[-\frac{\Lambda^2}{3} + m_t^2 \left(\ln\left(\frac{\Lambda^2}{m_t^2} - \frac{2}{3} \right) \right) + \mathcal{O}\left(\frac{1}{\Lambda^2} \right) \right], \tag{1.10}$$

with the Yukawa coupling y_t and the number of colors N_c. There is a quadratic dependence on the cutoff Λ as seen in Eq. (1.10). If the cutoff Λ is proportional to the Planck scale, the counter terms have to be tuned in a very delicate way removing the divergences at the electroweak scale. This phenomenon is referred to as the *fine–tuning problem* of the Higgs mass. Another important point is that the Higgs mass is renormalized additively in contrast to the multiplicative renormalization of the other SM particles. As a consequence, the quantum corrections are uncorrelated to the bare Higgs mass that is the non–renormalized Higgs mass and the quantum correction can be numerically larger than expected. The additive renormalization terms originate from a non–existing symmetry enhancement in the limit of a vanishing Higgs mass that would violate the criterion for technical naturalness. Then, the SM Lagrangian can be regarded as classically conformal, because the Higgs mass term in Eq. (1.9) vanishes. Assuming implicitly a connection of the cutoff scale Λ of an underlying UV theory with its corresponding mass scale which breaks the conformal symmetry explicitly, the technical naturalness would still be violated. Despite the Higgs mass corrections, the other SM particles are renormalized multiplicatively as they are protected by either the chiral symmetry or the gauge symmetry. This stems from the fact that the fermion spins in the chiral limit transform independently from each other. Hence, the chiral symmetry implies a logarithmic dependence of the radiative corrections, *i.e.* $m_f \sim m_f \ln\left(\Lambda^2/m_f^2\right)$.

Nota bene: Here, the natural logarithm of a variable x based on the Euler number e is denoted by $\ln(x)$ in order to avoid any confusion with $\log(x)$ that is more conveniently used in the English literature with the same meaning.

Changing the renormalization scheme does not remove the additive corrections to the Higgs mass. Considering the case of the fundamental UV theory with its mass scale M, particles could interact with the Higgs. Without the introduction of additional symmetries, the resulting radiative corrections would be quadratically sensitive to the new mass scale. For large new particle masses, this would be a reintroduction of the fine–tuning problem of the Higgs mass.

Another point concerns the criticality of the Higgs sector of the electroweak vacuum stability and the symmetry breaking in the SM. Assuming the validity of the SM up to the Planck scale, leads to an effective potential $V_{\text{eff}}(h) = \frac{1}{4}\lambda_{\text{eff}}^{(n)}(h)$. The parameter λ_{eff} is the effective quartic running coupling at the energy scale μ. This effective coupling is numerically close to $\lambda(\mu)$ resulting from the one obtained *via* renormalization group (RG)–running [77]. At one loop level and ignoring the gauge couplings, the running for

the quartic coupling in the $\overline{\text{MS}}$ [78] scheme leads to

$$\frac{\mathrm{d}\lambda(\mu)}{\mathrm{d}\ln(\mu^2)} = \frac{1}{(4\pi)^2}\left[-3y_t^4 + 6y_t^2\lambda + 12\lambda^2 + ...\right], \tag{1.11}$$

with the running couplings λ at the energy scale μ indicated on the left hand side of the equation. The first term dominates and leads to negative values with growing energy and the vacuum stability of the SM requires a positive value for $\lambda(M_{\text{Pl}})$ [76]. With today's SM input parameters, the metastable and long-living electroweak vacuum stability is just achieved with fixed gauge couplings. The electroweak vacuum is metastable if the probability of quantum tunnel effects out of the electroweak vacuum is sufficiently small so that the lifetime of the SM vacuum is longer than the age of the universe. Smaller values for both $y_t(M_{\text{Pl}})$ and $\lambda(M_{\text{Pl}})$ would either lead to an unstable electroweak vacuum with a lifetime smaller than the age of the universe or to no EWSB below the Planck scale. An upper bound on the mass parameter $\mu(M_{\text{Pl}})$ of the quadratic Higgs term can be the condition for a minimal potential including the logarithmic running of $\lambda(M_{\text{Pl}})$[76]. Here, μ^2 is considered as the parameter determining the size of the transition between the symmetric phase $\left(\mu^2 > 0\right)$ and the broken phase $\left(\mu^2 < 0\right)$ [79]. Furthermore, μ^2 is in the range of $\left(-M_{\text{Pl}}^2, M_{\text{Pl}}^2\right)$. The interpretation of the hierarchy problem is that the value of running of $\mu^2(M_{\text{Pl}}) \approx (140.3\,\text{GeV})^2$ is close to $\mu = 0$ compared to the Planck scale [76]. The boundary between the symmetric phase and the broken phase is described by $\mu = 0$. Under the assumption that the SM is valid up to the Planck scale, the two parameters $\lambda(M_{\text{Pl}})$ and $\mu(M_{\text{Pl}})$ are in between these phases. The two most important explanations are

1. The appearance of the near criticality could stem from a broken symmetry. This means that the Higgs can be regarded as a pseudo Nambu Goldstone Boson (PNGB) of a theory of strong interactions, where both μ^2 and λ^2 vanish at tree level. Loop–suppressed radiative corrections could then trigger a potential leading to negative values for λ at the Planck scale [80–90].

2. In the case of a zero Higgs mass, the SM can be regarded as a conformal theory and contains dimensionful couplings. Radiative corrections to the Higgs potential trigger EWSB and the approximate conformal symmetry leads to a stabilization of the Higgs mass at the electroweak scale [91]. The crucial point is the question of the origin of a conformal SM through gravity as the SM is not conformally invariant at all due to the existence of the dimensionful Planck scale.

1.4 Extra–dimensional theories

We have now established the reasons, why the SM as an EFT is a solid foundation for more general theories. The EFT approach of the SM is valid up to the electroweak scale with the inherent cutoff Λ_{UV}. Furthermore, the power law dependence highlights the challenge of the incalculability of certain observables, because the divergences cannot be treated in the same way as in the SM. The reason is that the effects of higher–dimensional operators in both extra–dimensional theories and all non–renormalizable theories, respectively, scale after the application of the renormalization procedure with $(E/\Lambda_{\text{UV}})^n$, where E denotes the energy scale for a given process. At energies around Λ_{UV}

there are two main reasons for which the contribution of higher dimensional operators become relevant. The first reason is that the higher–dimensional operators contribute to tree–level processes, and contributions from loop–level processes can be of the same order of magnitude as tree–level processes [113].
One possibility for embedding the SM into a more fundamental theory is a generic theory with at least one extra dimension. Originally, this scenario was developed in the early 20^{th} century by Kaluza, Klein and Nordstrom [92–94]. After a gap of almost 80 years the model was re–discovered and further developed [95–100]. In the following, some short remarks about the challenges of the SM as an EFT for extra–dimensional models are given and we will review two of them. More detailed and further literature can be found in [101, 102]. The fundamental idea is a compact extra dimension in which the particles or the forces propagate. In case of considering particles along the extra dimension, the particles show excitations. These excitations are referred to as Kaluza Klein (KK) excitations and will be explained in greater detail in Ch. 2. An imagination of this behavior could be a string of a violin where the SM particle is the empty string of the violin. Playing a note that is a higher harmonic excitation on the string leads to its excitations. The different notes on this string represent the different particles excitations.
A careful treatment of observables is necessary if they are sensitive or close to Λ_{UV}. Extra–dimensional models posses an intrinsic UV cutoff. In this case other higher–dimensional operators have to be considered whose coefficients have to determined by experiment. In the case of the Randall Sundrum (RS) model that is explained in the following chapter, there is only a contribution of the KK modes, which are below the cutoff. This is an important fact considering loop–induced processes, because otherwise the sum over the infinite excitations does not commute and the amplitude of the considered process diverges.
The idea of extra dimensions can be also applied to the hierarchy problem, because such theories postulate particles close to the TeV scale. If these particles are experimentally found, they could be a hint that a given cutoff is close to this scale, because then the observables would be close to the theory's intrinsic UV cutoff. As a consequence, the hierarchy problem brings the electroweak scale and the TeV scale closer together. Furthermore, the hierarchy of the electroweak scale and the cutoff of the extra dimensional theory has to be understood.

1.4.1 Flat extra dimensions

Flat extra dimensions were introduced in the model of [96] in 1998, which offers an explanation to the hierarchy problem. Although in general this setup is possible with n additional extra dimensions, the explanation is restricted to one additional extra dimension for the sake of clarity. With the help of a flat extra dimension, gravity can be introduced [96]. The existence of (an) additional compactified spatial extra dimension(s) as long as gravity propagates along the extra dimension is a possible explanation for the deviation of the $1/r$–behavior of Newton's potential. The additional space time is compactified on a manifold. The SM is confined on a 3 brane that is a sub–manifold with the dimensions of the SM. In this model, only one particle, the graviton, possesses excitations, which are referred to as *KK excitations* that are explained in further detail in Ch. 2. The d–dimensional Planck scale M_d sets the theory's cutoff, at which gravity is realistically described up to either the electroweak scale $M_d \sim M_{\text{EW}}$ or up to a higher (TeV) range. Then, the solution of the hierarchy problem is that quantum corrections to

the Higgs mass m_h possess a cutoff at this scale. At the same time, higher dimensional operators are not suppressed, which leads to flavor changing neutral currents. While the concept of flat extra dimensions does not address the flavor problem, this is achieved by moving the fermions into the bulk of the extra dimension that is the space between the two branes. If the fermions are moved into the bulk of the extra dimension, they also obtain KK excitations. A suppression of the fermion overlap profiles on the brane may lead to a suppression of the couplings, *c.f.* [97]. Theories, in which this procedure appears are also known as *split fermion* theories [97].

1.4.2 Universal extra dimensions

If fermions are confined along the flat space time and the space time is included into n additional dimensions, then the concept of *universal extra dimensions* (UED) [103] emerges. As the concept of UED has to be in agreement with electroweak precision data, the radius r has to fulfill $r \sim \frac{1}{\text{TeV}}$ setting the fundamental cutoff to $M_5 \sim 10^{15}\,\text{GeV}$ [104]. At tree–level, there is only a production of higher KK states *via* pair production in contrast to the case at one loop–level where a single KK particle production is possible. The reason for this is the so–called *KK parity* following from the invariance of the 5D theory that is now a projection of the extra dimension onto 4 dimensions, which is described by the transformation $\Phi \rightarrow (-1)^n \Phi_n$ of the field Φ and the extra–dimensional coordinate ϕ. The KK parity is an exact symmetry that assures a loop suppression of a single KK mode in the case of an even number of KK modes. Finally, the KK parity is responsible for stable KK particles [112, 113]. On one hand, the KK photon is the lightest KK particle, which is also an ideal dark matter candidate, because it it offers an explanation for relic abundance [114]. On the other hand, the KK gluon is the most massive particle [119]. Relic abundance is the amount of - in this case - KK dark matter particles that are still present. The amount of these particles decreased after a temperature transition due to the expansion of the universe to those that are colder than needed to produce these particles in chemical equilibrium [117]. An upper bound of the KK photon mass of 1.6 TeV is proposed by the WMAP collaboration [115, 116] whereas the authors of [117] come to a 900 GeV bound.This would be in agreement with FCNC bounds [118].

2 Extra dimensions

The idea of an extra–dimensional field theory was developed by Kaluza, Klein and Nordstrom [92–94] about hundred years ago. Kaluza and Klein laid the foundation to the ideas of a realization of an extra dimension with the aim to find a combination of gravity and electromagnetism. At this time, the two forces have been the only two known forces. They considered a tiny and compact extra dimension as there was no hint for an extra dimension with large size at this time. After this, the theory was forgotten over almost 100 years, BSM physicists such as Arkani-Hamed, Randall and Sundrum, adopted their foundations in order to resolve the SM's discrepancies.
In this chapter, these ideas are summarized based on [95, 97–102, 120–125] as well as various other reviews, Diploma and PhD theses written in this group [126–131] and books [3]. This builds the framework of the calculations in this thesis.
The setup that is first presented after the general introduction in Sec. 2 is the *minimal* RS model. The word *minimal* refers to the fact that the SM gauge group, Eq. (1.1), is incorporated as a bulk symmetry. In this setup, the differences between the SM and the RS model are highlighted by discussing the particle content. In Sec. 2.5 the so–called *custodial* RS model with its enlarged bulk gauge group is considered. A comparison of the differences between the minimal RS model and the custodial RS model highlights the differences between these two setups. Here, the SM gauge group is enlarged by a P_{LR} symmetry that yields a protection of too large corrections to the electroweak precision parameters. Another advantage of the custodial RS model is that KK particles might be in reach for a detection at the LHC. First, the general idea to put the SM into a five–dimensional slice of Anti de Sitter space AdS_5 that motivates the Randall Sundrum (RS) model [98, 99], as well as all other warped extra–dimensional theories. These theories are referred to as RS models if they contain only one extra dimension. The RS model is introduced as the underlying model of this thesis.
The extra dimension is considered to be a $S^1/\mathbb{Z}_2$ orbifold that is considered as a circle with a so–called *compactification radius* r_c and with a parametrization $\phi \in [-\pi, \pi]$. The points on the circle are related to each other *via* a $\mathbb{Z}_2$ symmetry transformation

$$(x^\mu, \phi) \leftrightarrow (x^\mu, -\phi)\,. \tag{2.1}$$

This is a two–dimensional projection such as the shadow of a building on the ground and the orbifolding procedure is depicted in Fig. 2.1. For a 5D field Φ, the requirement has to be fulfilled that the transformation mentioned in Eq. (2.1) result in the same function

$$\Phi\,(x, \phi) \overset{\mathbb{Z}_2}{\to} \pm\Phi\,(x, \phi)\,, \tag{2.2}$$

which may differ by their eigenvalues $+1(-1)$ that are referred to as $\mathbb{Z}_2$–even ($\mathbb{Z}_2$–odd). As an asset, the S^1 symmetry leads to periodic boundary conditions (BC)

$$\Phi\,(x, -\pi) = \Phi\,(x, \pi)\,. \tag{2.3}$$

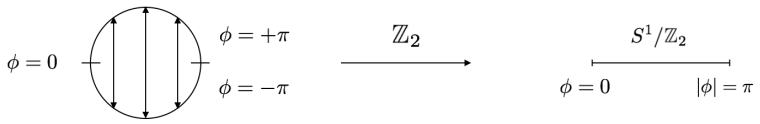

Figure 2.1: The $\mathbb{Z}_2$ symmetry transformation that happens during the procedure of orbifolding. At the beginning, the $S^1/\mathbb{Z}_2$ orbifold that represents the extra dimension is a circle. Then, the coordinates $\phi = -\pi$ and $\phi = \pi$ are identified to each other *via* Eq. (2.1) and a half–circle emerges. After the symmetry transformation that is a two–dimensional projection, the fixed points at the circle are related to each other. Taken from [132].

Both the requirement of the transformation behavior of the 5D field Φ and the S^1 symmetry, respectively, lead to vanishing $\mathbb{Z}_2$–odd functions at the orbifold fixed points $\phi = \pm\pi$. The orbifold fixed points are three sub–manifolds with one time dimension and three spatial dimensions. The region between the branes is the so–called *bulk*. In other words, the low–energy spectrum of Φ depends on the $\mathbb{Z}_2$ parity and is mediated *via* the BCs, which are in general

$$\Phi(x, \phi)\Big|_{\phi=\pm\pi} = 0, \tag{2.4}$$

$$\partial_\phi \Phi(x, \phi)\Big|_{\phi=\pm\pi} = 0. \tag{2.5}$$

They are known as *Dirichlet* BCs Eq. (2.4) and *Neumann* BCs, Eq. (2.5). On the one hand, Dirichlet BCs are applied to $\mathbb{Z}_2$–odd functions to remove those functions in the spectrum. On the other hand, Neumann BCs add solutions to the spectrum if the fields obey $\mathbb{Z}_2$–even parity. The orbifold construction visible in the BCs can be used to remove unwanted degrees of freedom from the theory's low energy spectrum.
In the 90s, Lisa Randall and Raman Sundrum proposed a model based on a non–flat 4D Minkowski spacetime [98, 99] in contrast to flat extra dimensions [95, 97, 100]. Their advantage is a so–called warped extra dimension, which addresses the hierarchy problem with the introduction of a non–flat Minkowski metric

$$\mathrm{d}s^2 = G_{MN}\mathrm{d}x^M\mathrm{d}x^N = e^{-2\sigma(\phi)}\eta_{\mu\nu}\mathrm{d}x^\mu\mathrm{d}x^\nu - r_c^2\mathrm{d}\phi^2 \tag{2.6}$$

and a description of the extra dimension as a $S_1/\mathbb{Z}_2$ orbifold. This leads to two fixed points at $\phi = 0$ and $\phi = \pi$ that are referred to as the *Planck brane* at $\phi = 0$ and the *IR brane*, respectively, the *TeV brane*, at $\phi = \pi$.
Originally, Randall and Sundrum introduced a compactification radius r_c in the order of the Planck length l_{Pl}. Consequently, the origin of the hierarchy stems from a choice of a negative cosmological constant.
The so–called warp factor

$$e^{-2\sigma(\phi)} \tag{2.7}$$

in Eq. (2.6) describes the curvature of the 5D metric and relates both energy units and length units along the extra dimension. Furthermore, the warp factor is also one of the main ingredients to the solution of the hierarchy problem. In the case of so–called

flat extra dimensions, the exponent of the warp factor is 0. With the help of the 4D Minkowski metric $\eta_{\mu\nu}$, the determinant's representation of the 5D metric G_{MN} reads

$$G_{MN} = \begin{pmatrix} \eta_{\mu\nu} e^{-2\sigma(\phi)} & 0 \\ 0 & 1 \end{pmatrix} = \begin{pmatrix} \eta^{\mu\nu} & \bar{A}^M \\ \bar{A}^{MT} & \bar{g}^{55} \end{pmatrix}. \tag{2.8}$$

It is included in the flat description of the 5D Einstein Hilbert action

$$\mathcal{S} = \int \mathrm{d}x^5 \left(-\frac{1}{2} M_5^3 \sqrt{G} R_5[G] \right), \tag{2.9}$$

in which R_5 is the 5D Ricci scalar and M_5 is 5D Planck mass. The scalar $\bar{g}^{55}$ from the 4D point of view, which acquires a VEV measuring the size of the extra dimension is called *Radion*. The 5D Einstein equations, which are obtained using the variational principle on Eq. (2.9) lead to

$$k = \sqrt{\frac{-\Lambda_5}{24 M_5^3}}, \qquad \sigma(\phi) = kr\pi, \tag{2.10}$$

where k is the curvature due to its relation to the 5D Ricci scalar $R_5 = 24k^2$. This follows the convention of the Anti de Sitter space time that is used in this thesis and results at the same time in a negative cosmological constant.
The warp factor can be used for a determination of the reduced 4D Planck mass $M_{\mathrm{Pl}} = (M_5^3/k)\left(1 - e^{-2k\pi r}\right)$. The reduced Planck mass M_{Pl} depends only very weak on the warp factor, because otherwise the hierarchy problem could not be solved. Furthermore, M_5 is assumed to be of the same size of the curvature k. In combination with the last argument and the latter equation, M_5 is assumed to be of order of the Planck size. The *volume* of the extra dimension is approximately $L \approx k\pi$ and is stabilized by the Goldberger Wise mechanism [105].
RS models are regarded as EFTs, because they have negative mass dimensions in their coupling. They posses an inherent position–dependent UV cutoff [98]

$$\Lambda_{\mathrm{UV}}(\phi) \approx M_{\mathrm{Pl}} e^{-kr\pi} \tag{2.11}$$

that is expressed *via* the reduced Planck mass [106–110]. This means that the position–dependent cutoff has an impact on quantum gravity on energy scales that are above the Planck scale. As a consequence, RS models do not offer a description of quantum gravity. The cosmological constant problem remains unsolved, because there is no answer provided for the fact that contributions from energy densities cancel with the cosmological constant. Furthermore, if Feynman diagrams are calculated, each vertex depends on the position ϕ and at the same time on $\Lambda_{\mathrm{UV}}(\phi)$. Thus, the euclidean loop–momentum possesses an upper bound at $p_E = \min\left(\Lambda_{\mathrm{UV}}(\phi_1), \Lambda_{\mathrm{UV}}(\phi_2)\right) = \Lambda_{\mathrm{TeV}}$ due to the position–dependent 4D cutoff. The values for the position–dependent cutoff $\Lambda_{\mathrm{UV}}(t)$ vary between $M_{\mathrm{Pl}} e^{-kr\pi}$ and the fundamental Planck scale, because ϕ is integrated along the extra dimension.
For the later phenomenological discussion, a switch to dimensionless variables is more convenient. This change is provided by introducing

$$t = M_{\mathrm{kk}} \frac{e^{2\sigma(\phi)}}{k} \tag{2.12}$$

with the KK scale

$$M_{\mathrm{kk}} = \epsilon\, k. \tag{2.13}$$

Nota bene: the variable t does not correspond to the time.
With the change of the notation, Eq.(2.6) now reads

$$\mathrm{d}s^2 = \left(\frac{\epsilon}{t}\right)^2 \left(\eta_{\mu\nu}\mathrm{d}x^\mu \mathrm{d}x^\nu - M_{\mathrm{kk}}^{-2}\mathrm{d}t^2\right). \tag{2.14}$$

As a next step, a general overview of the properties for general bulk fields is given and is based on [111, 113]. The SM particles including the Higgs boson were originally confined to the UV brane. Furthermore, the SM gauge group is extended into the bulk of the extra dimension and the action for a general 5D field $A_M\left(x_\mu, t\right)$ results in

$$S_{5D} = S_{\mathrm{gauge}} + S_{\mathrm{matter}} + S_{\mathrm{Yukawa}}. \tag{2.15}$$

Writing explicitly the variation of Eq. (2.15):

$$\delta S_{5D} = \int \mathrm{d}^4x \frac{2\pi r_c}{L} \int_\epsilon^1 \frac{\mathrm{d}t}{t} \delta A_M \left(\mathcal{D}A_M\right) + \int \mathrm{d}^4x \delta A_M \left(\mathcal{B}A_M\right)\Big|_{t=\epsilon,1} = 0 \tag{2.16}$$

that includes the differential operators $\mathcal{D}$ and $\mathcal{B}$ and leads to the equation of motion (EOM) for an arbitrary 5D Lorentz vector $A_M\left(x,t\right)$

$$\left(-t\partial_t \frac{1}{t}\partial_t + \frac{c_A^2}{t^2}\right) A_M\left(t\right) = x_M^2 A_M\left(t\right) \tag{2.17}$$

that are obtained from the term proportional to $\mathcal{D}A_M$ in Eq. (2.16). Furthermore, the EOM are distinct depending on the particle's spin. The bulk field A_M in Eq. (2.23) consists of both a vector field and a scalar field, respectively, because the vector representation of the 5D Lorentz group is decomposed into both a four dimensional Lorentz vector and a Lorentz scalar $A_M\left(x_\mu, t\right) = \left(A_\mu\left(x_\mu, t\right), A_5\left(x_\mu, t\right)\right)$, respectively.
The second term of Eq. (2.16) yields the BCs of the field A_M at both branes, because the boundary term is evaluated at the fixed points 1 and ϵ of the orbifold. The BCs introduced in both Eq. (2.4) and Eq. (2.5) determine the mass spectrum of the KK resonance. The lightest resonance is associated with the SM particle. The vector component of the 5D Lorentz scalar obeys Neumann BCs on both branes, which means that the SM fields are the massless zero modes of the theory. The energy eigenfunctions of the bulk fields are the KK modes as well as the energy eigenvalues are the mass terms. Neumann BCs are chosen in analogy to a Schrödinger particle in a box potential well, where a solution for zero energy requires the same BCs on both ends of the box. This choice is intuitive from the point of view that the SM consists of left–handed doublets, which are embedded in the context of the RS model. The scalar components of the fields have Dirichlet BCs on both branes, in contrast to the vector components. This is motivated by the requirement that the underlying theory is 5D Lorentz invariant. Other combinations of BCs on the branes exist and lead to a different physical interpretation for a particle with its given spin. The introduction of a regularized δ function $\delta^\eta\left(t-1\right)$ is necessary, because otherwise discontinuities arise, *e.g.* in the fermion case that will be discussed in Sec. 2.4. Otherwise the BCs would have to be modified. This modification of the BCs can be avoided if the delta function is properly regularized. With the use of a regularized

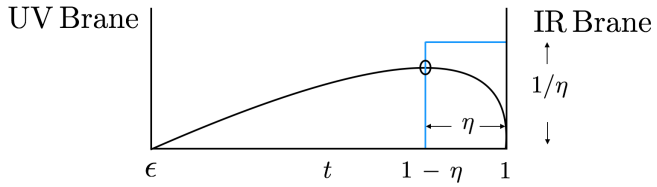

Figure 2.2: The blue colored rectangular box that is denoted in the text by $\delta^{\eta}(t-1)$, Eq. (2.18), with a height $1/\eta$ and a width η. The extra dimension is divided into two parts by $\delta^{\eta}(t-1)$. These two parts are referred to as *bulk* and *sliver*. This choice is, *e.g.* important for the derivation of the fermion propagator, because the solutions have to be obtained in the two parts of the extra dimension separately and then have to be matched at $t = 1-\eta$.

profile it is then possible to shift the profile by an infinitesimal width η into the bulk, *i.e.* $[1-\eta, 1]$. In the limit of $\eta \to 0$, the results are independent of the regularized delta function. A regulator η is introduced and the procedure can be regarded as a box with a height $\frac{1}{\eta}$ and a width η, illustrated in Fig. 2.2. Now, the rectangular regularization reads

$$\delta^{\eta}(t-1) = \frac{1}{\eta}\theta(t-1+\eta), \qquad \forall \ \eta \ll 1 \tag{2.18}$$

and contains the Heavyside step function θ that divides the extra dimension into two parts. One part is referred to as the *bulk*, *i.e.* $t < 1-\eta$ and the other part is the so–called *sliver*, *i.e.* $t > 1-\eta$. The discontinuities that would appear when fermions are considered are thus avoided. At the same time, the $\mathbb{Z}_2$ parity assignments are ensured to leave the Lagrangian hermitian and avoid boundary terms. Another asset of the introduction of this regularization procedure is the smooth transition between the brane Higgs and the bulk Higgs. Furthermore, the partial derivative ∂_t is odd under the $\mathbb{Z}_2$ symmetry, which is relevant for the transformation

$$A_M \to A_M + \partial_\mu \alpha_\mu + \partial_t \alpha_t. \tag{2.19}$$

An integration over the fifth dimension results in a 4D effective theory that contains both SM particles as well as massive KK modes. This is referred to as the *Kaluza Klein (KK)–decomposed theory*. Equation (2.23) suggests a separation of variables in the KK decomposition of the bulk field

$$A_M(x_\mu, t) = \begin{pmatrix} A_\mu(x_\mu, t) \\ A_5(x_\mu, t) \end{pmatrix} = \frac{1}{\sqrt{r_c}} \sum_n \begin{pmatrix} A_\mu^{(n)}(x_\mu)\,\chi^{(n),A}(t) \\ M_{\mathrm{kk}} A_5^{(n)}(x_\mu)\,\partial_t \chi^{(n),A}(t) \end{pmatrix}. \tag{2.20}$$

As a next step, the profile functions $\chi(t)$ depending on the location of the extra dimension have to be normalized. The orthonormality condition [120, 122, 123] reads

$$\frac{2\pi}{L}\int_{\epsilon}^{1} \frac{\mathrm{d}t}{t} \chi_n(t)\,\chi_m(t) = \delta_{nm}. \tag{2.21}$$

At the zero mode level, additional degrees of freedom (dof) are not available, but the number of dofs are doubled if higher KK levels are considered. Choosing Neumann BCs

on both branes, $\chi^{(n),A}(t) = 1$ is a valid choice even in the massless case. The derivative $\partial_t \chi^{(n),A}(t) = \chi_5^{(n),A}(t) = 0$ shows that there is no longitudinal polarization for a zero mode and is massless. The zero mode profile is flat and connected with gauge invariance as well as the universality of the gauge interactions. If the zero mode profile would not be flat, the couplings would not be as simple as they are, but would allow the adjustment of gauge couplings in an arbitrary way.
S_{5D} in Eq. (2.15) contains the gauge part, the Yukawa part, and the matter part, which consist of different sub–parts. For instance, the gauge sector of the 5D actions contains the following parts

$$S_{\text{gauge}} = \int \mathrm{d}^4x \frac{2\pi r_c}{L} \int_\epsilon^1 \frac{\mathrm{d}t}{t} \sqrt{|G|} \left(\mathcal{L} + \mathcal{L}_{\text{GF}} + \mathcal{L}_{\text{Mass}} + \mathcal{L}_{\text{Higgs}} + \mathcal{L}_{\text{FP}}\right) \tag{2.22}$$

After an integration by parts that includes an arbitrary bulk field $A_M(x,t)$, the first three parts of Eq. (2.22) read more explicitly

$$\begin{aligned} S_{\text{gauge}} \ni & \int \mathrm{d}^4x \frac{2\pi r_c}{L} \int_\epsilon^1 \frac{\mathrm{d}t}{t} \left(\mathcal{L} + \mathcal{L}_{\text{GF}} + \mathcal{L}_{\text{Mass}}\right) \\ = & \int \mathrm{d}^4x \frac{2\pi r_c}{L} \int_\epsilon^1 \frac{\mathrm{d}t}{t} \frac{r_c}{2} \Bigg[A_\nu \Bigg(\partial^2 \eta^{\mu\nu} - \left(1 - \frac{1}{\xi}\right) \partial^\nu \partial^\mu - \partial_t + \left(\frac{\epsilon}{t}\right)^2 M_A^2 \Bigg) A_\mu \\ & \left(\frac{\epsilon}{t r_c}\right)^2 \Bigg(A_5 \Big(- \left(\frac{\epsilon}{t r_c}\right)^2 \partial^2 + \frac{\xi}{r_c^4} \left(\frac{\epsilon}{t}\right)^2 \partial_t^2 \left(\frac{\epsilon}{t}\right)^2 - \left(\frac{\epsilon}{t r_c}\right)^4 r_c^2 M_A^2 \Big) A_5 \Bigg] \end{aligned} \tag{2.23}$$

The setup of the RS model used in this thesis consists of a Higgs boson confined on the brane and the matter sector containing both bosons and fermions localized in the bulk. It is important for the discussion of the decay $h \to \gamma\gamma$. The discussion includes the derivation of the boson profiles, which is also necessary for the consideration of the propagators in Ch. 3. After the introduction of the profiles of bosons the fermion sector is derived. The fermion sector is important for both the $h \to \gamma\gamma$ decay and for the investigation of the Wilson coefficient for of a four fermion operator. The four fermion operator contains a scalar connection to the fermions by a possible extra-dimensional scalar S that could act as a fermion localizer field. For the latter investigation, it is necessary to consider the fermion profile function in the so–called *zero mode approximation* (ZMA). Leading contributions in the full theory stem from tree–level diagrams with external fermions and an arbitrary scalar S that propagates between the vertices. The setup of the model used in this thesis is displayed in Fig. 2.3.

2.1 Boson interaction in the minimal RS model

The gauge sector of the RS model is highlighted in the following, because it is necessary for the decay $h \to \gamma\gamma$.
After electroweak symmetry breaking (EWSB), the RS gauge bosons are defined analogously to the SM gauge bosons

$$\begin{aligned} W_M^\pm &= \frac{1}{\sqrt{2}} \left(W_M^1 \mp i W_M^2\right), \\ Z_M &= \frac{1}{\sqrt{g_5^2 + g_5^{'2}}} \left(g_5 W_M^3 - g_5^{'} B_M\right), \end{aligned} \tag{2.24}$$

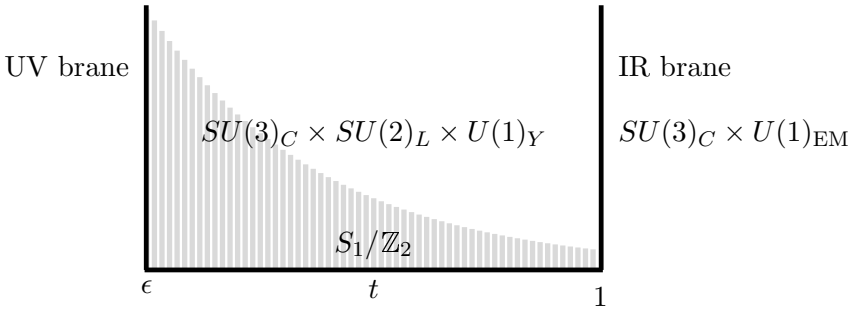

Figure 2.3: Illustration of the minimal RS model considered in this thesis. The electroweak symmetry is broken on the IR brane by the IR localized Higgs. The SM gauge group is placed in the bulk, as well as all SM particles except for the Higgs boson. The gray shaded area denotes the warp factor that affects all dimensionful parameters. Taken from [127] and also appears in [128, 129].

$$A_M = \frac{1}{\sqrt{g_5^2 + g_5^{'2}}} \left(g_5^{'} W_M^3 + g_5 B_M \right)$$

with the exception of both the dimensionful 5D gauge couplings of $SU(2)_L, g_5$ and of $U(1)_Y, g_5'$, which are commonly defined in a way to look like SM couplings. The reason for this exception is that the strength of the weak coupling constant is determined by the coupling of the profile functions of the light fermions to the non–flat profile functions of the gauge bosons. As the profile function of the gauge bosons coupling to both the electric coupling constant e_5 and strong coupling constant g_{s_5} is flat, an identification to the SM value is possible *via* [122, 123]

$$e = \frac{e_5}{\sqrt{2\pi r}} \qquad g_s = \frac{g_{s_5}}{\sqrt{2\pi r}}. \tag{2.25}$$

Furthermore, the gauge boson profile functions are defined as bulk fields. Contrary to the definition of gauge bosons field as bulk fields, a confinement of the gauge boson fields to the IR brane would lead to a localization dependence of the gauge couplings as well as to a non–diagonal coupling for both their excitations and their zero mode. As a consequence, a discrepancy with both the diagonal coupling of the gluon and the diagonal coupling of the photon would exist, respectively. The gauge bosons have a mass in the order of the electroweak scale and their corresponding zero modes are given by the SM gauge bosons. This setup is realized in a scenario that consists of bulk fields transforming as an arbitrary 5D Lorentz vector $A_M(x,t)$.
The Lagrangian of the gauge part of the action Eq. (2.22) reads

$$\mathcal{L}_{\text{gauge}} = G^{KM} G^{LN} \left(-\frac{1}{4} G^i_{KL} G^i_{MN} - \frac{1}{4} W^b_{KL} W^b_{MN} - \frac{1}{4} B_{KL} B_{MN} \right), \tag{2.26}$$

in which the superscripts of the field strength tensors denote $i = 1, ..., 8$ for the $SU(3)_c$ generators and $b = 1, 2, 3$ for the for the $SU(2)_L$ generators, respectively. Just as in the SM, the gauge fixing term of Eq.(2.51) has to be added to the matter part and to the gauge part of the Lagrangian. As quadratic couplings of gauge bosons are more relevant

for this thesis, only they are quoted, but the result of terms containing trilinear or even quartic gauge boson terms can be obtained analogously [120]. The action then reads

$$
\begin{aligned}
S_{\text{gauge,bil}} \ni & \int \mathrm{d}^4x \frac{2\pi r}{L} \int_\epsilon^1 \frac{\mathrm{d}t}{t} \\
& \Bigg\{ -\frac{1}{4}F_{\mu\nu}F^{\mu\nu} - \frac{1}{2\xi}\left(\partial^\mu A_\mu\right)^2 + \frac{1}{2}\left(\partial_\mu A_5 \partial^\mu A_5 + M_{\text{kk}}^2 \partial_t A_\mu \partial_t A^\mu\right) \\
& - \frac{1}{4}Z_{\mu\nu}Z^{\mu\nu} - \frac{1}{2\xi}\left(\partial^\mu Z_\mu\right)^2 + \frac{1}{2}\left(\partial_\mu Z_5 \partial^\mu Z_5 + M_{\text{kk}}^2 \partial_t Z_\mu \partial_t Z^\mu\right) \\
& - \frac{1}{2}W^+_{\mu\nu}W^{-\mu\nu} - \frac{1}{\xi}\left(\partial^\mu W_\mu^+\right)\left(\partial_\nu W_\nu^-\right) + \left(\partial_\mu W_5^+ \partial^\mu W_5^- + M_{\text{kk}}^2 \partial_t W_\mu^+ \partial_t W^{-\mu}\right) \\
& + \frac{k}{2}\delta\left(t-1\right)\Bigg(\frac{1}{2}(\partial_\mu h \partial^\mu h - \lambda v^2 h^2 + \partial_\mu \varphi^+ \partial^\mu \varphi^- + \frac{1}{2}\partial_\mu \varphi^3 \partial^\mu \varphi^3 + \frac{M_{\text{Z}}^2}{2} Z_\mu Z^\mu \\
& + M_{\text{W}}^2 W_\mu^+ W^{-\mu}\Bigg) - \frac{\xi}{2}\left(M_{\text{kk}} t \partial_t \frac{1}{t} A_5\right)^2 - \frac{\xi}{2}\left(\delta\left(t-1\right) k M_{\text{Z}}^2 \varphi^3 + 2 M_{\text{kk}} t \partial_t \frac{1}{t} Z_5\right)^2 \\
& - \frac{\xi}{4}\left(\delta\left(t-1\right) k M_{\text{W}}^2 \varphi^+ + M_{\text{kk}} t \partial_t \frac{1}{t} W_5^+\right)\left(\delta\left(t-1\right) k M_{\text{W}}^2 \varphi^- + M_{\text{kk}} t \partial_t \frac{1}{t} W_5^-\right)
\end{aligned}
\tag{2.27}
$$

The KK decomposition of the gauge fields has an additional t dependence of the form

$$
X_\mu\left(x,t\right) = \frac{1}{\sqrt{r}} \sum_n X_\mu^{(n)}\left(x\right) \chi_n^X\left(t\right), \tag{2.28}
$$

$$
X_5\left(x,t\right) = \frac{M_{\text{kk}}}{\sqrt{r}} \sum_n a_n^X \varphi_X^{(n)}\left(x\right) \partial_t \chi_n^X\left(t\right), \quad X = W, A, Z. \tag{2.29}
$$

In Equation (2.28), the expression of the profile functions $\chi^X\left(t\right)$ are obtained *via* the relation $\chi^X\left(t\right) = a_n^X \partial_t \chi^X\left(t\right)$ that includes an *a priori* parameter a^X. These parameters are determined in the next step after the insertion of the KK modes, *c.f.* Eq.(2.28). Given these considerations, the fifth dimension can be integrated out now and the Fourier coefficients a_n^X can be fixed. The vector components of the KK modes in Eq. (2.28) absorb the KK modes of the scalar KK modes X_5 and become massive. The profile functions $X_\mu^{(n)}\left(x\right)$ denote the KK excitation of the gauge bosons and m_n^X denotes their mass. The profile functions $\varphi_A^{(n)}\left(x\right)$ are the admixture of the KK modes with the profile functions of the Goldstone bosons $\varphi^{\pm,3}\left(x\right)$ that are derived by an expansion in the mass eigenstates, reading [120]

$$
\varphi^\pm\left(x\right) = \sum_m b_m \varphi_W^{(m)}\left(x\right), \qquad \tilde{m}_W = \frac{v}{2}\sqrt{\frac{g_5}{2\pi r}}, \tag{2.30}
$$

$$
\varphi^3\left(x\right) = \sum_n a_m \varphi_Z^{(n)}\left(x\right), \qquad \tilde{m}_Z = \frac{v}{2}\sqrt{\frac{g_5 + g_5'}{2\pi r}}. \tag{2.31}
$$

Using the Fourier coefficients a_n^X, b_n^X, and the orthonormality condition of the profile functions Eq. (2.21), the KK decomposition Eq. (2.28) is inserted into the action

Eq. (2.27). Integrating out the fifth dimension results in

$$
\begin{aligned}
S_{\text{gauge,bil}} \ni \int \mathrm{d}^4x \Bigg\{ & -\frac{1}{4}F^{(n)}_{\mu\nu}F^{(n)\mu\nu} - \frac{1}{2\xi}\left(\partial^\mu A^{(n)}_\mu\right)^2 + \frac{\left(m^{(n)}_A\right)^2}{2}A^{(n)}_\mu A^{(n)\mu} \\
& - \frac{1}{4}Z^{(n)}_{\mu\nu}Z^{(n)\mu\nu} - \frac{1}{2\xi}\left(\partial^\mu Z^{(n)}_\mu\right)^2 + \frac{\left(m^{(n)}_Z\right)^2}{2}Z^{(n)}_\mu Z^{(n)\mu} - \frac{1}{2}W^{+(n)}_{\mu\nu}W^{-(n)\mu\nu} \\
& - \frac{1}{\xi}\left(\partial^\mu W^{+(n)}_\mu\right)\left(\partial_\nu W^{-(n)}_\nu\right) + \frac{\left(m^{(n)}_W\right)^2}{2}W^{+(n)}_\mu W^{-\mu(n)} + \frac{1}{2}\partial_\mu\varphi^{+(n)}_W\partial^\mu\varphi^{-(n)}_W \\
& - \xi\left(m^{(n)}_W\right)^2\varphi^{+(n)}_W\varphi^{-(n)}_W + \frac{1}{2}\partial_\mu\varphi^{(n)}_Z\partial^\mu\varphi^{(n)}_Z - \frac{\xi\left(m^{(n)}_Z\right)^2}{2}\varphi^{(n)}_Z\varphi^{(n)}_Z \\
& + \frac{1}{2}\partial_\mu\varphi^{(n)}_A\partial^\mu\varphi^{(n)}_A - \frac{\xi\left(m^{(n)}_A\right)^2}{2}\varphi^{(n)}_A\varphi^{(n)}_A \Bigg\} + \int \mathrm{d}^4x\left(\frac{1}{2}\partial_\mu h\partial^\mu h - \lambda v^2h^2\right)
\end{aligned}
\tag{2.32}
$$

After a comparison of coefficients, the Fourier coefficients a^X_n and b^X_n read [120]

$$
a^X_n = -\frac{1}{m^X_n}, \qquad b^X_n = -\frac{\tilde{m}^X}{m^X_n}\sqrt{2\pi}\chi^X_n(1). \tag{2.33}
$$

The action describes the gauge bosons with an infinite tower of KK modes and masses m^X_n. The masses of the corresponding Goldstone bosons $\sqrt{\xi}m^X_n$ and the zero modes are associated to the SM Goldstone bosons. In principle mixing effects can occur between both physical zero modes and their excitations. Such a mixing results in different couplings of the gauge boson zero modes to the fermions. After inserting the KK decomposition Eq. (2.28) in the 5D action Eq. (2.26), the profile functions of the gauge bosons become [120]

$$
\left(t\partial_t\frac{1}{t}\partial_t + x^2_{X_n}\chi^X_n(t) - c_A\right)\chi^X_n(t) = 0, \qquad c_A = \delta^\eta(t-1)\frac{L\tilde{m}^2_X}{2M^2_{\text{kk}}}, \tag{2.34}
$$

with $x^2_{X_n} = m^2_X/M_{\text{kk}}$. The δ function stems from the Higgs Lagrangian and implies that two regions exist, which are divided by the regulator η *via* $t < 1-\eta$ and $t > 1-\eta$. The Neumann BC in the UV is applied in the first region and results in an expression for the profile function

$$
\chi^X_n(t) = N_n\sqrt{L/\pi}t\left(Y_0(x_n\epsilon)J_1(x_nt) - J_0(x_n\epsilon)Y_1(x_nt)\right) \tag{2.35}
$$

with the normalization constant N_n. The procedure is repeated in the region $t > 1-\eta$ and the IR BC $\partial_t\chi^X_n(t)|_{t=1^-} = 0$ leads to

$$
\chi^X_n(t) = N_n\sqrt{L/\pi}t\Big(K_0\left(\eta^{-1/2}S_n\right)I_1\left(\eta^{-1/2}S_nt\right) + I_0\left(\eta^{-1/2}S_n\right)K_1\left(\eta^{-1/2}S_nt\right)\Big) \tag{2.36}
$$

with coefficients N_n and $S_n = \left(L\tilde{m}^2_X/2M^2_{\text{kk}} - \eta x^2_{X_n}\right)^{1/2}$. The two coefficients are determined by the continuity equation at $t = 1-\eta$ as well as with the help of the orthonormality condition Eq. (2.21) and lead to a solution for finite values of η. An analytical

solution is found in the region $\eta \ll 1$ *via* an integration of Eq. (2.34) in the interval $[1-\eta, 1]$. In the limit $\eta \to 0$, the $\mathbb{Z}_2$–odd profile functions show a discontinuity at $t = 1$. This means that the profile functions of the W and Z boson are not smoothly differentiable, whereas the profile functions for the photon and the gluon are continuous at $t = 1$. The IR boundary condition then reads

$$\partial_t \chi^X(t)\Big|_{t=1^-} = \lim_{\eta \to 0^+} \partial_t \chi_n^X(t)(t-\eta) = -\frac{L\tilde{m}_X^2}{M_{\mathrm{kk}}^2}\chi^X\left(1^-\right). \tag{2.37}$$

The exact results of the boson profile functions are

$$\chi_n^X(t) = N_n \sqrt{\frac{L}{\pi}} t c^+(t) \tag{2.38}$$

with the normalization constant

$$N_n^{-2} = \left[c^+(1)\right]^2 + \left[c^-\left(1^-\right)\right]^2 - \frac{2}{x_n} c^+(1) c^-\left(1^-\right) - \epsilon^2 \left[c^+(\epsilon)\right]^2 \tag{2.39}$$

and the linear combination of the Bessel functions

$$c^{\pm}(t) = Y_0(x_n\epsilon) J_{1/0}(x_n t) - J_0(x_n\epsilon) Y_{1/0}(x_n t). \tag{2.40}$$

Later, the zero mode profile needs to be expanded in v^2/M_{kk}^2 in the following way

$$\chi_0^{A,G}(t) = \frac{1}{\sqrt{2\pi}}, \tag{2.41}$$

$$\chi_0^{W,Z}(t) = \frac{1}{\sqrt{2\pi}}\left[1 - \frac{m_{W,Z}^2}{2M_{\mathrm{kk}}^2}\left(t^2\left(L - \frac{1}{2} + \ln t\right) - \frac{1}{2} + \frac{1}{2L}\right) + \mathcal{O}\left(v^4/M_{\mathrm{kk}}^4\right)\right]. \tag{2.42}$$

The expression for the zero mode profiles are exact in the case of the photon and the gluon. The contributions proportional to v^2/M_{kk}^2 stem from the IR localized Higgs term, which is contained in c_A [120]. Gauge invariance is broken at the massive KK level, because the fifth mode acts as a Goldstone boson that is absorbed and consequently leads to a mass term of the KK modes and a massive physical KK spectrum. As a consequence, the KK mass spectrum only consists of massive spin 1 particles that contain a non–trivial profile function and lead to non–trivial couplings.
The masses of the KK modes also are the zeros of the Bessel functions that result from the differential equation Eq. (2.34). The KK masses are approximately given by $m_{X_{n+1}} \approx m_{X_n} + n\pi M_{\mathrm{kk}}$ and result in an equidistant spacing. The physical W and Z boson masses are expanded in v^2/M_{kk}^2

$$m_{W,Z}^2 = \tilde{m}_{W,Z}^2\left[1 - \frac{\tilde{m}_{W,Z}^2}{2M_{\mathrm{kk}}^2}\left(L - 1 + \frac{1}{2L}\right) + \mathcal{O}\left(v^4/M_{\mathrm{kk}}^4\right)\right] \tag{2.43}$$

with $\tilde{m}_{W,Z}$ defined in Eq. (2.30) [120].

2.2 Localization of the Higgs sector in Randall Sundrum models and solution of the hierarchy problem

In the RS model, the localization of the Higgs boson is not fixed *a priori*, because both the brane–localized Higgs boson as well as the bulk–localized Higgs boson solve

the hierarchy problem [98] if both are defined close enough to the IR brane. For this thesis, the setup of the RS model with a focus of a brane–localized Higgs is considered in more detail in Sec. 2.2.2 that is based on [98, 120, 121]. The different situation of a Higgs that propagates in a narrow area in the bulk (*narrow bulk Higgs*) is explained and investigated in Sec. 2.2.3. This also offers an implementation of another scalar boson S without an SM analogue that is also considered in this thesis with an introduction based on [133, 134]. A relation between both the brane–localized Higgs scenario and the narrow bulk–localized Higgs scenario is established and discussed also in several theses [128–131]. As mentioned, both brane–localized Higgs and bulk–localized Higgs solve the hierarchy problem as long as both are localized sufficiently close to the IR brane, which is explained in the following [86, 98, 120, 121, 133, 135–138]. After this explanation and before the implementation of a scalar boson S is introduced, the meaning of the general statement "close to the IR brane" is investigated for both cases starting with the brane–localized Higgs sector.

2.2.1 Solution to the hierarchy problem

In [98], the hierarchy problem is addressed in the context of warped extra dimensions. Furthermore, [98] assumes that the fundamental parameters of the RS model are of the order of the Planck mass $M_{\mathrm{Pl}} \sim M_5 \sim k \sim r^{-1}$. The argumentation is as follows: we use the more illustrative ϕ notation, in which the Higgs field Φ in the 5D Higgs action, *c.f.* Eq. (2.22), becomes

$$\mathcal{S}_{\mathrm{Higgs}} = \int \mathrm{d}^4x \int_{-\pi}^{\pi} \mathrm{d}\phi \, \sqrt{|G|}\delta\left(|\phi| - \pi\right) \left[G^{\mu\nu} \left(D_\mu \Phi\right)^\dagger \left(D_\nu \Phi\right) - \frac{\lambda_5}{2} \left(\Phi^\dagger \Phi - \frac{v_5^2}{2} \right)^2 \right]. \tag{2.44}$$

This action is for a Higgs field localized at the IR brane. In Equation (2.44), λ_5 denotes the quartic coupling and is assumed to be of the order of $\mathcal{O}(1)$ and the 5 dimensional Higgs VEV v_5 is in the order of the Planck scale M_{Pl}. Furthermore, the normalized kinetic term in Eq. (2.44) is shifted by the redefinition of the Higgs field $\Phi \to e^{kr\pi}\Phi$. The Higgs VEV is shifted by the same amount:

$$\mathcal{S}_{\mathrm{Higgs}} = \int \mathrm{d}^4x \left[\eta^{\mu\nu} \left(D_\mu \Phi\right)^\dagger \left(D_\nu \Phi\right) - \frac{\lambda_5}{2} \left(\Phi^\dagger \Phi - e^{-2kr\pi} \frac{v_5^2}{2} \right)^2 \right]. \tag{2.45}$$

Now, the connection between the 4–dimensional effective Higgs VEV v_4 and the 5 dimensional Higgs VEV v_5 is given by $v_4 = e^{-kr\pi} v_5$, in which the exponential factor is the warp factor, as given in Eq. (2.7) and is evaluated on the IR brane $\phi = \pm\pi$. The tree level Higgs mass is given by

$$m_h = e^{-kr\pi} m_{h,5} = e^{-kr\pi} \sqrt{2\lambda_5} v_5. \tag{2.46}$$

Although the dimensionful parameters of the RS model are of $\mathcal{O}(M_{\mathrm{Pl}})$, the Higgs localized at the IR brane leads to a position dependence of the dimensionful variables, which are also of the order of the electroweak scale $\mathcal{O}(M_{\mathrm{EW}})$ at the TeV brane. In [98], all SM particles were confined on the IR brane, which leads to FCNCs. Proton decay became possible as well as the cutoff scale would not be large enough for a suppression of higher–dimensional operators. It turned out that Eq. (2.44) requires only the Higgs

confined on the IR brane, because the compactification radius r_c enters only in the Higgs Lagrangian [98]. Moving the gauge boson fields away from the brane and into the bulk [122] and considering bulk fermions [125, 139], as well, SM discrepancies could be resolved that occur if they are confined on the IR brane. The next step is to solve the hierarchy problem with a Higgs that is confined on the IR brane.

2.2.2 Brane–localized Higgs

The 5D Higgs Lagrangian from Eq. (2.22) for a brane–localized Higgs is given in t notation by

$$\mathcal{L}_{\text{Higgs}} = \int_{\epsilon}^{1} \frac{\mathrm{d}t}{t} \delta^{\eta}(t-1) \sqrt{|G|} \Big[G^{\mu\nu} \left(D_\mu \Phi\right)^\dagger \left(D_\nu \Phi\right) + \mu^2 \Phi^\dagger \Phi - \lambda \left(\Phi^\dagger \Phi\right)^2 \Big] \tag{2.47}$$

with the covariant derivative

$$\mathrm{D}_\mu = \partial_M - \frac{i g_5}{2\sqrt{2}} \left(\sigma^+ W_M^+ + \sigma^- W_M^-\right) - \frac{i g_5}{2 c_{\theta_W}} Z_M \left(\sigma^3 - 2Q s^2_{\theta_W}\right) - i e_5 A_M \tag{2.48}$$

acting on the Higgs field

$$\Phi_h(x,t) = \frac{1}{\epsilon} \begin{pmatrix} -i\varphi^+(x) \\ \frac{1}{\sqrt{2}} \left[v + h(x) + i\varphi_3(x)\right] \end{pmatrix} \tag{2.49}$$

and leads to

$$\mathrm{D}_\mu \Phi_h(x,t) = \frac{1}{\sqrt{2}} \begin{pmatrix} -i\sqrt{2} \left(\partial_\mu \varphi^+(x) + M_{\mathrm{W}} W_\mu^+\right) \\ \partial_\mu h + i \left(\partial_\mu \varphi^3 + M_{\mathrm{Z}} Z_\mu\right) \end{pmatrix}. \tag{2.50}$$

The couplings $g_{s,5}, g_5, e_5$, and g_5' have mass dimension -1/2.. The gauge fixing term reads in the case for a brane–localized Higgs

$$\begin{aligned} \mathcal{L}_{GF} = &- \frac{1}{2\xi} \left(\partial^\mu A_\mu - \xi \left[M_{\mathrm{kk}} t \partial_t \frac{1}{t} A_5\right]\right)^2 \\ &- \frac{1}{2\xi} \left(\partial^\mu Z_\mu - \frac{\xi}{2} \left[\delta(t-1)\, k M_Z \varphi^3 + 2 M_{\mathrm{kk}} t \partial_t \frac{1}{t} Z_5\right]\right)^2 \\ &- \frac{1}{2\xi} \left(\partial^\mu W_\mu^+ - \frac{\xi}{2} \left[\delta(t-1)\, k M_W \varphi^+ + 2 M_{\mathrm{kk}} t \partial_t \frac{1}{t} W_5^+\right]\right) \\ &\times \left(\partial^\mu W_\mu^- - \frac{\xi}{2} \left[\delta(t-1)\, k M_W \varphi^- + 2 M_{\mathrm{kk}} t \partial_t \frac{1}{t} W_5^-\right]\right). \end{aligned} \tag{2.51}$$

This gauge fixing term implies that the couplings from the vector component have to be adjusted if the result should remain 4D Lorentz invariant. Then, there exists no other excitation of the Higgs boson, and there are only zero modes for the Goldstone bosons φ_A with mass dimension $[\varphi_A] = 1$. The terms containing a squared delta function in Eq. (2.51) cancel out after the KK decomposition. Besides this procedure, there is also the possibility to introduce a separate brane gauge fixing term. Then, the EOM for a vector boson in Eq. (2.17) changes to

$$c_A^2 \to L \frac{g_5^2 v^2}{4 r M_{\mathrm{kk}}^2} \left(\delta\left(t - 1^-\right) + \delta\left(t + \varepsilon^+\right)\right). \tag{2.52}$$

A non–zero width of the Higgs profile function is assumed, which is described by a delta function on the IR brane $\delta(t-1)$. This can be considered as a limiting procedure of an infinitesimal shift of the Higgs profile function into the bulk, which reads

$$\delta\left(t-1^{-}\right)=\lim_{\eta\to 0}\delta\left(t-1+\eta\right). \tag{2.53}$$

Such an approach is satisfied as long as the Higgs profile function has no impact on observables or the profile function of the Higgs boson is not resolved by other modes. The two mentioned conditions confine the maximum of the Higgs profile function width η to

$$\eta \ll \frac{v\left|Y_q\right|}{\Lambda_{\mathrm{TeV}}}. \tag{2.54}$$

In this relation, Y_q reflects the scale of the dimensionless 5D Yukawa coupling. In this limit, the width of the Higgs profile function is resolved by other fermion modes of the theory. An equivalent explanation is the dominance of the Yukawa term compared to the mass term that follows from $\eta \ll |Y_q|$ and leads to modified BCs at $t=1^{-}$, as well. The limit of η corresponds to the theory's inherent UV cutoff Λ_{TeV}. Ideally, all results are considered in the limit $\eta \to 0$. However, this is not possible every time: As long as the condition Eq. (2.54) is fulfilled, the Higgs localization can still be regarded as a brane Higgs.
Following this discussion, the case of a so–called bulk–localized Higgs is given, whenever the condition in Eq. (2.54) is not fulfilled anymore.

2.2.3 Narrow bulk–localized Higgs

Considering the bulk Higgs, there are a few more remarks to make. The spontaneous symmetry breaking (SSB) now happens in the bulk, which leads to an introduction of Goldstone bosons φ_A in the gauge fixing term of Eq. (2.23). Now there exists a linear combination of the fields $A_5(x_\mu,t)$ and φ_A, which is absorbed by the KK modes of $A_\mu(x_\mu,t)$. The other combinations remain and as a consequence, an additional tower of pseudo scalar bosons appears in the gauge fixing term. In case of a bulk Higgs, η lies in the interval

$$\frac{v\left|Y_q\right|}{\Lambda_{\mathrm{TeV}}} \ll \eta \ll \frac{v\left|Y_q\right|}{M_{\mathrm{kk}}}. \tag{2.55}$$

In the limit $\eta \to 0$, a model independent solution can be derived under the following circumstances. Within the region $\frac{v|Y_q|}{\Lambda_{\mathrm{TeV}}} > \eta$, the Higgs profile function is completely resolved by both the fermion and gauge boson modes and leads to competing contributions to the amplitude of the processes under investigation.
An arbitrary scalar boson S is considered with almost the same properties as the bulk Higgs analogously to the bulk–localized Higgs boson. The Lagrangian of a bulk–localized Higgs boson is given by

$$\begin{aligned}\mathcal{L}_{h/S}(x,t)=\int_{\epsilon}^{1}\mathrm{d}t\frac{2\pi r}{Lt}\sqrt{|G|}\Bigg[\, & G^{MN}D_M\Phi^{\dagger}(x,t)\,D_N\Phi(x,t)-\mu^2\left|\Phi(x,t)\right|^2 \\ & -\frac{M_{\mathrm{kk}}}{2}V_{UV}(\Phi)\,\delta(t-\epsilon)-\frac{k}{2}V_{IR}(\Phi)\,\delta(t-1)\Bigg],\end{aligned} \tag{2.56}$$

with the bulk mass μ and a scalar doublet field Φ with mass dimension 3/2. The Lagrangian of a bulk scalar is different compared to the brane–localized Higgs boson, because additional brane terms appear. In Equation (2.56), the terms $V_{UV} = M_{UV} |\Phi|^2$ and $V_{IR} = -M_{IR} |\Phi|^2 + \lambda_{IR} |\Phi|^4$ indicate the potentials in the UV and IR regions, respectively, and define the BCs of the scalar fields. Furthermore, they may induce EWSB at the same time. The mass dimensions of the terms of the potential are $\left[M_{UV}\right] = \left[M_{IR}\right] = 1$ and $\left[\lambda_{IR}\right] = -2$. They are rescaled to the dimensionless quantities

$$m_{IR} = \frac{M_{IR}}{2k}, \qquad m_{UV} = \frac{M_{UV}}{2k}, \qquad \lambda_{IR} = \frac{\lambda_{IR} k}{4r}. \tag{2.57}$$

The mass terms M_{IR}, M_{UV} and λ_{IR} scale with terms proportional to M_{Pl}. Equation (2.56) is valid for any scalar boson and therefore also applies to the scalar S. The difference between the scalar S and the bulk–localized Higgs boson is that the scalar S is a gauge singlet

$$\Phi_S (t) = \frac{1}{\sqrt{2}} \left(v_s (t) + s (x,t) \right) \tag{2.58}$$

with a scalar VEV $v_s (t)$ and $s (x,t)$, being the profile function of the scalar. In contrast, the Higgs field is a doublet

$$\Phi_h (x,t) = \frac{1}{\epsilon \sqrt{r}} \begin{pmatrix} -i\varphi^+ (x,t) \\ \frac{1}{\sqrt{2}} \left[v_h (t) + h (x,t) + i\varphi_3 (x,t) \right] \end{pmatrix}. \tag{2.59}$$

Here, $v_h (t)$ denotes the Higgs VEV, $h (x,t)$ the corresponding physical Higgs field after a rotation into the mass basis, whereas $\varphi^+ (x,t)$ and $\varphi_3 (x,t)$ denote the Goldstone bosons. Now, all 5D fields and the VEV in the Higgs doublet $\Phi_h (x,t)$ also possess a position in the extra dimension, indicated by the letter t. Furthermore, this advantage allows a decomposition into KK modes, but as a consequence the profiles now mix with KK modes of other extra–dimensional particles [140]. Further, the additional scalars $\phi^{\pm(n)} (x,t)$ and $\phi_Z^{(m)} (x,t)$ do not possess a zero mode. In Ch.4, the Higgs decay into two photons and the charged scalars are discussed. Their analysis follows analogously to the one of both the Higgs boson and the scalar boson S.
After an integration by parts, the corresponding Lagrangian $\mathcal{L}_{h/S}$ to the action in Eq.(2.56) reads

$$\begin{aligned} \mathcal{L}_{h/S}^{bulk} =& \frac{2\pi}{L} \int_\epsilon^1 \frac{\mathrm{d}t}{t} \left[\frac{1}{2} \partial_\mu h (x,t) \, \partial^\mu h (x,t) + \frac{M_{\mathrm{kk}}^2}{2} \left[\frac{v (t) + 2h (x,t)}{t} \left(t^2 \partial_t^2 + t\partial_t - \beta^2 \right) \frac{v (t)}{t} \right. \right. \\ & \left. \left. + \frac{h (x,t)}{t} \left(t^2 \partial_t^2 + t\partial_t - \beta^2 \right) \frac{h (x,t)}{t} \right] \right] \\ & - \frac{\pi M_{\mathrm{kk}}^2}{L} \left[\left[\frac{v (t) + 2h (x,t)}{t^2} \partial_t \left[t v (t) \right] + \frac{h (x,t)}{t^2} \partial_t \left[t h (x,t) \right] \right]_{t=\epsilon}^1 \right. \\ & \left. + \frac{m_{\mathrm{UV}}}{\epsilon^2} \left[v (\epsilon) + h (x,\epsilon) \right]^2 - m_{\mathrm{IR}} \left[v (1) + h (x,1) \right]^2 + \frac{\lambda}{M_{\mathrm{kk}}^2} \left[v (1) + h (x,1) \right]^4 \right], \end{aligned} \tag{2.60}$$

and includes the bulk localization parameter $\beta = \sqrt{4 + \mu^2/k^2}$. For clarity, only the Higgs field $h (x,t)$ is written, but the Lagrangian also holds if the Higgs would be a general scalar S. The BCs are obtained by an integration of Eq.(2.60) over an infinitesimal

interval around the branes. With the further restriction that both quadratic and linear terms vanish on the branes, the BCs are

$$\partial_t \left[tv\left(t\right)\right]|_{t=\epsilon^+} = m_{\mathrm{UV}} v\left(\epsilon\right), \qquad \partial_t \left[tv\left(t\right)\right]|_{t=1^-} = m_{\mathrm{IR}} v\left(1\right) - \frac{2\lambda_{\mathrm{IR}}}{M_{\mathrm{kk}}^2} v^3\left(1\right), \tag{2.61}$$

$$\partial_t \left[th\left(t\right)\right]|_{t=\epsilon^+} = m_{\mathrm{UV}} h\left(x,\epsilon\right), \qquad \partial_t \left[th\left(t\right)\right]|_{t=1^-} = m_{\mathrm{IR}} h\left(x,1\right) - \frac{6\lambda_{\mathrm{IR}}}{M_{\mathrm{kk}}^2} v^2\left(1\right) h\left(x,1\right). \tag{2.62}$$

Such a restriction is necessary for a description of the Higgs field $h\left(x,t\right)$ in the desired way, but for an arbitrary scalar S, these restrictions do not necessarily apply and are subject to further specifications. Nevertheless, Eq.(2.62) can be recovered for an arbitrary scalar S if both quadratic and quartic terms on the branes are allowed. Throughout this thesis, the same BCs for both the Higgs boson and the arbitrary scalar boson S are used.
In order to obtain the profile function for an arbitrary scalar field, the scalar field is decomposed by

$$s\left(x,t\right) = \sum_n^{\infty} \chi_S^n\left(t\right) s_n\left(x\right). \tag{2.63}$$

For the zero mode of a bulk Higgs and after applying the BC, the EOM of a bulk scalar is obtained from the Lagrangian, Eq. (2.60):

$$\left(t^2\partial_t^2 + t\partial_t + t^2 x_n^2 - \beta^2\right) \frac{\chi_S^{(n)}\left(t\right)}{t} = 0 \tag{2.64}$$

with $x_n = m_{\mathrm{sc}}/M_{\mathrm{kk}}$. A general solution of the EOM in Eq. (2.64) is

$$S\left(p^2;t,t'\right) = N_n t\left[J_\beta\left(x_n t\right) - r_n J_{-\beta}\left(x_n t\right)\right] \tag{2.65}$$

with the normalization constant N_n and $J_\beta\left(x_n t\right)$ denoting a Bessel function. The mass for the SM Higgs boson is derived *via* the application of appropriate BCs

$$\frac{x_n J_{\beta+1}\left(x_n t\right)}{J_\beta\left(x_n t\right)} = 2\left(m_{\mathrm{IR}} - 2 - \beta\right) = \delta \tag{2.66}$$

and as a consequence, the Higgs mass should be of $\mathcal{O}\left(M_{\mathrm{kk}}\right)$, which is not the case and referred to as *little hierarchy problem*. A realistic expression for the mass is obtained *via* $\delta \ll 1$. After that, an expansion in δ is possible that results in the expression for the bulk Higgs mass

$$x_0^2 = \frac{m_h^2}{M_{\mathrm{kk}}^2} = 4\left(1+\beta\right)\delta\left[1 - \frac{\delta}{2+\beta} + \frac{2\delta^2}{\left(2+\beta\right)^2\left(3+\beta\right)+...}\right] \tag{2.67}$$

and the profile function for the bulk Higgs

$$\chi_0^h\left(t\right) = \sqrt{\frac{L}{\pi}\left(1+\beta\right)} t^{1+\beta}\left[1 - \frac{x_0^2}{4}\left(\frac{t^2}{1+\beta} - \frac{1}{2+\beta}\right) + ...\right]. \tag{2.68}$$

In the case of an arbitrary bulk scalar with no SM equivalent, Eq. (2.68) differs by an interchange of

$$x_0^2 \leftrightarrow x_1^2 = \frac{m_{\mathrm{sc}}^2}{M_{\mathrm{kk}}^2} \approx \frac{4\left(1+\beta\right)\left[1-\xi\left(1+\beta\right)\right]}{1-\xi\left(3+\beta\right)} \tag{2.69}$$

and the lightest mode results in the case of the singlet scalar S in

$$\begin{aligned}\chi_S(t) &= \sqrt{\frac{L(1+\beta)}{\pi}} t^{1+\beta}\left[1-\frac{x_1^2}{4}\left(\frac{t^2}{1+\beta}-\frac{1}{2+\beta}\right)+...\right], \\ \chi_S(t) &\overset{\beta\to\infty}{=} \sqrt{\frac{L(1+\beta)}{\pi}}\frac{1}{2+\beta}\delta(t-1).\end{aligned} \tag{2.70}$$

Here it is clearly visible that the profile function of $\chi_S(t)$ approaches a localization near the IR brane in the case of $\beta \to \infty$, as the delta function $\delta(t-1)$ appears in Eq. (2.70). If $\beta = \mathcal{O}(1)$, the profile lies wide along the extra dimension [141].
The differential equation for the profile function of the 5D Higgs–VEV $v(t)$ is

$$\left[t^2\partial_t^2 + t\partial_t - \beta^2\right]\frac{v(t)}{t} = 0. \tag{2.71}$$

The latter equation is obtained with the application of the principle of variation on the action, Eq.(2.56), that ensures that tadpole terms vanish. The Lagrangian $\mathcal{L}_{h/S}^{bulk}$ of Eq.(2.60) now reads

$$\begin{aligned}\mathcal{L}_{h/S}^{\text{Bulk}}(x) = \frac{2\pi}{L}\int_\epsilon^1 \frac{d}{t}\left[\frac{1}{2}\partial_\mu h(x,t)\,\partial^\mu h(x,t) + \frac{M_{\text{kk}}^2}{2}\frac{h(x,t)}{t}\left(t^2\partial_t^2 + t\partial_t - \beta^2\right)\frac{h(x,t)}{t}\right] \\ -\frac{\pi}{L}\lambda\left[-v^4(1) + 4v(1)\,h^3(x,1) + h^4(x,1)\right].\end{aligned} \tag{2.72}$$

The general solution of Eq.(2.71) with the BCs Eq.(2.61) is

$$v(t) = N_v\left(t^{1+\beta} - r_v\, t^{1-\beta}\right), \tag{2.73}$$

with the normalization

$$N_v = \frac{M_{\text{kk}}^2}{2\lambda}\frac{(m_{\text{IR}}-2-\beta) - r_v(m_{\text{IR}}-2+\beta)}{(1-r_v)^3} \tag{2.74}$$

and the radius

$$r_v = \epsilon^{2\beta}\frac{2+\beta-m_{\text{UV}}}{2-\beta-m_{\text{UV}}}. \tag{2.75}$$

If the 5D scalar field obeys the Breitenlohner-Freedman bound $\mu^2 \geq -4k^2$ [142], β is assumed to be a real positive number. The assumption of β being a real positive number follows from the observation that the energy–momentum flux in a pure Anti–de–Sitter space in the limit $r \to \infty$ vanishes at the bound, *i.e.* without an IR brane. The prevention of the little hierarchy problem is realized by the scaling dimension $(2+\beta)$ and the relation of the source to the operator *via* $\Lambda_{\text{UV}}^{1-\beta}\Phi_0\mathcal{O}$. Here, Φ_0 denotes the scalar and $\mathcal{O}$ denotes the operator [133, 143, 144]. At the same time, the lower bound is set to $\beta \geq 1$ by these requirements. With this bound, the contribution of $r_v \propto \epsilon^{2\beta}$ remains insignificant as long as t is sufficiently close to the UV brane, which means $t \sim \epsilon$. The upper bound on β is set by the fact that the Higgs VEV is a positive real number

$$v(t) = v(1)\,t^{1+\beta} \quad \text{with} \quad v(1) = M_{\text{kk}}\sqrt{\frac{m_{\text{IR}}-2-\beta}{2\lambda}}, \tag{2.76}$$

and keeping in mind that λ is positive for the reason of a stable vacuum.Although there is an expression for $v\,(1)$, the expression depends on input parameters of the theory. A more intuitive way is an expression by a relation of the two VEVs, which is derived next with the help of the gauge boson profile functions.
In order to obtain a relation from the 4D Higgs VEV to the 5D Higgs VEV profile, the next step is to consider the mass terms of the W and Z boson in the action

$$S^{(5)}_{\text{GB masses}} = \int d^4x \frac{2\pi}{L} \int_\epsilon^1 \frac{dt}{t} \frac{v\,(t)^2}{4} \left[g_5^2 W^+_\mu(x,t) W^{-\mu}(x,t) + \frac{g_5^2 + g_5'^2}{2} Z_\mu(x,t) Z^\mu(x,t) \right]. \quad (2.77)$$

Next, the KK decomposition is inserted that relates v_4 to the 5D Higgs VEV:

$$\begin{aligned} v_4^2 &\equiv \frac{2\pi}{L} \int_\epsilon^1 \frac{dt}{t} v^2\,(t) \left(\chi_0^W\,(t)\, 2\pi\right)^2 \\ &= \frac{N_v^2}{k} \left[\frac{1-\epsilon^{2(1+\beta)}}{2\,(1+\beta)} + r_v^2 \frac{2\,(2-\beta)\,(1-\epsilon) - \epsilon^{2(1-\beta)}}{2\,(1-\beta)} \right] \\ &= \frac{\pi}{L} \frac{v^2\,(1)}{1+\beta}. \end{aligned} \quad (2.78)$$

Up to an expansion in $\mathcal{O}\left(\frac{v^2}{M_{\text{kk}}^2}\right)$, v_4 is identical to the SM Higgs VEV. The exact derivation is challenging as it requires the knowledge of the profile function $\chi^W_{\text{bulk}}\,(t)$ of the W boson that cannot be obtained in a closed form. However, it can be obtained by an expansion of the EOM, Eq.(2.17), with $c_A^2 \to \frac{g_5^2 v(1)^2}{4 r M_{\text{kk}}^2}$. As one is too involved with the derivation of the profile function, an expansion fits the purpose better. Thus, the Higgs VEV becomes

$$v\,(t) = v_4 \sqrt{\frac{L}{\pi}\,(1+\beta) t^{1+\beta}}. \quad (2.79)$$

As one can see, both VEV profile, Eq. (2.79), and the bulk Higgs zero mode profile, Eq. (2.68), coincide for $\beta \to \infty$

$$\delta_v^{1/\beta}\,(t-1) = (2+\beta)\,t^{1+\beta}, \quad (2.80)$$

$$\delta_h^{1/\beta}\,(t-1) = (2+\beta)\,t^{1+\beta} \left[1 - \frac{x_0^2}{4\,(1+\beta)} \left(t^2 - \frac{2+\beta}{4+\beta} \right) + ... \right]. \quad (2.81)$$

This leads to the profile function of both the bulk Higgs VEV and the bulk Higgs profile

$$v\,(t) = v_4 \sqrt{\frac{L}{\pi}} \frac{\sqrt{(1+\beta)}}{2+\beta} \delta_v^{1/\beta}\,(t-1), \quad (2.82)$$

$$\chi_0\,(t) = \sqrt{\frac{L}{\pi}} \frac{\sqrt{(1+\beta)}}{2+\beta} \left[1 + \frac{x_0^2 \beta}{4\,(1+\beta)\,(2+\beta)\,(4+\beta)} + ... \right] \delta_h^{1/\beta}\,(t-1) \quad (2.83)$$

with the regulator $1/\beta$ and η that is the regulator for the brane–localized Higgs scenario. These considerations are also necessary for bulk fermions that are discussed now.

2.3 Yukawa interactions in the RS model

The matter sector of the 5D action Eq. (2.15) consists of the kinetic terms of the fermions and the Yukawa action S_{Yuk}. These parts are investigated in the following, because they

are necessary to understand the derivation of both the profile functions of the fermions and their propagator. Starting with the Yukawa sector, the derivation of the fermion profile functions follows immediately. The matter part of Eq. (2.15) reads

$$\begin{aligned}\mathcal{L}_{\text{Yuk}} = -\int_{\epsilon}^{1} \frac{\mathrm{d}t}{t} \frac{M_{\text{kk}}}{2} \delta^{\eta}(t-1) \Bigg[& \overline{Q}_L(x,t)\, \Phi(x)\, Y_d^{5D} d_R(x,t) \\ & + \overline{Q}_R(x,t)\, \Phi(x)\, Y_d^{5D} d_L(x,t) + \epsilon_{ab} \overline{Q}_{a,L}(x,t)\, \Phi_b^{\dagger}(x)\, Y_u^{5D} u_R(x,t) \\ & + \epsilon_{ab} \overline{Q}_{a,R}(x,t)\, \Phi_b^{\dagger}(x)\, Y_u^{5D} u_L(x,t) + \text{h.c.} \end{aligned} \tag{2.84}$$

The 5D Yukawa matrices are defined *via*

$$Y = \frac{k}{2} Y^{5D}, \tag{2.85}$$

and lead to the mass dimension of $\left[Y^{5D}\right] = -1$ and the two–dimensional Levi Civita symbol $\epsilon = i\sigma^2$ also appears with $\epsilon_{12} = 1$. Compared to the SM Yukawa matrices, these Yukawa matrices are assumed to be anarchical, which means that there is no hierarchical structure as it is the case for SM Yukawa matrices. The upper bound of the absolute value of the Yukawa matrices $y_\star$ is 3 in both Ch.4 and Ch.5, in which the phenomenology of both $h \to \gamma\gamma$ and the coupling for an arbitrary bulk scalar S are discussed. This value corresponds to the perturbativity bound, which is explained in Sec. 2.3.1. For the phenomenological analysis also other values for the Yukawa matrices are discussed, *via* $y_\star = 0.5, 1, 1.5, 2, 2.5$.
The Yukawa couplings are described by

$$\mathcal{L}_Y^{\text{bulk}} = -\int_{\epsilon}^{1} dt \sum_{q=u,d} \frac{v(t) + \sum_n h_n(x)\, \chi_h^n(t)}{\sqrt{2}} \overline{\mathcal{Q}}_L(x,t) \frac{1}{\sqrt{r}} \begin{pmatrix} 0 & Y_{b,q}^{(5D)} \\ Y_{b,q}^{(5D)\dagger} & 0 \end{pmatrix} \mathcal{Q}_R(x,t) + \text{h.c.} \tag{2.86}$$

for a bulk localized Higgs boson. The requirement of $\beta = \sqrt{4 + \frac{\mu^2}{k^2}}$ in $\mathcal{O}(1)$ leads to the modification of the Yukawa matrix for the bulk Higgs case to

$$Y_q \equiv \frac{k}{2} Y_q^5 = \frac{\sqrt{k(1+\beta)}}{2+\beta} Y_q^{5,bulk}, \tag{2.87}$$

which is bound from above by $y_\star$. In the limit $\beta \gg 1$ which also means that $\eta \to 0$, the profile functions Eq. (2.82) become IR localized. Then, the dimensionless Yukawa matrices are related *via* $Y_q \sim \sqrt{(k/\beta)}\, Y_q^{5,bulk}$ and are interpreted as quantities that relate an observed mass to a mixing angle following the relation from [120]. Then, the relation

$$\frac{\delta_h^{1/\beta}(t-1)}{\delta_v^{1/\beta}(t-1)} = 1 + \mathcal{O}\left(\frac{m_h^2}{\beta^2 M_{\text{kk}}^2}\right) \tag{2.88}$$

shows that the delta functions are equal at $\mathcal{O}\left(\frac{m_h^2}{\beta^2 M_{\text{kk}}^2}\right)$ and the Yukawa coupling for a brane–localized Higgs boson is recovered. One additional note is that for a very large β a double hierarchy in the following relation exists:

$$\frac{1}{r} \ll k \ll \mu \approx \frac{m_{\text{IR}}}{2}, \tag{2.89}$$

which can be achieved if k is chosen to be smaller than the Planck scale. In the above Eq. (2.86), both $\mathcal{Q}_R(x,t)$ and $\mathcal{Q}_L(x,t)$ denote the fermion profile functions, whose properties are now being investigated.

2.3.1 Perturbativity bounds on the Yukawa couplings

A perturbative treatment of the Yukawa interaction in the RS model that is under consideration requires here an upper bound to the 5D Yukawa couplings [134, 145]. In the so–called naïve dimensional analysis (NDA) approach, it is visible that the Yukawa interactions at 1–loop get corrections from a brane–localized Higgs sector and might exhibit quadratic divergences, resulting from [113]

$$c_g \left(\frac{\left| Y_q^{5D} \right|}{\sqrt{2}} \right)^2 \frac{l_4}{l_5} M_{\rm Pl}^2 = \frac{c_g \left| Y_q \right|^2}{18\pi^4} \left(\frac{\Lambda_{\rm TeV}}{M_{\rm kk}} \right)^2 < 1. \tag{2.90}$$

The scale for the dimensionful Yukawa matrices is defined by $\frac{\left| Y_q^{5D} \right|}{k}$, and $l_4 = 16\pi^2, l_5 = 24\pi^3$ denote the phase space factors for the 4D and the 5D case, respectively. The scale $\Lambda_{\rm TeV} = M_{\rm Pl}\epsilon$ denotes the IR cutoff whereas $M_{\rm Pl}^2$ denotes the UV cutoff. The quantity $M_{\rm kk}$ is defined as $M_{\rm kk} = k\epsilon$. As the last ingredient for Eq. (2.90), c_g defines the multiplicity of the fermion generation. In the present discussion, c_g is defined as

$$c_g = 2N_g - 1 \tag{2.91}$$

for N_g fermion generation(s), which is related *via*

$$\left\langle \left(Y_q Y_q^\dagger Y_q \right)_{ij} \right\rangle = (2N_g - 1) \left| Y_q \right|^2 (Y_q)_{ij} \,. \tag{2.92}$$

The latter equation is meant to be an expectation value for both complex and anarchic 5D Yukawa matrices. In the KK picture, Eq. (2.90) is expressed *via* the KK modes. There is a contribution of the quadratic cutoff that stems from the double sum of the $N_{\rm KK}$ states below the cutoff value $\Lambda_{\rm TeV}$ [145], which yields

$$c_g \left(\frac{\left| Y_q^{5D} \right|}{\sqrt{2}} \right)^2 \frac{N_{\rm KK}^2}{l_4} \approx \frac{c_g \left| Y_q \right|^2}{32\pi^4} \left(\frac{\Lambda_{\rm TeV}}{M_{\rm kk}} \right)^2 < 1 \tag{2.93}$$

with

$$\left| Y_q \right|^2 = \langle |Y_q|_{ij}^2 \rangle = \frac{y_*^2}{2}. \tag{2.94}$$

Depending on the choice of formulae, it is possible to derive two similar upper bounds for $y_\star^2$. Using Eq. (2.90), the upper bound becomes

$$y_* \leq y_{\rm max} = \frac{6\pi^2}{\sqrt{c_g}} \frac{M_{\rm kk}}{\Lambda_{\rm TeV}}. \tag{2.95}$$

While for Eq. (2.93) the upper bound for y_*^2 becomes

$$y_* \leq y_{\rm max} = \frac{8\pi^2}{\sqrt{c_g}} \frac{M_{\rm kk}}{\Lambda_{\rm TeV}}. \tag{2.96}$$

If the scale of $\Lambda_{\rm TeV} \sim 10 M_{\rm kk}$ is considered, the upper bounds become $y_{\rm max} \approx 2.6$ and $y_{\rm max} \approx 3.5$, which justifies an assumption of $y_{\rm max} = 3$ in both the phenomenological analyses and use in the literature, *e.g.* [120, 121, 131, 179, 194]. Usually the values for

$y_{\max}$ are derived without a dependence of N_g. In the case of a bulk Higgs model, Eq. (2.93) turns into

$$c_g \left(\frac{|Y_q^{5D}|}{\sqrt{2}} \right)^2 \frac{1}{l_5} M_{\rm Pl} = \frac{c_g |Y_q|^2}{48\pi^3} \frac{(2+\beta)^2}{1+\beta} \frac{M_{\rm kk}}{\Lambda_{\rm TeV}} \tag{2.97}$$

that shifts y_* to

$$y_* \leq y_{\max} = \sqrt{96\pi^3/c_g} \frac{\sqrt{1+\beta}}{2+\beta} \sqrt{M_{\rm kk}/\Lambda_{\rm TeV}}. \tag{2.98}$$

This includes $\beta \sim 1/\eta$ that sets the Higgs profile width. For a broad Higgs with $\beta \to 0$, the value for $y_{\max}$ takes 3.9, which is also weakened by $\sqrt{M_{\rm kk}/\Lambda_{\rm TeV}}$. In the case of a narrow bulk Higgs with $\eta = 1/\beta$, Eq. (2.98) simplifies to

$$y_{\max} = \sqrt{96\pi^3/c_g} \sqrt{\eta M_{\rm kk}/\Lambda_{\rm TeV}} \approx 7.7\sqrt{\eta} \tag{2.99}$$

that can be used if $\eta > M_{\rm kk}/\Lambda_{\rm TeV} \approx 0.1$. For a smaller value of η, the bound of $y_{\max}$ corresponds to the brane Higgs [129, 130].

2.4 Fermion profile functions

A bulk fermion is a four component Dirac spinor in the 5D representation of the Lorentz group, because the bulk fermion has to fulfill the 5D Clifford algebra

$$\left\{ \Gamma_M, \Gamma_N \right\} = 2\eta_{MN}. \tag{2.100}$$

Five gamma matrices are required and the relation

$$\Gamma_M = (\gamma_\mu, i\gamma_5) \tag{2.101}$$

follows from the anticommutation relation. The choice of Γ_M makes a construction of projection operators challenging. The construction of the orbifold resolves this discrepancy *via* a projection of a different choice of BCs. As a consequence, a 5D fermion is decomposed into two Weyl representations.
Confining the fermions along the extra dimension leads to a suppression of higher–dimensional operators, because the overlap integrals of their wave function determine the size of the coupling [125, 139]. These characteristics offer an explanation for the definition of the boson profiles along the extra dimension. Otherwise, the bulk–localized gauge sector would be localization–independent. This would lead to non–diagonal gauge couplings for the KK excitations and to problems if couplings between a photon and a gluon are considered. The 5D fermion Lagrangian

$$\mathcal{L}_{\rm Ferm} = \int_\epsilon^1 \frac{{\rm d}t}{t} \sqrt{|G|} \sum_{\mathcal{Q}=\mathcal{U},\mathcal{D}} \bar{\mathcal{Q}}(x,t) \left[i\partial\!\!\!/ - M_{\rm kk}\gamma_5\partial_t - \frac{M_{\rm kk}}{t} \begin{pmatrix} c_Q & 0 \\ 0 & -c_q \end{pmatrix} \right] \mathcal{Q}(x,t) \tag{2.102}$$

includes the so–called *bulk mass parameters* $c_{Q,q}$ that indicate the position along the extra dimension. They are 3×3 diagonal matrices in generation space and a basis may be chosen in which the bulk mass parameters are diagonal. The bulk mass parameter

of the $SU(2)_L$ doublets is c_Q, while c_q is the bulk mass parameter of the singlet under $SU(2)_L$ [120]. There are also $SU(2)_L$ doublets with the left–handed and right–handed fields of the six component vectors $\mathcal{Q}(x,t) = \mathcal{Q}_L(x,t) + \mathcal{Q}_R(x,t)$ as well as the singlets $u_L(x,t)$, and $d_L(x,t)$ under $SU(2)_L$ that are four component Dirac spinors [125, 139]. Left–handed quark fields are chosen to have $\mathbb{Z}_2$–even parity whereas the right–handed quark field is described by a $\mathbb{Z}_2$–odd component and the six component vector

$$\mathcal{Q}_A(x_\mu,t) = \sqrt{\frac{2\pi r}{L\epsilon}} \begin{pmatrix} Q_A(x_\mu,t) \\ q_A(x_\mu,t) \end{pmatrix}. \tag{2.103}$$

Either the up–type quark or the down–type quark under consideration is represented by $(\mathcal{Q},Q,q) = (\mathcal{U},U,u),(\mathcal{D},D,d)$ and the subscript $A = L,R$ refers to the chirality of the profile under consideration. One asset of this compact notation is that the factors appearing in the integrals are absorbed into Eq. (2.103). Furthermore, $\mathcal{Q}_A(x_\mu,t)$ is the abbreviation of

$$\mathcal{Q}_{L,R}(x,t) = \sum_n Q^{(n)}_{L,R}(t)\, q^{(n)}_{L,R}(x). \tag{2.104}$$

The wave functions of both left–handed and right–handed components of the n^{th} KK eigenstates are $q^{(n)}_{L,R}(xu)$. With the insertion of the KK decomposition, Eq. (2.104) becomes

$$\mathcal{Q}^{(n)}_L(t) = \sqrt{\frac{2\pi}{L\epsilon}} \begin{pmatrix} C^Q_n(t)\, a^Q_n \\ S^q_n(t)\, a^q_n \end{pmatrix}, \qquad \mathcal{Q}^{(n)}_R(t) = \sqrt{\frac{2\pi}{L\epsilon}} \begin{pmatrix} S^Q_n(t)\, a^Q_n \\ C^q_n(t)\, a^q_n \end{pmatrix}. \tag{2.105}$$

Some comments on Eq. (2.105) are necessary. The even (odd) quark profile function are $C^{Q,q}$ ($S^{Q,q}$), which corresponds to NN (DD) BCs. Furthermore, both $C^{Q,q}$ and $S^{Q,q}$ are 3×3 matrices in generation space and the $SU(2)_L$ symmetry implies that the doublet quark fields have the same profile functions for both the up–type quark sector and the down–type quark sector. Another advantage lies in the fact of the freedom to choose the functions in such a way that the resulting profile functions are both real and diagonal. As a consequence, the $a^{Q,q}$–vectors in Eq. (2.105) are then imaginary. The $a^{Q,q}$–vectors contain the description of flavor mixing of the 5D interaction to the 4D eigenstates, which are generated by the Yukawa interaction on the IR brane. If there is no Yukawa interaction, *i.e.* $v \to 0$, this corresponds to the case of the absence of flavor mixing and the $a^{Q,q}$ vectors then become unit vectors [120].
The EOM of the fermion profiles are obtained in the same way as in the gauge boson case, *i.e.* matching the 5D action onto the 4D canonical term

$$S_{4D} = \sum_{q=u,d} \sum_n \int \mathrm{d}^4x \left[\bar{q}^{(n)}(x)\, i\partial\!\!\!/\, q^{(n)}(x) - m_n \bar{q}^{(n)}(x)\, q^{(n)}(x) \right] \tag{2.106}$$

after the insertion of the KK decomposition of Eq. (2.105) and Eq. (2.104) into Eq. (2.102) with the orthonormality relation

$$\begin{aligned} \frac{2\pi}{L\epsilon} \int_\epsilon^1 \mathrm{d}t \Big\{ & a^{(Q,q)\dagger}_m C^{(Q,q)}_m(t) C^{(Q,q)}_n(t) a^{(Q,q)}_n \\ & + a^{(q,Q)\dagger}_m S^{(q,Q)}_m(t) S^{(q,Q)}_n(t) a^{(q,Q)}_n \Big\} = \delta_{mn}. \end{aligned} \tag{2.107}$$

Then, the EOM read

$$\partial_t \mathcal{Q}_L^{(n)}(t) = -x_n^q \mathcal{Q}_R(t) + \mathcal{M}_q(t)\, \mathcal{Q}_L^{(n)}(t), \tag{2.108}$$

$$\partial_t \mathcal{Q}_R^{(n)}(t) = x_n^q \mathcal{Q}_L(t) - \mathcal{M}_q(t)\, \mathcal{Q}_R^{(n)}(t). \tag{2.109}$$

In Eq. (2.108), $x_n = m_{q_n}/M_{\mathrm{kk}}$ denotes the normalized bulk mass of the fermions to the KK scale and $\mathcal{M}$ is a 6×6 t–dependent mass matrix

$$\mathcal{M}_q(t) = \frac{1}{t}\begin{pmatrix} c_Q & 0 \\ 0 & -c_q \end{pmatrix} + \frac{v}{\sqrt{2}M_{\mathrm{kk}}}\delta^\eta(t-1)\begin{pmatrix} 0 & Y_q \\ Y_q^\dagger & 0 \end{pmatrix} + \mathcal{O}\left(\frac{M_{\mathrm{kk}}}{v\,|Y_q|}\right), \quad q = u, d \tag{2.110}$$

that contains the bulk mass parameters $c_{Q,q} = \pm M_{Q,q}/k$ and the regularized delta function $\delta^\eta(t-1)$. A naïve treatment of the delta function in Eq. (3.56) would lead to an ill–defined definition [151] of the upper component of Eq. (2.108),

$$\left(\partial_t + \frac{1}{t}c_Q\right) S_n^Q(t)\, a_n^Q = x_{q_n} C_n^Q(t)\, a_n^Q - \frac{v}{\sqrt{2}M_{\mathrm{kk}}}\delta^\eta(t-1)\, Y_q C_n^q(t)\, a_n^q, \tag{2.111}$$

because the right–hand side of Eq. (2.111) would lead to 0 at the IR brane, as the delta function is 0 at $t = 1$ after an integration around an infinitesimal interval of $t = 1$. As a consequence, $S_n^Q(1)$ would not be zero, but both the BC and the $\mathbb{Z}_2$–odd profile function dictate $S_n^Q(1) = 0$. Treating the Yukawa matrices as a small perturbation, the resulting solution is valid up to $\mathcal{O}\left(v^2/M_{\mathrm{kk}}^2\right)$. Solving then the free EOM leads to the BCs

$$\begin{pmatrix} 0 & 1 \end{pmatrix} \mathcal{Q}_L^{(n)}(t) = 0, \qquad \begin{pmatrix} 1 & 0 \end{pmatrix} \mathcal{Q}_R^{(n)}(t) = 0, \quad \forall t \in [\epsilon, 1]. \tag{2.112}$$

This is a standard operation, *c.f.* [120, 139, 146–149]. After a rotation into the mass basis, the Yukawa interactions are already contained and regularized. The solution of this discrepancy is a shift of the delta function into the bulk by a small amount that leads to a discontinuity of the $\mathbb{Z}_2$–odd fermion profile functions at $t = 1 - \eta$ using Eq. (2.53) [150]. In this case, a delta function is used that is assumed as a box of a width η and a height $1/\eta$, *c.f.* Eq. (2.18). In the following, solutions containing an exact dependence of the Yukawa matrices are derived, *c.f.* [120, 121, 139, 151, 152]. The infinitesimal small regulator η divides the extra dimension into two parts,*i.e.* $t \in [\epsilon, 1-\eta)$ and a part $t \in (1-\eta, 1,]$. First, the second region is investigated, as here the desired mixed BCs can be obtained. After the derivation of the modified BCs, the quark profiles can be derived and the final IR BCs can be obtained in the brane–localized Higgs scenario *via* a limiting procedure, where $\eta \to 0$. In the region $t > 1 - \eta$, the delta function is approximated as $1/\eta$ in the generalized mass matrix Eq. (3.56), and the EOM result in the second order differential equation

$$\left[\partial_t^2 - \frac{1}{\eta^2}\begin{pmatrix} X_q^2 - \eta^2 x_{q_n}^2 & 0 \\ 0 & \bar{X}_q^2 - \eta^2 x_{q_n}^2 \end{pmatrix}\right] \mathcal{Q}_A^{(n)}(t) = 0, \quad A = L, R \tag{2.113}$$

with the hermitian 3×3 matrices

$$X_q = \frac{v}{\sqrt{2}M_{\mathrm{kk}}}\sqrt{Y_q Y_q^\dagger}, \qquad \bar{X}_q = \frac{v}{\sqrt{2}M_{\mathrm{kk}}}\sqrt{Y_q^\dagger Y_q}, \tag{2.114}$$

where the square root has to be interpreted as an expansion. The general solution of Eq. (2.113) is given by

$$\mathcal{S}(t) = \sinh\left(S_q \frac{1-t}{\eta}\right), \quad \mathcal{C}(t) = \cosh\left(S_q \frac{1-t}{\eta}\right), \quad S_q \equiv \sqrt{X_q^2 - \eta^2 x_{q_n}^2} \tag{2.115}$$

as well as their corresponding conjugate expressions $\bar{\mathcal{S}}(t)$ and $\bar{\mathcal{C}}(t)$. After the application of the Neumann (Dirichlet) BCs of the $\mathbb{Z}_2$–even (odd) profile functions, the quark profiles on the IR brane result in

$$\mathcal{Q}_L^{(n)}(t) = \begin{pmatrix} \frac{\mathcal{C}(t)}{\mathcal{C}(1_\eta)} & 0 \\ 0 & \frac{\bar{\mathcal{S}}(t)}{\mathcal{S}(1_\eta)} \end{pmatrix} \mathcal{Q}_L^{(n)}(1_\eta), \quad \mathcal{Q}_R^{(n)}(t) = \begin{pmatrix} \frac{\mathcal{S}(t)}{\mathcal{S}(1_\eta)} & 0 \\ 0 & \frac{\bar{\mathcal{C}}(t)}{\mathcal{C}(1_\eta)} \end{pmatrix} \mathcal{Q}_R^{(n)}(1_\eta) \tag{2.116}$$

with $1_\eta = 1-\eta$ and the coefficients $\mathcal{Q}_{L,R}^{(n)}(1_\eta)$ that depend on the continuity conditions at $t = 1-\eta$. As $\frac{v|Y_q|}{\Lambda_{\mathrm{TeV}}} \gg \eta$ is already assumed, the KK mass is replaced by the corresponding KK fermion mass, $M_{\mathrm{kk}} \to m_{q_n}$ that allows to consider the mass terms to be negligible, which leads to $S_q \to X_q$. After the insertion of Eq. (2.116) into the first order differential equation, the modified BCs read in the limit $\eta \to 0$

$$\left(\frac{v\tilde{Y}_q^\dagger}{\sqrt{2}M_{\mathrm{kk}}} \quad 1\right) \mathcal{Q}_L^{(n)}(1^-) = 0, \qquad \left(1 \quad -\frac{v\tilde{Y}_q}{\sqrt{2}M_{\mathrm{kk}}}\right) \mathcal{Q}_R^{(n)}(1^-) = 0. \tag{2.117}$$

The limiting procedure is necessary due to the discontinuity of the $\mathbb{Z}_2$–odd profile appearing in the upper (lower) component of $\mathcal{Q}_L^{(n)}(t)\left(\mathcal{Q}_R^{(n)}(t)\right)$. In addition, Eq. (2.117) serves as a crosscheck during the derivation of the fermion propagator in the brane–localized Higgs scenario in Sec. 2.2.2. Another quantity introduced in Eq. (2.117) is the so–called *modified Yukawa matrix*

$$\tilde{Y}_q = \frac{\tanh(X_q)}{X_q} Y_q \tag{2.118}$$

that differs by factors of v^2/M_{kk}^2 compared to the original Yukawa matrix Y_q. An exact solution in the limit $\eta \to 0$ is obtained with the help of the EOM Eq. (2.108) and the modified BCs:

$$\mathcal{Q}_L^{(n)}(t) = \sqrt{2t} \begin{pmatrix} \mathcal{N}_n(c_Q) f_n^+(t, c_Q) a_n^Q \\ -\mathcal{N}_n(c_q) f_n^-(t, c_q) a_n^q \end{pmatrix}, \tag{2.119}$$

$$\mathcal{Q}_R^{(n)}(t) = \sqrt{2t} \begin{pmatrix} \mathcal{N}_n(c_Q) f_n^-(t, c_Q) a_n^Q \\ \mathcal{N}_n(c_q) f_n^+(t, c_q) a_n^q \end{pmatrix}, \tag{2.120}$$

in which the functions

$$f^\pm(t, c_{Q,q}) = J_{-\frac{1}{2}-c}(x_n\epsilon) J_{\mp\frac{1}{2}+c}(x_n t) \pm J_{\frac{1}{2}+c}(x_n\epsilon) J_{\pm\frac{1}{2}-c}(x_n t) \tag{2.121}$$

are product of Bessel functions. For non–integer values of $c_{Q,q}$ the orthonormality condition requires a normalization

$$2\int_\epsilon^1 \mathrm{d}t\, t = \frac{1}{\mathcal{N}_n^2(c_{Q,q})} \pm \frac{f_n^+(1, c_{Q,q}) f_n^-(1^-, c_{Q,q})}{x_n} \tag{2.122}$$

including the value of $\mathcal{N}^{-2}$

$$\mathcal{N}_n^{-2}\left(c_{Q,q}\right)=\left[f_n^+\left(1,c_{Q,q}\right)\right]^2\left[f_n^-\left(1,c_{Q,q}\right)\right]^2-\frac{2c_{Q,q}}{x_n}f_n^+(1,c_{Q,q})f_n^-(1,c_{Q,q})-\epsilon\left[f_n^+\left(\epsilon,c_{Q,q}\right)\right]^2. \tag{2.123}$$

Solutions for $C_n^{Q,q}\left(t\right)$ and $S_n^{Q,q}\left(t\right)$ are obtained with the help of Eq. (2.121) and Eq. (2.123), leading to

$$C_n^{Q,q}\left(t\right)=\mathcal{N}_n\left(c_{Q,q}\right)\sqrt{\frac{L\epsilon t}{\pi}}f_n^+\left(t,c_{Q,q}\right), \tag{2.124}$$

$$S_n^{Q,q}\left(t\right)=\pm\mathcal{N}_n\left(c_{Q,q}\right)\sqrt{\frac{L\epsilon t}{\pi}}f_n^-\left(t,c_{Q,q}\right). \tag{2.125}$$

Performing an expansion in the limit $x_n \ll 1$, in which the masses are assumed to be much smaller compared to the KK scale, Eq. (2.124) results in the ZMA

$$C_n^{Q,q}\left(t\right)\approx F\left(c_{Q,q}\right)t^{c_{Q,q}}\hat{a}_n^{Q,q}, \tag{2.126}$$

$$S_n^{Q,q}\left(t\right)\approx x_nF\left(c_{Q,q}\right)\frac{t^{1+c_{Q,q}}-\epsilon^{1+2c_{Q,q}}t^{-c_{Q,q}}}{1+2c_{Q,q}}\hat{a}_n^{Q,q} \tag{2.127}$$

that contains the localization *zero mode profile function*

$$F\left(c_{Q,q}\right)\equiv\sqrt{\frac{1+2c_{Q,q}}{1-\epsilon^{1+2c_{Q,q}}}}, \tag{2.128}$$

which determines the localization in the IR of the C–profile in Eq. (2.126). In the case of the S-profile in Eq. (2.127), this is the inverse function approaching from the left to 1^-. Eq. (2.128) can also be divided into two ranges by the values of the bulk mass parameters

$$F\left(c\right)=\begin{cases}-\sqrt{-1-2c}\,\epsilon^{-c-1/2}, & -3/2<c<-1/2\\ \sqrt{1+2c}, & -1/2<c<1/2\end{cases} \tag{2.129}$$

The sign of the bulk mass parameters depends on their localization and reflects at the same time the chirality of the fermions. If $c_{Q,q}<-1/2$ the fermion is UV localized, otherwise it is localized in the IR. It is remarkable that the sensitivity of the F–profiles depends exponentially on $\mathcal{O}\left(1\right)$ variations of the bulk mass parameters, which are used for the generation of large fermion hierarchies. With the insertion of Eq. (2.126) and Eq. (2.127) into Eq. (2.117), an expression for both the zeroth order masses is obtained that are the eigenvalues. The $\hat{a}_n^{Q,q}$ vectors are the eigenvectors of

$$\left(m_{q_{n,0}}\mathbf{1}-\frac{v^2}{2}Y_q^{eff}\left(Y_q^{eff}\right)^\dagger\right)\hat{a}_n^Q=0,\ \left(m_{q_{n,0}}\mathbf{1}-\frac{v^2}{2}\left(Y_q^{eff}\right)^\dagger Y_q^{eff}\right)\hat{a}_n^q=0. \tag{2.130}$$

Equation (2.130) includes the effective Yukawa matrix

$$Y_q^{eff}=F\left(c_Q\right)\tilde{Y}_qF\left(c_q\right). \tag{2.131}$$

Now it is possible to derive an analytical expression for the quark masses

$$m_{q_i}\approx\frac{v}{\sqrt{2}}\left|Y_q\right|\left|F\left(c_{Q_i}\right)\right|\left|F\left(c_{q_i}\right)\right|, \tag{2.132}$$

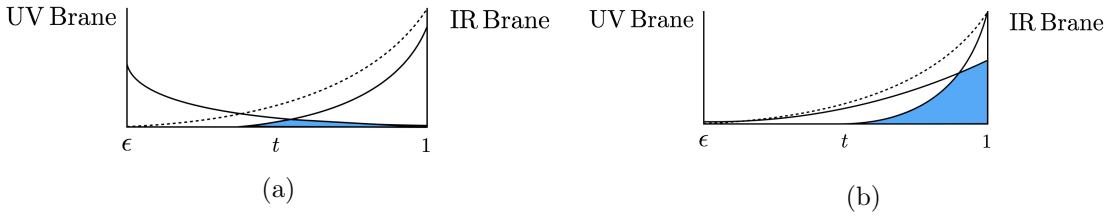

Figure 2.4: A qualitative display of the RS GIM mechanism. The dashed line represents a t^2 behavior and the solid lines display the fermion profiles along the extra dimension. Fermions that are considered to be localized towards the UV brane are assumed to be lighter and show a small overlap with the IR brane compared to fermion profile functions that are localized towards the IR brane, *c.f.* Fig. 2.4a. The colored blue area in Fig. 2.4a and Fig. 2.4b gets larger if the fermion profile functions are localized in the same region. Furthermore, the size of FCNC that results from the coupling of the overlap integrals is sketched by the blue colored area. At the same time the overlap determines the size of the 4D Yukawa coupling that generates the fermion masses. This illustration is based on [127, 129, 130].

in which the bulk mass parameter $c_{Q,q}$ determine the size of the overlap of the profile functions. The generation of realistic mass hierarchies requires the bulk mass parameters to be in the interval of $c_{Q,q} \in (-1, 1)$. The light quark masses have a profile function near the UV brane, which is indicated by the values of $c_{Q,q} < -1/2$, while the overlap profile function of the heavy fermions are localized towards the IR brane [120]. This leads to a FCNC suppression if fermions couple to gauge bosons. FCNCs are in the RS model possible at tree–level that is in contrast to the SM. If light fermions are involved, the size of the coupling will be small due to the value of the bulk mass parameter. Another benefit is that only terms with a positive exponent of t or t' is present. As a consequence, the whole tower of the massive KK modes is either localized on or near the IR brane, or is delocalized [120, 130]. This effect is referred to as the *RS–GIM mechanism* [153–155] and is depicted in Fig. 2.4. The solid lines in Fig. 2.4 display the fermion profile functions along the extra dimension qualitatively whereas the dashed line displays a t^2 behavior as an illustration. The RS GIM mechanism is discussed in more detail in Ch. 5 as this mechanism is explained in the context of a tree–level diagram with two external fermions that couple to a scalar boson. As already mentioned, mass hierarchies are generated using the bulk–mass parameters. Not only the localization of the fermions along the extra dimension is important for a suppression of contributions of higher–dimensional operators, but also their suppression that stems from the position–dependent cutoff. The latter suppression also depends on the localization of both fermions and bosons in the bulk. FCNCs can already arise at tree–level, because the couplings of KK fermions to massive (gauge) bosons are in general not diagonal. The suppression by the masses of the fermions are proportional to the zero mode profile as shown in Eq. (2.132) and are proportional to

$$\frac{m_f^2}{M_{\mathrm{kk}}^2} \approx \frac{1}{16\pi} \frac{m_f^2}{m_W^2}, \tag{2.133}$$

if M_{kk} is associated with $4\pi m_W$. This is suppression is of the same order as in the SM. Suppressions that stem from first or second fermion generations are stronger compared

to the suppressions that stem from the third fermion generation. As a consequence, the latter case can lead to sizable contributions if third generation fermions are involved in diagrams.
The absolute values of all fundamental parameters of the fermion sector in the RS model are of $\mathcal{O}(1)$, which are the Yukawa matrix Y_q on the one hand as well as the bulk–mass parameter $c_{Q,q}$ on the other hand. Small changes in the values of $c_{Q,q}$ may lead to a different localization of the fermion profiles along the extra dimension resulting in a different overlap with the IR brane. Exactly this overlap determines the size of the effective 4D Yukawa couplings that are responsible for the generation of the quark masses.

2.5 Custodial RS model

The custodial RS model bases on [124, 156, 157]. Here, the probability to detect lightest KK resonances is higher compared to the minimal RS model [87, 158–160]. In addition, the difference between the minimal RS model and the custodial RS model lies in the enlarged bulk gauge symmetry

$$SU(3)_C \times SU(2)_L \times SU(2)_R \times U(1)_X \times P_{LR} \tag{2.134}$$

that is enforced to protect both ρ parameter *via* the symmetry breaking of the $SU(2)_L \times SU(2)_R \to SU(2)_V$ at the IR brane that also generates at the same time EWSB [124]. The P_{LR} symmetry in Eq. (2.134) interchanges the $SU(2)_L$ group with the $SU(2)_R$ group, and leads to a protection of the $Z\bar{b}b$ couplings for both flavor changing counterparts [161] and too large corrections [157]. Generally speaking, the P_{LR} interchange symmetry is imposed for both a charge conjugation and a space reflection at the Lagrangian level [3]. On the UV brane, the breakdown of $SU(2)_R \times U(1)_X \to U(1)_Y$ leads to a generation of the SM gauge group *via* both the interaction of the UV brane and the IR brane, respectively. In the following section, technical details and notations are based on [121, 162].

2.5.1 Gauge sector in the custodial RS model

In the custodial RS model, the action of the gauge sector $\mathcal{S}^{(CRS)}_{gauge}$ reads

$$\mathcal{S}^{(CRS)}_{gauge} = \int_{\epsilon}^{1} \frac{\mathrm{d}t}{t} \left(\mathcal{L}_{L,R,X} + \mathcal{L}_{Higgs} + \mathcal{L}_{GF} \right), \tag{2.135}$$

in which the Higgs Lagrangian of Eq. (2.135) reads explicitly

$$\mathcal{L}_{\text{Higgs}} = \int_{\epsilon}^{1} \frac{\mathrm{d}t}{t} \sqrt{|G|} \delta^{\eta}(t-1) \left(\frac{1}{2} \text{Tr} \left[(D^{\mu}\Phi)^{\dagger} D^{\mu}\Phi \right] - V(\Phi) \right). \tag{2.136}$$

with $V(\Phi) = -\mu \Phi^{\dagger}\Phi + \Phi^{\dagger}\Phi^2$. The Higgs field is a bi–doublet $(2,2)_0$

$$\Phi(x) = \frac{1}{\epsilon\sqrt{2}} \begin{pmatrix} v + h(x) - i\phi^3(x) & -i\sqrt{2}\phi^+(x) \\ -i\sqrt{2}\phi^-(x) & v + h(x) + i\phi^3(x) \end{pmatrix}, \tag{2.137}$$

with the scalar fields $\phi^{\pm} = \left(\phi^1 \mp \phi^2\right)/\sqrt{2}$. The variable v denotes the Higgs VEV in the custodial RS model. The Higgs field acts under the representation $SU(2)_L \times SU(2)_R$ and has a neutral charge under $U(1)_X$. The proper implementation of the $SU(2)_L \times SU(2)_R \to SU(2)_V$ symmetry breaking requires the covariant derivative in Eq. (2.136) to be written as $D_\mu\Phi = \partial_\mu - ig_{L,5}L^i_\mu T^i_L\Phi + ig_{R,5}\Phi R^i_\mu T^i_R$, in which T^i denote the generators $\sigma^i/2$ and $g_{L/R,5}$ denotes the 5D gauge coupling [121]. Furthermore, it follows that $g_{L,5} = g_{R,5}$ and $c_{\theta_W} = \frac{1}{\sqrt{2}} = s_{\theta_W}$ because of the P_{LR} symmetry in Eq. (2.134).
In the gauge Lagrangian

$$\mathcal{L}_{L,R,X} = \left(-\frac{1}{4}L^a_{KM}L^a_{LN} - \frac{1}{4}R^a_{KM}R^a_{LN} - \frac{1}{4}X^a_{KM}X^a_{LN}\right), \tag{2.138}$$

the 5D gauge boson fields act under $SU(2)_{L/R}$ and $U(1)_X$. They are abbreviated with $L^i_M, R^i_M, i = 1,2,3$, and X_M. All vector components of the gauge fields are even under a $\mathbb{Z}_2$–parity. This reflects the compatibility of the current observations while the fifth component is odd under a $\mathbb{Z}_2$–parity. The kinetic term of the scalar bi–doublet is kept due to a rotation of the fields in the basis of both the fields $\tilde{A}^i_M$ and V^i_M [163]

$$\begin{pmatrix}\tilde{A}^i_M \\ V^i_M\end{pmatrix} = \begin{pmatrix}\cos(\theta_W) & -\sin(\theta_W) \\ \sin(\theta_W) & \cos(\theta_W)\end{pmatrix}\begin{pmatrix}L^i_M \\ R^i_M\end{pmatrix} \equiv \mathbf{R}_{\theta_W}\begin{pmatrix}L^i_M \\ R^i_M\end{pmatrix}. \tag{2.139}$$

The Higgs VEV in the custodial model $\langle\phi\rangle$, denoted by V, generates the mass term $M^2_{\tilde{A}_M} = \frac{g^2_{L,5}+g^2_{R,5}}{4}$ for the fields $\tilde{A}^i_M$, while the fields V^i_M remain massless. The coupling of both $\tilde{A}^i_M$ and V^i_M is read off after the shift $v^2 \to (v+h)^2$. Introducing the fields [121]

$$\begin{pmatrix}Z'_M \\ B_M\end{pmatrix} = \frac{1}{\sqrt{g^2_{R,5}+g^2_{X,5}}}\begin{pmatrix}g_{R,5} & -g_{X,5} \\ g_{X,5} & g_{R,5}\end{pmatrix}\begin{pmatrix}R^3_M \\ X_M\end{pmatrix} \tag{2.140}$$

with an appropriate choice of the BC, the breaking of the extended electroweak gauge group on the UV brane into the SM group $SU(2)_R \times U(1)_X \to U(1)_Y$ is achieved. Dirichlet BCs are chosen for the fields Z'_μ and $R^{1,3}_\mu$. The $U(1)_X$ gauge coupling in Eq. (2.140) is g_X and B_μ denotes the $U(1)_X$ gauge field in Eq. (2.140). The corresponding particles to the SM neutral particles are defined *via* [121]

$$\begin{pmatrix}Z_M \\ A_M\end{pmatrix} = \frac{1}{\sqrt{g^2_{L,5}+g^2_{Y,5}}}\begin{pmatrix}g_{L,5} & -g_{Y,5} \\ g_{Y,5} & g_{L,5}\end{pmatrix}\begin{pmatrix}L^3_M \\ Y_M\end{pmatrix}, \qquad g_{Y,5} \equiv \frac{g_{X,5}g_{R,5}}{\sqrt{g^2_{R,5}+g^2_{X,5}}}. \tag{2.141}$$

The electroweak mixing angle is defined as $s_{\theta_W} = g_{Y,5}/(g^2_{L,5}+g^2_{Y,5})^{1/2}$ and the 5D electromagnetic gauge coupling is defined as $e_5 = g_{L,5}s_{\theta_W}$ in the same way as in the minimal RS model if the replacements $g_{L,5} \to g_5$ and $g_Y \to g'_5$ are performed. In the custodial RS model, there exist two bases. One is the so-called *UV basis* in which the fields $L/R^{\mp}_\mu = L/R^1_\mu \mp L/R^2_\mu, A_M, Z_M$ and Z'_M are defined. Except for Z'_M and $R^{\mp}_M$ the vector component of them obeys Neumann BCs at the UV brane, whereas all other fields obey Dirichlet BCs. The vector components of the photon obeys Neumann BCs, whereas its scalar component obeys Dirichlet BCs. The BCs for all other fields are in general more challenging to derive. A solution to this challenge offers the so–called IR basis, where

the fields $\tilde{Z}_M$ and Z_M^H are related to those in the UV basis (Z_M and Z'_M) *via*

$$\begin{pmatrix} \tilde{Z}_M \\ Z_M^H \end{pmatrix} = \begin{pmatrix} \cos(\theta_Z) & -\sin(\theta_Z) \\ \sin(\theta_Z) & \cos(\theta_Z) \end{pmatrix} \begin{pmatrix} Z_M \\ Z'_M \end{pmatrix} \equiv \mathbf{R}_{\theta_Z} \begin{pmatrix} Z_M \\ Z'_M \end{pmatrix} \tag{2.142}$$

with a rotation matrix $\mathbf{R}_{\theta_Z}^T$ and *via* the mixing angle $\sin(\theta_Z) = g_{R,5}^2/((g_{R,5}^2+g_{L,5}^2)(g_{R,5}^2+g_{X,5}^2))^{1/2}$ [121]. Now, the choice of either the UV basis or the IR basis is possible *via* the rotation matrices $\mathbf{R}_{\theta_{W/Z}}$. With these rotation matrices, the vector bosons $\vec{W}^\pm$ and $\vec{Z}_M$

$$\vec{W}^\pm \equiv \begin{pmatrix} \tilde{A}_M^\pm \\ V_M^\pm \end{pmatrix} = \mathbf{R}_{\theta_W} \begin{pmatrix} L_M^\pm \\ R_M^\pm \end{pmatrix}, \qquad \vec{Z}_M \equiv \begin{pmatrix} \tilde{Z}_M \\ Z_M^H \end{pmatrix} = \mathbf{R}_{\theta_Z} \begin{pmatrix} Z_M \\ Z'_M \end{pmatrix} \tag{2.143}$$

read in the KK decomposition

$$\vec{B}_\mu(x,t) = \frac{\mathbf{R}_{\theta_B}}{\sqrt{r}} \sum_{n=0}^{\infty} \vec{\chi}_n^B(t)\, B_\mu^{(n)}(x), \tag{2.144}$$

$$\vec{B}_5(x,t) = \frac{\mathbf{R}_{\theta_B}}{\sqrt{r}} \sum_{n=0}^{\infty} \frac{-kt}{m_{B_n}} \varphi_B^{(n)}(x)\, \partial_t \vec{\chi}_n^B(t)\, B_\mu^{(n)}(x), \tag{2.145}$$

$$B = W^\pm, Z \tag{2.146}$$

including the $\mathbb{Z}_2$–even profile function

$$\vec{\chi}_n^B(t) = \begin{pmatrix} \vec{\chi}_n^{B,+}(t) & 0 \\ 0 & \vec{\chi}_n^{B,-}(t) \end{pmatrix}. \tag{2.147}$$

The upper (lower) component of Eq. (2.147) is the so–called *untwisted* (*twisted*) profile function. Light zero modes result from the application of Neumann BCs in the UV on untwisted even profile functions, whereas the twisted even profile functions are not smooth on the orbifold fixed point and obey Dirichlet BCs. The KK decompositions for both the photon and the gluon are the same as in the minimal RS model [121]. Expanded in the mass eigenbasis, the KK decomposition of the four NGBs and their corresponding mass terms are

$$\varphi_B(x) = \sum_n \frac{\tilde{m}_B}{m_{B_n}} \sqrt{2\pi} \mathbf{P}_+ \mathbf{R}_{\theta_B}^T \vec{\chi}_n^B(1)\, \varphi_B^{(n)}(x), \tag{2.148}$$

$$\tilde{m}_W = \frac{g_{L,5}}{\sqrt{2\pi r}} \frac{v}{2}, \qquad \tilde{m}_Z = \sqrt{\frac{g_{L,5}^2 + g_{Y,5}^2}{2\pi r}} \frac{v}{2}. \tag{2.149}$$

This is done in analogy to Eq. (2.30). The matrix $\mathbf{P}_+$ in Eq. (2.148) denotes the projection operator of the upper component. The masses in Eq. (2.149) denote an expansion in v^2/M_{kk}^2 of both the W and Z boson mass as in the minimal RS model. With the insertion of Eq. (2.144)–Eq. (2.149) into the action, Eq. (2.135), the differential equation is $\left(t\partial_t t^{-1}\partial_t + x_{B_n}^2\right)\vec{\chi}_n^B(t) = 0$ [121] which will be discussed in further detail in Sec. 3.1, because this differential equation is needed for the derivation of the gauge boson propagator and leads to the IR BCs

$$\left(\mathbf{P}_+\partial_t + \mathbf{P}_-\right)\vec{\chi}_n^B(t)\Big|_{t=\epsilon^+} = 0, \qquad \left(1 + \frac{L\tilde{m}_W^2}{c_{\theta_W}^2 M_{\text{kk}}^2}\mathbf{P}_+\right)\mathbf{R}_{\theta_B}\partial_t\vec{\chi}_n^B(t)\Big|_{t=1^-} = 0. \tag{2.150}$$

With the application of the IR BCs and with the masses defined in Eq. (2.149), the expressions for both W and Z boson masses are obtained in a leading order expansion v^2/M_{kk}^2 to

$$m_W^2 = \tilde{m}_W^2 \left[1 - \frac{\tilde{m}_W^2}{2M_{\mathrm{kk}}^2}\left(\frac{L}{c_{\theta_W}^2} - 1 + \frac{1}{2L}\right) + \mathcal{O}\left(v^4/M_{\mathrm{kk}}^4\right)\right], \tag{2.151}$$

$$m_Z^2 = \tilde{m}_Z^2 \left[1 - \frac{\tilde{m}_W^2}{2M_{\mathrm{kk}}^2}\left(\frac{L}{c_{\theta_W}^2} - 1 + \frac{1}{2L}\right) + \frac{\tilde{m}_Z^2}{2M_{\mathrm{kk}}^2}\left(1 - \frac{1}{2L}\right) + \mathcal{O}\left(v^4/M_{\mathrm{kk}}^4\right)\right], \tag{2.152}$$

in which the term containing the leading order correction in Eq. (2.152) stems from the enlarged P_{LR} gauge symmetry and is proportional to the W boson mass. The zero mode profiles read expanded to the same order [121]

$$\vec{\chi}_0^W(t) = \frac{1}{\sqrt{2\pi}} \begin{pmatrix} 1 - \frac{m_W^2}{2M_{\mathrm{kk}}^2}\left[t^2\left(L - \frac{1}{2} + \ln t\right) - \frac{1}{2} + \frac{1}{2L}\right] \\ \frac{\sin(\theta_W)}{\cos(\theta_W)} \frac{Lm_W^2}{2M_{\mathrm{kk}}^2} t^2 \end{pmatrix}, \tag{2.153}$$

$$\vec{\chi}_0^Z(t) = \frac{1}{\sqrt{2\pi}} \begin{pmatrix} 1 - \frac{m_Z^2}{2M_{\mathrm{kk}}^2}\left[t^2\left(L - \frac{1}{2} + \ln t\right) - \frac{1}{2} + \frac{1}{2L}\right] \\ \frac{\sin(\theta_Z)\cos(\theta_Z)}{\cos^2(\theta_W)} \frac{Lm_W^2}{2M_{\mathrm{kk}}^2} t^2 \end{pmatrix}, \tag{2.154}$$

in which the upper component of the profile functions in Eq. (2.153) reflect the untwisted component, while the lower twisted component is suppressed by a factor of v^2/M_{kk}^2.

2.5.2 Fermion sector in the custodial RS model

Due to the enlarged bulk gauge symmetry singlets, the quark representation in the custodial RS model contains bi–doublets and triplets under the $SU(2)$ groups. It is possible to embed the quark representation into $SO(5)$ multiplets. This appears in gauge Higgs unification models [87, 160, 164], which is convenient. The P_{LR} symmetry is introduced for the avoidance of both large corrections to the coupling of the $Z\bar{b}b$ vertex [157] and for the prevention of large flavor changing counterparts [161]. Starting with this, it is deduced that the left–handed bottom quark has to be embedded into the $SU(2)_L \times SU(2)_R$ group with its isospin quantum number $T^3 = -T_R^3 = -\frac{1}{2}$. With this choice, all other quantum numbers of the remaining fields are fixed. As a consequence, the right–handed quarks have to be embedded into a $SU(2)_R$ triplet that results into a $U(1)_X$ invariant Yukawa interaction. Quark fields with an even $\mathbb{Z}_2$ parity are defined as

$$Q_L = \begin{pmatrix} u_{L,\frac{2}{3}}^{(+)} & \lambda_{L,\frac{5}{3}}^{(-)} \\ d_{L,-\frac{1}{3}}^{(+)} & u_{R,\frac{2}{3}}^{\prime(+)} \end{pmatrix}_{\frac{2}{3}}, \quad u^{c(+)} = \left(u_{R,\frac{2}{3}}^{c(+)}\right)_{\frac{2}{3}}, \tag{2.155}$$

and

$$\mathcal{T}_R = \mathcal{T}_{1R} \otimes \mathcal{T}_{2R} = \begin{pmatrix} \Lambda_{R,\frac{5}{3}}^{\prime(-)} \\ U_{R,\frac{2}{3}}^{\prime(-)} \\ D_{R,-\frac{1}{3}}^{\prime(-)} \end{pmatrix}_{\frac{2}{3}} \otimes \left(D_{R,-\frac{1}{3}}^{\prime(+)} \quad U_{R,\frac{2}{3}}^{(-)} \quad \Lambda_{R,\frac{5}{3}}^{(-)}\right)_{\frac{2}{3}}, \tag{2.156}$$

in which Q_L acts as a bi–doublet under $SU(2)_L \times SU(2)_R$ and $\mathcal{T}_R$ transforms as a $(3,1) \otimes (1,3)$ representation. The fields with odd–parity represent the fields with opposite handedness. The profile functions of the $\mathbb{Z}_2$–even fields to the $\mathbb{Z}_2$–odd fields are connected *via* the field equations. In Eq. (2.155)–Eq. (2.156), both inner and outer subscripts denote the charge under $U(1)_{\mathrm{EM}}$ and under $U(1)_Y$, connected *via* $Y = -T_R^3 + Q_X$ and $Q = T_L^3 + Y$. The superscripts "(+)" and "(−)" specify the type of BC at the UV brane. The superscript "(+)" refers to mixed BCs. This results into light zero modes that can be identified with SM quarks and denote an application of Dirichlet BC on the $\mathbb{Z}_2$–odd profiles. In contrast to the generation of light zero modes, profile functions with the superscript "(−)" refer to the new heavy, exotic fermion states that do not have a SM counterpart. This is achieved *via* the application of Dirichlet BC on the $\mathbb{Z}_2$–even profiles. The other UV BC are of the mixed type.
The requirement that the quark mixing in the full anarchic flavor approach in a warped extra dimensions has to be embedded consistently into the theory and leads to the same $SU(2)_L \times SU(2)_R$ representation for all quark generations available in this model, playing at the same time a vital role in the suppression of flavor changing left–handed couplings to the Z boson [121, 161]. In total, there are 15 different quark states in the up–type quark sector as well as 9 different quark states in the down–type quark sector. In each sector, the application of the BCs lead to 3 light states that are identified as the SM quarks, which are accompanied by a tower of 15 + 9 additional KK modes. The new heavy exotic fermion states contribute with a tower of 9 KK excitations per KK level and with an electric charge of 5/3. Following again the notation of [121], the fields are collected in vectors with the same electric charge, *i.e.* 2/3,-1/3 and 5/3,

$$\vec{U} = \begin{pmatrix} u \\ u' \end{pmatrix}, \ \vec{u} = \begin{pmatrix} u^c \\ U' \\ U \end{pmatrix}, \ \vec{D} = d, \ \vec{d} = \begin{pmatrix} D \\ D' \end{pmatrix}, \ \vec{\Lambda} = \vec{\lambda}, \ \vec{\lambda} = \begin{pmatrix} \Lambda' \\ \Lambda \end{pmatrix}. \tag{2.157}$$

The fields are collected to their corresponding chirality, *i.e.* $\left(\vec{U}_A, \vec{u}_A, \right)^T$, $\left(\vec{D}_A, \vec{d}_A, \right)^T$ and $\left(\vec{\Lambda}_A, \vec{\lambda}_A, \right)^T$ into both 15 + 9 component vectors, which then result in the form $\mathcal{Q} = \mathcal{U}, \mathcal{D}, \Lambda$ and lead to a slightly modified fermion action

$$\mathcal{L}_{\mathrm{Ferm}} = \int_{\epsilon}^{1} \frac{\mathrm{d}t}{t} \sqrt{|G|} \sum_{\mathcal{Q}=\mathcal{U},\mathcal{D},\Lambda} \bar{\mathcal{Q}}(x,t) \left[i\partial\!\!\!/ - M_{\mathrm{kk}} \gamma_5 \partial_t - \frac{M_{\mathrm{kk}}}{t} \begin{pmatrix} c_{\vec{Q}} & 0 \\ 0 & -c_{\vec{q}} \end{pmatrix} \right] \mathcal{Q}(x,t) \tag{2.158}$$

compared to the one in the minimal RS model in Eq. (2.102). Furthermore, Eq. (2.158) contains the bulk mass parameters

$$c_{\vec{U}} = \mathrm{diag}\left(c_Q, c_Q\right), \qquad c_{\vec{D}} = -c_Q, \qquad c_{\vec{\Lambda}} = c_Q, \tag{2.159}$$

$$c_{\vec{u}} = \mathrm{diag}\left(c_{u^c}, c_{\tau_1}, c_{\tau_2}\right), \quad c_{\vec{d}} = \mathrm{diag}\left(c_{\tau_2}, c_{\tau_1}\right), \quad c_{\vec{\lambda}} = \mathrm{diag}\left(c_{\tau_1}, c_{\tau_2}\right), \tag{2.160}$$

which are now 3×3 diagonal matrices in generation space. As it is visible in Eq. (2.159)–Eq. (2.160), the bulk mass parameters of the fields $\vec{U}, \vec{D}$ and $\vec{\Lambda}$ consist of the bulk mass matrix c_Q already present in the minimal RS model. In contrast to this, the bulk mass matrices for $\vec{u}, \vec{d}$ and $\vec{\lambda}$ consist of three mass matrices c_{u^c}, c_{τ_1} and c_{τ_2}. Two mass matrices appear already in the minimal RS model, *i.e.* $c_u \equiv c_{u^c}$ and $c_d \equiv c_{\tau_2}$, reducing

the parameter space to only one new mass matrix c_{τ_1}. The new bulk mass matrix c_{τ_1} is connected to the P_{LR} symmetry and mixes with the left–handed zero modes. This requires the action to be invariant under an exchange of D' and D. The P_{LR} symmetry is enlarged to the quark sector and one of its assets is $c_{\tau_1} = c_{\tau_2}$. This reduces again the parameter space of the bulk mass matrices and leads to an equivalent parameter space as in the minimal RS model [121]. In the custodial model, the Yukawa Lagrangian without the consideration of NGBs of Eq. (2.137) reads

$$\mathcal{L}_{\text{Yuk}} = -\sum_{\vec{q}=\vec{u},\vec{d},\vec{\lambda}} \int_{\epsilon}^{1} \mathrm{dt}\, \delta^{\eta}(t-1)\, \frac{v+h(x)}{\sqrt{2}} \bar{\mathcal{Q}}_L(x,t) \begin{pmatrix} 0 & Y_{\vec{q}} \\ Y_{\vec{q}}^{\dagger} & 0 \end{pmatrix} \mathcal{Q}_R(x,t) + \text{h.c.} \tag{2.161}$$

with the same Yukawa matrices Y_q as in the minimal RS model, as they are connected *via*

$$Y_{\vec{u}} = \begin{pmatrix} Y_u & \frac{1}{\sqrt{2}} Y_d & \frac{1}{\sqrt{2}} Y_d \\ Y_u & -\frac{1}{\sqrt{2}} Y_d & -\frac{1}{\sqrt{2}} Y_d \end{pmatrix}, \qquad Y_{\vec{d}} = \begin{pmatrix} Y_d & Y_d \end{pmatrix} = Y_{\vec{\lambda}}. \tag{2.162}$$

After the introduction of the extended symmetry, the custodial RS model contains the same parameters as in the minimal RS model, although the custodial RS model has a richer structure compared to the minimal RS model. With the application of the same KK decomposition as in the minimal RS model, the fermion profile functions $\mathcal{Q}_{L,R}^{(n)}(x,t)$ with $(\mathcal{Q},Q,q) = (\mathcal{U},U,u),(\mathcal{D},D,d)$ now become

$$\mathcal{Q}_L^{(n)}(t) = \sqrt{\frac{2\pi}{L\epsilon}} \begin{pmatrix} C_n^Q(t)\, \vec{a}_n^Q \\ S_n^q(t)\, \vec{a}_n^q \end{pmatrix}, \qquad \mathcal{Q}_R^{(n)}(t) = \sqrt{\frac{2\pi}{L\epsilon}} \begin{pmatrix} S_n^Q(t)\, \vec{a}_n^Q \\ C_n^q(t)\, \vec{a}_n^q \end{pmatrix}. \tag{2.163}$$

Here, the first three excitations denote the SM quarks, whereas the other modes, especially the modes $n = 4, ..., 18$ denote the new quark modes of the first level. In the case of the λ-type quarks, there would be only 9. Furthermore, $C_n^A(t)$ and $S_n^A(t)$ are defined as in Eq. (2.124) and the a_n^A vectors are defined in an analogous way as in the minimal RS model, *c.f.* [121].

2.6 Electroweak precision observables

The Peskin–Takeuchi parameters S,T and U [52, 53] measure deviations to the SM *via* quantifying new physics. They are zero in the SM. New physics contributes to the electroweak gauge boson propagators.
One possibility to define S,T, and U is in terms of the Fermi constant G_F, the Z boson mass m_Z, the sine of the weak mixing angle $\sin(\theta_W)$, and α. In the following, the parametrization *via* the self energy functions of the gauge boson propagators derived in Ch. 3 is applied.
The self–energy of a vector boson (VV) $\Sigma_{VV}\left(p^2\right)$ is the sum of all 1–particle–irreducible diagrams.
In general, the Ward identities read [165]

$$p_\mu p_\nu \Delta_W^{\mu\nu}(p) - 2m_W p_\mu \Delta_{W\varphi_W}^{\mu\nu} + m_W^2 \Delta_{\varphi_W}^{\mu\nu} = -i, \tag{2.164}$$

$$p_\mu p_\nu \Delta_Z^{\mu\nu}(p) - 2m_Z p_\mu \Delta_{Z\varphi_Z}^{\mu\nu} + m_Z^2 \Delta_{\varphi_Z}^{\mu\nu} = -i, \tag{2.165}$$

$$p_\mu p_\nu \Delta_\gamma^{\mu\nu}(p) = -i, \tag{2.166}$$

$$p_\mu p_\nu \Delta_{Z\gamma}^{\mu\nu}(p) + i m_Z p_\mu \Delta_{Z\gamma}^{\mu\nu} = 0, \tag{2.167}$$

but we will restrict us to the unitary gauge, in which the contribution of the Goldstone bosons vanishes. Then, the second and third term of Eq. (2.164) and Eq. (2.165) vanish. The propagator $\Delta_{\alpha\beta}^{\mu\nu}\left(p^2\right)$ is then decomposed into is transverse (T) components and in its longitudinal (L) components

$$\Delta_{\alpha\beta}^{\mu\nu}\left(p^2\right) = \left(-g^{\mu\nu} + \frac{p^\mu p^\nu}{p^2}\right)\Delta_{\alpha\beta,T}\left(p^2\right) - \frac{p^\mu p^\nu}{p^2}\Delta_{\alpha\beta,L}\left(p^2\right) \tag{2.168}$$

$$\Delta_{\alpha\beta}^{\mu}(p) = ip^\mu \Delta_{\alpha\beta}\left(p^2\right) = \frac{ip^\mu}{p^2 - m_\alpha^2}\Sigma_{\alpha\beta}\left(p^2\right)\frac{i}{p^2 - m_\beta^2} \tag{2.169}$$

$$\Delta(p) = \frac{i}{p^2 - m^2 + \Sigma\left(p^2\right)}, \tag{2.170}$$

$$\Delta_{\alpha\beta,T,L}(p) = \frac{i}{p^2 - m_\alpha^2}\Sigma_{\alpha\beta,T,L}\left(p^2\right)\frac{i}{p^2 - m_\beta^2}. \tag{2.171}$$

Then, the self–energy reads

$$\Sigma^{\mu\nu}\left(p^2\right) = \left(p^2 g^{\mu\nu} - p^\mu p^\nu\right)\Sigma\left(p^2\right), \tag{2.172}$$

and the vacuum polarization functions result in [2]

$$\Pi_{VV}\left(p^2\right) = \frac{\Sigma_{VV}\left(p^2\right)}{p^2 - m_{VV}^2}. \tag{2.173}$$

S,T, and U read in the definition of the vacuum polarization functions [52, 53]

$$\alpha S = 4e^2\left[\Pi'_{ZZ}(0) - \Pi'_{Z\gamma}(0)\right], \tag{2.174}$$

$$\alpha T = \frac{e^2}{s_{\theta_W}^2 c_{\theta_W}^2 m_Z^2}\left[\Pi_{WW}(0) - \Pi_{ZZ}(0)\right], \tag{2.175}$$

$$\alpha U = 4e^2\left[\Pi'_{WW}(0) - \Pi'_{ZZ}(0)\right], \tag{2.176}$$

with [52, 53]

$$\Sigma_{WW}\left(p^2\right) = \frac{e^2}{s_{\theta_W}^2}\Pi_{WW}\left(p^2\right), \tag{2.177}$$

$$\Sigma_{ZZ}\left(p^2\right) = \frac{e^2}{c_{\theta_W}^2 s_{\theta_W}^2}\left(\Pi_{ZZ}\left(p^2\right) - 2s_{\theta_W}^2\Pi_{Z\gamma}\left(p^2\right) + s_{\theta_W}^4\Pi_{\gamma\gamma}\left(p^2\right)\right), \tag{2.178}$$

$$\Pi_{XY}\left(p^2\right) \approx \Pi_{XY}(0) + p^2\Pi'_{XY}(0), \tag{2.179}$$

with $XY = WW, ZZ, Z\gamma, \gamma\gamma$. In the case of $XY = Z\gamma, \gamma\gamma$, the vacuum polarization function at zero momentum transfer $\Pi_{XY}(0)$ vanishes in Eq. (2.179) due to the Ward identities.
The current values for S,T, and U are

$$\mathrm{S_{exp.}} = 0.07 \pm 0.08,\ \mathrm{T_{exp.}} = 0.10 \pm 0.08,\ \mathrm{U_{exp.}} = 0. \tag{2.180}$$

The experimental values of the PDG [6] differ by a small amount to the values obtained by the analysis of the authors of [166].
In the case of the RS model, the assumption that the new physics scale is much larger than the gauge boson masses is justified, because the LHC did not yet find any heavy new particles so far. As a consequence, a possible shift in the S,T, and U parameters is a result from contributions that stem from particles in the RS model. Furthermore, corrections to gauge bosons stemming from fermions are chiral suppressed. The derivation starts with the definition of the self–energy function in Eq. (3.28). The self–energy function is shown in terms of the W boson, but it is the same in the case of the Z boson, except for the change $\tilde{m}_W^2 \to \tilde{m}_Z^2$ in b_1 in Eq. (3.19) and of course, in the expansion for the propagator in Eq. (3.27). Following [53], the self energy functions are defined in the RS model as

$$\Sigma_{WW}^{\mathrm{RS}}\left(p^2\right) \approx \tilde{m}_W^2 \frac{4}{v^2} \Pi_{WW}\left(p^2\right), \tag{2.181}$$

$$\Sigma_{ZZ}^{\mathrm{RS}}\left(p^2\right) \approx \tilde{m}_Z^2 \frac{4}{v^2} \left(\Pi_{ZZ}\left(p^2\right) - 2 s_{\theta_W}^2 \Pi_{Z\gamma}\left(p^2\right)\right) \tag{2.182}$$

with Π_{XY}, $XY = WW, ZZ, Z\gamma, \gamma\gamma$ defined in Eq. (2.179). The polarization functions read in the minimal RS model

$$\Pi_{WW}(0) = \frac{\tilde{m}_W^2 L}{2 M_{\mathrm{kk}}^2}, \tag{2.183}$$

$$\Pi_{ZZ}(0) = \frac{\tilde{m}_Z^2 L}{2 M_{\mathrm{kk}}^2}, \tag{2.184}$$

$$\Pi'_{WW}(0) = -\frac{1}{2 M_{\mathrm{kk}}^2}, \tag{2.185}$$

$$\Pi'_{ZZ}(0) = -\frac{1}{2 M_{\mathrm{kk}}^2}, \tag{2.186}$$

$$\Pi'_{Z\gamma} = \frac{1}{2 L M_{\mathrm{kk}}^2}. \tag{2.187}$$

With equations Eq. (2.183)–Eq. (2.187), the electroweak precision parameters are derived in the minimal RS model by an insertion into Eq. (2.174)–Eq. (2.176) and using $4\pi\alpha = e^2$. They read in Eq. (2.192) S and $\mathrm{T}_{\mathrm{min}}$. In the custodial RS model, the vacuum polarization functions read

$$\Pi_{WW}(0) = \frac{\tilde{m}_W^2 L}{2 M_{\mathrm{kk}}^2 c_{\theta_W}^2}, \tag{2.188}$$

$$\Pi_{ZZ}(0) = \frac{\tilde{m}_W^2 L}{2 M_{\mathrm{kk}}^2 c_{\theta_W}^2} - \frac{\tilde{m}_Z^2 L}{2 M_{\mathrm{kk}}^2}\left(1 - \frac{1}{2L}\right), \tag{2.189}$$

$$\Pi'_{WW/ZZ}(0) = -\frac{1}{2 M_{\mathrm{kk}}^2}, \tag{2.190}$$

$$\Pi'_{Z\gamma}(0) = \frac{1}{2 L M_{\mathrm{kk}}^2}. \tag{2.191}$$

The S and T parameter are obtained in the custodial RS model by an insertion of Eq. (2.188)–Eq. (2.191) into Eq. (2.174)–Eq. (2.176) and using $4\pi\alpha = e^2$. The expression

for the S parameter remains unchanged in both models. The resulting expressions for the S,T, and U parameters in the minimal and custodial RS model are then given by

$$\mathrm{S} = \frac{2\pi v^2}{M_{\mathrm{kk}}^2}\left(1 - \frac{1}{L}\right), \quad \mathrm{U} = 0, \tag{2.192}$$

$$\mathrm{T}_{\mathrm{min.}} = \frac{\pi v^2 L}{2c_{\theta_W}^2 M_{\mathrm{kk}}^2}, \quad \mathrm{T}_{\mathrm{cust.}} = -\frac{\pi v^2}{2c_{\theta_W}^2 M_{\mathrm{kk}}^2}\left(L - \frac{1}{2L}\right). \tag{2.193}$$

The expression for T differs in the custodial RS model compared to the minimal RS model due to the enlarged gauge symmetry. There is a large contribution to the S parameter visible in Eq. (2.192) if the fermions are localized in the UV as in holographic Higgs–less models [167], while the opposite is true if the fermions are localized in the IR yielding a large negative contribution [168]. So the S parameter is sensitive to the fermion localization [169]. A fact that is not visible in Eq. (2.192) as there have been only universal corrections taken into account.
The T parameter shows an enhancement by the volume factor L in the minimal model and is therefore larger compared to the naïve dimensional analysis. In the custodial model the T parameter is protected by the global $SU(2)_L \times SU(2)_R$ symmetry in contrast to the minimal model. The $SU(2)_R$ symmetry is absent in the minimal RS model as there is only the SM gauge group in the bulk. Thus, the T parameter is enhanced. An other way to lower the values of T is the consideration of a minimal RS model with a small volume L. Those models are referred to as *little RS models* based on little Higgs models [170]. The challenge in these models is that the hierarchy problem is shifted to an intermediate scale $\Lambda_{\mathrm{UV}} = e^L\,\mathrm{TeV}$ that would lower the scale for the UV completion, as well. Furthermore, the lowering of the scale of the UV completion also affects CP violation and especially ϵ_K [171].
In the bulk–localized Higgs model, the self–energy function for the vector bosons VV, $\Sigma_{VV,\mathrm{bulk}}\left(p^2\right)$, is derived in the same way as in the brane–localized Higgs scenario and turns into

$$\Sigma_{VV,\mathrm{bulk}}\left(p^2\right) = \frac{\tilde{m}_W^4}{2M_{\mathrm{kk}}^2} - \left[L\frac{2(1+\beta)^2}{(2+\beta)(3+2\beta)} - \frac{(1+\beta)(3+\beta)}{(2+\beta)^2}\frac{p^2}{\tilde{m}_W^2} + \frac{1}{2L}\frac{p^4}{\tilde{m}_W^4}\right]. \tag{2.194}$$

Proceeding analogously to the brane–localized case, the electroweak S,T, and U parameters become in the bulk–localized Higgs scenario

$$\mathrm{S} = \frac{2\pi v^2}{M_{\mathrm{kk}}^2}\left(1 - \frac{1}{(2+\beta)^2} - \frac{1}{2L}\right), \quad \mathrm{U} = 0, \tag{2.195}$$

$$\mathrm{T} = \frac{\pi v^2}{2c_{\theta_W}^2 M_{\mathrm{kk}}^2}\frac{2L(1+\beta)^2}{(2+\beta)(3+2\beta)}. \tag{2.196}$$

This result coincides with the findings of [140, 172]. In the limit $\beta \to \infty$ the expressions for the electroweak parameters in Eq. (2.192) for the brane–localized Higgs scenario are recovered. The results for S and T are plotted in both custodial RS model and in the minimal RS model in the ST plane in Fig. 2.5. The blue ellipses show the values for the SM electroweak parameter obtained by an analysis published in [6]. In the minimal RS model, the T parameter for the brane–localized Higgs scenario (dark blue) and the

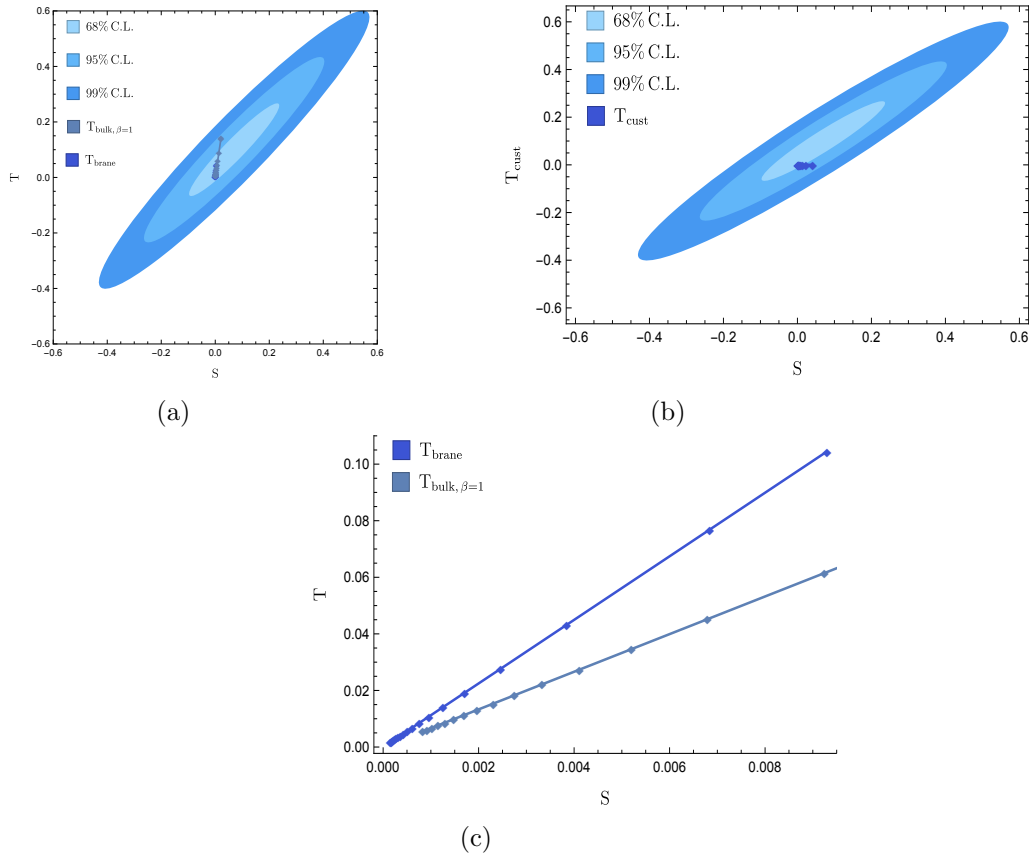

Figure 2.5: The T and S parameters of both brane–localized Higgs scenario and bulk–localized Higgs scenario with $\beta = 1$ in the minimal RS model in the S,T plane of the SM values are shown in Fig. 2.5a. The dark blue (lavender blue) line connects values for the T parameter in the brane–localized (bulk–localized) Higgs scenario for different KK masses for a better visualization. The specific values for the T parameter in the RS model are displayed as diamonds. The blue ellipses in Fig. 2.5a and Fig. 2.5b correspond to 99%, 95%, and 68% CL. The values for the S and T parameters of the SM have been obtained by electroweak precision tests [6]. For values lager than $M_{\text{kk}} \geq 3$ TeV, the S and T parameters in the brane–localized Higgs scenario are in agreement with the current data. In the minimal model with a bulk–localized Higgs scenario and $\beta = 1$, values for S and T parameters with $M_{\text{kk}} \geq 5$ TeV are in agreement with the current data. Then, Fig. 2.5c shows a comparison of the values for different M_{kk}^2 and their model–dependent behavior. In Fig. 2.5b the behavior of the T parameter in the custodial RS model is shown with a brane–localized Higgs.

bulk–localized Higgs scenario (lavender blue) with $\beta = 1$ are included in Fig. 2.5a. The values for the S and T parameters in the brane–localized Higgs scenario are for values of $M_{\text{kk}} \geq 3$ TeV in agreement with the current data, while the S and T parameters in the bulk–localized Higgs scenario are in agreement with the current data for values of $M_{\text{kk}} \geq 5$ TeV. A comparison of both scenarios gets clearer by showing a smaller

region in Fig. 2.5a, in which the results of the T parameter in the different model setups is plotted against the belonging S parameter. In this picture it is visible that the T parameter is closer to zero in the bulk–localized Higgs scenario (lavender blue) than in the brane–localized Higgs scenario (dark blue).

2.7 RS Parameter space and experimental survey

The RS model has more fundamental parameters compared to the 19 input parameters in the SM that consists of 9 moduli, 6 quark masses, 3 mixing angles of the CKM matrix and a CP violating phase. The number of parameters in both the minimal RS model and the custodial RS model are the same. In particular, the RS model contains the bulk mass parameters $c_{Q,q}$ (3×3 hermitian matrices), 27 additional parameters as well as 18 moduli and 9 complex phases in the custodial model with the additional P_{LR} symmetry. Furthermore, 36 parameters enter in the electroweak sector *via* Y_u and Y_d. In the quark sector of the RS model, the global symmetry $U(3)_Q \times U(3)_u \times U(3)_d$ shows 27 parameters and is broken by $U(1)_B$. In total, there remain 27 parameters and 10 phases [153].
Experimental values for the quark masses and the Wolfenstein parameter [6] fix 10 parameters of the RS model. Other parameters could be fixed *via* experimental searches. The RS model postulates heavy resonances of the SM particles and particles, which are not present in the SM. Their masses lie in the TeV range. As a consequence, there is a chance for their detection. A possible pure RS particle is outside of the reach of the LHC due to its mass. Bounds on the mass of the KK gluon $M_{g^{(1)}}$ and the KK graviton $h^{(1)}_{\mu\nu}$ are derived, *e.g.* from the invariant mass spectrum from the $t\bar{t}$ production. The current values at $\sqrt{s} = 8\,\text{TeV}$ are

$$M_{g^{(1)}}\Big|_{\text{ATLAS}} \geq 2.2\,\text{TeV}\,[174], \qquad M_{g^{(1)}}\Big|_{\text{CMS}} \geq 2.8\,\text{TeV}\,[175,\ 176] \tag{2.197}$$

$$M_{g^{(1)}}\Big|_{\text{PDG}} \geq 2.5\,\text{TeV}\,[6] \tag{2.198}$$

at 95% CL with an integrated luminosity of $20.3\,\text{fb}^{-1}$ (ATLAS) [174] and $19.7\,\text{fb}^{-1}$ (CMS) [175]. The advantage of a choice of a KK gluon is that the gluon profile function is flat and is therefore independent of the localization of the scalar sector in RS models. Furthermore, the gluon profile function is also unaffected by the electroweak gauge group in the bulk of the extra dimension. The coupling of the KK gluon in the RS model to quarks is given by $c_{gq\bar{q}} \approx \left(1/\sqrt{L}\right) g_s$, and the coupling of the KK gluon to left–handed quarks is dominated by the top quark coupling, *i.e.* $c_{gt_L\bar{t}_L} \approx -g_s$. The coupling to right–handed top quarks is $c_{gt_R\bar{t}_R} \approx -\sqrt{L} g_s$, where g_s denotes the QCD coupling constant. A more precise estimation can only be given *via* a detailed knowledge of the particular overlap integrals of the first KK gluon mode to the overlap integrals of the quarks under consideration. The knowledge of this expression depends on the setup of the RS model under consideration and the results of the analyses should be read carefully as the specific values depend on a specific choice and therefore may be misleading. Another interesting channel for its investigation would be a diphoton resonance with a signal rate $(\sigma \cdot \text{Br})\left(pp \to h^{(1)} \to \gamma\gamma\right)$ besides the mentioned production channel for the KK gluon. The signal rate would depend on both the KK graviton mass $m_{h^{(1)}}$ and the ratio $k/\bar{M}_{\text{Pl}} = M_{\text{Pl}}/\sqrt{8\pi} M_{\text{kk}}/\Lambda_{\text{TeV}}$. The ratio includes the reduced Planck mass $\bar{M}_{\text{Pl}}$

and sets the interaction strength of the coupling of the graviton to either two gluons or 2 photons. This results in $\mathcal{L}(x) \ni 0.054 \cdot 1/m_{h^{(1)}} k/\bar{M}_{\mathrm{Pl}} h^{(1)}_{\mu\nu}(x) T^{\mu\nu}(x)$ [177] with the 4D energy momentum tensor $T^{\mu\nu}$ of the gluon.
Alternatively, couplings of KK excitations of the other vector bosons, *i.e.* $Z, W^{\pm}$ to fermions, could be also measured and some prospects are published in [178]. This turns out to be challenging, because their corresponding production and decay channels strongly depend on the fermion localization given *via* the 5D Yukawa matrices and the 5D bulk mass parameters. Numerical simulations that are presented in Ch. 4 are done using the bounds on the KK gluon masses to test the validity of the RS model.
Model–independent bounds are the Peskin Takeuchi parameter S, T and U [52, 53].

2.8 Generation of the RS data sets

Based on the program derived in [120, 179] and its numerical implementation in Mathematica [180, 181], the data sets for the phenomenology part of this thesis were generated. In the following, a summary of the procedure is given.
First, the anarchic Yukawa matrices are implemented and filled with a complex number derived on a computer time based random number generator to check the consistency with the observables. The elements of the Yukawa matrices are constrained *via*

$$\left|(Y_q)_{ij}\right| \leq y_\star \tag{2.199}$$

for different values of $y_\star$. An upper limit on $y_\star \leq y_{\max}$ is only necessary if the perturbativity for the Yukawa sector is required, where $y_\star \leq y_{\max} \approx 3$ is a suitable value, *c.f.* Sec. 2.3.1 and [145]. In the current analyses, the values for $y_\star \in [0.5, 3]$ are used. The obtained parameters of the Yukawa matrices are flat distributed in the complex plane. Even $Y_{u_{33}}$ shows a small deviation due to either the contribution of the top mass m_t or if $Y_{u_{33}} \geq 1/2$.
In leading order v^2/M_{kk}^2 the ZMA can be applied to express the Wolfenstein parameter. $\bar{\rho}$ and $\bar{\eta}$ can be solely expressed *via* the entries of the Yukawa matrices $(Y_q)_{ij}$ and the corresponding minors M_{ij} of $(Y_q)_{ij}$ [182]

$$\bar{\rho} - i\bar{\eta} = \frac{(Y_d)_{33}(M_u)_{31} - (Y_d)_{23}(M_u)_{21} + (Y_d)_{13}(M_u)_{11}}{(Y_d)_{33}(M_u)_{11}\left[\frac{(Y_d)_{23}}{(Y_d)_{33}} - \frac{(Y_u)_{23}}{(Y_u)_{33}}\right]\left[\frac{(M_d)_{21}}{(M_d)_{11}} - \frac{(M_u)_{21}}{(M_u)_{11}}\right]} \tag{2.200}$$

Additionally, the F profiles $F(c_{u_3}) \in [0, 3]$ are generated with $c_{u_3} \in [-1/2, 1]$ as the right–handed top is required to have an $\mathcal{O}(1)$ overlap with the IR brane and the other limit is set by the fact that the 5D bulk mass does not exceed the curvature k. Now, as well as with the Wolfenstein parameters A and λ, all parameters are derived to express the remaining F profiles [120, 182]

$$|F(c_{Q_1})| = \frac{\sqrt{2}m_t}{v}\left(|(Y_u)_{33}|\left|\frac{(Y_d)_{23}}{(Y_d)_{33}} - \frac{(Y_u)_{23}}{(Y_u)_{33}}\right|\left|\frac{(M_d)_{21}}{(M_d)_{11}} - \frac{(M_u)_{21}}{(M_u)_{11}}\right|\right)^{-1}\frac{\lambda^3 A}{|F(c_{u_3})|}, \tag{2.201}$$

$$|F(c_{Q_2})| = \frac{\sqrt{2}m_t}{v}\left(|(Y_u)_{33}|\left|\frac{(Y_d)_{23}}{(Y_d)_{33}} - \frac{(Y_u)_{23}}{(Y_u)_{33}}\right|\right)^{-1}\frac{\lambda^2 A}{|F(c_{u_3})|}, \tag{2.202}$$

$$|F(c_{Q_2})| = \frac{\sqrt{2}m_t}{v}\frac{1}{|(Y_u)_{33}|\,|F(c_{u_3})|}, \tag{2.203}$$

$$|F(c_{u_1})| = \frac{m_u}{m_t}\frac{|(Y_u)_{33}|\,|(M_u)_{11}|}{\det Y_u}\left|\frac{(Y_d)_{23}}{(Y_d)_{33}} - \frac{(Y_u)_{23}}{(Y_u)_{33}}\right|\left|\frac{(M_d)_{21}}{(M_d)_{11}} - \frac{(M_u)_{21}}{(M_u)_{11}}\right|\frac{|F(c_{u_3})|}{\lambda^3 A}, \tag{2.204}$$

$$|F(c_{u_2})| = \frac{m_c}{m_t}\frac{|(Y_u)_{33}|^2}{|(M_u)_{11}|}\left|\frac{(Y_d)_{23}}{(Y_d)_{33}} - \frac{(Y_u)_{23}}{(Y_u)_{33}}\right|\frac{|F(c_{u_3})|}{\lambda^2 A}, \tag{2.205}$$

$$|F(c_{d_1})| = \frac{m_d}{m_t}\frac{|(Y_u)_{33}|\,|(M_d)_{11}|}{\det Y_d}\left|\frac{(Y_d)_{23}}{(Y_d)_{33}} - \frac{(Y_u)_{23}}{(Y_u)_{33}}\right|\left|\frac{(M_d)_{21}}{(M_d)_{11}} - \frac{(M_u)_{21}}{(M_u)_{11}}\right|\frac{|F(c_{u_3})|}{\lambda^3 A}, \tag{2.206}$$

$$|F(c_{d_2})| = \frac{m_s}{m_t}\frac{|(Y_u)_{33}|\,|(Y_d)_{33}|}{|(M_d)_{11}|}\left|\frac{(Y_d)_{23}}{(Y_d)_{33}} - \frac{(Y_u)_{23}}{(Y_u)_{33}}\right|\frac{|F(c_{u_3})|}{\lambda^2 A}, \tag{2.207}$$

$$|F(c_{d_3})| = \frac{m_b}{m_t}\frac{|(Y_u)_{33}|}{|(Y_d)_{33}|}|F(c_{u_3})|. \tag{2.208}$$

The fraction of the profiles scale with

$$\frac{|F(c_{Q_1})|}{|F(c_{Q_2})|} \sim \lambda \quad \frac{|F(c_{Q_2})|}{|F(c_{Q_3})|} \sim \lambda^2, \quad \frac{|F(c_{Q_1})|}{|F(c_{Q_3})|} \sim \lambda^3 \tag{2.209}$$

The input masses are obtained in the $\bar{M}S$ scheme evaluated at $\mu = 1\,\text{TeV}$ [6]

$$m_u = (1.0 \pm 0.7)\,\text{MeV}, \quad m_c = (500 \pm 25)\,\text{MeV}, \quad m_t = (141 \pm 5)\,\text{GeV}, \tag{2.210}$$

$$m_d = (2.2 \pm 0.5)\,\text{MeV}, \quad m_s = (43 \pm 5)\,\text{MeV}, \quad m_b = (2.31 \pm 0.03)\,\text{GeV}, \tag{2.211}$$

$$\lambda = 0.22548^{+0.00068}_{-0.00034}, \quad \bar{\eta} = 0.343^{+.0.0011}_{-0.0012}, \quad \bar{\rho} = 0.145^{+0.013}_{-0.007}, \quad A = 0.810^{0.018}_{-0.024} \tag{2.212}$$

and the values for the Wolfenstein parameters from [183]. These result in the parameter $x = \{m_u, m_d, m_s, m_c, m_b, m_t, A, \lambda, \rho, \eta\}$ in the RS model which is valid up to v^2/M_{kk}^2. The parameter x now has to fulfill a χ^2 test. With

$$\chi^2 = \left(\frac{x_{\text{exp}}(n) - x_{\text{th}}(n)}{\sigma_{\text{exp}}(n)}\right)^2, \tag{2.213}$$

the value for the parameter $x_{\text{exp}}(n)$ is accepted if $\chi^2/\text{dof} > 68\%$ [184].

3 Propagators in the warped extra dimension

The 5D propagators for bosons and fermions are derived in this chapter, because they are important for the calculation of the loop–induced process $h \to \gamma\gamma$ that is discussed in Ch. 4. The calculation of the 5D propagators is done in the framework of warped extra dimensions. The 5D propagators are functions that depend on the coordinates in the extra dimension, *e.g.* t and t', and on the 4–momentum p^μ. This dependence is referred to as the *mixed–momentum position representation*, because the coordinates in the extra dimension lie in the position space [106, 185–188]. With the use of the AdS/CFT correspondence [189–191], the two point function of the 5D propagator is expressed in the KK decomposition as an infinite sum over all KK modes and their profile functions $\chi_n(t), \chi_n(t')$ [192]

$$D\left(t, t'; p^2\right) \approx \sum_{n=0}^{\infty} \frac{\chi_n(t)\,\chi_n(t')}{p^2 - m_n^2}. \tag{3.1}$$

There are some advantages of the 5D descriptions that should be mentioned. The 5D propagator contains all KK modes, *c.f.* Eq. (3.1), by encoding the full 5D theory. This also includes the expression for the 5D propagator that is valid to all orders in an expansion in powers of $\mathcal{O}\left(v^2/M_{\text{kk}}^2\right)$. Furthermore, one finds a closed analytic expression for amplitudes of loop–induced processes with the help of the 5D propagator. Thus, it is possible to check the full structure of the warped 5D propagators. This would not have been possible if only a part of the KK modes had been considered in the KK–decomposed theory. An example for this is the investigation of the fermion contributions in the decay $h \to \gamma\gamma$ that are discussed in Ch. 4.
In this chapter, the 5D propagator for bosons is derived in Sec. 3.1 based on our publication [193]. The section starts with the derivation for arbitrary scalar fields in Sec. 3.1.1 and is followed by the derivation of the vector boson propagator in Sec. 3.1.1 for both the minimal and the custodial RS model with a brane–localized Higgs boson and a narrow bulk–localized Higgs boson. The propagators of both vector bosons and scalar bosons are necessary for the investigation of the decay $h \to \gamma\gamma$. In Sec. 3.2 the fermion propagator is derived in both the minimal and the custodial RS model with a brane localized Higgs boson and a narrow bulk localized Higgs boson, in analogy to the derivation of the vector boson propagator. This section is based on our publication [131] and in [128–130], the fermion propagator is derived in the corresponding theses in more detail.

3.1 Boson propagators

3.1.1 Derivation of both vector boson and scalar boson propagator

The derivation of the gauge boson propagator is needed for the decay $h \to \gamma\gamma$. The propagator of the W boson is derived now, valid for both massive and massless vector

bosons. Parts of this section are based on [193]. The derivation is valid for the case of the Z boson, however, small modifications due to both the different coupling and the different mass have to be considered. In the case of both the photon and the gluon, some other adjustments have to be made which are mentioned in the text below. Originally, the propagator was also derived in [126, 106, 188, 168]. The achievement of [193] is a closed expression for the brane–localized Higgs model, the custodial RS model, as well as for the bulk–localized Higgs model. The boson propagator for the bulk–localized Higgs model is needed, because the decay $h \to \gamma\gamma$ is also studied for a narrow bulk Higgs model as explained in Sec.2.2.3. In this case, there are contributions from diagrams containing a W propagator with a narrow bulk–localized Higgs boson.
Beginning with the derivation of the gauge boson propagator in the brane localized Higgs model, the study of the propagator in the narrow bulk localized Higgs model follows analogously. As a conclusion of the whole derivation in both models, it is shown that both results coincide under given circumstances.
For an arbitrary R_ξ gauge in the minimal RS model for a brane–localized Higgs boson, the general 5D action reads [106]

$$S_{\text{Gauge}} = \frac{1}{2}\int \mathrm{d}^4x \frac{2\pi r}{L}\int_\epsilon^1 \frac{\mathrm{d}t}{t} B_M\left(x,t\right) K^{MN}_{B,\xi} B_N\left(x,t\right) \tag{3.2}$$

In Eq. (3.2) only terms bilinear in the fields occur with

$$K^{MN}_{B,\xi} = \begin{pmatrix} \left(\partial^2 - M^2_{\text{kk}} t\partial_t \frac{1}{t}\partial_t\right)\eta^{\mu\nu} - \left(1-\frac{1}{\epsilon}\right)\partial^\mu\partial^\nu & 0 \\ 0 & -\partial^2\frac{1}{t^2} + \xi M^2_{\text{kk}} t\partial_t t\partial_t \frac{1}{t^2} \end{pmatrix}, \tag{3.3}$$

which contains differential operators. The off–diagonal elements of Eq. (3.3) vanish with an appropriate choice of the gauge-fixing, *c.f.* [120, 106]. As a consequence, both scalar components and vector components of the 5D propagator decouple. Rescaling the propagator B_M with $\frac{1}{\sqrt{r}}$ yields the consistent mass dimension of $[B_M] = 3/2$. After the application of the rescaling with the factor $\frac{1}{\sqrt{r}}$, it turns out that the propagator can be written as a sum of infinitely many KK modes including the zero mode. The differential equations then read, after a Fourier transformation of the non–compact directions

$$\left[\left(\hat{p}^2 + t\partial_t\frac{1}{t}\partial_t\right)\eta^{\mu\nu} - \left(1-\frac{1}{\epsilon}\right)\hat{p}^\mu\hat{p}^\nu\right] D^\xi_{B,\nu\rho}\left(t,t';p\right) = -\frac{Lt'}{2\pi M^2_{\text{kk}}}\delta^\mu_\rho\delta\left(t-t'\right), \tag{3.4}$$

$$\left[\hat{p}^2 + \xi t\partial_t t\partial_t\frac{1}{t^2}\right] D^\xi_{B,55}\left(t,t';p\right) = \frac{Lt'^3}{2\pi\epsilon^2 M^2_{\text{kk}}}\delta\left(t-t'\right), \tag{3.5}$$

in which Eq. (3.4) is the differential equation for the vector component. The differential equation of the scalar component of the propagator is given by Eq. (3.5). The vector component can be obtained *via*

$$D^\xi_{B,\nu\rho}\left(t,t';p\right) = A^\xi_B\left(t,t';-p^2\right)\frac{p_\nu p_\mu}{p^2} + B_B\left(t,t';-p^2\right)\left(\eta_{\nu\rho} - \frac{p_\nu p_\mu}{p^2}\right), \tag{3.6}$$

in which Lorentz invariance was used to obtain the two separate scalar functions $A^\xi_B\left(t,t';-p^2\right)$ and $B_B\left(t,t';-p^2\right)$. If Eq. (3.6) is inserted into Eq. (3.4), this relates $A^\xi_B\left(t,t';-p^2\right)$ to

$B_B\left(t,t';-p^2\right)$ and one will yield two partial differential equations

$$\left(\frac{\hat{p}^2}{\xi}+t\partial_t\frac{1}{t}\partial_t\right)A_B^{\xi}\left(t,t';-p^2\right)=\left(\hat{p}^2+t\partial_t\frac{1}{t}\partial_t\right)B_B\left(t,t';-p^2\right), \tag{3.7}$$

$$\left(\hat{p}^2+t\partial_t\frac{1}{t}\partial_t\right)B_B\left(t,t';-p^2\right)=-\frac{Lt'}{2\pi M_{\mathrm{kk}}^2}\delta\left(t-t'\right). \tag{3.8}$$

It is sufficient to obtain an expression for $B_B\left(t,t';-p^2\right)$, because $A_B^{\xi}\left(t,t';-p^2\right)$ and $B_B\left(t,t';-p^2\right)$ are related *via* Eq. (3.7). The insertion of the KK decomposition of the field $B_M\left(x,t\right)$, which is defined in the first line of Eq. (2.28), into the action Eq. (3.2) yields an expression for $B_B\left(t,t';-p^2\right)$

$$B_B\left(t,t';-p^2\right)=\sum_{n=0}^{\infty}\frac{\chi_n^B\left(t\right)\chi_n^B\left(t'\right)}{m_{B_n}^2-p^2}. \tag{3.9}$$

Now, the propagator function is related to the KK decomposition. A parametrization with $D_{B,55}^{\xi}\left(t,t';p\right)=-\frac{1}{\xi}B_{B,55}\left(t,t';-p/\xi\right)$ yields the 5^{th} scalar component of Eq. (3.9)

$$B_{B,55}\left(t,t';-p^2\right)=\sum_{n=0}^{\infty}\frac{k^2tt'}{m_{B_n}^2}\frac{\partial_t\chi_n^B\left(t\right)\partial_{t'}\chi_n^B\left(t'\right)}{m_{B_n}^2-p^2} \tag{3.10}$$

with the curvature k. Eq. (3.10) can be re–expressed *via* Eq. (3.9)

$$B_{B,55}\left(t,t';-p^2\right)=\frac{k^2tt'}{p^2}\partial_t\partial_{t'}\left[B_B\left(t,t';0\right)-B_B\left(t,t';-p^2\right)\right]. \tag{3.11}$$

If an expression for the vector component is known, only the knowledge of Eq. (3.9) will be necessary for the whole derivation. Proceeding to obtain an expression for $B_B\left(t,t';-p^2\right)$, Eq. (3.8) can be re–expressed *via* a second order partial differential equation which has to be solved, leading to

$$\left(t^2\hat{p}^2-t^2\partial_t^2+t\partial_t-1\right)\frac{B_B\left(t,t';-p^2\right)}{t}=-\frac{Lt'}{2\pi M_{\mathrm{kk}}^2}\delta\left(t-t'\right). \tag{3.12}$$

This requires a distinction between $t>t'$ and $t<t'$ and this yields 4 coefficients $C_1^<,C_1^>,C_2^<,C_2^>$ with

$$t_<=\min\left(t,t'\right) \tag{3.13}$$

and

$$t_>=\max\left(t,t'\right) \tag{3.14}$$

Then it is possible to determine the 4 coefficients $C_1^<,C_1^>,C_2^<,C_2^>$. One coefficient is obtained *via* the continuity of the solution at $t=t'$

$$B_B\left(t,t';-p^2\right)\big|_{t=t'-0}^{t=t'+0}=0 \tag{3.15}$$

and a second coefficient is obtained *via* the so–called jump condition

$$\partial_tB_B\left(t,t';-p^2\right)\big|_{t=t'+0}^{t=t'-0}=-\frac{Lt'}{2\pi M_{\mathrm{kk}}} \tag{3.16}$$

that is obtained after an integration of Eq. (3.12) over an infinitesimal interval. The last two coefficients in

$$B_B\left(t,t';-p^2\right)=\frac{Ltt'}{4M_{\mathrm{kk}}^2}\frac{\left[C_1^{>}J_1\left(\hat{p}t_{>}\right)+C_2^{>}Y_1\left(\hat{p}t_{>}\right)\right]\left[C_1^{<}J_1\left(\hat{p}t_{<}\right)+C_2^{<}Y_1\left(\hat{p}t_{<}\right)\right]}{C_1^{>}C_2^{<}-C_1^{<}C_2^{>}} \tag{3.17}$$

are determined *via* the BCs b_ϵ and b_1 on both the UV brane and IR brane

$$\left(\partial_t-\frac{b_\epsilon}{\epsilon}\right)B_B\left(t,t';-p^2\right)\Big|_{t=\epsilon^+}=0,\quad \left(\partial_t-b_1\right)B_B\left(t,t';-p^2\right)\Big|_{t=1^-}=0. \tag{3.18}$$

In case of massive vector bosons $B=W,Z$, b_1 contains the leading order mass term defined in Eq. (2.30) and results in

$$b_1\Big|_{B\,\mathrm{boson}}=-\frac{L\tilde{m}_B^2}{M_{\mathrm{kk}}^2}, \tag{3.19}$$

whereas b_ϵ is consequently set to zero. Furthermore, Eq. (3.17) can be used to derive the propagator for a general gauge boson, *c.f.* [126, 106, 168]. For a W boson, the coefficients $C_1^{<},C_1^{>},C_2^{<},C_2^{>}$ are

$$C_1^{>}\left(\hat{p}\right)=-\hat{p}Y_0\left(\hat{p}\right)+b_1Y_1\left(\hat{p}\right),\qquad C_1^{<}\left(\hat{p}\right)=-\hat{p}\epsilon Y_0\left(\hat{p}\epsilon\right)+b_\epsilon Y_1\left(\hat{p}\epsilon\right), \tag{3.20}$$

$$C_2^{>}\left(\hat{p}\right)=\hat{p}J_0\left(\hat{p}\right)-b_1J_1\left(\hat{p}\right),\qquad C_2^{<}\left(\hat{p}\right)=\hat{p}\epsilon J_0\left(\hat{p}\epsilon\right)-b_\epsilon J_1\left(\hat{p}\epsilon\right). \tag{3.21}$$

Inserting the coefficients of Eq. (3.20) into Eq. (3.17), Eq. (3.17) results in

$$B_B\left(t,t';-p^2\right)=\frac{Ltt'}{4M_{\mathrm{kk}}^2}\frac{\left[\hat{p}D_{10}\left(t_{>},1\right)-b_1D_{11}\left(t_{>},1\right)\right]D_{10}\left(t_{<},\epsilon\right)}{\hat{p}D_{00}\left(1,\epsilon\right)-b_1D_{10}\left(1,\epsilon\right)} \tag{3.22}$$

with the abbreviation for time like momenta $p^2>0,\hat{p}^2=p^2/M_{\mathrm{kk}}^2$

$$D_{ij}\left(t,t'\right)=J_i\left(\hat{p}t\right)Y_j\left(\hat{p}t'\right)-Y_i\left(\hat{p}t\right)J_j\left(\hat{p}t'\right). \tag{3.23}$$

The solution for the propagator is needed for time like momenta after the Wick rotation with Euclidean momenta $p_E^2=-p^2>0,\hat{p}_E\equiv p_E^2/M_{\mathrm{kk}}^2$, and is given by

$$B_B\left(t,t';p_E^2\right)=\frac{Ltt'}{2\pi M_{\mathrm{kk}}^2}\frac{\left[\hat{p}_ED_{10}\left(t_{>},1\right)+b_1D_{11}\left(t_{>},1\right)\right]D_{10}\left(t_{<},\epsilon\right)}{\hat{p}_ED_{00}\left(1,\epsilon\right)-b_1D_{10}\left(1,\epsilon\right)}. \tag{3.24}$$

Due to the change of the argument in both Bessel functions $J_i\left(\hat{p}t\right)$ and $Y_i\left(\hat{p}t\right)$, $D_{ij}\left(t,t'\right)$ results in

$$D_{ij}\left(t,t'\right)=I_i\left(\hat{p}_Et\right)K_j\left(\hat{p}_Et'\right)-(-1)^{i+j}K_i\left(\hat{p}_Et\right)I_j\left(\hat{p}_Et'\right). \tag{3.25}$$

As a next step, the self–energy function $\Sigma\left(p^2\right)$ for the boson propagator is derived. Knowing, that the mass of the propagator is the residue of the propagator [195], the self–energy function $\Sigma\left(p^2\right)$ and the wave–function renormalization is derived, because around $p^2=m_{B_n}^2$

$$\frac{1}{2\pi}\frac{-1}{\left(p^2-\tilde{m}_{B_n}^2\right)\left[1+\Pi\left(t,t';p^2\right)\right]+\Sigma\left(p^2\right)+i0}=\frac{1}{2\pi}\frac{Z_2\left(t,t'\right)}{p^2-m_{B_n}^2+i0}. \tag{3.26}$$

Furthermore, the expression for the boson propagator expanded in $v^2/M_{\rm kk}^2$ is needed that keeps both p^2 and m_W^2 fixed in Eq. (3.24) and results in the case of the W boson propagator in

$$B_W\left(t,t';-p^2\right)=\frac{1}{2\pi}\frac{-1}{\left(p^2-\tilde{m}_W^2\right)\left[1+\Pi\left(t,t';p^2\right)+\Sigma\left(p^2\right)\right]+i0} \tag{3.27}$$

with the self–energy function $\Sigma\left(p^2\right)$ with the t–dependent part $\Pi\left(t,t';p^2\right)$

$$\Sigma\left(p^2\right)=\frac{\tilde{m}_W^4}{2M_{\rm kk}^2}\left(L-\frac{p^2}{\tilde{m}_W^2}+\frac{1}{2L}\frac{p^4}{\tilde{m}_W^4}\right), \tag{3.28}$$

$$\Pi\left(t,t';p^2\right)=\frac{\tilde{m}_W^2}{2M_{\rm kk}^2}\left\{Lt_>^2+\frac{p^2}{\tilde{m}_W^2}\left[Lt_<^2-t^2\left(\frac{1}{2}-\ln t\right)-t'^2\left(\frac{1}{2}-\ln t'\right)\right]\right\}. \tag{3.29}$$

The results are valid at $\mathcal{O}\left(v^4/M_{\rm kk}^4\right)$. The zero in the propagator Eq. (3.27) is determined *via* $m_W^2=\tilde{m}_W^2-\Sigma\left(m_W^2\right)$ that is the physical W boson mass of the ground state. With the same strategy, the exact expression for the zero mode profile function $\chi_0^W(t)$ defined in Eq. (2.42) can be derived at $v^2/M_{\rm kk}^2$ *via* the residue of the propagator that is determined *via*

$$\begin{aligned}B_W\left(t,t';-p^2\right)&=\frac{1}{2\pi}\frac{Z_2\left(t,t'\right)}{p^2-m_{W_n}^2+i0},\\ Z_2\left(t,t'\right)&=2\pi\chi_0^W(t)\,\chi_0^W\left(t'\right)\\&=1-\Pi\left(t,t';m_W^2\right)-\partial\Sigma\left(p^2\right)/\partial p^2\big|_{p^2=m_W^2}.\end{aligned} \tag{3.30}$$

For time like momenta $p^2\geq v^2$, at leading order $\mathcal{O}\left(v^2/M_{\rm kk}^2\right)$. The expansion of the propagator is then given by

$$B_W\left(t,t';-p^2\right)=\frac{1}{2\pi}\left[\frac{c_1\left(t,t'\right)}{m_W^2-p^2}+\frac{c_2\left(t,t'\right)}{2M_{\rm kk}^2}\right]+\mathcal{O}\left(\frac{v^4}{M_{\rm kk}^4}\right) \tag{3.31}$$

with

$$c_1\left(t,t'\right)=2\pi\chi_0^W(t)\,\chi_0^W\left(t'\right), \tag{3.32}$$

$$c_2\left(t,t'\right)=Lt_<^2+\frac{1}{2L}+t^2\left(\ln t-\frac{1}{2}\right)+t'^2\left(\ln t'-\frac{1}{2}\right). \tag{3.33}$$

The expansion allows a distinction in which both the contributions stemming from the KK modes and the zero modes can be separated. Furthermore, Eq. (3.31) is a more lucid expression compared to the full result in Eq. (3.24).

3.1.1.1 The vector boson propagator in the custodial model

As a next step, the W boson propagator is derived in the custodial RS model with a brane–localized Higgs model. In [193], a closed and exact expression for the W boson propagator is derived in the custodial model described in Sec. 2.5 for both the brane–localized Higgs scenario and the narrow bulk localized Higgs scenario.

In the UV basis, the differential equation of the gauge boson propagator is the same as in the minimal RS model

$$\left(\mathbf{P}_+\partial_t + \mathbf{P}_-\right) B_W^{\mathrm{UV}}\left(t,t';-p^2\right)\Big|_{t=\epsilon} = 0, \tag{3.34}$$

$$\left(\partial_t - b_1 \mathbf{R}_{\theta_W}^T \mathbf{P}_+ \mathbf{R}_{\theta_W}\right) B_W^{\mathrm{UV}}\left(t,t';-p^2\right)\Big|_{t=1^-} = 0, \qquad b_1 = -\frac{L\tilde{m}_W^2}{c_{\theta_W}^2 M_{\mathrm{kk}}^2}, \tag{3.35}$$

in which the BCs are changed due to the enlarged gauge symmetry. The first equation, Eq. (3.34), results from the field $A_M^{\pm}$ with $A = L, R$. The general solution for the propagator in the UV basis $B_W^{\mathrm{UV}}\left(t,t';-p^2\right)$ reads

$$\begin{aligned} B_W^{\mathrm{UV}}\left(t,t';-p^2\right) = \frac{Ltt'}{4M_{\mathrm{kk}}^2} & \frac{1}{\left[\hat{p}D_{00}\left(1,\epsilon\right) - b_1 D_{10}\left(1,\epsilon\right)\right] D_{01}\left(1,\epsilon\right) - b_1 \frac{4s_{\theta_W}^2}{\pi^2\hat{p}^2\varepsilon}} \\ & \Bigg\{ \left[\left[\hat{p}D_{10}\left(t_>,1\right) - b_1 D_{11}\left(t_>,1\right)\right] D_{01}\left(1,\epsilon\right) - b_1 \frac{2s_{\theta_W}^2}{\pi\hat{p}} D_{11}\left(t_>,\epsilon\right) \right] D_{10}\left(t_<,\epsilon\right)\mathbf{P}_+ \\ & \left[\left[\hat{p}D_{00}\left(1,\epsilon\right) - b_1 D_{10}\left(1,\epsilon\right)\right] D_{10}\left(t_>,1\right) + b_1 \frac{2s_{\theta_W}^2}{\pi\hat{p}} D_{10}\left(t_>,\epsilon\right) \right] D_{11}\left(t_<,\epsilon\right)\mathbf{P}_- \\ & - b_1 \frac{2s_{\theta_W}c_{\theta_W}}{\pi\hat{p}} \left[D_{10}\left(t,\epsilon\right) D_{11}\left(t',\epsilon\right)\mathbf{P}_{12} + D_{11}\left(t,\epsilon\right) D_{10}\left(t',\epsilon\right)\mathbf{P}_{21}\right] \Bigg\} \end{aligned} \tag{3.36}$$

and is valid at $\mathcal{O}\left(v^2/M_{\mathrm{kk}}^2\right)$. The expressions $D_{ij}\left(t,t'\right)$ are already known from Eq. (3.23) and the 2×2 matrices $\mathbf{P}_{12,21}$ denote the entry of 1on the place indicated by their subscript. The expansion of the Bessel functions in $D_{ij}\left(t,t'\right)$ can be used for a simplification *via* $\hat{p}\epsilon D_{n1}\left(t,t'\right) = -\frac{2}{\pi}J_n\left(\hat{p}\epsilon\right)$ valid at $\mathcal{O}\left(\epsilon^2\right)$ for $n = 0, 1$. As a consequence, the parameter $\frac{1}{\epsilon}$ in the denominator of Eq. (3.36) cancels. Considering Eq. (3.36) in the limit for vanishing s_{θ_W}, the term proportional to $\mathbf{P}_+$ coincides with the result for the boson propagator obtained in the minimal RS model. An expansion of Eq. (3.36) in $\mathcal{O}\left(v^2/M_{\mathrm{kk}}^2\right)$ for general $p^2 \leq v^2$,

$$2\pi B_W^{\mathrm{UV}}\left(t,t';-p^2\right) = \begin{pmatrix} \frac{c_1(t,t')}{m_W^2-p^2} + \frac{c_2(t,t')}{2M_{\mathrm{kk}}^2} & \frac{Lm_W^2\tan(\theta_W)}{2M_{\mathrm{kk}}^2\left(m_W^2-p^2\right)}t'^2 \\ \frac{Lm_W^2\tan(\theta_W)}{2M_{\mathrm{kk}}^2\left(m_W^2-p^2\right)}t^2 & \frac{Lt_<^2}{2M_{\mathrm{kk}}^2} \end{pmatrix} \tag{3.37}$$

is obtained, in which the expression for $c_2\left(t,t'\right)$ corresponds to Eq. (3.33) obtained in the minimal RS model and $c_1\left(t,t'\right)$ corresponds to Eq. (3.32). In the case of $p^2 = 0$, the propagator corresponds to Eq. (54) from [121].

3.1.2 The vector boson propagator in the bulk Higgs model

3.1.2.1 The vector boson propagator in the bulk Higgs model in the minimal RS model

Now, the expression for the W boson propagator that is needed for the investigation in Ch. 4 is derived in the narrow bulk Higgs model. The gauge boson action remains almost the same as in Eq. (3.2) with the difference that an additional bulk mass for the bulk

field is needed. The procedure to obtain the expression for the second order differential equation follows in the same way as for the brane–localized Higgs, reading

$$\left(t^2\hat{p}^2 - t^2\partial_t^2 + t\partial_t - c_A^2(t) - 1\right)\frac{B_B\left(t,t';-p^2\right)}{t} = -\frac{Lt'^{,2}}{2\pi M_{\rm kk}^2}\delta\left(t-t'\right) \tag{3.38}$$

with the t dependent bulk mass present in the coefficient

$$c_A^2(t) = \frac{2\pi\tilde{m}_W^2}{M_{\rm kk}^2}\frac{t^2v^2(t)}{v^2} = \frac{L\tilde{m}_W^2}{M_{\rm kk}^2}(1+\beta)t^{4+2\beta}. \tag{3.39}$$

This is different for the brane–localized Higgs scenario due to the additional term in the 5D action, and $v^2 = v_4^2$ and $\tilde{m}_w = vg_5/\left(2\sqrt{2\pi r}\right)$. A solution in leading order $\mathcal{O}\left(v^2/M_{\rm kk}^2\right)$ is obtained justifying the expansion in $\hat{\epsilon}$ which counts the order proportional to $v^2/M_{\rm kk}^2$

$$B_W\left(t,t';-p^2\right) = B_0\left(t,t';-p^2\right) + \hat{\epsilon}B_1\left(t,t';-p^2\right) + \hat{\epsilon}^2B_2\left(t,t';-p^2\right) + \mathcal{O}\left(\epsilon^3\right). \tag{3.40}$$

The insertion of Eq. (3.40) into Eq. (3.38) and the powers of $\mathcal{O}\left(v^2/M_{\rm kk}^2\right)$ results in three differential equations

$$t\partial_t\frac{1}{t}\partial_tB_0\left(t,t';-p^2\right) = 0, \tag{3.41}$$

$$t\partial_t\frac{1}{t}\partial_tB_1\left(t,t';-p^2\right) + \left(\hat{p}^2 - \frac{c_A^2(t)}{t^2}\right)B_0\left(t,t';-p^2\right) = -\frac{Lt'}{2\pi M_{\rm kk}^2}\delta\left(t-t'\right), \tag{3.42}$$

$$t\partial_t\frac{1}{t}\partial_tB_2\left(t,t';-p^2\right) + \left(\hat{p}^2 - \frac{c_A^2(t)}{t^2}\right)B_1\left(t,t';-p^2\right) = 0. \tag{3.43}$$

For every $B_i\left(t,t';-p^2\right)$, $i=0,1,2$, the procedure of the application of both the Neumann BC and the continuity condition at $t=t'$ on the propagator has to be done. Both $B_0\left(t,t';-p^2\right)$ and $B_2\left(t,t';-p^2\right)$ are continuous at $t=t'$. The application of the continuity condition to Eq. (3.41) results in

$$B_0\left(t,t';-p^2\right) = C\left(t'\right), \tag{3.44}$$

that suggests a t' dependence. After applying both the jump condition and the BCs to Eq. (3.42) leads to the result that $C(t')$ is a constant. A solution for $B_1\left(t,t';-p^2\right)$ can be obtained *via* the same procedure applied to Eq. (3.43). With respect to $\left|p^2\right| \leq v^2$ at leading order $\mathcal{O}\left(v^2/M_{\rm kk}^2\right)$, the expression for the propagator $B_W\left(t,t';-p^2\right)$ can be obtained with the insertion of

$$\begin{aligned} c_1\left(t,t'\right) = 1 + \frac{m_W^2}{2M_{\rm kk}^2}\Bigg[& \frac{L\left(t^{4+2\beta}+t'^{\,4+2\beta}\right)}{2+\beta} + \frac{(1+\beta)(3+\beta)}{(2+\beta)^2} - \frac{1}{L} \\ & - t^2\left(L - \frac{1}{2} + \ln(t)\right) - t'^2\left(L + \ln\left(t'\right) - \frac{1}{2}\right)\Bigg] \end{aligned} \tag{3.45}$$

into Eq. (3.31). For $\beta\to\infty$, Eq. (3.45) is identical to Eq. (3.32) recovering the expression for the brane localized Higgs scenario.
For $p^2=0$ we find the solution

$$B_W\left(t,t';0\right) = -\frac{L\alpha tt'}{4M_{\rm kk}^2\sin(\pi\alpha)}\frac{D_1\left(t_>,1\right)D_1\left(t_<,\epsilon\right)}{D_2\left(1,\epsilon\right)} \tag{3.46}$$

with $\alpha \equiv 1/(2+\beta)$ and

$$D_1(t,t') = \tilde{I}_\alpha(t)\,\tilde{I}_{1-\alpha}(t') - \tilde{I}_{-\alpha}(t)\,\tilde{I}_{\alpha-1}(t'), \tag{3.47}$$

$$D_2(t,t') = \tilde{I}_{\alpha-1}(t)\,\tilde{I}_{1-\alpha}(t') - \tilde{I}_{1-\alpha}(t)\,\tilde{I}_{\alpha-1}(t') \tag{3.48}$$

including

$$\tilde{I}_\alpha(t) \equiv \left(\frac{2L\tilde{m}_W^2}{M_{\rm kk}^2}\frac{1+\beta}{2+\beta}t^{2+\beta}\right). \tag{3.49}$$

The expansion to $\mathcal{O}\left(v^2/M_{\rm kk}^2\right)$ yields

$$B_W(t,t';0) = \frac{1}{2\pi\tilde{m}_W^2} + \frac{L}{4\pi M_{\rm kk}^2}\left[\frac{2(1+\beta)^2}{(2+\beta)(3+\beta)} + \frac{t^{4+2\beta}t'^{4+2\beta}}{2+\beta} - t_>^2\right]. \tag{3.50}$$

In the case of $\beta \to \infty$ or $\alpha \to 0$, the result of the expansion in the brane–localized Higgs scenario is recovered.

3.1.2.2 The vector boson propagator in the bulk Higgs model in the custodial RS model

The W boson propagator in the custodial model with a narrow bulk localized Higgs is derived in the IR basis with the differential equation

$$\left(t^2\hat{p}^2 - t^2\partial_t^2 + t\partial_t - \frac{c_A^2(t)}{c_{\theta_W}^2}\mathbf{P}_+ - 1\right)\frac{B_W^{\rm IR}(t,t';-p^2)}{t} = -\frac{Lt'^2}{2\pi M_{\rm kk}^2}\delta(t-t') \tag{3.51}$$

that decouples for $c_W(t) = c_A(t)$ as defined in Eq. (3.39). The BCs

$$(\mathbf{P}_+\partial_t + \mathbf{P}_-)\,\mathbf{R}_{\theta_W}^T B_W^{\rm IR}(t,t';-p^2)\Big|_{t=\epsilon} = 0, \quad \partial_t B_W^{\rm IR}(t,t';-p^2)\Big|_{t=1^-} = 0 \tag{3.52}$$

contain the rotation matrix $\mathbf{R}_{\theta_W}^T$ that rotates the fields in the IR basis. Both the continuity equations and jump conditions are applied in the same way as in the minimal RS model receiving for $p^2 = 0$

$$B_W^{\rm IR}(t,t';0) = \frac{L}{4\pi M_{\rm kk}^2}\left\{-\frac{\pi\alpha tt'}{\sin(\alpha)}\frac{D_1(t,\epsilon)\,D_1(t',\epsilon)}{D_2(1,\epsilon)}\mathbf{P}_+ + \left[t_<^2 - \epsilon^2 - \frac{2\tan(\theta_W)}{c_W(1)\,\epsilon^\beta}\frac{D_1(\epsilon,1)}{D_2(\epsilon,1)}\right]\mathbf{P}_- \right.$$
$$\left. + \frac{2\tan(\theta_W)}{c_W(1)\,\epsilon^{1+\beta}}\left[\frac{tD_1(t,1)}{D_2(1,\epsilon)}\mathbf{P}_{12} + \frac{t'D_1(t',1)}{D_2(1,\epsilon)}\mathbf{P}_{12}\right]\right. \tag{3.53}$$

with $\alpha = 1/(2+\beta)$, $c_W(1) = \frac{\tilde{m}_W}{m_W}\sqrt{2L(1+\beta)}$ and $D_{1,2}(t,t')$ defined in Eq. (3.47). As in the case for the brane localized Higgs scenario, the expression proportional to $\mathbf{P}_+$ coincides with the result in the minimal model. After a Taylor expansion in $\mathcal{O}\left(v^2/M_{\rm kk}^2\right)$ of Eq. (3.53) as well as a rotation into the UV basis, Eq. (3.53) now results in

$$B_W^{\rm UV}(t,t';0) = \frac{\mathbf{P}_+}{2\pi\tilde{m}_W^2} + \frac{L}{4\pi M_{\rm kk}^2}\left[\left(\frac{2(1+\beta)^2}{c_{\theta_W}^2(2+\beta)(3+2\beta)} + \frac{t^{4+2\beta}+t'^{4+2\beta}}{2+\beta} - t_>^2\right)\mathbf{P}_+ \right.$$
$$\left. + \tan(\theta_W)\left(t'^2\left(1-\frac{t'^{2+2\beta}}{2+\beta}\right)\mathbf{P}_{12} + t^2\left(1-\frac{t^{2+2\beta}}{2+\beta}\right)\mathbf{P}_{21}\right) + t_<^2\mathbf{P}_-\right] \tag{3.54}$$

that coincides with the result obtained in the custodial RS model in the brane localized Higgs scenario in the limit $\beta \to \infty$.

3.2 Fermion propagator

The derivation of the fermion propagator in both the minimal and the custodial RS model for both the brane and the narrow bulk Higgs scenario is needed for computing the contributions to the the decay amplitude $h \to \gamma\gamma$. Originally the fermion propagator in the RS model has been calculated in [185, 186] for one fermion generation. The results of [185, 186] have been extended in [188]. The authors of [188] derived the result for three fermion generations, without the Yukawa interactions on the IR brane. As a consequence, the results of [188] are only valid at zeroth order v^2/M_{kk}^2. As a next step, [126, 194] included the Yukawa interactions on the IR brane for three generations in the case of a brane–localized Higgs in the limit $\eta \to 0$ of the width of the regularized delta function $\delta^\eta(t-1)$.
The analysis presented here based on [131] is summarized. An alternative derivation without using the regularized δ function is mentioned in the text at the important steps. Only in the brane–localized Higgs scenario this alternative is valid and marks a crosscheck to the derivation presented in the following. Furthermore, the analysis presented here is also valid in the case for the custodial RS model. Therefore, the shifts $(q, Q) \to \left(\vec{q}, \vec{Q}\right) = \left(\vec{u}, \vec{U}\right), \left(\vec{d}, \vec{D}\right), \left(\vec{\lambda}, \vec{\Lambda}\right)$ have to be performed. Whenever functions are explained in more detail, the contributions from the additional fermion fields in the custodial model are presented.
As in the case of the bosons, the starting point for the analysis is the 5D fermion action that contains terms bilinear in the quark fields

$$S_{\text{Ferm}} = \sum_{\mathcal{Q}=\mathcal{U},\mathcal{D}} \int \mathrm{d}^4x \int_\epsilon^1 \mathrm{d}t \bar{\mathcal{Q}}_L(x,t) \left[\partial\!\!\!/ - M_{KK}\,\gamma_5\,\partial_t - M_{KK}\,\mathcal{M}_{\vec{q}}(t)\right] \mathcal{Q}_R(x,t) \tag{3.55}$$

with the spinor fields $\mathcal{Q}$. The fermion action also contains the generalized mass matrix $\mathcal{M}_q$, which reads

$$\mathcal{M}_q(t) = \frac{1}{t}\begin{pmatrix} c_Q & 0 \\ 0 & -c_q \end{pmatrix} + \frac{v}{\sqrt{2}M_{\text{kk}}}\delta^\eta(t-1)\begin{pmatrix} 0 & Y_q \\ Y_q^\dagger & 0 \end{pmatrix}, \tag{3.56}$$

and contains the bulk mass parameter $c_{Q,q}$ as well as the regularized delta function $\delta^\eta(t-1)$ that is defined in Eq. (2.18). As mentioned above, in both Eq. (3.55) and Eq. (3.56) fields have to be added in the case of the custodial RS model. The partial differential equation Eq. (3.57) is obtained from Eq. (3.55) and reads

$$\left[p\!\!\!/ - M_{KK}\,\gamma_5\,\partial_t - M_{KK}\,\mathcal{M}_q(t)\right] S^q\left(t,t';p^2\right) = \delta\left(t-t'\right). \tag{3.57}$$

In Eq. (3.57), $S^q\left(t,t';p^2\right)$ denotes the fermion propagator

$$\begin{aligned} iS^{\vec{q}}\left(t,t';p\right) &= \int d^4x\, e^{ip\cdot x} \langle 0|\mathbf{T}\left(\mathcal{Q}_L(x,t) + \mathcal{Q}_R(x,t)\right)\left(\overline{\mathcal{Q}}_L(t,0) + \overline{\mathcal{Q}}_R(t,0)\right)|0\rangle \\ &= \left[\Delta^q_{LL}(t,t';-p^2)p\!\!\!/ + \Delta^q_{RL}(t,t';-p^2)\right] P_R + (L \leftrightarrow R), \end{aligned} \tag{3.58}$$

with the time ordering T and $\Delta^q_{AB}\left(t,t';-p^2\right)$ with $A,B = R,L$ denotes the 5D fermion propagator that is a 15×15 matrix for the up–type quarks and a 9×9 matrix for both down–type quarks as well as for the λ–type quarks in the custodial RS model and

includes the multiplicity of the generations. The KK decomposition of the propagator functions with the KK–decomposed fermions in Eq. (3.58) read

$$\Delta^q_{AA}(t,t';-p^2) = \sum_n \frac{1}{p^2-m_n^2}\mathcal{Q}^{(n)}_A(t)\,\mathcal{Q}^{(n)\dagger}_A\left(t'\right),$$
$$\Delta^q_{BA}(t,t';-p^2) = \sum_n \frac{m_{q_n}}{p^2-m_{q_n}^2}\mathcal{Q}^{(n)}_B(t)\,\mathcal{Q}^{(n)\dagger}_A\left(t'\right), \quad A,B=R,L \tag{3.59}$$

in which the subscripts denote the handedness of the fermion fields that are outgoing and incoming. In the case of $\Delta^u_{RL}(t,t';-p^2)$, u_R denotes the right–handed outgoing fermion field, which is odd under the $\mathbb{Z}_2$ parity and requires Dirichlet BC at the UV brane. It is also part of the $SU(2)_L \times SU(2)_R$ bi–doublet. In contrast to u_R, the incoming left–handed field is even under the $\mathbb{Z}_2$ parity and transforms as a triplet under $SU(2)_L \times SU(2)_R$. Using the KK representation of the fermion fields, the EOM, Eq. (2.108), as well as the orthonormality condition, Eq. (2.107), the propagator functions of Eq. (3.59) have been proven to be consistent [131]. The first–order differential equations

$$p^2\Delta^q_{AA}\left(t,t';-p^2\right) - M_{kk}\mathcal{D}^{\vec{q}}_{\pm}\Delta^q_{BA}\left(t,t';-p^2\right) = \delta\left(t-t'\right), \tag{3.60}$$
$$\Delta^q_{BA}\left(t,t';-p^2\right) - M_{kk}\mathcal{D}^{\vec{q}}_{\mp}\Delta^q_{AA}\left(t,t';-p^2\right) = 0. \tag{3.61}$$

with $\mathcal{D}^{\vec{q}}_{\pm} = \pm\partial_t + \mathcal{M}_q$ are obtained *via* an insertion of Eq. (3.58) in Eq. (3.55). Furthermore, Eq. (3.60) is decoupled into the second–order differential equations

$$\left(\hat{p}^2 - \mathcal{D}^q_+\mathcal{D}^q_-\right)\Delta^q_{LL}\left(t,t';-p^2\right) = M_{\rm kk}^{-2}\delta\left(t-t'\right), \tag{3.62}$$
$$\left(\hat{p}^2 - \mathcal{D}^q_-\mathcal{D}^q_+\right)\Delta^q_{RR}\left(t,t';-p^2\right) = M_{\rm kk}^{-2}\delta\left(t-t'\right), \tag{3.63}$$
$$\left(\hat{p}^2 - \mathcal{D}^q_-\mathcal{D}^q_+\right)\Delta^q_{RL}\left(t,t';-p^2\right) = M_{\rm kk}^{-1}\mathcal{D}^q_-\delta\left(t-t'\right), \tag{3.64}$$
$$\left(\hat{p}^2 - \mathcal{D}^q_+\mathcal{D}^q_-\right)\Delta^q_{LR}\left(t,t';-p^2\right) = M_{\rm kk}^{-1}\mathcal{D}^q_+\delta\left(t-t'\right) \tag{3.65}$$

with $\hat{p} = p^2/M_{\rm kk}$, *i.e.* the momentum normalized to $M_{\rm kk}$. The continuity equations

$$\Delta^q_{AA}\left(t'+0,t';-p^2\right) - \Delta^q_{AA}\left(t'-0,t';-p^2\right) = 0, \qquad A=L,R \tag{3.66}$$
$$\Delta^q_{RL}\left(t'+0,t';-p^2\right) - \Delta^q_{RL}\left(t'-0,t';-p^2\right) = -M_{\rm kk}^{-1}, \tag{3.67}$$
$$\Delta^q_{LR}\left(t'+0,t';-p^2\right) - \Delta^q_{LR}\left(t'-0,t';-p^2\right) = M_{\rm kk}^{-1} \tag{3.68}$$

are obtained after the integration of Eq. (3.62) over an infinitesimal interval $t \in [t'-0, t'+0]$. Here, Eq. (3.66) does not show a discontinuity at $t = t'$ in contrast to both Eq. (3.67) and Eq. (3.68). If the derivative of Eq. (3.66) is considered, the discontinuity will appear for Eq. (3.66). Before the solutions of the fermion propagator are obtained, the implementation of the BCs on both branes have to be considered. On the IR brane, they read

$$\mathrm{diag}\begin{pmatrix}0 & 1\end{pmatrix}\Delta^q_{LA}\left(1,t';-p^2\right) = 0 = \mathrm{diag}\begin{pmatrix}1 & 0\end{pmatrix}\Delta^q_{RA}\left(1,t';-p^2\right), \quad A=L,R \tag{3.69}$$

with zero entries and the rank of the unit matrices that correspond to the structure of the propagator function. In the case of the alternative derivation in the brane Higgs case, in which the Yukawa matrices are implemented *via* the IR BCs, the IR BCs read in contrast to Eq. (3.69)

$$\begin{pmatrix}\frac{v}{\sqrt{2}M_{\rm kk}}\tilde{Y}_q^\dagger & 1\end{pmatrix}\Delta^q_{LL}\left(1^-,t';-p^2\right) = 0 = \begin{pmatrix}1 & -\frac{v}{\sqrt{2}M_{\rm kk}}\tilde{Y}_q\end{pmatrix}\Delta^q_{LA}\left(1,t'\right)\Delta^q_{RL}\left(1^-,t',-p^2\right) \tag{3.70}$$

However, the BC on the UV brane can not be written as general as in Eq. (3.69), because they differ for each quark type. In the custodial RS model, the additional BCs for the $\vec{\lambda}$–type quarks are

$$\mathrm{diag}\left(0,\quad 1,\quad 1,\quad 0,\quad 0\right)\Delta^{\vec{u}}_{LA}\left(\epsilon,t';-p^2\right)=0=\mathrm{diag}\left(1,\quad 0,\quad 0,\quad 1,\quad 1\right)\Delta^{\vec{u}}_{RA}\left(\epsilon,t';-p^2\right), \tag{3.71}$$

$$\mathrm{diag}\left(0,\quad 1,\quad 0\right)\Delta^{\vec{d}}_{LA}\left(\epsilon,t';-p^2\right)=0=\mathrm{diag}\left(1,\quad 0,\quad 1\right)\Delta^{\vec{d}}_{RA}\left(\epsilon,t';-p^2\right), \tag{3.72}$$

$$\mathrm{diag}\left(1,\quad 0,\quad 0\right)\Delta^{\vec{\lambda}}_{LA}\left(\epsilon,t';-p^2\right)=0=\mathrm{diag}\left(0,\quad 1,\quad 1\right)\Delta^{\vec{d}}_{RA}\left(\epsilon,t';-p^2\right). \tag{3.73}$$

Now, all ingredients are available for the derivation of the propagator functions $\Delta^{q}_{LA}\left(t,t'\right)$ with $A=L,R$. After the derivation of the propagator functions $\Delta^{q}_{LL}\left(t,t'\right)$ and $\Delta^{q}_{RL}\left(t,t'\right)$ are considered. The translation, which is necessary to obtain the results of both $\Delta^{q}_{LR}\left(t,t'\right)$ and $\Delta^{q}_{LL}\left(t,t'\right)$ is given afterward. The presence of the regulator η divides the whole bulk into two regions. While one region is described by $t<1-\eta$, which is referred to as the bulk, the other region $t>1-\eta$ is referred to as the sliver. For every region, the solution of both $\Delta^{q}_{LL}\left(t,t'\right)$ and $\Delta^{q}_{RL}\left(t,t'\right)$ are obtained in the euclidean momentum space with the general ansatz $af\left(p_E\right)$, in which a is a coefficient that depends on the region as well as a (well–behaved) function $f\left(\hat{p}_E\right)$ for every entry in $\Delta^{q}_{LL}\left(t,t'\right)$ and $\Delta^{q}_{RL}\left(t,t'\right)$. An additional case study with respect to $t_<=t<t'$ and $t_>=t>t'$ has to be done, before applying the jump condition, the BCs, and the continuity equations. The propagator functions will depend in total on 8 matrix valued functions $K_i\left(t'\right)$ appearing in the bulk, whereas $C_i\left(t'\right)$, with $i=1,...,4$ that appear in the sliver are to be determined with the matching condition at $t=1-\eta$. Once they are fixed, the propagator solution is obtained.

3.2.0.3 Solution of the propagator functions in the region $t<1-\eta$

In the limit $t<1-\eta$, the delta function plays no role, because the Yukawa matrices in the generalized mass matrix Eq. (3.56) do not appear. As a consequence, the solution of both $\Delta^{q}_{LL}\left(t,t'\right)$ and $\Delta^{q}_{RL}\left(t,t'\right)$ is given *via* the Bessel functions $\sqrt{t}I_{(-)\alpha}\left(\hat{p}_E,t\right)$ with α being a non–integer value and depending on the bulk mass parameter. In the case of $\alpha\in\mathbb{N}$, a solution can be obtained *via* a limiting procedure. Thus, the solutions for $t_<$ with the UV BCs are given by

$$\Delta^{q<}_{LL}\left(t,t';p_E^2\right)=\sqrt{t}\begin{pmatrix}D^{Q}_{1}\left(\hat{p}_E,t\right) & 0\\ 0 & D^{q}_{2}\left(\hat{p}_E,t\right)\end{pmatrix}\begin{pmatrix}K_1\left(t'\right) & K_2\left(t'\right)\\ K_3\left(t'\right) & K_4\left(t'\right)\end{pmatrix}, \tag{3.74}$$

$$\Delta^{A<}_{RL}\left(t,t';p_E^2\right)=-M_{\mathrm{kk}}p_E\sqrt{t}\begin{pmatrix}D^{Q}_{1}\left(\hat{p}_E,t\right) & 0\\ 0 & D^{q}_{2}\left(\hat{p}_E,t\right)\end{pmatrix}\begin{pmatrix}K_1\left(t'\right) & K_2\left(t'\right)\\ K_3\left(t'\right) & K_4\left(t'\right)\end{pmatrix}, \tag{3.75}$$

whereas Eq. (3.75) is obtained *via* the insertion of Eq. (3.74) into Eq. (3.60), in which $K_i\left(t'\right),i=1,...,4$ are matrix–valued functions with the appropriate rank. The functions $D^{A}_{1,2}\left(\hat{p}_E,t\right)$ depend on $A=\vec{Q},\vec{q},Q,q$ and $\left(\hat{p}_E,t\right)$ is the short hand notation for $\left(\hat{p}_E,t,\epsilon\right)$. $D^{A}_{i}\left(\hat{p}_E,t,\epsilon\right)$ are 3×3 matrices in generation space and are given in the custodial RS model by

$$D^{\vec{U}}_{1,2}\left(\hat{p}_E,t\right)=\mathrm{diag}\left(D^{Q}_{1,2}\left(\hat{p}_E,t\right),D^{Q}_{3,4}\left(\hat{p}_E,t\right)\right), \tag{3.76}$$

$$D^{\vec{u}}_{1,2}\left(\hat{p}_E,t\right)=\mathrm{diag}\left(D^{u^c}_{1,2}\left(\hat{p}_E,t\right),D^{\tau_1}_{3,4}\left(\hat{p}_E,t\right),D^{\tau_2}_{3,4}\left(\hat{p}_E,t\right)\right), \tag{3.77}$$

$$D^{\vec{D}}_{1,2}\left(\hat{p}_E,t\right)=D^{Q}_{1,2}\left(\hat{p}_E,t\right), \tag{3.78}$$

$$D^{\vec{d}}_{1,2}\left(\hat{p}_E,t\right)=\mathrm{diag}\left(D^{\tau_2}_{1,2}\left(\hat{p}_E,t\right),D^{\tau_1}_{3,4}\left(\hat{p}_E,t\right)\right), \tag{3.79}$$

$$D^{\vec{\Lambda}}_{1,2}\left(\hat{p}_E,t\right)=D^{Q}_{3,4}\left(\hat{p}_E,t\right), \tag{3.80}$$

$$D^{\vec{\lambda}}_{1,2}\left(\hat{p}_E,t\right)=\mathrm{diag}\left(D^{\tau_1}_{3,4}\left(\hat{p}_E,t\right),D^{\tau_2}_{3,4}\left(\hat{p}_E,t\right)\right), \tag{3.81}$$

$$\tag{3.82}$$

with

$$D^{A}_{1,2}\left(\hat{p}_E,t,t'\right)=I_{-c_A-\frac{1}{2}}\left(\hat{p}_E,t'\right)\,I_{c_A\mp\frac{1}{2}}\left(\hat{p}_E,t\right)-I_{c_A+\frac{1}{2}}\left(\hat{p}_E,t'\right)\,I_{-c_A\pm\frac{1}{2}}\left(\hat{p}_E,t\right), \tag{3.83}$$

$$D^{A}_{3,4}\left(\hat{p}_E,t,t'\right)=I_{-c_A+\frac{1}{2}}\left(\hat{p}_E,t'\right)\,I_{c_A\mp\frac{1}{2}}\left(\hat{p}_E,t\right)-I_{c_A-\frac{1}{2}}\left(\hat{p}_E,t'\right)\,I_{-c_A\pm\frac{1}{2}}\left(\hat{p}_E,t\right). \tag{3.84}$$

The antisymmetry leads to $D^{A}_{2,3}\left(\hat{p}_E,t,t\right)=0=D^{A}_{2,3}\left(\hat{p}_E,t,\epsilon\right)$. The procedure is repeated for the case $t_>$ and results in

$$\Delta^{A>}_{LL}\left(t,t';p^2_E\right)=\Delta^{A<}_{LL}\left(t,t';p^2_E\right)+\frac{\sqrt{tt'}}{p_E M_{\mathrm{kk}}1_\eta}\begin{pmatrix}-L^{Q}_{3}\left(\hat{p}_E,t,t'\right) & 0\\ 0 & L^{q}_{2}\left(\hat{p}_E,t,t'\right)\end{pmatrix}, \tag{3.85}$$

$$\Delta^{A>}_{RL}\left(t,t';p^2_E\right)=\Delta^{A<}_{RL}\left(t,t';p^2_E\right)+\frac{\sqrt{tt'}}{M_{\mathrm{kk}}1_\eta}\begin{pmatrix}L^{Q}_{4}\left(\hat{p}_E,t,t'\right) & 0\\ 0 & -L^{q}_{1}\left(\hat{p}_E,t,t'\right)\end{pmatrix}, \tag{3.86}$$

with $L^{A}_{i}\left(\hat{p}_E,t,t'\right)=\frac{\pi p_E 1_\eta}{2\cos(c_A\pi)}D^{A}_{i}\left(\hat{p}_E,t,t'\right)$ and $1_\eta=1-\eta$. In conclusion, the equations Eq. (3.74), Eq. (3.75), Eq. (3.85) and Eq. (3.86) depend on the matrix functions $K\left(t'\right),i=1,...,4$.

3.2.0.4 Solution of the propagator functions in the region $t>(1-\eta)$

There is no exact solution of a general choice of η in the region $t>(1-\eta)$, in which the Yukawa matrices are relevant. In the case of $\eta\ll 1$, the contribution is enhanced proportional to a factor of η^{-1} and dominates over the term that contains the bulk mass parameter. Terms proportional $\eta\ll v\left|Y_q\right|/M_{\mathrm{kk}}$ are suppressed and this inequality is at the same time an upper bound for the regulator η and the definition of the narrow bulk Higgs scenario that is described in Sec. 2.2.3. The solutions read in the case of $t_>$:

$$\Delta^{A>}_{LL}\left(t,t';p^2_E\right)=\begin{pmatrix}\mathcal{C}^\dagger\left(t\right) & 0\\ 0 & \bar{\mathcal{S}}^\dagger\left(t\right)\end{pmatrix}\begin{pmatrix}C_1\left(t'\right) & C_2\left(t'\right)\\ C_3\left(t'\right) & C_4\left(t'\right)\end{pmatrix}, \tag{3.87}$$

$$\Delta^{A>}_{RL}\left(t,t';p^2_E\right)=\frac{M_{\mathrm{kk}}}{\eta}\begin{pmatrix}S^\dagger_q\mathcal{S}^\dagger\left(t\right) & \frac{v}{\sqrt{2}M_{\mathrm{kk}}}Y_q\bar{\mathcal{S}}^\dagger\left(t\right)\\ \frac{v}{\sqrt{2}M_{\mathrm{kk}}}Y^\dagger_q\mathcal{C}^\dagger\left(t\right) & S^\dagger_q\bar{\mathcal{C}}^\dagger\left(t\right)\end{pmatrix}\begin{pmatrix}C_1\left(t'\right) & C_2\left(t'\right)\\ C_3\left(t'\right) & C_4\left(t'\right)\end{pmatrix} \tag{3.88}$$

that contain the 3×3 matrices

$$S=\sqrt{X^2_q+\eta^2p^2_E},\quad X_q=\frac{v}{\sqrt{2}M_{\mathrm{kk}}}\sqrt{Y_qY^\dagger_q}, \tag{3.89}$$

$$\bar{S}=\sqrt{\bar{X}^2_q+\eta^2p^2_E},\quad \bar{X}_q=\frac{v}{\sqrt{2}M_{\mathrm{kk}}}\sqrt{Y^\dagger_qY_q}, \tag{3.90}$$

and the trigonometric functions

$$\mathcal{S}(t)=\sinh\left(S_q\frac{1-t}{\eta}\right),\quad \mathcal{C}(t)=\cosh\left(S_q\frac{1-t}{\eta}\right). \tag{3.91}$$

In the case of $t_<$, the jump conditions should be taken into account. Then, the following expressions for the propagators are obtained:

$$\Delta_{LL}^{A<}\left(t,t';p_E^2\right)=\Delta_{LL}^{A>}\left(t,t';p_E^2\right)+\frac{\eta}{M_{\rm kk}^2}\begin{pmatrix}\frac{\mathcal{S}^\dagger(1-t'+t)}{S_q^\dagger} & 0\\ 0 & \frac{\bar{\mathcal{S}}^\dagger(1-t'+t)}{\bar{S}_q^\dagger}\end{pmatrix}, \tag{3.92}$$

$$\Delta_{RL}^{A<}\left(t,t';p_E^2\right)=\Delta_{RL}^{A>}\left(t,t';p_E^2\right)+\frac{1}{M_{\rm kk}}\begin{pmatrix}\mathcal{C}^\dagger(1-t'+t) & \frac{v}{\sqrt{2}M_{\rm kk}}Y_q\frac{\bar{\mathcal{S}}^\dagger(1-t'+t)}{\bar{S}_q^\dagger}\\ \frac{v}{\sqrt{2}M_{\rm kk}}Y_q^\dagger\frac{\mathcal{S}^\dagger(1-t'+t)}{S_q^\dagger} & \bar{\mathcal{C}}^\dagger(1-t'+t)\end{pmatrix} \tag{3.93}$$

Now, all functions are derived that are needed for an exact solution of the propagator functions in both regions $t_<$ and $t_>$, respectively, in order to determine the 8 matrix functions $K_i(t')$ and $C_i(t')$, $i=1,...,4$.

3.2.0.5 Matching at $t=(1-\eta)$ and results

The requirement of the continuity at $t=1-\eta$ implies a specification of $t'_<=t'<1-\eta$ and $t'_>=t'>1-\eta$. Continuous solutions for the coefficients in the region $t'_<$ are obtained by using the equation

$$\Delta_{BL}^{A<}\left(1-\eta-0,t';p_E^2\right)=\Delta_{BL}^{A>}\left(1-\eta+0,t';p_E^2\right),\quad B=L,R, \tag{3.94}$$

where both Eq. (3.74) and Eq. (3.87) are used in the case of $\Delta_{LL}^{A}\left(t,t';p_E^2\right)$ as well as Eq. (3.75) and Eq. (3.88) are used in the case of $\Delta_{RL}^{A}\left(t,t';p_E^2\right)$. As a consequence, the matrix valued functions $K_i(t')$ and $C_i(t')$, $i=1,...,4$ are determined unambiguously for $t'\in[\epsilon,1]$. In the brane localized Higgs scenario where $t,t'\,[\epsilon,1-\eta]$, the components for $\Delta_{LL}^{q}\left(t,t';p_E^2\right)$ read

$$\Delta_{LL}^{q}\left(t,t';-p^2\right)\Big|_{11}=-\frac{\sqrt{t\,t'}}{p_E M_{\rm kk}}\left[\frac{\mathrm{D}_1^Q(p_E t)}{\mathrm{D}_1^Q(p_E)}R_Q\frac{1}{1+Z_q}\frac{\mathrm{D}_1^Q(p_E t')}{\mathrm{D}_1^Q(p_E)}-\frac{\mathrm{D}_1^Q(p_E t_<)}{\mathrm{D}_1^Q(p_E)}\mathrm{L}_3^Q(p_E,p_E\,t_>)\right] \tag{3.95}$$

$$\Delta_{LL}^{q}\left(t,t';-p^2\right)\Big|_{12}=\frac{\sqrt{t\,t'}}{p_E M_{\rm kk}}\frac{\mathrm{D}_1^Q(p_E t)}{\mathrm{D}_1^Q(p_E)}R_Q\frac{1}{1+Z_q}\rho\tilde{Y}_q\frac{\mathrm{D}_2^q(p_E t')}{\mathrm{D}_2^q(p_E)} \tag{3.96}$$

$$\Delta_{LL}^{q}\left(t,t';-p^2\right)\Big|_{21}=\frac{\sqrt{t\,t'}}{p_E M_{\rm kk}}\frac{\mathrm{D}_2^q(p_E t')}{\mathrm{D}_2^q(p_E)}\rho\tilde{Y}_q^\dagger R_Q\frac{1}{1+Z_q}\frac{\mathrm{D}_1^Q(p_E t)}{\mathrm{D}_1^Q(p_E)} \tag{3.97}$$

$$\Delta_{LL}^{q}\left(t,t';-p^2\right)\Big|_{22}=-\frac{\sqrt{t\,t'}}{p_E M_{\rm kk}}\left[\frac{\mathrm{D}_2^q(p_E t')}{\mathrm{D}_2^q(p_E)}\rho\tilde{Y}_q^\dagger R_Q\frac{1}{1+Z_q}\rho\tilde{Y}_q\frac{\mathrm{D}_2^q(p_E t')}{\mathrm{D}_2^q(p_E)}+\frac{\mathrm{D}_2^q(p_E t_<)}{\mathrm{D}_2^q(p_E)}\mathrm{L}_2^q(p_E,p_E\,t_>)\right] \tag{3.98}$$

and the components for $\Delta_{RL}^{q}\left(t,t';p_E^2\right)$ read

$$\Delta_{RL}^{q,11}=\frac{-\sqrt{tt'}}{M_{\rm kk}}\begin{cases}\frac{D_2^Q(\hat{p}_E,t)}{D_2^Q(\hat{p}_E,1)}\frac{Z_q}{1+Z_q}\frac{D_1^Q(\hat{p}_E,t')}{D_1^Q(\hat{p}_E,1)}+\frac{D_2^Q(\hat{p}_E,t)}{D_2^Q(\hat{p}_E,1)}L_4^Q(\hat{p}_E,t',\epsilon), & t<t',\\ \frac{D_2^Q(\hat{p}_E,t)}{D_2^Q(\hat{p}_E,1)}\frac{Z_q}{1+Z_q}\frac{D_1^Q(\hat{p}_E,t')}{D_2^Q(\hat{p}_E,1)}+\frac{D_1^Q(\hat{p}_E,t')}{D_1^Q(\hat{p}_E,1)}R_Q L_4^Q(\hat{p}_E,1,t), & t'>t\end{cases}$$

$$\Delta_{RL}^{q,12} = \frac{-\sqrt{tt'}}{M_{\rm kk}} \frac{D_2^Q\left(\hat{p}_E,t\right)}{D_2^Q\left(\hat{p}_E,1\right)} \frac{1}{1+Z_q} \frac{v}{\sqrt{2}M_{\rm kk}\tilde{Y}_q} \frac{D_2^q\left(\hat{p}_E,t'\right)}{D_2^q\left(\hat{p}_E,1\right)} \tag{3.99}$$

$$\Delta_{RL}^{q,21} = \frac{-\sqrt{tt'}}{M_{\rm kk}} \frac{D_1^q\left(\hat{p}_E,t\right)}{D_1^q\left(\hat{p}_E,1\right)} \frac{\sqrt{2}M_{\rm kk}}{v\tilde{Y}_q} \frac{Z_q}{1+Z_q} \frac{D_1^Q\left(\hat{p}_E,t'\right)}{D_1^Q\left(\hat{p}_E,1\right)} \tag{3.100}$$

$$\Delta_{RL}^{q,22} = \frac{\sqrt{tt'}}{M_{\rm kk}} \begin{cases} \frac{D_1^q(\hat{p}_E,t)}{D_1^q(\hat{p}_E,1)} \frac{1}{\tilde{Y}_q} \frac{Z_q}{1+Z_q} \tilde{Y}_q \frac{D_2^q(\hat{p}_E,t')}{D_2^q(\hat{p}_E,1)} + \frac{D_1^q(\hat{p}_E,t)}{D_1^q(\hat{p}_E,1)} R_q L_2^q\left(\hat{p}_E,1,t'\right) & t<t', \\ \frac{D_1^q(\hat{p}_E,t)}{D_1^q(\hat{p}_E,1)} \frac{1}{\tilde{Y}_q} \frac{Z_q}{1+Z_q} \tilde{Y}_q \frac{D_2^q(\hat{p}_E,t')}{D_2^q(\hat{p}_E,1)} + \frac{D_2^q(\hat{p}_E,t')}{D_2^q(\hat{p}_E,1)} L_4^q\left(\hat{p}_E,1,t\right), & t'>t \end{cases}, \tag{3.101}$$

with the substitutions

$$1_\eta \to 1,\ S_q \to X_q,\ \bar{S}_q \to \bar{X}_q,\ Z_q^{\eta,i} \to Z_q,\ N^{\eta,i} \to 1+Z_q \tag{3.102}$$

whereas in the case of a narrow bulk localized Higgs in which $t,t' \in [1-\eta,1]$, the components for $\Delta_{RL}^q\left(t,t';p_E^2\right)$ read

$$\begin{aligned} \Delta_{RL}^{q,11} = &-\frac{1}{M_{\rm kk}}\Bigg[\frac{\mathcal{S}\left(t\right)}{\mathcal{S}\left(1_\eta\right)} \left(Z_q^{\eta,1} + \eta\hat{p}_E \frac{\tanh S_q}{S_q} R_Q \right) \frac{1}{N_q^{\eta,1}} \frac{\mathcal{C}\left(t'\right)}{\mathcal{C}\left(1_\eta\right)} \\ &- \frac{\mathcal{C}\left(t+\eta\right)\mathcal{C}\left(t'\right)}{\mathcal{C}\left(1_\eta\right)} + \theta\left(t-t'\right)\mathcal{C}\left(1+t-t'\right) \Bigg] \\ \Delta_{RL}^{q,12} = &-\frac{1}{M_{\rm kk}}\Bigg[\frac{\mathcal{S}\left(t\right)}{\mathcal{S}\left(1_\eta\right)} \frac{1-N_q^{\eta,2}}{N_q^{\eta,2}} \frac{v\tilde{Y}_q}{\sqrt{2}M_{\rm kk}} \frac{\bar{\mathcal{S}}\left(t'\right)}{\bar{\mathcal{S}}\left(1_\eta\right)} + \frac{\mathcal{S}\left(t_>\right)\mathcal{C}\left(t_<+\eta\right)}{\mathcal{S}\left(1_\eta\right)} \frac{v\tilde{Y}_q}{\sqrt{2}M_{\rm kk}} \Bigg] \\ \Delta_{RL}^{q,21} = &-\frac{1}{M_{\rm kk}}\Bigg[\frac{\bar{\mathcal{C}}\left(t\right)\sqrt{2}M_{\rm kk}}{\bar{\mathcal{C}}\left(1_\eta\right)v\tilde{Y}_q} \frac{X_q^2}{S_q^2} \frac{Z_q^{\eta,1}}{N_q^{\eta,1}} \frac{\mathcal{C}\left(t\right)}{\mathcal{C}\left(1_\eta\right)} - \frac{\sqrt{2}M_{\rm kk}}{v\tilde{Y}_q} \frac{X_q^2}{S_q^2} \frac{\mathcal{C}\left(t_>\right)\mathcal{S}\left(t_<+\eta\right)}{\mathcal{C}\left(1_\eta\right)\coth S_q} \Bigg] \\ \Delta_{RL}^{q,22} = &-\frac{1}{M_{\rm kk}}\Bigg[\frac{\bar{\mathcal{C}}\left(t\right)}{\bar{\mathcal{C}}\left(1_\eta\right)} \frac{1}{\tilde{Y}_q} \Bigg[1 - N_q^{\eta,2} + \eta\hat{p}_E \frac{\tanh S_q}{S_q} R_Q \Bigg] \frac{\tilde{Y}_q}{N_q^{\eta,1}} \frac{\bar{\mathcal{S}}\left(t'\right)}{\bar{\mathcal{S}}\left(1_\eta\right)} \\ &+ \frac{\bar{\mathcal{S}}\left(t+\eta\right)\bar{\mathcal{S}}\left(t'\right)}{\bar{\mathcal{C}}\left(1_\eta\right)} + \theta\left(t-t'\right)\mathcal{C}\left(1+t-t'\right) \Bigg] \end{aligned} \tag{3.103}$$

In Eq. (3.99), the arguments $\left(t,t';p_E^2\right)$ that appear in the propagator have been omitted as well as the arguments of both $Z^{\eta,i}\left(p_E^2\right)$ and $N^{\eta,i}\left(p_E^2\right)$. The results obtained for both $\Delta_{LL}^A\left(t,t';p_E^2\right)$ and $\Delta_{RL}^A\left(t,t';p_E^2\right)$ are extended to $\Delta_{RR}^A\left(t,t';p_E^2\right)$ and $\Delta_{LR}^A\left(t,t';p_E^2\right)$ *via*

$$D_{1,2}^A\left(\hat{p}_E,t,t'\right) \to D_{2,1}^A\left(\hat{p}_E,t,t'\right), \qquad \mathcal{S}\left(t\right) \leftrightarrow \mathcal{C}\left(t\right), \tag{3.104}$$

$$L_{2,3}^A\left(\hat{p}_E,1_\eta,t\right) \to -L_{3,2}^A\left(\hat{p}_E,1_\eta,t\right), \qquad L_{1,4}^A\left(\hat{p}_E,1_\eta,t\right) \to -L_{4,1}^A\left(\hat{p}_E,1_\eta,t\right), \tag{3.105}$$

$$R_{Q,q}\left(\hat{p}_E\right) = \frac{D_1^{Q,q}\left(\hat{p}_E,1_\eta\right)}{D_2^{Q,q}\left(\hat{p}_E,1_\eta\right)}, \qquad Y_q \to -Y_q, \qquad \tilde{Y}_q = \frac{\tanh S_q}{S_q} Y_q, \tag{3.106}$$

$$Z_q^{\eta,1}\left(p_E^2\right) = \frac{v^2}{2M_{\rm kk}^2} \frac{S_q^2}{X_q^2} \tilde{Y}_q R_q\left(\hat{p}_E\right) \tilde{Y}_q^\dagger R_Q\left(\hat{p}_E\right), \tag{3.107}$$

$$Z_q^{\eta,2}\left(p_E^2\right) = \frac{v^2}{2M_{\rm kk}^2} \tilde{Y}_q R_q\left(\hat{p}_E\right) \tilde{Y}_q^\dagger \frac{S_q^2}{X_q^2} R_Q\left(\hat{p}_E\right), \tag{3.108}$$

$$N_q^{\eta,1}\left(p_E^2\right) = 1 + Z_q^{\eta,1}\left(p_E^2\right) + \eta\hat{p}_E \left[\frac{\coth S_q}{R_Q\left(\hat{p}_E\right) S_q} Z_q^{\eta,1}\left(p_E^2\right) + \frac{\tanh S_q}{S_q} R_q\left(\hat{p}_E\right) \right], \tag{3.109}$$

$$N_q^{\eta,2}\left(p_E^2\right) = 1 + Z_q^{\eta,2}\left(p_E^2\right) + \eta\hat{p}_E\left[Z_q^{\eta,2}\left(p_E^2\right)\frac{\coth S_q}{R_Q\left(\hat{p}_E\right)S_q} + \frac{\tanh S_q}{S_q}R_q\left(\hat{p}_E\right)\right], \quad (3.110)$$

$$Z_q^{\eta,i}\left(p_E^2\right) \to R_Q\left(\hat{p}_E\right)\frac{1}{Z_q^{\eta,i}\left(p_E^2\right)}\frac{1}{R_Q\left(\hat{p}_E\right)}, \quad (3.111)$$

$$\frac{1}{N_q^{\eta,1}\left(p_E^2\right)} \to R_Q\left(\hat{p}_E\right) Z_q^{\eta,1}\left(p_E^2\right)\frac{1}{N_q^{\eta,1}\left(p_E^2\right)}\frac{1}{R_Q\left(\hat{p}_E\right)}, \quad (3.112)$$

$$\frac{1}{N_q^{\eta,2}\left(p_E^2\right)} \to R_Q\left(\hat{p}_E\right)\frac{1}{N_q^{\eta,1}\left(p_E^2\right)} Z_q^{\eta,2}\left(p_E^2\right)\frac{1}{R_Q\left(\hat{p}_E\right)} \quad (3.113)$$

with an overall minus sign in the case of $\Delta_{LR}^A\left(t,t';p_E^2\right)$. Furthermore, the propagator functions $\Delta_{RL}^A\left(t,t';p_E^2\right)$ and $\Delta_{RL}^A\left(t,t';p_E^2\right)$ are connected to each other *via* both a complex conjugation as well as an interchange of $t \leftrightarrow t'$. The propagator function $\Delta_{LL}^A\left(t,t';p_E^2\right)$ gets the same result with its hermitian conjugate $\Delta_{RR}^A\left(t,t';p_E^2\right)$ if $t \leftrightarrow t'$ are interchanged. This can be proven *via* the KK representation of the 5D fermion propagator in Eq. (3.59).

4 Loop–induced Higgs decay into two photons $h \to \gamma\gamma$ in the RS model

The decay $h \to \gamma\gamma$ was studied originally by [196] in the middle of the 70s. Another consideration of this decay was done by [197]. The authors of [197] considered the $h \to \gamma\gamma$ decay with a Higgs mass m_h in both Feynman t'Hooft gauge and in non–linear gauges. For small masses, the results of [196, 197] agree.
In this Chapter, the publication [193] is discussed at greater detail as the author of this thesis is one of the authors of this publication. The calculation has been done by every author of [193] independently, and led to several diploma theses, master theses, and PhD theses [129, 130, 198, 199]. Furthermore, the calculation served the co–authors as a crosscheck of both their and the other authors' calculations, respectively. The calculation for an arbitrary R_ξ gauge has been done by J. Hahn in [198]. The aim of this investigation of the $h \to \gamma\gamma$ decay in RS models was a determination of possible effects from the KK modes that could give sizable contributions to the SM value. If these deviations from the SM value had existed, they could have given a hint for new physics.

4.1 Introduction and first steps

The decay $h \to \gamma\gamma$ has been studied originally by various authors [121, 200–203] in the context of extra dimensions/ The proof of the gauge invariance of $h \to \gamma\gamma$ that has been done in the SM [204]. The authors of [121, 200–202] highlighted different points and their work led to discussions, which the following analysis addresses. The analysis in [202] was the first calculation that considered the impact of the full KK tower of W bosons in the decay $h \to \gamma\gamma$. In [121], the calculation of both the contribution of $\mathbb{Z}_2$–even and $\mathbb{Z}_2$–odd fermions as well as the impact of the corresponding Yukawa couplings to $h \to \gamma\gamma$ were addressed. The results of [121] suggested an enhancement of the decay rate $\Gamma(h \to \gamma\gamma)$ compared to the SM, because of the contributions of the fermion KK tower, whereas the authors of [200] came to the opposite conclusion. It turned out that the discrepancies in the results of [121, 200] occurred due to the Higgs localization in the RS model, because [121] considered the scenario with a brane–localized Higgs and [200] investigated the $h \to \gamma\gamma$ decay in the narrow bulk Higgs scenario. The two Higgs scenarios mentioned are described in Sec.2.2.
As a next step, the gauge boson contributions to the $h \to \gamma\gamma$ decay are discussed and the scalar components are investigated in more detail, because their profile functions show the same discontinuity behavior as both the $\mathbb{Z}_2$–even and $\mathbb{Z}_2$–odd fermion profile functions at the IR brane. At the best knowledge of the authors of [193], a formula has not been published before. The two main goals were to show the gauge independence of the decay amplitude in the RS model and the independence of the Higgs localization. The gauge independence is shown and explained in Sec. 4.3 and the results of [121] are

confirmed if the the result is expanded at $\mathcal{O}\left(v^2/M_{\text{kk}}^2\right)$. This was done to distinguish the W bosons and their KK tower. Applied in the framework of the custodial model, the analysis yielded an exact expression for the $h \to \gamma\gamma$ decay, as well and the result has been expanded. This leads to a confirmation of the results obtained in [200].
The investigation of both fermion contributions and boson contribution is motivated by the fact that all particles that couple to both the Higgs and the photon have to be taken into account for the consideration of the virtual particles that run in the loop. Fermion contributions are considered in Sec. 4.5, because they couple in Eq. (2.86) to the Higgs *via* the Yukawa couplings and the kinetic term in Eq. (2.44) to the photon. The W boson is another particle that also couples to both the Higgs boson and the photon *via* the kinetic term in Eq. (2.44).

4.2 Details of the calculation of the amplitude

The following steps are necessary to achieve a complete description of the $h \to \gamma\gamma$ amplitude from a pure 5D perspective. The goal is to express the amplitude using both the 5D boson and fermion propagators. Then, the KK decomposition is inserted into the propagator. The exact formula that is going to be derived describes the overlap integrals of the Higgs boson with the transverse polarization of the W boson. It includes the exact dependence of the Higgs mass. As a preparation, the gauge independence of the $h \to \gamma\gamma$ decay is investigated in Sec. 4.3. As a next step, the contributions of the vector bosons are investigated using the KK decomposition showing that the whole tower of the KK excitations is gauge independent. The decay is further investigated in the unitary gauge, as there is only one contribution containing the vector bosons which can be expressed *via* the gauge boson propagator. Before the investigation is continued in the custodial RS model, the decay in the RS minimal model is discussed.
In unitary gauge, the diagrams Fig. 4.1a–Fig. 4.1c of Fig. 4.1 contribute to the calculation of the $h \to \gamma\gamma$ amplitude. The amplitude itself is considered in an effective field theory expansion that contains the following Wilson coefficients

$$\mathcal{A}\left(h \to \gamma\gamma\right) = C_{1\gamma}\frac{\alpha}{6\pi v}\langle\gamma\gamma\big|\ F_{\mu\nu}F^{\mu\nu}\big|0\rangle - C_{5\gamma}\frac{\alpha}{4\pi v}\langle\gamma\gamma\big|\ F_{\mu\nu}\tilde{F}^{\mu\nu}\big|0\rangle, \tag{4.1}$$

where the Wilson coefficient $C_{1\gamma}$ corresponds to the CP even term of the effective Lagrangian

$$\mathcal{L}_{\text{eff}} \ni C_{1\gamma} v h F_{\mu\nu}F^{\mu\nu} + C_{5\gamma} v h F_{\mu\nu}\tilde{F}^{\mu\nu} = \mathcal{L}_{\text{CPeven}} + \mathcal{L}_{\text{CPodd}} \tag{4.2}$$

and $C_{5\gamma}$ corresponds to the CP odd term of Eq. (4.2). Each of the two Wilson coefficients in Eq. (4.1) involve contributions from fermions. Furthermore, they include contributions from the W boson, ghosts, and Goldstone bosons and read

$$C_{i,\gamma} = C_{i,\gamma}^{W} + C_{i,\gamma}^{q} + C_{i,\gamma}^{l} \qquad \forall i = 1, 5. \tag{4.3}$$

4.3 Gauge independence of the $h \to \gamma\gamma$ amplitude

The gauge independence of the $h \to \gamma\gamma$ amplitude in arbitrary R_ξ gauge was proven in [204]. It was shown by [204] that it is possible to perform the calculation in the unitary gauge consistently. For the consideration of the ξ independence in the RS model, it is suitable to consider the KK decomposed theory in a first step, because both the Feynman

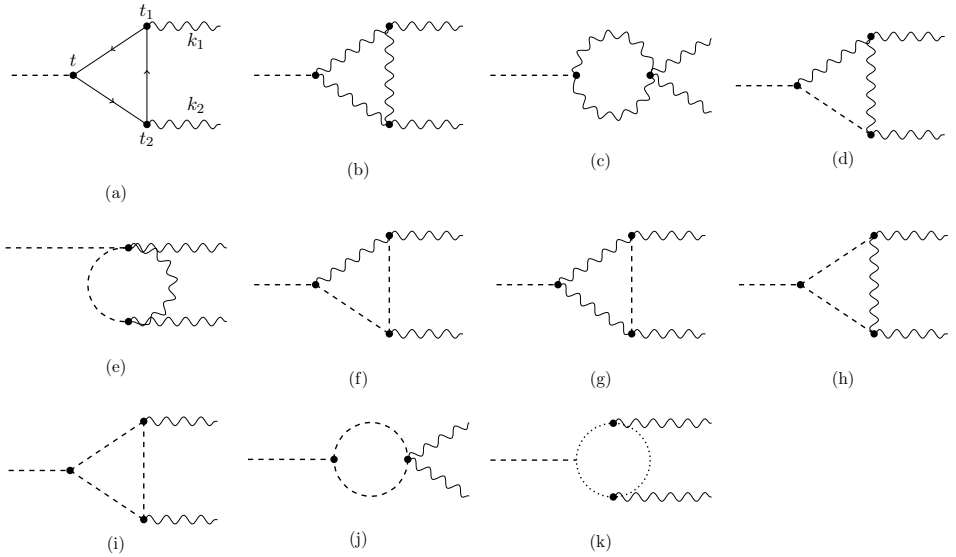

Figure 4.1: Diagrams contributing in the R_ξ gauge to the decay $h \to \gamma\gamma$. The momenta and extra–dimensional coordinates of the diagrams Fig. 4.1b–Fig. 4.1k are labeled in the same way as Fig. 4.1a.

rules in the KK decomposed theory and the structure of the Feynman propagator follow analogously to the SM case. As a consequence, the amplitude of the contributions of the bosons in the KK decomposed theory in the RS model

$$\mathcal{A}^W_{\mathrm{RS}}\left(h \to \gamma\gamma\right) = \frac{\tilde{m}^2_W}{v} \sum_{n=0}^{\infty} 2\pi \left[\chi^W_n\left(1\right)\right]^2 \left[\frac{v_{\mathrm{SM}}}{m^2_W} \mathcal{A}^W_{\mathrm{SM}}\left(h \to \gamma\gamma\right)\right]_{m_W \to m^{(n)}_W} \tag{4.4}$$

differs only in small substitutions compared to the SM expression that stem from the requirements of the RS model, which are explained in the following. The Feynman rules in the KK decomposed theory can be found in Sec. A.1.

Three main facts are discussed in further details below and are elaborated by considering the analogy between the SM model and the RS model in its KK decomposed theory:

The fact that the couplings of the KK modes to external photons (*i.e.* one or more, *c.f.* Fig. 4.1j) are solely diagonal after the integration of the extra dimensional coordinate $\int_{\epsilon}^{1} \mathrm{d}t \, \frac{2\pi}{L} \frac{\mathrm{d}t}{t}$. An additional comparison of coefficients leads to the relation $e = e_5/\sqrt{2\pi r}$ and furthermore to an analogous form of the Feynman rules in the RS model compared to the Feynman rules in the SM. In the case of a mass dependent vertex, *i.e.* a coupling including $W^{\pm,(n)}$ or $\varphi^{\pm,(n)}_W$ particles to the photon, the mass shift $m_W \to m^{(n)}_W$ has to be made.

This has the consequence that only one KK particle runs in the loop of all 1–loop diagrams that contribute to $h \to \gamma\gamma$. Thus, only diagonal couplings of the Higgs profile to the KK profiles are required.

The last statement leads to the result that the couplings of the Higgs to the KK profiles have the same structure as in the SM, but differ by an overall factor

$$\frac{v}{2} \frac{g^2_5}{2\pi r} 2\pi \left[\chi^W_n\left(1\right)\right]^2 = \frac{2\tilde{m}^2_W}{v} 2\pi \left[\chi^W_n\left(1\right)\right]^2 \tag{4.5}$$

compared to the SM expression. The SM expression $gm_W = 2m_W^2/v_{\text{SM}}$ in which v_{SM} denotes the SM VEV that is defined by $v_{\text{SM}} = \left(\sqrt{2}G_F\right)^{-\frac{1}{2}}$ *via* the Fermi constant is replaced by Eq. (4.5). As already mentioned, the W mass has to be replaced by its corresponding expression for the Feynman rule in the KK picture whenever a W mass appears that enters through a scalar NGB $\varphi^{\pm,(n)}$ or a W boson at the corresponding vertex. The Feynman rule for the diagram Fig. 4.1j results after the integration of the vertex in

$$2ie^2\eta_{\mu\nu}\left[\frac{M_{\text{kk}}^2}{m_W^n m_W^m}\frac{2\pi}{L}\int\limits_{\epsilon}^{1}\frac{\mathrm{d}t}{t}\left[\partial_t\chi_m^W(t)\right]\left[\partial_t\chi_n^W(t)\right]+\frac{2\pi\tilde{m}_W^2}{m_W^n m_W^m}\chi_n^W(1)\,\chi_m^W(1)\right]. \tag{4.6}$$

The first term of Eq. (4.6) originates from the $W_5W_5A_\mu A^\mu$ term of the Yang-Mills action of the W boson and its corresponding KK decomposition, whereas the second term of Eq. (4.6) stems from the kinetic term of the Higgs doublet with its KK decomposition, to be more precise from $\varphi^-\varphi^+A_\mu A^\mu$. Thus, the boundary terms cancel the contribution of the term stemming from the $\varphi^-\varphi^+A_\mu A^\mu$ part after an integration by parts of the first term and after the application of the EOM, Eq. (4.6) now reads

$$2ie^2\eta_{\mu\nu}\left[\frac{m_W^n}{m_W^m}\frac{2\pi}{L}\int\limits_{\epsilon}^{1}\frac{\mathrm{d}t}{t}\,\chi_n^W(t)\,\chi_m^W(t)\right]. \tag{4.7}$$

The SM expression for Eq. (4.7) is $2ie^2\eta_{\mu\nu}$. The similarity of Eq. (4.7) compared to the SM expression for the vertex is apparently after the application of the orthonormality condition Eq. (2.21). The gauge invariance of the full amplitude $\mathcal{A}_{\text{RS}}^W(h\to\gamma\gamma)$ to the decay $h\to\gamma\gamma$ is fulfilled for each KK mode in the RS model as long as the amplitude remains gauge invariant in the SM. In the RS model, the 5D gauge invariance is a consequence of the convergent sum over all KK modes that can be traced back to Eq. (3.9). In the SM, the gauge invariance is shown *via* a separation of the gauge boson propagator in the R_ξ gauge:

$$\frac{i}{p^2-m_W^2}\left(\frac{(1-\xi)\,p^\mu p^\nu}{p^2-\xi m_W^2}-\eta^{\mu\nu}\right)=\frac{i}{p^2-m_W^2}\left(\frac{p^\mu p^\nu}{m_W^2}-\eta^{\mu\nu}\right)-\frac{i}{p^2-m_W^2}\frac{p^\mu p^\nu}{\xi m_W^2}. \tag{4.8}$$

Here, in the term $\frac{i}{p^2-m_W^2}\left(\frac{p^\mu p^\nu}{m_W^2}-\eta^{\mu\nu}\right)$ denotes the propagator in unitary gauge and the ξ dependent part $\frac{i}{p^2-\xi m_W^2}\frac{p^\mu p^\nu}{m_W^2}$ has the same structure as both the scalar propagator and the ghost propagator, respectively. Marciano et al. showed in [204] that the ξ–dependent contributions of Eq. (4.8) cancel after some transformations of the contributions of the ξ–dependent expressions. As a consequence, only the diagrams in Fig. 4.1b and Fig. 4.1c remain, which contains the W boson propagator in the unitary gauge. The fermion contributions are ξ independent and the diagram in Fig. 4.1a remains, as well.
In the RS model, the calculation is performed in the unitary gauge after the confirmation of the gauge invariance of the amplitude in the RS model by a comparison to the results obtained in [204].

4.4 Contributions of boson diagrams to the $h\to\gamma\gamma$ amplitude

Besides the fermion contributions, diagrams that contain vector bosons are considered, as well. Only the diagrams Fig. 4.1b–Fig. 4.1c of Fig. 4.1 contribute in the unitary gauge

and lead to the following amplitude

$$i\mathcal{A}\left(h\to\gamma\gamma\right)=-\frac{2\tilde{m}_W^2}{v}2\pi e^2\varepsilon_\mu^*\left(k_1\right)\varepsilon_\nu^*\left(k_2\right)\eta^{\alpha\beta}\int\frac{d^dp}{\left(2\pi\right)^d}\int\limits_\epsilon^1\mathrm{d}t\,\delta^\eta\left(t-1\right)\frac{2\pi}{L}\int\limits_\epsilon^1\frac{\mathrm{d}t_1}{t_1}$$
$$\left[\frac{2\pi}{L}\int\limits_\epsilon^1\frac{\mathrm{d}t_2}{t_2}2V^{\gamma\mu\lambda\rho\nu\delta}D_{W,\alpha\gamma}^{\xi\to\infty}\left(t,t_1,p+k_1\right)D_{W,\lambda\rho}^{\xi\to\infty}\left(t_1,t_2,p\right)D_{W,\delta\beta}^{\xi\to\infty}\left(t_2,t,p-k_2\right)\right.$$
$$\left.\left(2\eta^{\gamma\delta}\eta^{\mu\nu}-\eta^{\delta\nu}\eta^{\gamma\mu}-\eta^{\nu\gamma}\eta^{\mu\delta}\right)D_{W,\alpha\gamma}^{\xi\to\infty}\left(t,t_1,p+k_1\right)D_{W,\beta\delta}^{\xi\to\infty}\left(t_1,t,p-k_2\right)\right]\tag{4.9}$$

with $V^{\gamma\mu\lambda\rho\nu\delta}=V^{\gamma\mu\lambda}\left(p+k_1,-k_1,-p\right)V^{\rho\nu\delta}\left(p,-k_2,k_2+p\right)$ that is the abbreviation for the triple gauge coupling $V^{\mu\nu\rho}\left(k,p,q\right)=\eta^{\mu\nu}\left(k-p\right)^\rho+\eta^{\nu\rho}\left(p-q\right)^\mu+\eta^{\rho\mu}\left(q-k\right)^\nu$. The main interest is the expression in Eq. (4.9), in which the Feynman parameter integral and the 5D propagator of the gauge boson appear. Before the amplitude is expressed with the help of the 5D gauge boson propagator, the 5D boson propagator is re–expressed by an insertion of the KK decomposition similar to the result obtained in Eq. (3.9). It turns out that only one mode runs in the loop in the KK–decomposed theory. Writing the 5D boson propagator in its KK–decomposed equivalent is the same trick as the introduction of the Feynman parametrization. With the application of the KK decomposition, it is possible to simplify the expression using the orthonormality relation in Eq. (2.21), which eliminates an extra–dimensional coordinate. This procedure is repeated in the case of the decay amplitude for $h\to\gamma\gamma$, because the amplitude depends on three extra–dimensional coordinates t, t_1, t_2, and two external photons. This leads to a dependence on only one extra–dimensional coordinate t. The possibility to apply the orthonormality relation in Eq. (2.21) is a direct consequence of the diagonality of the photon vertex. As a next step, the expression in the KK decomposition is rewritten in the 5D picture and results in the expression of the 5D boson propagator. As a consequence, the KK decomposition does not appear anymore. This is shown in the following with the Wilson coefficients for the boson contribution. A further simplification is done *via* the Passarino Veltman reduction [205, 206] that simplifies the expression to scalar integrals after the deduction of the Dirac structure in Eq. (4.9). Summing the contributions of all diagrams and setting the regulator $\hat{\epsilon}=0$ leads to the boson contribution of the Wilson coefficient $C_{1\gamma}^W$ with its full expression in the KK decomposition

$$C_{1\gamma}^W=-3\pi\tilde{m}_W^2\int\limits_\epsilon^1\mathrm{d}t\,\delta^h\left(t-1\right)\sum_{n=0}^\infty\left[\chi_n^W\left(t\right)\right]^2\left(\frac{1}{m_W^{n,2}}+6\int\limits_0^1\mathrm{d}x\int\limits_0^{1-x}\mathrm{d}y\frac{1-2xy}{m_W^{n,2}-xym_h^2-i0}\right)\tag{4.10}$$
$$C_{5\gamma}^W=0.$$

Furthermore, the simplification of the latter equations is possible by an insertion of the 5D propagator into Eq. (4.10)

$$C_{1\gamma}^W=-3\pi\tilde{m}_W^2\left[T_W\left(0\right)+6\int\limits_0^1\mathrm{d}x\int\limits_0^{1-x}\mathrm{d}y\left(1-2xy\right)T_W\left(-xym_h^2\right)\right]\tag{4.11}$$

that includes

$$T_W\left(-p^2\right)=\int\limits_\epsilon^1\mathrm{d}t\,\delta^\eta\left(t-1\right)B_W\left(t,t;-p^2-i0\right)=B_W\left(1,1;-p^2-i0\right)+\mathcal{O}\left(\eta\right).\tag{4.12}$$

The expression $T_W\left(-p^2\right)$ is the overlap integral of the Higgs profile function and includes the transverse component of the W boson propagator that is now evaluated at $t = 1 = t'$. This is also true in the case for time–like momenta, *i.e.* $\hat{p} \equiv p/M_{\rm kk} + i0$. As a consequence, the exact result of the Wilson coefficient $C_{1\gamma}^W$ depends on both the Higgs profile function and the W boson propagator. After the Wick rotation, the denominator of Eq. (4.10) is expressed by $\left(p_E^2 + m_W^2 - xym_h^2\right)^{-3}$, for which $\partial_{p_E^2}^2 T_W\left(p_E^2 - xym_h^2\right)$ is an equivalent expression. The existence of the integral requires that the functions $T_W\left(p_E^2\right)$ and $p_E \partial_{p_E} T_W\left(p_E^2\right)$ have to vanish for large p_E^2. Thus, $T_W\left(p_E^2\right)$ results in an expression valid at $\mathcal{O}\left(v^2/M_{\rm kk}^2\right)$

$$T_W\left(-p^2\right) = \frac{1}{2\pi\tilde{m}_W^2}\left[1 + \frac{\hat{p}M_{\rm kk}^2}{L\tilde{m}_W^2}\frac{J_0\left(\hat{p}\right)Y_0\left(\hat{p}\hat{\epsilon}\right) - Y_0\left(\hat{p}\right)J_0\left(\hat{p}\hat{\epsilon}\right)}{J_1\left(\hat{p}\right)Y_0\left(\hat{p}\hat{\epsilon}\right) - Y_1\left(\hat{p}\right)J_0\left(\hat{p}\hat{\epsilon}\right)}\right]^{-1} \equiv \frac{1}{2\pi\tilde{m}_W^2}\hat{T}_W\left(-p^2\right). \quad (4.13)$$

Using an expansion of the Bessel functions for small arguments, Eq. (4.13) can be further simplified to $\hat{T}\left(0\right) = 1$. A closed analytic expression for the Wilson coefficient $C_{1\gamma}^W$ in Eq. (4.10) is derived in the minimal RS model with a brane–localized Higgs using the function $\hat{T}_W\left(-p^2\right)$. Keeping the leading order contribution to the physical W boson mass, $\tilde{m}_W$, m_W cancels the first term in Eq. (4.10). With these simplifications, $C_{1\gamma}^W$ now results in

$$C_{1\gamma}^W = -\frac{3}{2}\left[1 + 6\int_0^1 {\rm d}x \int_0^{1-x} {\rm d}y\,(1-2xy)\,\hat{T}_W\left(-xym_h^2\right)\right]. \quad (4.14)$$

In the case of a consideration of the propagator function in regions of space like momenta $p_E \gg M_{\rm kk}$, $T_W\left(p_E^2\right)$ shows a power–law dependence *via*

$$T_W\left(p_E^2\right) = \frac{L}{2\pi M_{\rm kk}}\frac{1}{p_E} + \mathcal{O}\left(p_E^{-2}\right). \quad (4.15)$$

If large euclidean momenta in the region $p_E^2 = -p^2 \to \infty$ are considered, both contributions $T_W\left(p_E^2\right)$ and $p_E\partial_{p_E}T_W\left(p_E^2\right)$ vanish and the conditions for an integration of Eq. (4.10) are fulfilled.

Besides the contributions to $C_{1\gamma}^W$, there are contributions that stem from the narrow bulk Higgs. For a general bulk Higgs field $\chi_n^h\left(t\right)$, Eq. (4.11) is still fulfilled using the results of [140] if the corresponding Higgs boson propagator is derived. The regularized delta function in Eq. (4.12) is replaced by

$$\delta^h\left(t-1\right) \to \frac{2\pi}{Lt}\frac{v\left(t\right)}{v}\chi_n^h\left(t\right) = 2\left(1+\beta\right)t^{1+2\beta} + ..., \quad (4.16)$$

with $v\left(t\right)$ being the profile function of the Higgs VEV that has been derived in Eq. (2.79) in Sec. 2.2. Considering $\beta \gg 1$, the function leads to a regularized delta function of width $\eta/(2\beta)$. The Higgs profile function contains a tower of scalar KK excitations that are considered to be physical, because the Higgs profile function $\chi_n^h\left(t\right)$ is not localized on the IR brane any more and gets a small width in a region where $\eta \ll v\left|Y_q\right|/\eta \ll \Lambda_{\rm TeV}$. These excitations originate from the $\varphi^\pm$ scalar in the Higgs doublet in Eq. (2.59). As the authors of [200] deduced in a clear way, these additional scalar field excitations are expressed *via* a superposition of both $W_\phi^\pm$ and $\varphi^\pm$. Furthermore, the authors of [200] summarized these contributions in

$$C_{1\gamma}^\phi = \frac{1}{8}\sum_{n=1}^{\infty}\frac{vg_{\phi\phi}^{(n,n)}}{\left(m_n^2\right)^2}A_\phi\left(\tau_n^\phi\right), \qquad C_{5\gamma}^\phi = 0 \quad (4.17)$$

with

$$A_\phi(\tau) = [3\tau f(\tau) - 1] \tag{4.18}$$

that includes the function

$$f(\tau) = \arctan^2\left(\frac{1}{\sqrt{\tau - 1}}\right) \quad \text{and} \quad \tau_n^\phi = 4\left(m_{(n)}^\phi\right)^2 / m_h^2 \tag{4.19}$$

and contributes to the full amplitude. The couplings $g_{\phi\phi}^{(n,n)}$ scale with $1/\eta$ in the case of an extremely narrow bulk Higgs profile. As a consequence, the particle masses scale with M_{kk}/η. The decoupling appears in the limit $\eta \to 0$, because $C_{1\gamma}^\phi = \mathcal{O}(\eta)$. The coefficient $C_{1\gamma}^\phi$ is 1 in the limit for large values of τ.

4.4.0.6 Contributions to the Wilson coefficients $C_{1\gamma}^W$ and $C_{1\gamma}^\phi$

The contributions to the Wilson coefficients $C_{1\gamma}^W$ and $C_{1\gamma}^\phi$ are in general separated into two parts. In the case of $C_{1\gamma}^W$, the function $T_W\left(-p^2\right)$ defined in Eq. (4.13) is an expression of the W boson propagator that contains SM particles visible in its zero mode and RS particles, which are described by a tower of KK excitations. The investigation of the contribution of both SM part and the KK tower is achieved *via* an application of the Taylor expansion at $\mathcal{O}\left(v^2/M_{\mathrm{kk}}^2\right)$, because the SM momenta are of the same order of the Higgs bosons mass m_h, *i.e.* $|p^2| + \mathcal{O}\left(m_h^2\right)$, which is far below the KK scale M_{kk}. In leading order $\mathcal{O}\left(v^2/M_{\mathrm{kk}}^2\right)$, Eq. (4.13) results in

$$\hat{T}_W\left(-p^2\right) = \frac{m_W^2}{m_W^2 - p^2 - i0}\left(1 - \frac{m_W^2}{2M_{\mathrm{kk}}^2}\left(\frac{L}{c_{\theta_W}^2} - 1 + \frac{1}{2L}\right)\right) + \frac{m_W^2}{2M_{\mathrm{kk}}^2}\left(\frac{L}{c_{\theta_W}^2} - 1 + \frac{1}{2L}\right). \tag{4.20}$$

Here, the value $c_{\theta_W}^2 = 1$ differs from the custodial RS model, which is discussed in the following section and $\tilde{m}_W$ is replaced by the physical W boson mass m_W defined in Eq. (2.43). After the integration of the Feynman parameter, Eq. (4.10) results in

$$C_{1\gamma}^W = -\frac{21}{4}\left[\kappa_W A_W(\tau_W) + \nu_W\right] + \mathcal{O}\left(\frac{v^4}{M_{\mathrm{kk}}^4}\right), \quad C_{5\gamma}^W = 0 \tag{4.21}$$

with $A_W(\tau) = \left[2 + 3\tau + 3\tau(2 - \tau) f(\tau)\right]/7$, $\tau_W = 4\left(m_W\right)^2/m_h^2$, in which the function $f(\tau)$ is 1 in the limit $\tau \to \infty$ [209]. The contribution of the SM W boson in Eq. (4.21) is given by k_W. This contribution contains a modified coupling to the Higgs field by a factor of v_{SM}/v that stems from Eq. (4.1) and ν_W contains the contribution that stems from the KK tower of the W bosons. Both κ_W and ν_W read

$$\begin{aligned} \kappa_W|_{\mathrm{braneHiggs}} &= \left(1 - \frac{m_W^2}{2M_{\mathrm{kk}}^2}\left(\frac{L}{c_{\theta_W}^2} - 1 + \frac{1}{2L}\right)\right), \\ \nu_W|_{\mathrm{braneHiggs}} &= \frac{m_W^2}{2M_{\mathrm{kk}}^2}\left(\frac{L}{c_{\theta_W}^2} - 1 + \frac{1}{2L}\right). \end{aligned} \tag{4.22}$$

Only in leading order and if the limit $\tau \to \infty$ is considered, $\nu_W = (1 = \kappa_W)$ cancels the contributions to Eq. (4.21) that stem from the RS model and the result for $C_{1\gamma}^W$ is the same as obtained in [202]. $\kappa_W = \tilde{m}_W^2 2\pi\left[\chi_0^W(1)\right]^2/m_W^2$ coincides with Eq. (4.5), as well.

In the case of the consideration of a narrow bulk Higgs, Eq. (4.22) changes due to the dependence on the width of the Higgs profile $\eta = 1/(2\beta) \ll 1$ to

$$\begin{aligned}\kappa_W|_{\text{bulkHiggs}} &= \kappa_W|_{\text{braneHiggs}} + \frac{3Lm_W^2}{2M_{\text{kk}}^2}\eta + \mathcal{O}\left(\eta^2\right),\\ \nu_W|_{\text{bulkHiggs}} &= \nu_W|_{\text{braneHiggs}} - \frac{Lm_W^2}{M_{\text{kk}}^2}\eta + \mathcal{O}\left(\eta^2\right).\end{aligned} \tag{4.23}$$

Both Eq. (4.23) and Eq. (4.22) become equivalent to each other in the case of the decay $h \to \gamma\gamma$, *i.e.* the narrow–bulk Higgs scenario transits to the brane–localized Higgs scenario. Of course, Eq. (4.12) only holds in the case for the narrow–bulk Higgs scenario if both the profile function of the Higgs and the gauge boson propagator are replaced by their equivalent expressions, see Eq. (2.81) and Eq. (3.40).
In the following, the investigation of boson contributions to the Wilson coefficients $C_{1\gamma}^W$ and $C_{1\gamma}^\phi$ of the decay $h \to \gamma\gamma$ in the minimal RS model is extended to the custodial RS model. Whenever possible, as much as necessary, as less as possible changes to the procedure how the Wilson coefficients in the minimal RS model case were made.

4.4.1 Contributions of $C_{1\gamma}^W$ and $C_{1\gamma}^\phi$ in the custodial RS model

The Feynman rules are obtained in a similar way to the Feynman rules in the minimal RS model and given in Sec. A.1. The couplings of the $W^\pm$ bosons to the photon γ do not change at all, because the orthonormality condition still holds. The validity of the orthonormality condition is basis–independent, as the rotation matrix $\mathbf{R}_{\theta_W}$ is not included in the orthonormality condition. The derivation of the Higgs coupling to the $W^\pm$ is more challenging as the Higgs profile couples on the IR brane to the basis fields $\tilde{A}_\mu^\pm$ with a coupling strength proportional to $\left(g_{L,5}^2 + g_{R,5}^2\right)$, *cf.* Sec. 2.1. This is resolved using the projection operator $\mathbf{P}_+$ by a rotation into the IR basis with an additional factor $1/c_{\theta_W}^2$. Compared to the SM, the coefficient of all diagonal KK modes that couple to the Higgs boson is now

$$\frac{2\tilde{m}_W^2}{c_{\theta_W}^2 v} 2\pi \vec{\chi}_n^W(1)^T \mathbf{R}_{\theta_W}^T \mathbf{P}_+ \mathbf{R}_{\theta_W} \vec{\chi}_n^W(1) = \frac{2\tilde{m}_W^2}{c_{\theta_W}^2 v} 2\pi \vec{\chi}_n^W(1)^T \mathbf{D}_{\theta_W} \vec{\chi}_n^W(1)\,. \tag{4.24}$$

Compared to the minimal RS model, see Eq. (4.5), this coefficient has an additional contribution of $\mathbf{D}_{\theta_W} = \mathbf{R}_{\theta_W}^T \mathbf{P}_+ \mathbf{R}_{\theta_W}$. Analogous to the expression of the amplitude in Eq. (4.4) in the minimal RS model, the $h \to \gamma\gamma$ amplitude in the custodial model reads

$$\mathcal{A}(h \to \gamma\gamma)\big|_{\text{cust}} = \frac{\tilde{m}_W^2}{c_{\theta_W}^2 v} \sum_{n=0}^{\infty} 2\pi \vec{\chi}_n^W(1)^T \mathbf{D}_{\theta_W} \vec{\chi}_n^W(1) \left[\frac{v_{\text{SM}}}{m_W^2} \mathcal{A}_{\text{SM}}^W(h \to \gamma\gamma)\right]_{m_W \to m_W^{(n)}}. \tag{4.25}$$

The integral of the Wilson coefficient $C_{1\gamma}^W$ in Eq. (4.14) remains valid if the expression for $T\left(-p^2\right)$ in Eq. (4.12) is replaced by

$$T\left(-p^2\right) = \text{Tr}\left[\frac{\mathbf{D}_{\theta_W}}{c_{\theta_W}^2} B^{\text{UV}}\left(1,1;-p^2 - i0\right)\right]. \tag{4.26}$$

This equation includes the expression for the boson propagator in the UV basis defined in Eq. (3.36). After an expansion of Eq. (4.26) at $\mathcal{O}\left(v^2/M_{\text{kk}}^2\right)$ with $\left|p^2\right|$ of $\mathcal{O}\left(m_h^2\right)$, Eq. (4.20)

is obtained. Compared to the expression in the minimal RS model, there is a difference by a factor $1/c^2_{\theta_W}$ in the term containing the L–enhanced correction that affects the contributions to both the W boson and the KK tower. Compared to the custodial RS model and its P_{LR}–symmetry, this enhancement results in a factor 2. Inserting $c^2_{\theta_W} = \frac{1}{2}$ in both ν_W and κ_W in Eq. (4.22), the results obtained in [121] are comparable. The results of the authors of [121] are not equal to those obtained in [193]. The authors of [121] connected the Wilson coefficient $C_{1\gamma}$ to $vhF_{\mu\nu}F^{\mu\nu}$ in contrast to [193] in Eq. (4.1). This results in the relation [121]

$$\kappa'_W = \kappa_W \frac{v^2_{\mathrm{SM}}}{v^2}. \tag{4.27}$$

4.5 Contributions of fermion diagrams to the $h \to \gamma\gamma$ amplitude

The amplitude for the fermion contribution in Fig. 4.1a reads

$$\begin{aligned} i\mathcal{A}^{\mathrm{ferm}}(h \to \gamma\gamma) = \sum_{q=u,d,e} \int \frac{d^d p}{(2\pi)^d} \int_\epsilon^1 \mathrm{d}\, t_1 \int_\epsilon^1 \mathrm{d}\, t_2 \delta_h^\eta (t-1)\, \mathrm{Tr}\Bigg[\frac{1}{\sqrt{2}} \begin{pmatrix} 0 & Y_q \\ Y_q^\dagger & 0 \end{pmatrix} \\ S^q(t, t_2; p - k_2) \not{\epsilon}(k_2)\, S^q(t_2, t_1; p) \not{\epsilon}(k_1)\, S^q(t_1, t; p + k_1) \Bigg] \end{aligned} \tag{4.28}$$

with an integration over the extra dimensional coordinate t_1 and t_2 at each vertex. The Yukawa interaction between the Higgs boson profile to both up–type quarks and down–type quarks is derived from the Yukawa Lagrangian

$$\begin{aligned} \mathcal{L}_{hqq}(x) &= -\sum_{q=u,d} \int_\epsilon^1 \mathrm{d}\, \delta_h^\eta (t-1)\, h(x)\, \bar{\mathcal{Q}}_L(x,t) \frac{1}{\sqrt{2}} \begin{pmatrix} 0 & Y_q \\ Y_q^\dagger & 0 \end{pmatrix} \mathcal{Q}_R(x,t) + \text{h.c.} \\ &= -\sum_{q=u,d} \sum_{n,m} g^q_{mn} h(x)\, \bar{q}_L^{(m)}(x)\, q_R^{(n)}(x) + \text{h.c.} \end{aligned} \tag{4.29}$$

with

$$\begin{aligned} g^q_{mn} &= \frac{1}{\sqrt{2}} \int_\epsilon^1 \mathrm{dt}\ \delta^\eta(t-1) \mathcal{U}_L^{\dagger,(m)}(t) \begin{pmatrix} 0 & Y_u \\ Y_u^\dagger & 0 \end{pmatrix} \mathcal{U}_R^{(n)}(t) \\ &= \frac{\sqrt{2}\pi}{L\epsilon} \int_\epsilon^1 \mathrm{dt}\ \delta^\eta(t-1) \left[a_m^{U,\dagger} C_m^Q(t)\, Y_u C_n^u(t)\, a_n^u + a_m^{u,\dagger} S_m^u(t)\, Y_u^\dagger S_n^Q(t)\, a_n^U \right]. \end{aligned} \tag{4.30}$$

For the evaluation of the results, the introduction of two regulators is mandatory. The first regulator is introduced, because the fermion profiles are discontinuous at the IR brane and the overlap integrals to the Higgs profile are not well–defined, *c.f.* Eq. (2.53). As a consequence, a finite width η has to be assigned to the Higgs profile [207] that leads to the expression $\delta_h^\eta(t-1)$, because the regularized delta function assigns a unit width in the interval $t \in [1-\eta, 1]$ to the Higgs profile. Many of the results are independent of the explicit shape η of the Higgs profile.

As in the SM, the second regulator is a UV consistent regulator N [194], which is introduced in order to obtain a UV consistent result. As a bonus, the UV regulator regulates the superficial divergent KK modes in the 5D theory [194]. Then, the relevant sum reads

$$\lim_{\substack{N\to\infty\\ \eta\to 0}} \sum_{q=u,d} \sum_{n=4}^{3+6N} \frac{v g^q_{mn}}{m_{q_n}} \left(\frac{\mu}{m_{q_n}}\right)^{4-d}, \tag{4.31}$$

for which $n = 4$ denotes the lightest KK excitation.
The expressions for the Wilson coefficients are derived when the amplitude in Eq. (4.28) is matched with the expression of the amplitude in the effective theory Eq. (4.1). The fermion contribution to $h \to \gamma\gamma$ is similar to the gluon fusion process considered in [128–131] except for a few coefficients and results in the following expressions for the fermion contribution to the Wilson coefficients:

$$C^q_{1\gamma} = 3N_c \sum_{q=u,d,e} Q^2_q \int_0^1 \mathrm{d}x \int_0^{1-x} \mathrm{d}y (1-4xy) \left[T^q_+\left(-xym^2_h\right) - T^q_+\left(\Lambda^2_{\mathrm{TeV}}\right)\right], \tag{4.32}$$

$$C^q_{5\gamma} = 2N_c \sum_{q=u,d,e} Q^2_q \int_0^1 \mathrm{d}x \int_0^{1-x} \mathrm{d}y \left[T^q_-\left(-xym^2_h\right) - T^q_-\left(\Lambda^2_{\mathrm{TeV}}\right)\right]. \tag{4.33}$$

In the quark case, the number of colors $N_c = 3$ and the respective charges for either up–type quarks $Q_u = 2/3$ or for down–type quarks $Q_d = -1/3$ have to be inserted in Eq. (4.32). If lepton contributions are considered, their contribution will be obtained for $N_c = 1$ and for $Q_e = -1$ in Eq. (4.32). In the calculation of Eq. (4.32), the fermion masses m_{q_n} are kept. Although it is a good approximation if the masses of the particle in the loop $m^2_{q_n} \gg m^2_n/4$ are neglected, the Higgs mass has to be kept for a valid result, which is satisfied for the KK modes, for the light SM particles, and even in the case of the top quark. In the 5D framework, there is no difference between zero modes and the KK modes anymore. As a consequence, the Higgs mass is kept if the SM contributions are implemented properly. As in the boson case, the expression $T^q_\pm\left(-p^2\right)$ denotes the linear combination of the overlap profile functions of the Higgs boson profile to the chirality–odd profile function, which is defined as

$$T^q_\pm(p^2_E) = -\sum_{q=u,d} \frac{v}{\sqrt{2}} \int_\epsilon^1 \mathrm{d}t \delta^\eta_h (t-1) \mathrm{Tr}\left[\begin{pmatrix} 0 & Y_q \\ Y^\dagger_q & 0 \end{pmatrix} \frac{\Delta^q_{RL}\left(t,t';p^2_E\right) \pm \Delta^q_{LR}\left(t,t';p^2_E\right)}{2}\right]. \tag{4.34}$$

The expression $T^q_\pm\left(p^2_E\right)$ consists of the mixed chirality components of the 5D propagator $\Delta^q_{RL}\left(t,t';p^2_E\right) = \left[\Delta^q_{LR}\left(t',t;p^2_E\right)\right]^\dagger$ that is valid for large space–like momenta. Their exact expressions are required in a region $t, t' > \eta$ and given in [128–131]. For an arbitrary Higgs profile along the extra dimension, Eq. (4.34) and Eq. (4.32) are still valid. As a bonus, Eq. (4.32) are used for the derivation of the effective couplings, if the mixed chirality components of the 5D fermion propagator are derived. The case of a brane–localized Higgs is recovered for the regulator in the limit $\eta \to 0$.
The exact results for the Wilson coefficients in Eq. (4.32) is expanded *via* a Taylor series at $\mathcal{O}\left(v^4/M^4_{\mathrm{kk}}\right)$ and with the negligence of chirality–odd terms at $\mathcal{O}\left(v^2/M^2_{\mathrm{kk}}\right)$, Eq. (4.32) turns into

$$C^q_{1\gamma} \approx \left[1 - \frac{v^2}{3M^2_{\mathrm{kk}}} \mathrm{Re} \frac{\left(Y_u Y^\dagger_u Y_u\right)_{33}}{(Y_u)_{33}}\right] N_c Q^2_u A_q(\tau_t) + N_c Q^2_d A_q(\tau_b)$$

$$+N_c \sum_{q=u,d} Q_q^2 \mathrm{Re}\,\mathrm{Tr} g\left(X_0\right), \tag{4.35}$$

$$C_{5\gamma}^q \approx -\frac{v^2}{3M_{\mathrm{kk}}^2}\mathrm{Im}\left[\frac{\left(Y_u Y_u^\dagger Y_u\right)_{33}}{\left(Y_u\right)_{33}}\right] N_c Q_u^2 B_q\left(\tau_t\right) + N_c \sum_{q=u,d} Q_q^2 \mathrm{Im}\,\mathrm{Tr} g\left(X_0\right) \tag{4.36}$$

with [208, 209]

$$A_q\left(\tau\right) = \frac{3\tau}{2}\left[1 + \left(1-\tau\right)\arctan^2\left(\frac{1}{\sqrt{\tau-1}}\right)\right], \tag{4.37}$$

$$B_q\left(\tau\right) = \tau \arctan^2\left(\frac{1}{\sqrt{\tau-1}}\right), \tag{4.38}$$

$$\tau_i = 4m_{q_i}^2/m_h^2 - i0. \tag{4.39}$$

For light SM quarks, an analytical continuation for $\tau < 1$, see Eq. (4.39), has to be performed. This was already taken into account *via* the term $-i0$ in Eq. (4.39). Furthermore, the analytical continuation in $f\left(\tau\right)$ has to be applied. In the limit $\tau \to \infty$, both Eq. (4.37) and Eq. (4.38) become 1. A distinction between the SM contribution and the contribution that stems from the RS model is now possible by adding the Wilson coefficients $C_{1\gamma}^q$ and $C_{5\gamma}^q$ in Eq. (4.35) to

$$C_{1\gamma}^q + C_{5\gamma}^q \approx Q_e^2 \mathrm{Tr}\left[g\left(X_e\right)\right] \tag{4.40}$$

with the hermitian matrix

$$X_f = \frac{v}{\sqrt{2}M_{\mathrm{kk}}}\sqrt{Y_f Y_f^\dagger}, \quad f = u,d,e \tag{4.41}$$

that includes the dimensionless Yukawa matrices Y_f. As the Bessel functions in Eq. (4.34) are momentum–dependent, the matrix X_f is derived *via* an expansion of the Bessel functions for both large momenta and small momenta. The trace over the matrix–valued function $g\left(X_e\right)$ leads to $C_{5\gamma}^e = 0$ and the remaining contribution to $C_{5\gamma}^q$ stems from the top quark, which is the first contribution of the right hand side of Eq. (4.35). The matrix valued function $g\left(X_f\right)$ is sensitive to the Higgs localization. The values differ at a first glance from each other, because

$$g\left(X_f\right)|_{\mathrm{braneHiggs}} = -\frac{X_q \tanh\left(X_q\right)}{\cosh\left(2X_q\right)} \approx -X_q^2, \tag{4.42}$$

$$g\left(X_f\right)|_{\mathrm{bulkHiggs}} = X_q \tanh\left(X_q\right) \approx X_q^2. \tag{4.43}$$

Here, Eq. (4.42) corresponds to the result obtained in [194] and Eq. (4.43) corresponds to the result derived in [200] at $\mathcal{O}\left(v^2/M_{\mathrm{kk}}^2\right)$. The difference between the results of Eq. (4.42) and Eq. (4.43) stems from the subtraction of large euclidean momenta in $T_+^q\left(-p^2\right)$ in Eq. (4.32). In the brane Higgs scenario, the function $T_+^q\left(\Lambda_{\mathrm{TeV}}^2\right) = \mathrm{Tr}\left[X_q \tanh\left(X_q\right)\right]$ arrives at a plateau in contrast to the narrow bulk Higgs scenario, in which the function $T_+^q\left(\Lambda_{\mathrm{TeV}}^2\right) \propto \frac{1}{p_E^2}$ vanishes for large euclidean momenta $p_E^2 = -p^2 \gg \left(v/\eta\right)^2$. Now it is clear that the difference of Eq. (4.42) and Eq. (4.43) is traced back to the heavy KK modes of the fermion masses that are proportional to the inverse Higgs width $\Delta_h = v/\eta$ and that contribute unsuppressed. This term originates for the subtraction of large euclidean

momenta in $C_{5\gamma}^{q}$ in Eq. (4.32), which is only relevant for $T_{+}^{q}\left(-p^{2}\right)$. As a consequence, the brane Higgs from [194] corresponds to a special case of the narrow bulk Higgs scenario. In the case of two different Yukawa matrices Y_f^S and Y_f^C belonging to the $\mathbb{Z}_2$–odd and $\mathbb{Z}_2$–even fields, the expression for $g\left(X_f\right)$ is no longer hermitian, but the function $g\left(Y_f^C, Y_f^S\right)$ is given by $g\left(Y_f^C, Y_f^S\right) \approx -\frac{v^2}{M_{\mathrm{kk}}^2} Y_f^C Y_f^{C\dagger}$ at leading order expansion. The exact function reads

$$g\left(\tilde{Y}_q, \tilde{Y}_q^{\dagger}\right)\Big|_{\text{branehiggs}}^{\text{typeII}} = -\frac{2X_q}{\sinh\left(X_q\right)} \frac{2M_{\mathrm{kk}}^2 \tilde{Y}_q \tilde{Y}_q^{\dagger}}{1+\frac{v^2}{M_{\mathrm{kk}}^2}\tilde{Y}_q \tilde{Y}_q^{\dagger}} = -\frac{v^2}{2M_{\mathrm{kk}}^2} Y_f^C Y_f^{C\dagger} \tag{4.44}$$

and its trace delivers a real negative number. At leading order, there is no difference with the result in Eq. (4.42) in the brane Higgs model for $Y_f^C = Y_f^S$. The numerical difference appears in the distribution of the parameter points. This latter case is not considered in the phenomenological analysis. As a next step, the fermion contributions for the $h \to \gamma\gamma$ decay are investigated, which enter the custodial RS model.

4.5.1 Fermion contributions in the custodial RS model

In the custodial RS model, an enlarged bulk symmetry is considered that leads to a suppression of the large corrections to the electroweak precision observables. Analogue to the minimal RS, the fermion contributions in the custodial RS are the same 3×3 matrices that differ in their coefficients and show the embedding of the different fermion generations under the enlarged bulk gauge group. The generalization of the quark contributions

$$\mathcal{L}_{hqq}\left(x\right) = -\sum_{q=u,d,\lambda} \int_{\epsilon}^{1} \mathrm{d}\, \delta_h^{\eta}\left(t-1\right) h\left(x\right) \bar{\mathcal{Q}}_L\left(x,t\right) \frac{1}{\sqrt{2}} \begin{pmatrix} 0 & Y_{\vec{q}} \\ Y_{\vec{q}}^{\dagger} & 0 \end{pmatrix} \mathcal{Q}_R\left(x,t\right) + \text{ h.c.} \tag{4.45}$$

needs some further explanations. Here, $\mathcal{Q}_{L,R}\left(x,t\right)$ does not only contain the left–handed fields or right–handed fields of the up–sector or the down–sector, but contains also contributions of the exotic particle sector. The Yukawa interactions have the same structure as in the minimal model. The only visible difference is in the UV BCs of the propagator, which is explicit with the addition of the superscripts $(+)$ and $(-)$ that lead to $R_A^{+}\left(p_E\right) = \frac{D_1^A(p_E,1)}{D_2^A(p_E,1)}$ and to $R_A^{-}\left(p_E\right) = \frac{D_3^A(p_E,1)}{D_4^A(p_E,1)}$, with $D_i^A\left(p_E,1\right), i = 1,2,3$. The index $A = Q, u^c, \tau_1, \tau_2$ is used in the same way as introduced in Eq. (2.159),Eq. (2.160). The results for the Wilson coefficients remain the same with respect to the extended flavor content. The squared Yukawa matrices in X_q are now given by the 6×6 matrices

$$Y_u Y_u^{\dagger} = V \begin{pmatrix} 2Y_d Y_d^{\dagger} & 0 \\ 0 & 2Y_u Y_u^{\dagger} \end{pmatrix} V^{\dagger}, \qquad V = \frac{1}{\sqrt{2}} \begin{pmatrix} -1 & 1 \\ 1 & 1 \end{pmatrix} = V^{\dagger}. \tag{4.46}$$

Hence, the sum over the traces becomes

$$\sum_{q=u,d,\lambda} \mathrm{Tr} g\left(X_q\right) = \mathrm{Tr} g\left(\sqrt{2}X_u\right) + 3\mathrm{Tr} g\left(\sqrt{2}X_q\right) \tag{4.47}$$

with the 3×3 matrices X_q as in the minimal RS model. The first term of the Taylor expansion of $g\left(X_q\right)$ is X_q^2 with an additional factor $\sqrt{2}$ in the quark contributions for

the custodial RS model. The result of the expansion is 2 times larger with respect to the minimal RS model. With the electroweak charge of the λ–particles, the quark contribution results in a factor 13 that originates from the higher multiplicity of the KK quark modes.
In the custodial RS model, the modified Yukawa matrices are given by
$\tilde{Y}_q = \left[\tanh\left(\sqrt{2}X_q\right)/\left(\sqrt{2}X_q\right)\right] Y_q$. With all modifications, the expressions for the Wilson coefficients become

$$C_{1\gamma}^q \approx \left[1 - \frac{2v^2}{3M_{\rm kk}^2}{\rm Re}\frac{\left(Y_u Y_u^\dagger Y_u\right)_{33}}{(Y_u)_{33}}\right] N_c Q_u^2 A_q(\tau_t) + N_c Q_d^2 A_q(\tau_b)$$
$$+ N_c Q_u^2 {\rm ReTr} g\left(\sqrt{2}X_u\right) + N_c\left(Q_u^2 + Q_d^2 + Q_\lambda^2\right){\rm ReTr}\, g\left(\sqrt{2}X_d\right), \tag{4.48}$$

$$C_{5\gamma}^q \approx -\frac{2v^2}{3M_{\rm kk}^2}{\rm Im}\left[\frac{\left(Y_u Y_u^\dagger Y_u\right)_{33}}{(Y_u)_{33}}\right] N_c Q_u^2 B_q(\tau_t)$$
$$+ N_c Q_u^2 {\rm ImTr} g\left(\sqrt{2}X_u\right) + N_c\left(Q_u^2 + Q_d^2 + Q_\lambda^2\right){\rm ImTr}\, g\left(\sqrt{2}X_d\right). \tag{4.49}$$

4.5.1.1 Charged lepton contribution in the custodial RS model

The charged lepton contributions to the decay $h \to \gamma\gamma$ can be implemented in two possible ways that depend on the embedding of the lepton fields in the extended gauge symmetry of the custodial RS model. One way is to choose the lepton multiplets in the same way as the quark multiplets, *i.e.*

$$\xi_{1L} = \begin{pmatrix} \nu_{L,0}^{(+)} & \psi_{L,1}^{(-)} \\ e_{L,-1}^{(+)} & \nu_{L,0}^{\prime(-)} \end{pmatrix}_0, \qquad \xi_{2R} = \left(\nu_{R,0}^{c(+)}\right)_0, \tag{4.50}$$

$$\xi_{3R} = \mathcal{T}_{3R} \otimes \mathcal{T}_{4R} = \begin{pmatrix} \Psi_{R,1}^{\prime(-)} \\ N_{R,0}^{\prime(-)} \\ E_{R,-1}^{\prime(-)} \end{pmatrix}_0 \otimes \left(E_{R,-1}^{(+)} \quad N_{R,0}^{(-)} \quad \Psi_{R,0}^{(-)}\right)_0. \tag{4.51}$$

In the neutrino sector, 15 different leptonic states exist and 9 different states exist in the charged lepton sector. The BCs lead to 3 light modes in every sector that are associated with the SM neutrinos and the charged SM leptons, respectively. These modes are accompanied by 15 and 9 groups in the corresponding sectors. Additionally, a KK tower with charge $Q_\psi = 1$ exists that contains the exotic leptons including 9 KK level/excitation. The gauge–invariant Yukawa interaction is written in the same way to the quark Yukawa interaction. Furthermore, the Yukawa matrices Y_ν and Y_e are considered to be 3×3 matrices with an anarchic structure that lead to the SM lepton masses if they are connected to fermion profiles on the IR brane. The resulting contributions have the same structure as those in the Wilson coefficients $C_{1\gamma}^q$ and $C_{5\gamma}^q$ in Eq. (4.48). The lepton masses are proportional to m_l^2/m_h^2. Together with the following replacements

$$Y_u \to Y_\nu, \qquad Q_u \to Q_\nu = 0, \tag{4.52}$$
$$Y_d \to Y_e, \qquad Q_d \to Q_e = -1, \tag{4.53}$$

$$N_c \to 1, \qquad Q_\lambda \to Q_\psi = 1, \tag{4.54}$$

the Wilson coefficients $C^l_{1\gamma} + iC^l_{5\gamma}$ change to

$$C^l_{1\gamma} + iC^l_{5\gamma} \approx \left(Q_e^2 + Q_\psi^2\right) \mathrm{Tr} g \left(\sqrt{2} X_e\right). \tag{4.55}$$

Then, the lepton contribution to the Wilson coefficients turns out to be 4 times larger compared to the minimal RS model. There is no zero mode.
Another embedding of the charged lepton sector in the extended gauge symmetry follows more analogously to the minimal RS model. Both left–handed neutrino and left–handed electron are cast into an $SU(2)_L$ doublet, and the right–handed electron are put together with the new exotic particle N_R in the $SU(2)_R$ doublet. The lepton fields with $\mathbb{Z}_2$–even (odd) parity transform as (2,1) and (1,2):

$$L_L = \begin{pmatrix} \nu^{(+)}_{L,0} \\ e^{(+)}_{L,-1} \end{pmatrix}_{-\frac{1}{2}}, \qquad L_R = \begin{pmatrix} e^{c(+)}_{R,-1} \\ N^{(-)}_{R,0} \end{pmatrix}_{-\frac{1}{2}} \tag{4.56}$$

The BCs are chosen in a way that the zero modes correspond to the SM leptons without the right–handed neutrino. Thus, the Yukawa interaction is given by

$$\mathcal{L}_{\mathrm{Yuk}} = -\int_\epsilon^1 \frac{\mathrm{d}t}{t} \frac{M_{\mathrm{kk}}}{2} \delta^\eta (t-1) \frac{2}{k} (Y_e)_{ij} \left(\bar{L}^i_L \Phi \varepsilon L^{c,j}_R + \bar{L}^i_R \Phi \varepsilon L^{c,j}_L\right) + \mathrm{h.c.} \tag{4.57}$$

with $\varepsilon = i\sigma^2$. At this order, the SM neutrinos remain massless as EWSB generates a mass term for the zero modes of the charged leptons. The masses are explained by higher dimensional operators. The additional lepton field is the right–handed neutrino that is charged under $SU(2)_R$ and does not affect the $h \to \gamma\gamma$ decay amplitude, because it is considered to be uncharged. Then, the lepton contribution remains the same as in the minimal RS model.

4.6 Phenomenological implications

The ratio $R_{\gamma\gamma}$ is the signal strength of the decay $\gamma\gamma$ and is defined as the production mechanism of a Higgs bosons and its decay into two photons in the RS model divided by the SM expression. That means, any deviation from 1 of this ratio is an implication for New physics. The function reads

$$R_{\gamma\gamma} = \frac{(\sigma \cdot \mathrm{BR})(pp \to h \to \gamma\gamma)_{\mathrm{RS}}}{(\sigma \cdot \mathrm{BR})(pp \to h \to \gamma\gamma)_{\mathrm{SM}}} \frac{\left[\left(|\kappa_g|^2 + |\kappa_{g_5}|^2\right) f_{GF} + \left(|\kappa_\gamma|^2\right) f_{GF} + \kappa_v^2 f_{VBF}\right]}{\kappa_v^2 \kappa_h} \tag{4.58}$$

with the quantities κ_i. The Wilson Coefficients $\mathcal{C}_i$ enter κ_i and are normalized in the RS model to their respective SM value $\mathcal{C}_{i,\mathrm{SM}}$. Explicitly,

$$\begin{aligned} \kappa_i &= \frac{\mathcal{C}_{1i}}{\mathcal{C}_{1i,\mathrm{SM}}}, \qquad & \kappa_{i,5} &= \frac{3}{2} \frac{\mathcal{C}_{5i}}{\mathcal{C}_{5i,\mathrm{SM}}}, \\ & & \mathcal{C}_{1i,\mathrm{SM}} &= \frac{4}{3} - \frac{21}{4} A_W(\tau_W) \approx -4.9. \end{aligned} \tag{4.59}$$

In general, new physics can enter in the production processes *via* contributions to the gluon fusion process, *via* contributions to the vector boson fusion process or *via* contributions to the $h \to \gamma\gamma$ cross section. The possible contributions to the gluon fusion process have been discussed earlier in [128, 131] and now we will concentrate on the possible contributions to the $h \to \gamma\gamma$ decay rate.
In the minimal RS model, κ_γ becomes

$$\begin{aligned}\kappa_\gamma\Big|_{\text{min}} \approx 1 - \frac{v^2}{2M_{\text{kk}}^2}\Bigg[&\frac{1}{C_{\gamma,\text{SM}}}\left(\pm\frac{8}{3}N_g^2 + \frac{16}{9}N_g - \frac{8}{9}\right)\langle|Y_{ij}|^2\rangle \\ &+\frac{Lm_W^2}{C_{\gamma,\text{SM}}v^2}\left(\frac{23}{4} + A_h^W(\tau_W)\right)\Bigg]\end{aligned} \tag{4.60}$$

and in the custodial RS model

$$\begin{aligned}\kappa_\gamma\Big|_{\text{cust}} \approx 1 - \frac{v^2}{2M_{\text{kk}}^2}\Bigg[&\frac{1}{C_{\gamma,\text{SM}}}\left(\pm\frac{71}{3}N_g^2 + \frac{32}{9}N_g - \frac{16}{9}\right)\langle|Y_{ij}|^2\rangle \\ &+\frac{Lm_W^2}{c_{\theta_W}^2 C_{\gamma,\text{SM}}v^2}\left(\frac{23}{4} + A_h^W(\tau_W)\right)\Bigg].\end{aligned}$$

with

$$C_{\gamma,\text{SM}} = N_c\left[Q_u^2 A_q(\tau_t) + Q_d^2 A_q(\tau_b)\right] - \frac{21}{4}A_W(\tau_W). \tag{4.61}$$

In Eq. (4.58), the ratio of the Wilson coefficients of the gluons, *via* κ_g is obtained in a similar way. The Wilson Coefficients $\mathcal{C}_{1,g}$ and $\mathcal{C}_{5,g}$ are obtained *via* the replacements $Q_{u,d} \to 1, Q_l \to 0, N_c \to 1$ in Eq. (4.35), whereas the SM coefficient $\mathcal{C}_{g,\text{SM}}$ has the following structure: $\mathcal{C}_{g,\text{SM}} = A_q(\tau_t) + A_q(\tau_b)$. The shift of the Higgs VEV in the RS model $\kappa_v = \frac{v}{v_{\text{SM}}} = 1 + Lm_W^2/(4c_{\theta_W}^2 M_{\text{kk}}^2)$ is normalized to its SM value. The relation for the Weinberg angle $c_{\theta_W}^2$ becomes 1 in the minimal RS model and 1/2 in the custodial RS model. Furthermore, the relation for the Higgs particle is $\kappa_h = \kappa_v \Gamma_h^{\text{RS}}/\Gamma_h^{\text{SM}}$.
As a next step, the $R_{\gamma\gamma}$ amplitude is investigated using the procedure that was described in Sec. 2.8. 5000 data points have been generated for each Yukawa matrix with an absolute value of $y_* = 0.5, 1.5, 3$. The value of $y_* = 3$ corresponds to the limit in which a perturbative treatment of the Yukawa matrices is satisfied according to Sec. 2.3.1. The obtained value has to fulfill the condition $\left|(Y)_{ij}\right| \leq y_* \approx \mathcal{O}(1)$ or the value is rejected during the scan of the amplitude. For a large amount of random numbers, the central limit theorem can be applied and leads to an average

$$\left\langle \frac{\left(Y_u Y_u^\dagger Y_u\right)_{33}}{(Y_u)_{33}} \right\rangle = (2N_g - 1)\frac{y_*}{2}, \quad \langle|Y_{ij}|^2\rangle = N_g\frac{y_*}{2}. \tag{4.62}$$

The latter expectation values highlight the insensitivity of the fermion profiles to the entries of the Yukawa matrices, because only the number of fermion generations N_g occurs. In addition, flavor changing corrections are affected by Eq. (4.62). The scan is performed assuming the current numerical values for both quarks and leptons and for values of the CKM matrix in the quark sector. For $y_* = 1$, the average value of Eq. (4.62) is 2.5 if anarchic Yukawa matrices are considered. With the insertion of the correct values for the quark sector, y_* turns out to be 2.7, while for the lepton sector y_* is 2.2. The

consideration of the neutrino sector is omitted in the following as it is irrelevant for the discussion. Furthermore, the neutrino sector requires a model–dependent specification of the neutrino sector or the PMNS matrix. Focusing on the gauge sector, there is an analogy to Eq. (4.62) that results in a proportionality of M_{kk}/y_*.
In the minimal RS model, the largest corrections stem from fermion loop contributions for Yukawa couplings around $y_* = 2$, which are sufficiently large. In contrast to the contributions to the gluon fusion process [128, 131], the $h \to \gamma\gamma$ decay rate shows a suppression (an enhancement) in the brane (bulk)–localized Higgs scenario. Regarding the SM contributions, the dominant contribution to the $h \to \gamma\gamma$ decay rate stems from diagrams containing W boson loops, which contribute in the opposite direction. Expanding Eq. (4.58) to v^2/M_{kk}^2 and assuming $A_W(\tau_W) \approx 1.19$, $A_q(\tau_t) \approx 1$, and $A_q(\tau_b) \approx 0$, the expression in the minimal RS model is found:

$$\begin{aligned} R_{\gamma\gamma}\Big|_{\mathrm{min}} \approx 1 + \frac{v^2}{2M_{\mathrm{kk}}^2}\Bigg[& \left(f_{GF} - \frac{4}{3\left|C_{\gamma,\mathrm{SM}}\right|}\right)\left(\mp 18 - \frac{10}{3}\right) y_*^2 \\ & - \left(f_{VBF} - \frac{21}{4\left|C_{\gamma,\mathrm{SM}}\right|}\left(1 + \frac{4}{21}A_W(\tau_W)\right)\right)\frac{2m_W^2}{v^2}\left(L - 1 + \frac{1}{2L}\right) \\ & - \frac{Lm_W^2}{v^2} + 0.57\frac{10}{3}y_*^2 + 0.22\frac{2m_W^2}{v^2}\left(L - 1 + \frac{1}{2L}\right) - 0.09\left(\mp 18 - \frac{10}{3}\right) y_*^2\Bigg] \\ \approx 1 - \frac{v^2}{2M_{\mathrm{kk}}^2}&\left[(\pm 9.7 - 0.1)\, y_*^2 + 4.1\right]. \end{aligned} \tag{4.63}$$

In the custodial RS model, the same expression is now:

$$\begin{aligned} R_{\gamma\gamma}\Big|_{\mathrm{cust}} \approx 1 + \frac{v^2}{2M_{\mathrm{kk}}^2}\Bigg[& \mp\left(72 f_{GF} - \frac{213}{\left|C_{\gamma,\mathrm{SM}}\right|}\right) y_*^2 - \frac{20}{3}\left(f_{GF} - \frac{4}{3\left|C_{\gamma,\mathrm{SM}}\right|}\right) y_*^2 \\ & - \left(f_{VBF} + \frac{21\left[A_W(\tau_W) - 1\right]}{4\left|C_{\gamma,\mathrm{SM}}\right|}\right)\frac{2m_W^2}{v^2}\left(2L - 1 + \frac{1}{2L}\right) - \frac{2Lm_W^2}{v^2} \\ & + 0.57\frac{20}{3}y_*^2 + 0.22\frac{2m_W^2}{v^2}\left(2L - 1 + \frac{1}{2L}\right) - 0.09\left(\mp 72 - \frac{20}{3}\right) y_*^2\Bigg] \\ \approx 1 - \frac{v^2}{2M_{\mathrm{kk}}^2}&\left[(\pm 15.0 - 0.2)\, y_*^2 + 8.3\right]. \end{aligned} \tag{4.64}$$

In Eq. (4.63) and in Eq. (4.64), the second term contributes to the gluon fusion process indicated by f_{GF}. The dominance of the production process of the Higgs *via* gluon fusion is emphasized by the dependence on the value of the Yukawa matrix y_*. Indicated by f_{VBF}, another Higgs production mechanism contributes, which is the vector boson fusion that is visible in the third term of Eq. (4.63) and the second term in Eq. (4.64). Considering the behavior of light gluon masses $M_g^{(n)}$ in the brane–localized Higgs scenario, it turns out that this particular scenario is bound from below by f_{VBF}. Terms stemming from the gluon fusion production cross section are canceled with the SM amplitude at around $M_g^{(1)} \approx 3.5$ TeV. The amplitude is non–zero due to the contribution from the value of the vector boson fusion cross section. The terms from the gluon fusion contain also a correction to the $h \to \gamma\gamma$ decay rate *via* $1/C_{\gamma,\mathrm{SM}}$ and $C_{\gamma,\mathrm{SM}}$, as defined in Eq. (4.61). The third line of both Eq. (4.63) and Eq. (4.64) contains corrections to

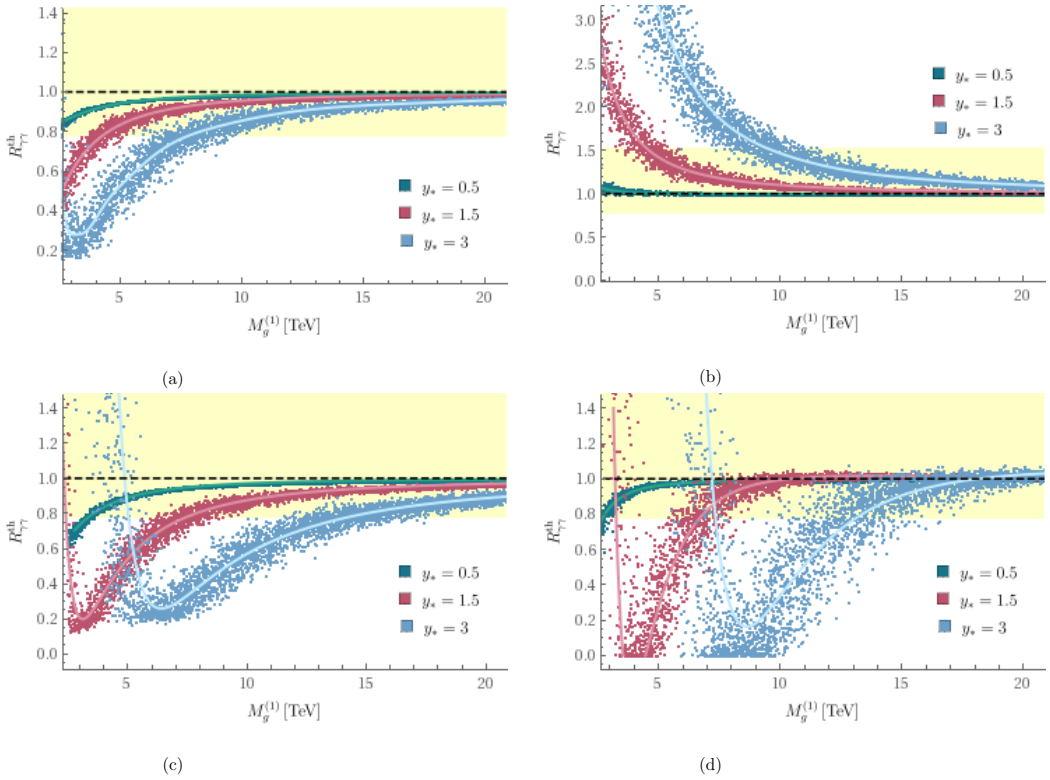

Figure 4.2: $R^{\text{th}}_{\gamma\gamma}$ is plotted against the RS gluon mass $M_g^{(1)}$. The scattered data points are obtained using the program described in Sec. 2.8. The blue, green and red dashed points correspond to the maximum values of $y_* = 0.5, 1.5, 3$. The yellow band denotes the combined signal strength $R^{\text{exp}}_{\gamma\gamma}$ with twice the error of the combined ATLAS and CMS experiment [210]. The first row shows the distribution of $R^{\text{th}}_{\gamma\gamma}$ in the minimal RS model. In Fig. 4.2a the distribution of $R^{\text{th}}_{\gamma\gamma}$ is shown for the brane–localized Higgs scenario, and Fig. 4.2b shows the distribution of $R^{\text{th}}_{\gamma\gamma}$ in the bulk–localized Higgs scenario.The second row shows the distribution of $R^{\text{th}}_{\gamma\gamma}$ in the custodial RS model. As in the case for the minimal RS model, the right figure Fig. 4.2c corresponds to the brane–localized Higgs scenario and the left figure Fig. 4.2d shows the distribution of $R^{\text{th}}_{\gamma\gamma}$ in the bulk–localized Higgs scenario. The detailed values for $R^{\text{exp}}_{\gamma\gamma}$ of the different experiments as well as the combined value of $R^{\text{exp}}_{\gamma\gamma}$ can be found in Tab. 4.1, as well.

the Higgs particle width. The two possibilities for signs in Eq. (4.63) and Eq. (4.64), are related to the brane (bulk)–localized Higgs scenario. The upper (lower) sign denotes the brane (bulk)–localized Higgs scenario.
Focusing only on the custodial model, the minimal lepton sector of Eq. (4.56) is considered in Eq. (4.64). For the extended lepton sector in Eq. (4.50), the factor 213 in the third term of Eq. (4.64) is changed to 240. In the last line of Eq. (4.64), the value ± 15.0 changes to ± 9.5. The linearized case of the equation leads to a slight difference between the expression in the custodial RS model and the expression in the minimal RS model. In Fig. 4.2, the $R_{\gamma\gamma}$ is plotted against the gluon mass $M_g^{(1)}$.
The signal strength $R_{\gamma\gamma}$ is plotted against the lowest gluon mass $M_g^{(1)}$ in units of TeV in Fig. 4.2 for three different absolute values of y_* to see the possibility for the existence of a possible signal of the $h \to \gamma\gamma$ from the RS model in the current experimental datasets. The yellow band denotes the measured region of the combined measurements of the $h \to \gamma\gamma$ decay in the SM by the experiments ATLAS and CMS including the errors twice. In the brane–localized Higgs scenario in the custodial RS model, the data points are similarly distributed as in the minimal RS model, although new physics effects are larger due to the enlarged particle content as can be seen in Fig. 4.2c. The enlarged particle content gives rise to a different behavior of the curves in the narrow–bulk localized model. This can bee seen by a comparison of Fig. 4.2b and Fig. 4.2d. It is also visible that less data points in the custodial RS model are compatible with the experimental data as in the case for the minimal RS models, because the scattered data points lie in the yellow band. The solid lines in Fig. 4.2a–Fig. 4.2d represent the fit curves to the data that are used to determine the intersection points with the yellow experimental band. The fit functions in the minimal RS model follow a polynomial function proportional to inverse powers of x. In the case of the custodial model, this function is modified by a factor of $\tanh\left(x^{-1}\right)$. These functions have been fitted to the right hand side and the parameter space was extrapolated that can be seen in the fit function for the custodial model with a bulk–localized Higgs in Fig. 4.2d for $y_* = 3$. This fit method was applied, because the data points are due to the absolute values in Eq. (4.64) either positive or zero. If there would have been negative values for the signal strength, the fit function could have been better estimated in the case of a bulk–localized Higgs in the custodial RS model for $y_* = 3$. The exact functions can be found in Sec. A.2.4. The exclusion show the possibility to detect the gluon mass $M_g^{(1)}$ within the σ regions of the signal strength $R_{\gamma\gamma}$. Therefore, the σ is the deviation of the ratio of the binned theoretical values of $R_{\gamma\gamma}^{\text{th}}$ to the measured signal strength $R_{\gamma\gamma}^{\text{exp}}$. Therefore, the parameter values are obtained in terms of 1, 2, 3 $-\sigma\left(R_{\gamma\gamma}^{\text{th,i}}/R_{\gamma\gamma}^{\text{exp}}\right)$, for which $R_{\gamma\gamma}^{\text{th}}/R_{\gamma\gamma}^{\text{exp}}$ deviate by 1

$$\sigma\left(R_{\gamma\gamma}^{\text{th,i}}/R_{\gamma\gamma}^{\text{exp}}\right) = \frac{R_{\gamma\gamma}^{\text{th,i}}}{R_{\gamma\gamma}^{\text{exp}}}\sqrt{\frac{\sigma\left(R_{\gamma\gamma}^{\text{th,i}}\right)^2}{R_{\gamma\gamma}^{\text{th}}} + \frac{\sigma\left(R_{\gamma\gamma}^{\text{th,i}}\right)^2}{R_{\gamma\gamma}^{\text{exp}}}}. \tag{4.65}$$

The experimental value $R_{\gamma\gamma}^{\text{exp}}$ is given in Tab. 4.1 and for each data point $R_{\gamma\gamma}^{\text{th}}$ a Gaussian standard deviation is assumed. The data points are sorted into bins, in order to minimize correlation effects and the errors of the experimental signal strength $R_{\gamma\gamma}^{\text{exp}}$ are averaged. With these results it is visible in the exclusion plots that the experimental lower bounds on $M_{g^{(n)}}$ [174–176] coincide with the results obtained here.

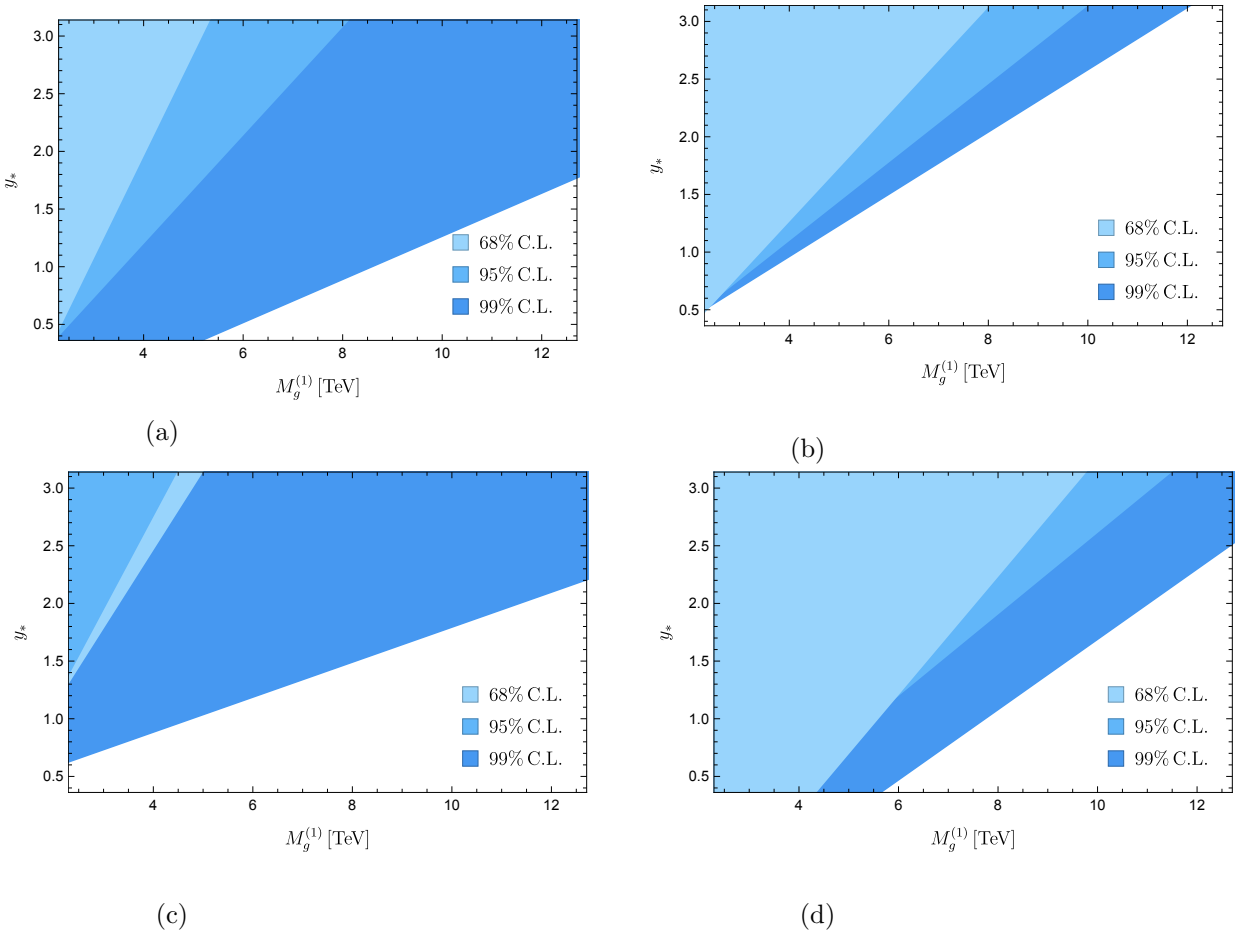

Figure 4.3: In the exclusion plots for the lowest gluon mass $M_{g^{(1)}}$ in the different setups of the RS model, y_* is plotted against the gluon mass $M_g^{(1)}$. The different blue colors correspond to the 1, 2, $3-\sigma$ region. The darkest color corresponds to 99% CL , whereas the lightest color corresponds to an exclusion of 68% CL. The lower experimental bound for the gluon mass $M_{g^{(1)}}$ from [174] is always fulfilled. Fig. 4.3a shows the excluded values of the RS signal strength $R_{\gamma\gamma}^{\text{th}}$ in the minimal RS model with a brane–localized Higgs, whereas Fig. 4.3b shows the same situation in the minimal RS model with a bulk–localized Higgs. In case of the exclusion of the signal strength $R_{\gamma\gamma}^{\text{th}}$ in the custodial RS model, the brane–localized Higgs scenario is displayed in Fig. 4.3c and Fig. 4.3d displays the excluded regions in the bulk–localized Higgs scenario.

values for the signal strength $R_{\gamma\gamma}$			
	combined	ATLAS	CMS
$R_{\gamma\gamma}$	$1.14^{+0.19}_{-0.18}$	$1.14^{+0.27}_{-0.25}$	$1.11^{+0.25}_{-0.23}$

Table 4.1: The values for the signal strength $R_{\gamma\gamma}$ from ATLAS and CMS and a combination of both values, published in [210].

From the contribution of the two production mechanisms, *i.e.* the gluon fusion and the vector boson fusion, only the contribution of the vector boson fusion remains explaining the minimal values of $R_{\gamma\gamma}$. For even smaller values of $M_g^{(n)}$, $R_{\gamma\gamma}$ grows and exceeds 1. These values are experimentally excluded.
In a nutshell, correction that stems from the fermions are large. Nonetheless, corrections stemming from the gluon fusion process exist and lead to cancellations.
In the bulk–localized Higgs scenario, the linearized approximation of both Eq. (4.63) and Eq. (4.64) breaks down for large values of y_*. Negative contributions to the $h \to \gamma\gamma$ decay are significant, such that positive values to the gluon fusion production rate are compensated. For small KK gluon masses, such contributions are dominant and lead to values for $R_{\gamma\gamma}$ below 1. For gluon masses $M_g^{(n)} \approx 5$ TeV, $R_{\gamma\gamma}$ vanishes completely.
Concluding, the cancellations that contribute to $R_{\gamma\gamma}$ seem to be independent in the case of the brane–localized Higgs scenario, while a careful treatment of the cancellations that contribute to $R_{\gamma\gamma}$ is necessary considering the bulk–localized Higgs scenario. In the latter case, a reliable estimation seems rather unlikely without knowing the exact model setup.

5 Flavor physics with an arbitrary bulk scalar S in the RS model

5.1 Motivation, setup and model description

During the data taking period in 2015, ATLAS [211] and CMS [212] observed an excess in the diphoton spectrum around 750 GeV (ATLAS) and 760 GeV (CMS) at $\sqrt{s} = 13$ TeV. Although this excess rose a discussion for the investigation of a possible BSM particle and its implementation in the various models, the signal was not confirmed after subsequent analyses with higher statistics. If the excess had been traced back to the existence of a new particle that decays into two photons, its spin could not be 1 following the Landau–Yang theorem [213, 214]. Applying this theorem, the new particle's spin could be 0. Then, the particle could be produced *via* gluon fusion and decayed into two photons *via* a virtual fermion loop. Assuming this to be true, the new scalar particle has to fulfill several tests. The existence of a new scalar particle is then excluded if changes in the SM values appear. The investigation of a pure BSM scalar in the context of extra–dimensions is not new as explained in Sec. 5.3.1, but its possible contribution to CP violating observables and decays was not investigated before in the context of warped extra–dimensions. As a consequence, the possibility of the existence of a general bulk scalar S as the lightest resonance of a bulk scalar S in the RS model is investigated in this chapter. This scalar particle is considered to be a singlet under the bulk gauge group of the RS model. In 2013, it was argued by the authors of [215] that a new scalar particle is rather likely to be a singlet under $SU(2)$. If not, the new scalar field belongs to a larger multiplet and the masses of its multiplet partners would be almost equal to the new scalar particle S [215]. Scalar multiplets are already discussed in the context of different models, *e.g.* in 2HDM [216]. In the framework of the RS model, there is a possibility of embedding a scalar that is a singlet under the entire gauge group. After the setup of the framework based on [141] and the investigation of the off–diagonal couplings of the scalar in Sec. 5.2 extending the work of [141], it is investigated if the contributions of this scalar particle are in conflict with the current measurements. Therefore, former work of this working group [179] is re–investigated in Sec. 5.6. Then, a possible contribution to electric dipole moments (EDMs) of the neutron and the deuteron is discussed in Sec. 5.7, based on [309].
The scalar boson S couples to the the matter fields by the term

$$\int_{\epsilon}^{1} \mathrm{d}\frac{2\pi}{Lt} r \frac{\epsilon^4}{t^4} \Big[\frac{g^{MN}}{2} \left(\partial_M S\right) \left(\partial_N S\right) - \frac{\mu^2}{2} S^2 - \sum_f \left(\bar{f} M_f f + S \bar{f} G_f f \right) \Big] \tag{5.1}$$

of the action, in which $\sum_f$ denotes the sum over all fermion states. The hermitian matrices M_f and G_f denote the bulk matrix M_f and the coupling G_f. In the following it is assumed that the mass matrices are connected to the coupling by $M_f = \omega G_f$ with

the VEV ω of the scalar field S. Furthermore, M_f is assumed to be diagonal, as we will work in the bulk–mass basis [141]. An effective theory approach justifies to integrate out the tower of KK fermions during the investigation of the bulk scalar $S(x,t)$. At the same time the mass of the new resonance $S(x,t)$ is assumed to be higher than the electroweak scale. As a consequence, the effective Lagrangian is written in the symmetric phase, *i.e.* v=0 that reads

$$\begin{aligned}\mathcal{L}_{\text{eff}} = &\frac{\alpha}{4\pi} c_{gg} S G^a_{\mu\nu} G^{\mu\nu,a} + \frac{\alpha}{4\pi s^2_{\theta_W}} c_{WW} S W^a_{\mu\nu} W^{\mu\nu,a} + \frac{\alpha}{4\pi c^2_{\theta_W}} c_{BB} S B^a_{\mu\nu} B^{\mu\nu,a} \\ &+ \left(S \bar{Q}_L \Lambda_u \tilde{\Phi} u_R + S \bar{Q}_L \Lambda_d \Phi d_R + S \bar{L}_L \Lambda_e \Phi e_R + \text{h.c.} \right).\end{aligned} \tag{5.2}$$

$\mathcal{L}_{\text{eff}}$ contains the field strength tensors $G^a_{\mu\nu}, W^a_{\mu\nu}, B^a_{\mu\nu}$ of $SU(3)_c, SU(2)_L, U(1)_Y$ and the scalar Higgs doublet Φ. In the last line of Eq. (5.2) the description of the couplings to quarks that are investigated in the following. The scalar field $S(x,t)$ itself is considered to be a $\mathbb{Z}_2$–odd field, because only then couplings to the scalar part of the Lagrangian density in Eq. (5.2) to the vector–like 5D fermions are allowed. These couplings from $S(x,t)$ to SM fermions appear at tree–level and are induced after EWSB in the same way as of [141, 131].
The term of the effective Lagrangian using the zero mode profile functions at $\mathcal{O}\left(m_h^2/M_{\text{kk}}^2\right)$ is given by

$$\begin{aligned}\mathcal{L}_{\text{ferm}} = &- \sum_{n,m=0}^{\infty} S(x)\, \bar{q}_L^{(m)}(x)\, q_R^{(n)}(x)\, (2+\beta) \int_0^1 \mathrm{d}t\, t^{1+\beta} \\ &\times \Bigg[x_n \hat{a}_m^{(c_Q)\dagger} F(c_Q)\, t^{c_Q} g_Q F(c_Q)\, \frac{t^{1+c_Q} - \epsilon^{-1+2c_Q} t^{-c_Q}}{1+2c_Q} \hat{a}_n^{(c_Q)} \\ &+ x_m \hat{a}_n^{(c_q)\dagger} F(c_q)\, t^{c_q} g_{c_q} F(c_q)\, \frac{t^{1+c_q} - \epsilon^{-1+2c_q} t^{-c_q}}{1+2c_q} \hat{a}_m^{(c_q)} \Bigg] \\ &+ \text{h.c.}\end{aligned} \tag{5.3}$$

and contains the fermion mass $x_n = m_n/M_{\text{kk}}$. n=1,2,3 labels the lowest lying KK modes. As the scalar singlet S only couples either to both singlets or to doublets, the integrand contains both $\mathbb{Z}_2$–even and $\mathbb{Z}_2$–odd profile functions Eq. (2.126) and Eq. (2.127). The fermion profile functions result from a mixing of the zero mode of the $\mathbb{Z}_2$–odd profile function with their KK excitations *via* EWSB. The overlap integrals scale with the involved fermion masses $x_{n,m}$. The three–dimensional $\hat{a}^{Q,q}$ vectors describe the mixing in flavor space and are normalized to unity [120].

5.2 Wilson coefficients and Fermion interactions to S

Couplings from the scalar boson S to fermions are parametrized in Eq. (5.3) by the matrix G_f. The fermion profile functions are parametrized *via* the bulk mass parameters $c_{Q,q_i} = \pm M/k$ already introduced in Sec. 2.4 and in [120]. Their sign depends on the

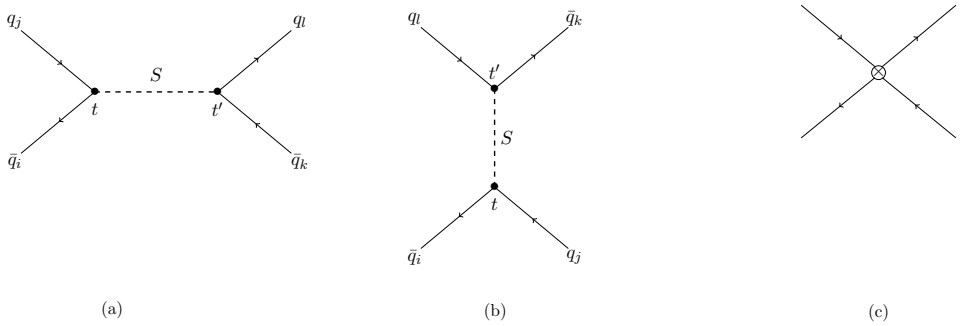

Figure 5.1: Tree–level process of a fermion exchange mediated by a bulk scalar S. Figure Fig. 5.1a and Fig. 5.1b describe the process in the full theory, whereas Fig. 5.1c describes the same process in the effective theory, in which the momentum p is considered to very much smaller than the KK mass M_{kk}.

fermion profiles $\mathbb{Z}_2$ symmetry transformation behavior. The scalar boson S couples *via*

$$\begin{aligned} g_{Q,q} &= \pm \frac{\sqrt{k\,(1+\beta)}}{(2+\beta)\,\omega} G_f \\ &= \pm \frac{\sqrt{k\,(1+\beta)}}{(2+\beta)} \begin{pmatrix} c_{Q,q_1} & 0 & 0 \\ 0 & c_{Q,q_2} & 0 \\ 0 & 0 & c_{Q,q_3} \end{pmatrix} \end{aligned} \tag{5.4}$$

including the VEV ω of the scalar particle to fermions that is analogous to the Yukawa couplings already defined in the context of RS models containing a bulk Higgs while β ensures a well–defined behavior in the limit $\beta \to \infty$ on the IR brane [131, 140, 141, 207]. Furthermore, it is assumed that the top Yukawa matrix has the dominant effect. This results from a hierarchical structure of the Yukawa matrices. The most important process for the investigation of the behavior of the couplings derived so far is the four fermion exchange displayed in Fig. 5.1. In the description of the four fermion interaction the exchange by a virtual KK boson has to be taken into account. Figure 5.1a describes the tree–level process in the full theory by a an s–channel diagram, while Fig. 5.1c describes the same diagram in the effective theory. The Wilson coefficients are obtained, if the diagram in Fig. 5.1c is identified with Fig. 5.1a. There is a combinatorial factor of $1/2$ compared to the t channel diagram in Fig. 5.1b. The operators have the dimension eight. The huge mass difference between the fermions and the scalar boson S has the advantage of an identification of the operator product expansion in the effective theory. The procedure is justified as the typical energy regime for flavor physics is at low energies. The importance of the four fermion exchange is the view from the effective theory in which the propagator of the scalar particle is expanded around small momenta $p \ll M_{\mathrm{kk}}$. In the effective theory approach, the Wilson coefficients arise as follows:

$$\mathcal{H}_{eff} = \sum_i \mathcal{C}_i \mathcal{O}_i \tag{5.5}$$

For the consideration of the processes in Fig. 5.1c, the following operators are important:

$$\tilde{\mathcal{O}}_2 = (\bar{s}_L d_R)\,(\bar{s}_L d_R)\,, \qquad\qquad \mathcal{O}_2 = (\bar{s}_R d_L)\,(\bar{s}_R d_L)\,,$$

$$\mathcal{O}_4 = (\bar{s}_L d_R)(\bar{s}_R d_L). \tag{5.6}$$

In the case of Fig. 5.1, the general Wilson coefficient $\mathcal{C}_i$ of the four quark operator of the coupling of a scalar boson S to a $SU(2)_L$ singlet is defined as the overlap integral c_{ijkl} of

$$\begin{aligned}
\mathcal{H}_{eff} \ni & \sum_{i,j,k,l,=1}^{3} c_{ijkl} (\bar{q}_{i,1,R} q_{j,2,L}) (\bar{q}_{l,1,R} q_{l,2,L}) \\
&= \frac{1}{m_{sc}^2} \Lambda^*_{\bar{q}_i q_l} \Lambda^*_{\bar{q}_k q_j} (\bar{q}_{i,1,L} q_{j,2,R}) (\bar{q}_{l,1,L} q_{k,2,R}) \\
&\quad + \frac{1}{m_{sc}^2} \Lambda_{\bar{q}_i q_j} \Lambda_{\bar{q}_k q_l} (\bar{q}_{i,1,R} q_{j,2,L}) (\bar{q}_{l,1,R} q_{k,2,L}) \\
&\quad + \frac{1}{2m_{sc}^2} \Lambda_{\bar{q}_i q_j} \Lambda^*_{\bar{q}_k q_l} (\bar{q}_{i,1,L} q_{j,2,R}) (\bar{q}_{l,2,R} q_{k,1,L})
\end{aligned} \tag{5.7}$$

with

$$\begin{aligned}
c_{ijkl} &\sim \Lambda_{ij}(t) \Lambda_{kl}(t') \\
&= \int_0^1 \mathrm{d}t t^{1+\beta} \int_0^1 \mathrm{d}t' t'^{,1+\beta} (2+\beta)^2 \Bigg[x_i \hat{a}_j^{(c_Q)\dagger} F(c_Q) t^{c_Q} g_Q F(c_Q) \frac{t^{1+c_Q} - \epsilon^{-1+2c_Q} t^{-c_Q}}{1+2c_Q} \hat{a}_i^{(c_Q)} \\
&\quad + x_j \hat{a}_i^{(c_q)\dagger} F(c_q) t^{c_q} g_q F(c_q) \frac{t^{1+c_q} - \epsilon^{-1+2c_q} t^{-c_q}}{1+2c_q} a_j^{(c_q)} \Bigg] \\
&\quad \times \Bigg[x_k \hat{a}_l^{(c_Q)\dagger} F(c_Q) t'^{,c_Q} g_Q F(c_Q) \frac{t'^{,1+c_Q} - \epsilon^{-1+2c_Q} t'^{,-c_Q}}{1+2c_Q} \hat{a}_k^{(c_Q)} \\
&\quad + x_l \hat{a}_k^{(c_q)\dagger} F(c_q) t'^{,c_q} g_q F(c_q) \frac{t'^{,1+c_q} - \epsilon^{-1+2c_q} t'^{,-c_q}}{1+2c_q} a_l^{(c_q)} \Bigg]
\end{aligned} \tag{5.8}$$

and contains the coupling $\Lambda_{ij}(t)$ of the scalar S to fermions. The coupling Λ_{ij} is a 3×3 matrix and differs from the CKM matrix in its phenomenological interpretation. While the CKM matrix describes charged transitions with different charges, the matrix Λ_{ij} describes transitions, in which the charge remains the same. Before going into more detail of the calculation, some remarks about the flavor suppression mechanism are necessary. The coupling of the scalar particle S consists always of an $\mathcal{S}(t)$ profile function and a $\mathcal{C}(t)$ profile function (Eq. (2.124)) of the 5D fermion (Eq. (2.105)), because the scalar particle couples only to doublets or singlets. The localization in the extra dimension of the overlap profile function of the fermions depends on the bulk–localization parameter $c_{Q/q}$. In Eq. (5.8) appear at each vertex and for either singlet fermion profile function or doublet fermion profile function three combinations: $t, t^{c_{Q/q}}$ and $t^{2c_{Q/q}}$. The first one, *i.e.* contributions that are proportional to t do not induce a flavor change, whereas the other two do so. The factors $t^{c_{Q/q}}$ and $t^{2c_{Q/q}}$ are only large and peaked towards the IR brane in case of the top quark. Considering light fermions, it turns out that the overlap between the profile functions of the fermion and the scalar bosons S are small, because the bulk–localization parameter is $c_{Q/q} \leq -1/2$ and the profile function of the scalar boson S is peaked due to the delta function towards the IR, as well. The coupling Eq. (5.8) scales in leading order in $F(c_{Q,q_i}) F(c_{Q,q_i})$ in the ZMA, in which Eq. (5.8) is

written. If the scalar S was a gauge boson, the situation would be similar. Differences occur in the scaling of the localization parameter in the coupling, because in this case, the transitions would be proportional to $t^{c_{Q_i}+c_{q_i}}$ [145, 153, 154, 161, 179, 271, 272]. The difference to the vector boson coupling to the fermions is the suppression by a factor of $1/M_{\mathrm{kk}}^4$ considering a tree–level diagram. The coupling is suppressed by a factor of $1/M_{\mathrm{kk}}$ that stems from the fermion mass at each vertex and the squared mass that stems from the propagator. Furthermore, the mass m_S is much larger than any other vector boson mass. This causes also a larger suppression. Considering the couplings of vector bosons to fermions, the inverse mass term is involved in couplings, in which doublets of right–handed fermions, or singlets of left–handed fermions are considered.
In the second row of Eq. (5.8), the coupling of the doublets is shown, whereas in the third line the coupling of the scalar particle to the singlet fermions is shown. The fourth and the fifth line describe the same coupling at t'. After integrating out the fifth dimension, the former t–dependent Λ_{ij} now reads

$$\begin{aligned}\Lambda_{ij} = x_i \frac{F\left(c_{Q_j}\right) F\left(c_{Q_i}\right)}{\left(1+2c_{Q_i}\right)} \hat{a}_j^{(c_Q)\dagger} g_{c_Q} \hat{a}_i^{(c_Q)} \left(\frac{1}{3+c_{Q_i}+c_{Q_j}+\beta} - \frac{\epsilon^{1+2c_{Q_i}}}{2+c_{Q_j}-c_{Q_i}+\beta} \right) \\ + x_j \frac{F\left(c_{q_i}\right) F\left(c_{q_j}\right)}{\left(1+2c_{q_j}\right)} \hat{a}_i^{(c_q)\dagger} g_{c_q} \hat{a}_j^{(c_q)} \left(\frac{1}{3+c_{q_i}+c_{q_j}+\beta} - \frac{\epsilon^{1+2c_{q_j}}}{2+c_{q_i}-c_{q_j}+\beta} \right). \end{aligned} \tag{5.9}$$

The coupling that depends on t' is obtained in the same way. With the insertion of the ZMA of the squared fermion mass Eq. (2.133) as well as replacing contributions of $\mathcal{O}\left(\epsilon^2\right)$ with Eq. (2.129), the term proportional to $1/\left(3+c_{q_i}+c_{q_j}+\beta\right)$ in Eq. (5.9) is negligible compared to the rest. Thus, the Wilson coefficients of the operators of Eq. (5.6) read

$$\begin{aligned}\mathcal{C}_2 &= \frac{1}{m_{sc}^2} \Lambda_{il}^* \Lambda_{kj}^* \\ &= \frac{(2+\beta)^2}{m_{\mathrm{sc}}^2 M_{\mathrm{kk}}^2} \Bigg[\Big(m_{f_i} F\left(c_{Q_j}\right) F\left(c_{Q_i}\right) g_{c_{Q_{ij}}}^* I_{ij}\left(c_{Q_j}, c_{Q_i}\right) \\ &\quad + m_{f_j} F\left(c_{q_j}\right) F\left(c_{q_i}\right) g_{c_{q_{ij}}}^* I_{ij}\left(c_{q_j}, c_{q_i}\right) \Big) \\ &\quad \Big(m_{f_k} F\left(c_{Q_l}\right) F\left(c_{Q_k}\right) g_{c_{Q_{kl}}}^* I_{kl}\left(c_{Q_k}, c_{Q_l}\right) \\ &\quad + m_{f_l} F\left(c_{q_l}\right) F\left(c_{q_k}\right) g_{c_q}^* I_{kl}\left(c_{q_l}, c_{q_k}\right) \Big) \Bigg], \end{aligned} \tag{5.10}$$

$$\begin{aligned}\tilde{\mathcal{C}}_2 &= \frac{1}{m_{sc}^2} \Lambda_{ik} \Lambda_{jl} \\ &= \frac{(2+\beta)^2}{m_{\mathrm{sc}}^2 M_{\mathrm{kk}}^2} \Bigg[\Big(m_{f_i} F\left(c_{Q_i}\right) g_{c_Q} I_{ij}\left(c_{Q_i}, c_{Q_j}\right) \\ &\quad + m_{f_j} F\left(c_{q_i}\right) F\left(c_{q_j}\right) g_{c_{q_{ij}}} I_{ij}\left(c_{q_i}, c_{q_j}\right) \Big) \\ &\quad \Big(m_{f_k} F\left(c_{q_k}\right) F\left(c_{q_l}\right) g_{c_{Q_{kl}}} I_{kl}\left(c_{Q_k}, c_{Q_l}\right) \\ &\quad + m_{f_l} F\left(c_{q_l}\right) F\left(c_{q_k}\right) g_{c_{q_{kl}}} I_{kl}\left(c_{q_l}, c_{q_k}\right) \Big) \Bigg] \end{aligned} \tag{5.11}$$

$$\mathcal{C}_4 = \frac{1}{2m_{sc}^2} \Lambda_{ij} \Lambda_{kl}^*$$

$$= \frac{(2+\beta)^2}{2m_{\text{sc}}^2 M_{\text{kk}}^2} \Bigg[\Big(m_{f_i} F\left(c_{Q_j}\right) F\left(c_{Q_i}\right) g_{c_{Q_{ij}}} I_{ij}\left(c_{Q_j}, c_{Q_i}\right) + m_{f_j} F\left(c_{q_i}\right) F\left(c_{q_j}\right) g_{c_{q_{ij}}} I_{ij}\left(c_{q_i}, c_{q_j}\right) \Big) \Big(m_{f_l} F\left(c_{Q_l}\right) F\left(c_{Q_k}\right) g^*_{c_{Q_{kl}}} I_{kl}\left(c_{Q_k}, c_{Q_l}\right) + m_{f_k} F\left(c_{q_l}\right) F\left(c_{q_k}\right) g^*_{c_{q_{kl}}} I_{kl}\left(c_{q_l}, c_{q_k}\right) \Big) \Bigg] \tag{5.12}$$

with

$$I_{ij}\left(c_{Q/q_i}, c_{Q/q_j}\right) = \left(-\frac{1}{2 + c_{Q/q_i} - c_{Q/q_j} + \beta} \right). \tag{5.13}$$

In the following phenomenological section, contributions of the flavor–changing neutral scalar S are estimated and compared to SM flavor observables in meson mixing in Sec. 5.4. Contributions of the flavor–changing scalar to the bounds on the neutron EDM and deuteron EDM are discussed in Sec. 5.7, as well. For these reasons, values for the coupling Eq. (5.9) $\Lambda_{ij}(t)$ have had to be obtained. This has been done using the c_{Q/q_i} parameters that have been obtained by the generation of the RS data point sets in Sec. 2.8 and are inserted into Eq. (5.9). The mass of the flavor–violating neutral scalar S is considered to be 750 GeV. The quark masses have been obtained by the RG running down to the scale of the top mass. In case of the B^0–$\overline{B}^0$ mixing the masses have been obtained at the B scale, and for the K^0–$\overline{K}^0$ mixing the masses have been obtained at the K scale. Therefore, the matrix Λ_{ij} contains values in the real part of its off–diagonal entries of $\mathcal{O}\left(10^{-6}\right)$, whereas the diagonal elements are larger. The imaginary part of the off–diagonal matrices is much smaller than the real part. The largest value is always Λ_{33} that is of order 1. Another approach to evaluate the couplings $\Lambda_{ij}(t)$ is done with the ZMA and rewriting the quark masses by $x_{i,j} = m_{f_{i,j}}/M_{\text{kk}} = vF\left(c_{Q_{i,j}}\right) y^* F\left(c_{q_{i,j}}\right)/(\sqrt{2}M_{\text{kk}})$ multiplied by a random number that is of order 1, because the other quantities in Eq. (5.9) are of order one. This assumption justifies to consider only diagonal entries in the matrix Eq. (5.4). Thus, the coupling $\Lambda_{i,j}$ (Eq. (5.9)) reads to leading order

$$\Lambda_{ij} = \frac{v y_*}{\sqrt{2} M_{\text{kk}}} F\left(c_{Q_i}\right) F\left(c_{q_j}\right). \tag{5.14}$$

5.3 Discussion and comparison to scalars in RS models

In the following, there is a short discussion, whether there are similarities between the scalar S under investigation and the most important scalar particles that appear in the context of warped extra dimensions.

In the literature, scalars in the RS model have been discussed before. If the scalar S acquired a VEV that generates fermion masses, S would create a mechanism that is responsible for the localization of the fermions along the extra dimension [125, 139, 141]. As a consequence, the scalar could also act as a localizer field, which was first introduced in split fermion theories [100, 141]. This possibility is discussed in greater detail below in Sec. 5.3.1. A possible new scalar S could exist in the context of flat extra dimensions, as well. Although no solution to the hierarchy problem as described in Sec. 2.2.1 exists, this model has a lot of similarities in calculations with models that contain a warped extra

dimension [217]. In [218], the scalar S couples to SM particles only *via* loops containing vector–like fermions. Leaving the possibility of generating flavor hierarchies *via* an extra–dimensional mechanism, the SM leptons are the only particles, which are in the bulk of the extra dimension in order to achieve the correct size of the couplings [219, 220]. Furthermore, this ansatz requires more than one extra dimension for the achievement of the size of the couplings [141]. The explanation that the scalar S could be a spin 2 KK graviton seems challenging, because the predictions of the 13 TeV dilepton data from CMS [221] seem to be in conflict with this hypothesis as they reject some parameter space [141, 222–224].

5.3.1 Localizer field

Arkani-Hamed and Schmaltz introduced a localizer field being a scalar [97] in the context of flat extra dimensions based on [95]. Besides the RS models [98, 99], also [95] is a milestone in the development of extra dimensional approaches. Arkani-Hamed and Schmaltz proposed that the KK excitations of the SM fermion fields live on a wall with a given volume L in the extra dimension, whereas gravity, the SM fields including the Higgs boson field propagate along the extra dimension. The KK excitations of the SM fermion fields are localized at a fixed point on the extra dimension and their wave functions are described by Gaussian distributions. Because of the overlap of the wave functions, the Yukawa couplings are suppressed exponentially as the wave function has the shape of a Gaussian distribution. The difference to the case of the warped extra dimensional models is that the exponential suppression does not stem from the metric, but from the profile of the fermionic wave function. Nevertheless, the prediction of non–universal couplings from the fermions to a scalar is model–independent and depends only on the localization in the wall. This localization breaks translational invariance leading to a local modification of the VEV in the extra dimension by the scalar. The VEV therefore has its origin imposed by a $\mathbb{Z}_2$ symmetric potential [97] and could be linear, if the corresponding scalar mass m_ϕ is zero. This means that the quartic interactions do not exist or the VEV an almost linear realization, if $m_\phi \neq 0$. Considering the $\mathbb{Z}_2$ symmetry, a so–called 'odd mass term'

$$\mathcal{L}_{\text{odd}} = m_\Psi \epsilon\left(t\right) \bar{\psi}\psi \tag{5.15}$$

has to be introduced for each fermion stemming from a second scalar field which is odd under the $\mathbb{Z}_2$ symmetry and which shifts the localization of the fermions away from the orbifold fixed points [100]. The localization of the Higgs field can be either on the boundary or in the bulk, where the VEV is in both scenarios confined to one orbifold fixed point. The localization of the Higgs on one of the boundary leads to EWSB which only occurs at this point in the extra dimension. Localizing the Higgs in the bulk leads to two more sub scenarios. If the Higgs mass would be positive, a belonging bulk VEV would not exist, but a separate negative mass term would exist on the boundary which leads to EWSB at this point. The other possibility is that the Higgs field is not the only scalar bulk field. The bulk Higgs field is coupled to more bulk fields which acquire a t-dependent VEV and trigger EWSB in the region near of t. A further fine–tuning would be required as well, because then $m_\phi \gg v$ follows for both boundary and bulk masses. The localizer field would have a small overlap with both the doublets and singlets of the first two generations, resulting in weaker interaction with the Higgs due to their

exponentially suppressed overlap functions. The opposite case is valid for the fermions of the third generation, where the coupling to the localizer field ϕ is weaker, resulting in a strong coupling to the Higgs [100].

5.3.2 Radion

As mentioned in Ch. 2 Sec. 2 the Radion is the VEV of the fifth component of the Minkowski metric in Eq. (2.8). Here is the main difference that the arbitrary scalar boson S stems from another part of the Lagrangian density. Furthermore, the Radion can be considered as fluctuation, as well [225]. There can be significant contributions to FCNCs if the Radion is considered as the lightest new resonance in the RS model [226]. If it exists, its mass would be of order the Higgs mass if the Goldberger-Wise potential is tuned but its mass would be rather of $\mathcal{O}\,(\text{TeV})$ in a general RS setup, although its couplings to fermions would be chiral suppressed, as well [226].
The authors of [232, 233] discussed a RS model, in which the SM fields are confined on the TeV brane. In this setup, the Higgs–Radion coupling is introduced by SSB on the brane that involves a stabilizing scalar field [232, 233]. This mixing is result from merging the stabilization mechanism of the size of the extra dimension together with SSB on the TeV brane [233]. The new state of 750 GeV is then regarded as a Radion–dominated state, but its production section is significantly smaller than in the original reports if ATLAS and CMS [232].

5.3.3 Bulk Higgs

As mentioned before in Sec. 2.2.3, the scalar S under consideration differs from a bulk Higgs only in the non–existence of a zero mode, and that is considered to be as a gauge singlet scalar. Possible flavor–changing couplings of the bulk Higgs have been studied before in *e.g.* [207, 227]. The contributions are larger compared to the case of a gauge–singlet scalar S that has no zero mode.

5.3.4 Scalar as a DM particle

The scalar particle S under investigation does not correspond to any of the other cases. This scalar can be regarded as a possible Dark Matter candidate and its possible implementation is discussed following [112]. Mirroring the IR brane and requiring the KK parity in the warped extra–dimensional scenario requires a light KK particle that is electric neutral, weakly interacting, and its profile function should peak towards the IR brane. As a consequence, the fermion profile functions to which this scalar couples have to due to the $\mathbb{Z}_2$–parity conservation an odd profile function and are peaked towards the IR brane. Then, the Lagrangian density in Eq. (5.2) has to be modified by adding negative coupling terms of the S to fermions [112]. The scalar that is investigated in this chapter fulfills all these properties, but the framework is different. In the publication [228], a $\mathbb{Z}_2$–odd scalar particle, which is in [228] called "dark–Higgs" χ as a dark matter candidate in the framework of [112] is discussed. The authors of [228] calculated the annihilation cross–section and the relic abundance and found that the abundance is $\Omega_\chi h < 10^{-4}$ if the electroweak precision bounds are fulfilled. The contribution that the authors found to the annihilation cross–section is classified into two main parts. The main contribution to the annihilation cross–section stems from contact interactions of

the dark Higgs to the W and Z boson. Contributions of the other final states, in which both Higgs bosons and top quarks are involved, are small [228]. In the past, another sector in which a singlet scalar as a dark matter candidate has been proposed as twin Higgs models [229]. The scalar is also compatible with electroweak precision tests. A 750 GeV scalar would then decay into two photons. Because of this reason, only an annihilation of this DM candidate into SM particles is possible [230, 231]. The authors of [234] discussed the Higgs–Radion mixing in context of a possible dark matter candidate $m_\phi = 750 \gg m_h$ GeV. They found that the cross–section depends strongly on the localization of the gauge fields in the extra–dimension and assumed a custodial symmetry. The Radion couplings to $\gamma\gamma, Z\gamma$ are not suppressed in contrast to the couplings of the Radion to other particles. If the fields of the other particles are allowed to propagate into the bulk of the extra–dimension, except for $t_{L,R}$ and b_L that are localized on the IR brane, the cross–section is higher than whether the gauge bosons are confined on the TeV brane [234]. In the context of UED with two universal extra dimensions, a neutral scalar particle has been studied as a possible DM candidate [235]. The interaction of the dark matter candidate B_H that is a scalar with the SM Higgs fields is induced by electroweak mixing and results in the additional term

$$\mathcal{L} = -g_Y^2/8 B_H B_H h\,(h + 2v)\,. \tag{5.16}$$

The authors of [236] mentioned that the first excitation of the Higgs particle, that has a mass range between 1 and 4 TeV, as a dark matter candidate is hard to find due to the Yukawa coupling that is small for fermions. Furthermore, an annihilation into pairs of $f\bar{f}$ is helicity suppressed. The authors of [237] estimated that the mass for the lightest KK particle as a dark matter candidate that is a scalar particle is in the range between 1 TeV and 2.4 TeV. Other dark matter candidates as scalar particles have been discussed in the overview [238]. In general, the possibility of gauge bosons as dark matter candidate in the context of UED and their estimation of a detection is discussed, as well. See, for example [239–242].

5.4 Meson mixing including a general bulk scalar S

In principle FCNCs occur at tree–level in new–physics models that might lead to corrections to SM couplings. For instance, very strong bounds on new physics models originate from measurements from both CP violation as well as from flavor physics *cf.* [3, 264, 265, 281–284]. The consideration of meson mixing is of particular interest for the investigation of such FCNCs as flavor–changing couplings in meson mixing occur in new physics model in tree–level diagrams that are displayed in Fig. 5.1.A general introduction to meson physics can be found in reviews *e.g.* [3]. Before the derivation of the Wilson coefficients and the matrix elements is explained, in which the new physics contribution is contained, the meson mixing is investigated in more detail.

5.4.1 Overview of Meson mixing in the SM

In the SM there exist only four mesons, which are both flavor eigenstates and share the same flavor content and mix with their antiparticle. These hadrons are the K, B and D meson and their particle content is

$$B_s^0 \sim \bar{b}s \qquad\qquad \overline{B}_s^0 \sim b\bar{s}, \tag{5.17}$$

$$B_d^0 \sim \bar{b}d \qquad \overline{B}_s^0 \sim b\bar{d}, \tag{5.18}$$

$$K_s^0 \sim \bar{s}d \qquad \overline{K}_s^0 \sim s\bar{d}, \tag{5.19}$$

$$D^0 \sim c\bar{u} \qquad \overline{D}^0 \sim \bar{c}u. \tag{5.20}$$

These meson states are eigenstates under the strong and the electromagnetic interactions. Furthermore, the mesons can be either produced by the strong interaction in $p\bar{p}$ collisions of by the electromagnetic interaction by e^+e^- collisions. The production mechanisms are flavor conserving [243]. If the weak interaction is neglected, the eigenstates of the mesons will have the same mass eigenstates for both meson and anti–meson, resulting in the same mass. Because of the weak interaction, the degeneration mentioned does not exist and as a consequence there is a difference in both the mass and the lifetime of both meson M and anti–meson $\overline{M}$ distinguishable [244]. These differences are expressed by a linear combination of the mass eigenstates of both M and anti–meson $\overline{M}$

$$|\, M_L\rangle = q|M\rangle + p|\overline{M}\rangle, \tag{5.21}$$

$$|M_H\rangle = q|M\rangle - p|\overline{M}\rangle, \tag{5.22}$$

with the normalization condition $|q|^2+|p|^2 = 1$ and the subscripts H, L refer to the heavy and light mass eigenstate. Further there exist oscillations between M and $\overline{M}$ evolving for times $t \gg 1/\Lambda_{\mathrm{QCD}}$. The evolution of the initial (anti)meson yields a superposition to its anti–meson (meson).The long duration of the oscillations indicated as $t \gg 1/\Lambda_{\mathrm{QCD}}$, because this time evolution allows an description by an effective Hamiltonian H which is only complete, if the Hilbert space spanned by M and $\overline{M}$ is complete. The application of a Schrödinger equation leads to

$$\frac{\partial}{\partial t}\begin{pmatrix}\overline{M}\\ M\end{pmatrix} = H\begin{pmatrix}\overline{M}\\ M\end{pmatrix}. \tag{5.23}$$

The decay into the different final states is described by the non–hermitian part of the 2×2 matrix H

$$H = M - \frac{i}{2}\Gamma \tag{5.24}$$

$$\begin{pmatrix}H_{11} & H_{12}\\ H_{21} & H_{22}\end{pmatrix} = \begin{pmatrix}M_{11} & M_{12}\\ M_{12}^* & M_{22}\end{pmatrix} - \frac{i}{2}\begin{pmatrix}\Gamma_{11} & \Gamma_{12}\\ \Gamma_{12}^* & \Gamma_{22}\end{pmatrix}, \tag{5.25}$$

where M describes the mass matrix and Γ denotes the decay matrix, which are both hermitian. The diagonal elements of Eq. (5.25) describe flavor conserving decays, whereas the off diagonal elements of Eq. (5.25) describe the flavor exchange mediated by virtual W bosons in box diagrams [243]. The detailed form of the off diagonal elements follows from CPT conservation [245]. The corresponding eigenvalues of Eq. (5.24) result in

$$\omega = H_{11} \pm \sqrt{H_{12}^* H_{12}} \tag{5.26}$$

The ratio of the complex quantities q and p appearing in Eq. (5.21) is given by

$$\left(\frac{q}{p}\right)^2 = \frac{M_{12}^* - \frac{i}{2}\Gamma_{12}^*}{M_{12} - \frac{i}{2}\Gamma_{12}}. \tag{5.27}$$

Eq. (5.27) becomes important when discussing asymmetries in CP violation for in Sec. B.1. Both mass difference and difference of the width of the mass eigenstates can be expressed by

$$\Delta m = m_H - m_L = 2\mathrm{Re}\sqrt{H_{12}^* H_{12}} \tag{5.28}$$

$$\Delta\Gamma = \Gamma_H - \Gamma_L = -4\mathrm{Im}\sqrt{H_{12}^* H_{12}}. \tag{5.29}$$

The presence of the eigenvalues Eq. (5.26) in Eqs. (5.28),(5.29) connect the off–diagonal elements to the mass eigenstates. The case of $K^0 - \overline{K}^0$ mixing is different, because there is a huge difference in their lifetime and both Δm and $\Delta\Gamma$ are expressed by the shorter and longer lived particle, denoted by L and S, respectively.
The dimensionless quantities described by the ratios involving the difference of the mass width Δm and the decay rate $\Delta\Gamma$ and the total decay rate Γ

$$x = \frac{\Delta m}{\Gamma}, \qquad y = \frac{\Delta\Gamma}{\Gamma} \tag{5.30}$$

give a hint of the amount of mixing. If $|x| = \infty$, the mixing is at its maximum, because $\frac{1}{\Delta m} \ll \frac{1}{\Gamma}$. As a consequence, the initial (anti)meson oscillates to its anti–meson (meson) and back results in an equal amount of both meson and anti–meson, respectively. The mixing of the mesons is at its maximum, as well, if $|y| = 1$ indicating that the two eigenstates M_L and M_H are decayed. Assuming CP conservation, the total decay of M_L and M_H, respectively, is equal to the same amount of both mesons and anti–mesons, *i.e.* $M = \overline{M}$ [243, 246]. Because of the different values in the parameters, *e.*g., Δm_M and $\Delta\Gamma$, the behavior of the oscillations of the meson systems is different [247, 248, 127].
The study of meson mixing is that the mixings belong to the FCNCs, because the quarks share the same electric charge. FCNCs appear at loop–level, because they are absent at tree level and as a consequence, they are sensitive to new physics and especially sensitive to CP violation.
There exist three systems, the B^0–$\overline{B}^0$ system, the Kaon system K^0–$\overline{K}^0$ and the D system D^0–$\overline{D}^0$. In the B^0–$\overline{B}^0$ system, diagrams with an internal top quark dominate compared to the contribution from other diagrams with lights quarks, as the result is proportional to the internal quark mass. In the case of both K^0–$\overline{K}^0$ and D^0–$\overline{D}^0$ this assumption is crucial, as these mixings are suppressed by the CKM matrix elements containing the top quark. Another possibility is that they are suppressed with the heaviest quark [244].

5.5 Derivation of the Wilson coefficients and matrix elements for meson mixing

Before the Wilson coefficients are derived, the matrix elements that contribute to meson mixing are discussed, the general expression for the matrix elements is discussed. The matrix elements of meson mixing consist of the box diagrams shown in Fig. 5.2. The new physics contributions enters by the additional diagram Fig. 5.1. Contributions to meson–mixing of the SM graphs and the NP contributions. The SM contribution is described by the two box diagrams in Fig. 5.2a and Fig. 5.2b, whereas the NP enters at tree–level and is described by Fig. 5.2c. The flavor of inner quark and its respective anti–quark in both diagrams Fig. 5.2a and Fig. 5.2b is independent from the meson under consideration and can be u, c, t or $\bar{u}, \bar{c}, \bar{t}$. In case of K^0–$\overline{K}^0$, $\bar{q}_1 = \bar{s}$,$q_1 = s$,$\bar{q}_2 = \bar{d}$,$q_2 = d$. In case of

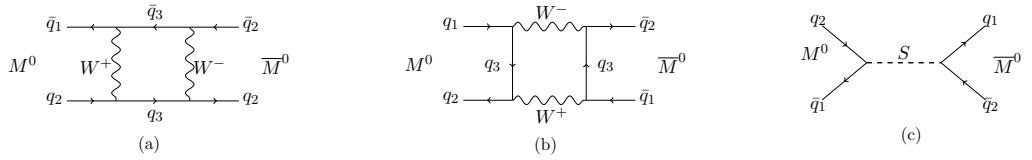

Figure 5.2: Contributions to meson–mixing of the SM graphs and the NP contributions. The SM contribution is described by the two box diagrams in Fig. 5.2a and Fig. 5.2b, whereas the NP enters at tree–level and is described by Fig. 5.2c. The flavor of inner quark and its respective anti–quark in both diagrams Fig. 5.2a and Fig. 5.2b is independent from the meson under consideration and can be u, c, t or $\bar{u}, \bar{c}, \bar{t}$. In case of K^0–$\overline{K}^0$, $\bar{q}_1 = \bar{s}$,$q_1 = s$,$\bar{q}_2 = \bar{d}$,$q_2 = d$. In case of $B^0_{d,s}$–$\overline{B}^0_{d,s}$ mixing $\bar{q}_1 = \bar{b}$, $q_1 = b, \bar{q}_2 = \bar{d}, \bar{s}$, $q_2 = d, s$. The particle content of the D^0–$\overline{D}^0$ meson mixing is $\bar{q}_1 = \bar{u}$, $q_1 = u\, \bar{q}_2 = \bar{c}$, $q_2 = c$.

$B^0_{d,s}$–$\overline{B}^0_{d,s}$ meson mixing is the particle content $\bar{q}_1 = \bar{b}$, $q_1 = b, \bar{q}_2 = \bar{d}, \bar{s}$, $q_2 = d, s$. The particle content of the D^0–$\overline{D}^0$ meson mixing is $\bar{q}_1 = \bar{u}$, $q_1 = u\, \bar{q}_2 = \bar{c}$, $q_2 = c$. The general expression for the evolution of the matrix elements of meson mixing from the high scale Λ down to the lower scale μ is [249]

$$\langle \overline{M}|\mathcal{H}_{\text{eff}}|M\rangle_i = \sum_{j=i}^{5}\sum_{r=i}^{5}\left(b_j^{(r,i)} + \left(\frac{\alpha_s\left(\Lambda\right)}{\alpha_s\left(m_t\right)}\right) c_j^{(r,i)}\right)\left(\frac{\alpha_s\left(\Lambda\right)}{\alpha_s\left(m_t\right)}\right)^{a_j} \mathcal{C}_i\left(\Lambda\right)\langle \overline{M}|\mathcal{O}_i|M\rangle. \tag{5.31}$$

The evolution from the higher scale Λ on the right hand side down to the lower scale on the left hand side of Eq. (5.31) is obtained by the so–called magic numbers a_j, b_j, c_j. The general derivation of the magic numbers is mentioned in Sec. 5.7, when the evolution matrix is discussed. The magic numbers have been obtained using the RI–MOM scheme in the Landau gauge [249]. The Wilson coefficients $C_{2,4}\left(\Lambda\right)$ are obtained at the higher scale Λ. At the high scale, the corresponding operators are considered. There is a possibility that the operators of the matrix elements mix with the other higher–dimensional operators due to the anomalous dimension matrix and as a consequence, in the magic numbers due to the renormalization procedure. As a consequence, all operators have to be taken into account, because the operators can induce a mixing to all other operators. The hadronic matrix elements on the right–hand side of the renormalized operators and are given by [334]

$$\langle \overline{M}|\mathcal{O}_1\left(\mu\right)|M\rangle = \frac{1}{3} m_M f_M^2 B_1\left(\mu\right), \tag{5.32}$$

$$\langle \overline{M}|\mathcal{O}_2\left(\mu\right)|M\rangle = -\frac{5}{24}\left(\frac{m_M}{m_{M_{q_i}}\left(\mu\right) + m_{M_{q_j}}\left(\mu\right)}\right)^2 m_M f_M^2 B_2\left(\mu\right), \tag{5.33}$$

$$\langle \overline{M}|\mathcal{O}_3\left(\mu\right)|M\rangle = \frac{1}{24}\left(\frac{m_M}{m_{M_{q_i}}\left(\mu\right) + m_{M_{q_j}}\left(\mu\right)}\right)^2 m_M f_M^2 B_3\left(\mu\right), \tag{5.34}$$

$$\langle \overline{M}|\mathcal{O}_4\left(\mu\right)|M\rangle = \frac{1}{4}\left(\frac{m_M}{m_{M_{q_i}}\left(\mu\right) + m_{M_{q_j}}\left(\mu\right)}\right)^2 m_M f_M^2 B_4\left(\mu\right), \tag{5.35}$$

$$\langle \overline{M}|\mathcal{O}_5\left(\mu\right)|M\rangle = \frac{1}{5}\left(\frac{m_M}{m_{M_{q_i}}\left(\mu\right)+m_{M_{q_j}}\left(\mu\right)}\right)^2 m_M f_M^2 B_5\left(\mu\right). \tag{5.36}$$

The operators that appear in Eq. (5.32)–Eq. (5.36) read [249]

$$\mathcal{O}_1 = \left(\bar{q}^{\alpha}_{i,L}\gamma^{\mu}q^{\alpha}_{j,L}\right)\left(\bar{q}^{\beta}_{i,R}\gamma^{\mu}q^{\beta}_{j,R}\right), \tag{5.37}$$

$$\mathcal{O}_2 = \left(\bar{q}^{\alpha}_{i,R}q^{\alpha}_{j,L}\right)\left(\bar{q}^{\beta}_{i,R}q^{\beta}_{j,L}\right), \tag{5.38}$$

$$\mathcal{O}_3 = \left(\bar{q}^{\alpha}_{i,R}q^{\beta}_{j,L}\right)\left(\bar{q}^{\beta}_{i,R}q^{\alpha}_{j,L}\right), \tag{5.39}$$

$$\mathcal{O}_4 = \left(\bar{q}^{\alpha}_{i,R}q^{\alpha}_{j,L}\right)\left(\bar{q}^{\beta}_{i,L}q^{\beta}_{j,R}\right), \tag{5.40}$$

$$\mathcal{O}_5 = \left(\bar{q}^{\alpha}_{i,R}q^{\beta}_{j,L}\right)\left(\bar{q}^{\beta}_{i,L}q^{\alpha}_{j,R}\right), \tag{5.41}$$

and the corresponding operator $\tilde{\mathcal{O}}$ is derived by the interchange of $L \leftrightarrow R$. The matrix elements in Eq. (5.32)–Eq. (5.36) have the following structure: they contain the mass of the meson m_M under consideration and, the respective decay constant f_M that is a measure of the probability of the distance between the quarks in the meson. This assumption is only true for point–like interactions, which is the case for the the weak interaction. Furthermore, all effects that stem from strong interactions are parametrized in f_M [251]. The so–called *bag* parameter $B_i\left(\mu\right)$ parametrizes deviations from the vacuum insertion approximation [127]. The vacuum insertion approximation splits the matrix element of a quartic operator into two matrix elements of two operators that are bilinear in the quark fields. Only the vacuum state is inserted, which is a appropriate approximation [250]. The remaining coefficient in Eq. (5.32)–Eq. (5.36) normalizes the bag parameter [251, 252].
The quark masses appear in Eq. (5.32)–Eq. (5.36) *via* a perturbation of higher orders and in an energy dependence of the effective quark masses. The running quark masses obey the RGE equation

$$\begin{aligned}\frac{\mathrm{d}}{\mathrm{d}\ln(\mu)}m_q\left(\mu\right) &= \gamma^m\left(\mu\right)m_q\left(\mu\right)\\ &= m_q\left(\mu\right)\left(\frac{\alpha_s\left(\mu\right)}{\alpha_s\left(\mu_0\right)}\right)^{-\frac{\gamma_0^m}{2\beta_0}},\end{aligned} \tag{5.42}$$

as well. In Eq. (5.42), the parameter μ_0 denotes the scale to which the masses are evolved down. In this thesis, the two–loop result [253]

$$m_q(\mu) = \left(\frac{\alpha_s\left(\mu\right)}{\alpha_s\left(\mu_0\right)}\right)^{-\frac{\gamma_0^m}{2\beta_0}}\left(1-\frac{\left(\alpha_s\left(\mu\right)-\alpha_s\left(\mu_0\right)\right)\left(\beta_0\gamma_1^m-\gamma_0^m\beta_1\right)}{\left(4\pi\right)\left(2\beta_0^2\right)}\right) \tag{5.43}$$

with the one–loop coefficients and the coefficients of the beta function

$$\gamma_0^m = -6C_F, \tag{5.44}$$

$$\gamma_1^m = -3C_F^2 - \frac{97}{3}C_FC_A + \frac{20}{3}C_An_fT_F - 4C_Fn_fT_F, \tag{5.45}$$

$$\beta_0 = \frac{11}{3}C_A - \frac{4}{3}n_fT_F, \tag{5.46}$$

$$\beta_1 = \frac{34}{3}C_A^2 - \frac{20}{3}C_A n_f T_F - 4C_F n_f T_F, \tag{5.47}$$

from [254–256] is used to obtain the values of the running quark masses. For $SU(3)_c$, the factors C_F, C_A, T_F have the values

$$C_A = 3, \quad C_F = \frac{4}{3}, \quad T_F = \frac{1}{2}. \tag{5.48}$$

Equation (5.31) holds for both B^0–$\overline{B}^0$, and D^0–$\overline{D}^0$ mixing and is used therefore. In the case of K^0–$\overline{K}^0$ mixing, the form of Eq. (5.31) changes to

$$\langle \overline{K}|\mathcal{H}_{\text{eff}}|K\rangle_i = \sum_{j=i}^{5}\sum_{r=i}^{5}\left(b_j^{(r,i)} + \eta\, c_j^{(r,i)}\right)\eta^{a_j} C_i(\Lambda)\, R_r \langle \overline{K}|\mathcal{O}_1|K\rangle, \tag{5.49}$$

with $\eta = \left(\frac{\alpha_s(\Lambda)}{\alpha_s(m_t)}\right)$. The difference to Eq. (5.31) is the evolution of the matrix element. Here, only the first hadronic matrix element

$$R_r \langle \overline{K}|\mathcal{O}_1^{sd}|K\rangle \tag{5.50}$$

is considered. Therefore, the rescaling parameters R_i are introduced that express with the matrix element $\langle \overline{K}|\mathcal{O}_1|K\rangle$ the remaining matrix elements in Eq. (5.33)–Eq. (5.36). The effective Hamiltonian for meson mixing $\mathcal{H}_{\text{eff}}$ is obtained by integrating out the scalar boson S and reads

$$\mathcal{H}_{\text{eff}} = \mathcal{C}_2\left(\overline{q}_{i,R}q_{j,L}\right)\left(\overline{q}_{i,R}q_{i,L}\right) + \tilde{\mathcal{C}}_2\left(\overline{q}_{i,L}q_{j,R}\right)\left(\overline{q}_{i,L}q_{j,R}\right) + \mathcal{C}_4\left(\overline{q}_{j,R}q_{i,L}\right)\left(\overline{q}_{i,L}q_{j,R}\right) \tag{5.51}$$

with the Wilson coefficients

$$\mathcal{C}_2 = -\frac{\left(\Lambda_{ij}^*\right)^2}{m_{\text{sc}}^2}, \quad \tilde{\mathcal{C}}_2 = -\frac{(\Lambda_{ji})^2}{m_{\text{sc}}^2} \tag{5.52}$$

$$\mathcal{C}_4 = -\frac{\Lambda_{ij}\Lambda_{ji}^*}{2m_{\text{sc}}^2}, \tag{5.53}$$

in which i and j denote the flavor of the corresponding meson. Using the leading order term of the coupling Λ_{ij} it is possible with help of Eq. (2.132) to see that the Wilson coefficient $\mathcal{C}_4$ is proportional to the contributing quark masses. The estimates for $\mathcal{C}_2$ and $\tilde{\mathcal{C}}_2$ read

$$\mathcal{C}_2 = \frac{v^2 y_* F(c_{Q_i}) F\left(c_{q_j}\right)}{M_{\text{kk}}^2 m_{\text{sc}}^2} \propto \lambda^{"M"}\frac{m_{M_{q_j}}}{M_{\text{kk}}^2 m_{\text{sc}}^2} \tag{5.54}$$

$$\tilde{\mathcal{C}}_2 = \frac{v^2 y_* F(c_{Q_i}) F\left(c_{q_j}\right)}{M_{\text{kk}}^2 m_{\text{sc}}^2} \propto \frac{m_{M_{q_j}}}{\lambda^{"M"} M_{\text{kk}}^2 m_{\text{sc}}^2}. \tag{5.55}$$

The exponent "M" of λ that occurs in the last two equations depends due to Eq. (2.209) on the meson mixing under consideration. While for K^0–$\overline{K}^0$ mixing "M" is 1, there is a factor of λ^3 in case of B_d^0–$\overline{B}_d^0$ mixing, and a factor of λ^2 in the case of B_s^0–$\overline{B}_s^0$ mixing. The mass difference of the meson system is expressed by the real part of the absolute value of the matrix element Eq. (5.31) in case of B^0–$\overline{B}^0$ and D^0–$\overline{D}^0$ mixing, whereas in case of K^0–$\overline{K}^0$ mixing the real part of the absolute value of the matrix element Eq. (5.49) is used.

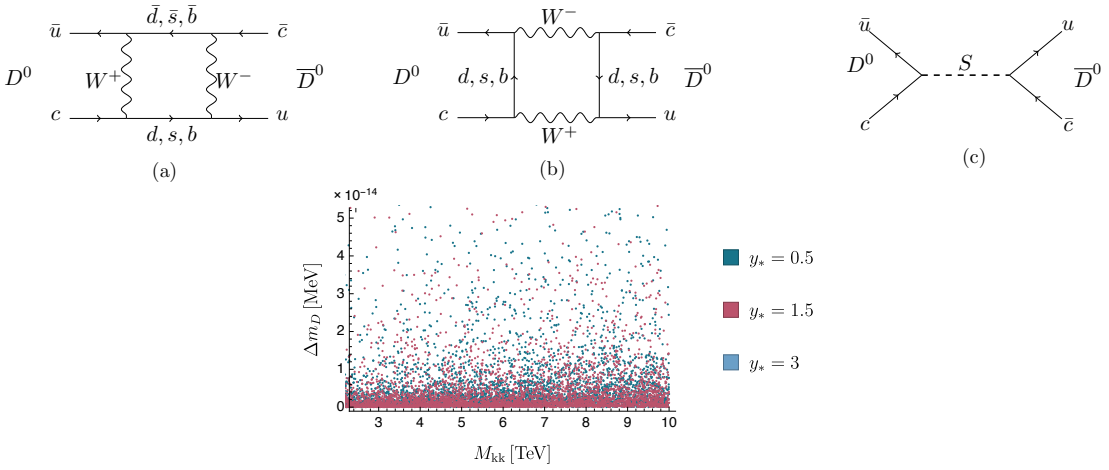

Figure 5.3: Contributions of the scalar S that induces FCNCs to Δm_D. These contributions are plotted in MeV against the $M_{\rm kk}$ mass in TeV. The corresponding Feynman diagrams that contribute are depicted in the first line. The first and the second diagram contribute in the SM, whereas the third diagram displays the new physics contribution. The contributions of a scalar S that induces FCNCs to Δm_D deviate from the SM value of $\Delta m_D = (5.26) \cdot 10^{-12}\,\text{MeV}$ [6] by a factor of $\mathcal{O}\left(10^{-2}\right)$. The two diagrams that contribution to the D^0–$\overline{D}^0$ mixing in the SM are depicted in Fig. 5.3a and Fig. 5.3b, whereas the new physics enter through the tree–level diagram in Fig. 5.3c.

5.5.1 D^0–$\overline{D}^0$ system

The D^0–$\overline{D}^0$ system is of particular interest as it is the only system containing up–type quarks in contrast to both B^0–$\overline{B}^0$ system and K^0–$\overline{K}^0$ system, which consist of only down–type quark mixings. The D^0–$\overline{D}^0$ system consists only of up–type quarks the quark in the loop is due to the W boson a down type quark. Those loops are suppressed by the bottom quark as the CKM elements are small. Additionally the masses of the internal particles can often be neglected. The long distance effects make predictions in the D^0–$\overline{D}^0$ mixing challenging to calculate. The short distant contributions are suppressed by two reasons: One reason is that contributions proportional to the inverse of the W boson mass are suppressed by the GIM mechanism and the contributions proportional to the inverse of the charm mass m_c are suppressed due to a contribution of the external momentum of the charm quark [257, 243]. The short distance contributions contain an equal amount of both box diagrams and penguin diagrams, as well.
In the D^0–$\overline{D}^0$ system CP violation not has been found since its discovery in 2007 [258–260] and confirmation [258, 261, 262]. The non–observation of CP violation is due to the fact that the decay width is much larger than the difference of the mass width Δm_D leading to a challenging observation of the mixing between the D^0 and $\overline{D}^0$ mesons [245, 258]. If CP violation is observed then this could be realized in different way, *e.g.* that the D^0–$\overline{D}^0$ mixing happens at tree–level leading to a FCNC coupling at the Z boson to vector–like singlet up–type quarks. Another realization would be multi–Higgs doublet models with both neutral or charged Higgs bosons which do not have to be

necessarily flavor conserving [230, 243, 258, 263]. The mass difference Δm_D is defined as

$$\Delta m_D = 2\left|\langle D^0|\mathcal{H}_{\text{eff}}^{\Delta S=1}|\bar{D}^0\rangle\right|, \tag{5.56}$$

measured to be as

$$\Delta m_D = (5.26)\cdot 10^{-12}\,\text{MeV}. \tag{5.57}$$

The contributions of the scalar particle S that induces FCNCs to Δm_D are displayed in MeV against the KK mass M_{kk} in TeV in Fig. 5.3. The contributions deviate by a relative factor of $\mathcal{O}\left(10^{-5}\right)$ to the SM value Eq. (5.57). The contributions consist of the Feynman diagrams in Fig. 5.3a and Fig. 5.3b that are the SM contribution. In Fig. 5.3c the Feynman diagram of the new physics contribution is shown.

5.6 Meson mixing and rare decays

5.6.1 B^0–$\overline{B}^0$ system

In the B^0–$\overline{B}^0$ system there exist two different mixings, *i.e.* the B_d^0–$\overline{B}_d^0$ and the B_s^0–$\overline{B}_s^0$ mixing [258]. The mixing in the B_s^0–$\overline{B}_s^0$ system was discovered in 2006 [264] and confirmed by measurements of the LHCb collaboration [265, 266]. Furthermore, this mixing appears in the decays $B_s^0 \to J/\psi K^+K^-$ [267] and $B_s^0 \to D_s^-\mu X$ [268], as well. The measurements of the mixing in the system offered a validation of the unitarity triangle and gave information about CP–violating asymmetries [3]. The mixing that is generated by the weak interaction takes place in lowest order as in the Kaon system and is mediated by an internal W boson and up–type quarks in the loop. The long–distance interaction effects can be ignored due to the large B meson mass, which is out of the range of hadronic resonances. Further, the mixing B_s^0–$\overline{B}_s^0$is very interesting as it is a $\Delta F = 2$ flavor transition that could be sensitive to new physics, because no quarks from the first generation are involved.
The mass difference of the B_X system are related to Eq. (5.31) *via*

$$\Delta m_{B_q} = 2\left|\langle B^0|\mathcal{H}_{\text{eff}}^{\Delta S=1,2}|\overline{B}^0\rangle\right| \tag{5.58}$$

with the normalization

$$C_{B_q}e^{2i\phi_{B_q}} = \frac{\langle B^0|\mathcal{H}_{\text{eff}}^{\Delta S=1,2}|\overline{B}^0\rangle}{\langle B^0|\mathcal{H}_{\text{eff,SM}}^{\Delta S=1,2}|\overline{B}^0\rangle}, \qquad C_{B_q} = \frac{\Delta m_{B_q}}{\left(\Delta m_{B_q}\right)_{\text{SM}}}. \tag{5.59}$$

C_{B_q} is considered to be a measure for the mass difference of Δm_{B_q} compared to the SM value, whereas the weak phase ϕ_{B_q} is a measure for the time–dependent asymmetry in the decay $B \to \psi\phi$. This phase is present in the SM [127, 6]. The current values for the world averages of Δm_{B_d} and Δm_{B_s} are [6, 258]

$$\Delta m_{B_d} = (3.333 \pm 0.013)\ 10^{-10}\,\text{MeV}, \tag{5.60}$$

$$\Delta m_{B_s} = (1.1688 \pm 0.0014)\ 10^{-8}\,\text{MeV}. \tag{5.61}$$

The contribution of the flavor–changing scalar particle S to the mass differences from neutral meson mixing Δm_{B_d} and Δm_{B_s} are considered in Fig. 5.4. Both SM contributions that enter by the box diagrams in Fig. 5.4a and Fig. 5.4b and the new physics

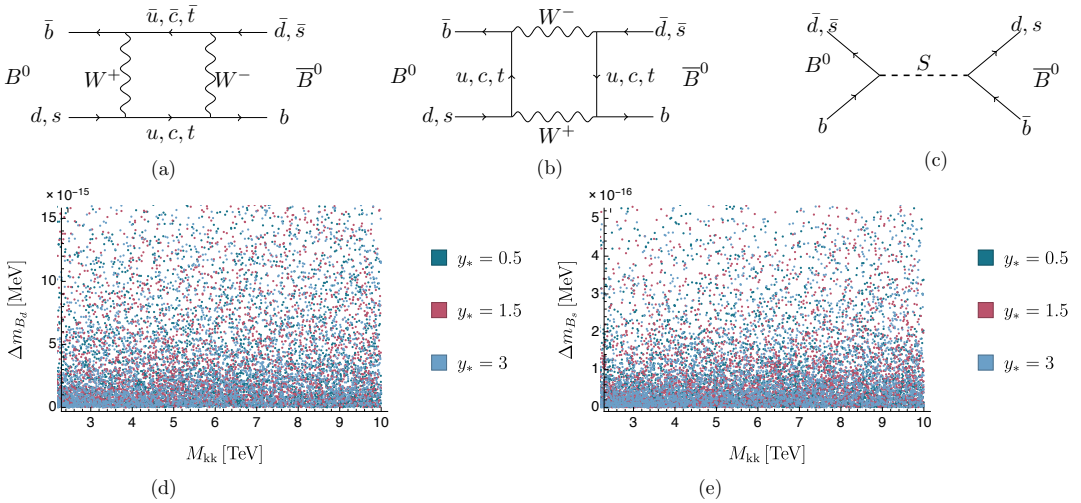

Figure 5.4: The first line shows with the two diagrams depicted in Fig. 5.4a and Fig. 5.4b the SM contribution to the neutral meson mixing, whereas Fig. 5.4c shows the tree–level contribution form a scalar particle. In Fig. 5.4d and Fig. 5.4e, the contributions of the scalar particle S to the mass differences Δm_{B_d} and Δm_{B_s} of B meson mixing are plotted in Fig. 5.4d and Fig. 5.4e in MeV against the KK mass in TeV. The predictions for Δm_{B_d} differ by a factor of 10^{-5} compared to the SM value, which is $\Delta m_{B_d} = (3.333 \pm 0.013)\ 10^{-10}$ MeV [6]. The contributions of a scalar particle S to the mass difference in neutral B_s mixing is smaller by a factor of 10^{-8} compared to the experimental value, which is shown in Eq. (5.61). The masses of the corresponding B mesons are $B_d = 5279.63 \pm 0.15$ MeV and $B_s = 5366.89 \pm 0.19$ MeV [6].

contribution is depicted in Fig. 5.4c. They are plotted in MeV against the KK mass in TeV. The contributions of the scalar particle S to the mass differences are smaller by a factor of 10^{-5} to the measured value of Δm_{B_d}. The contributions are also smaller by a factor of 10^{-8} compared to the experimental value of Δm_{B_s}. The experimental values for Δm_{B_d} and Δm_{B_s} are shown in Eq. (5.60) and Eq. (5.61).
If ϕ_{B_q} not equal to zero, the time–dependent asymmetry measures the new physics contribution

$$2\varphi_{B_q} = \arg\left(\langle B^0|\mathcal{H}_{\rm eff}^{\Delta S=1,2}|\overline{B}^0\rangle\right) \tag{5.62}$$

$$= \left|\beta_{B_q}\right| - \phi_{B_q}, \tag{5.63}$$

and not only β_{B_q} that defines the phase difference, which leads to the B^0–$\overline{B}^0$ mixing. In case of a vanishing phase and its experimental value is [6, 258]

$$\beta_{B_d} = \arg\left(-\frac{V_{cd}V_{cb}^*}{V_{td}V_{tb}^*}\right), \tag{5.64}$$

$$\beta_{B_s} = 0.0376 \pm 0.0012. \tag{5.65}$$

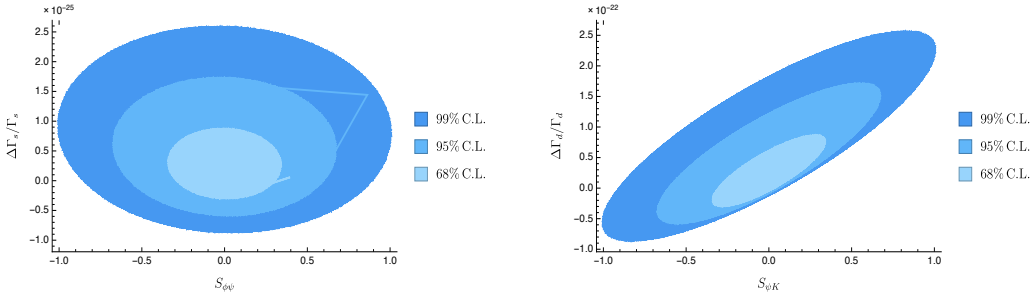

(a) (b)

Figure 5.5: The contribution of a scalar S that induces FCNCs to the asymmetries $\Delta\Gamma_{B_q}/\Gamma_{B_q}$, q=d,s. The contribution of the prediction of the phase $S_{\psi\phi}$ plotted against the prediction of $\Delta\Gamma_s/\Gamma_s$ in Fig. 5.5a. The predictions differ by a relative factor of $\mathcal{O}\left(10^{-25}\right)$ compared to the SM value of $\Delta\Gamma_s/\Gamma_s = 0.12943$ [6]. In case of the predicted contributions to $\Delta\Gamma_d/\Gamma_d$, the values deviate by a relative factor of $\mathcal{O}\left(10^{-22}\right)$ compared to the SM value of $\Delta\Gamma_d/\Gamma_d = 0.13072$ [6]. $\Delta\Gamma_d/\Gamma_d$ is plotted against $S_{\psi K_s}$ in Fig. 5.5b.

Furthermore, the CP asymmetries and the width differences of the semi–leptonic decays result in [127, 161, 269, 270]

$$\frac{\Delta\Gamma_{B_q}}{\Gamma_{B_q}} = -\left(\frac{\Delta m_{B_q}}{\Gamma_{B_q,\text{exp}}}\right)\left[\text{Re}\left(\frac{\Gamma_{12}^{B_q}}{M_{12}^{B_q}}\right)_{\text{SM}}\frac{\cos\left(2\phi_{B_q}\right)}{C_{B_q}} - \text{Im}\left(\frac{\Gamma_{12}^{B_q}}{M_{12}^{B_q}}\right)_{\text{SM}}\frac{\sin\left(2\phi_{B_q}\right)}{C_{B_q}}\right] \tag{5.66}$$

$$\mathcal{A}_{\text{SL},B_q} = \text{Im}\left(\frac{\Gamma_{12}^{B_q}}{M_{12}^{B_q}}\right)_{\text{SM}}\frac{\cos\left(2\phi_{B_q}\right)}{C_{B_q}} - \text{Re}\left(\frac{\Gamma_{12}^{B_q}}{M_{12}^{B_q}}\right)_{\text{SM}}\frac{\sin\left(2\phi_{B_q}\right)}{C_{B_q}} \tag{5.67}$$

with $q = s, d$, $\text{Im}\left(\frac{\Gamma_{12}^{B_q}}{M_{12}^{B_q}}\right)_{\text{SM}} = \frac{\Delta\Gamma^{B_q}}{\Delta M^{B_q}}\tan\left(\phi_{B_q}\right)$, $\text{Re}\left(\frac{\Gamma_{12}^{B_q}}{M_{12}^{B_q}}\right)_{\text{SM}} = \frac{\Delta\Gamma_{B_q}}{\Delta M^{B_q}}$ [258]. With the angle φ_{B_q} (Eq. (5.62)) and β_{B_q} it is possible to obtain a value for the phase ϕ_{B_q}. The width differences are then compared to [161, 270, 272]

$$S_{\psi K_s} = \sin\left(2\beta_{B_d} + 2\phi_{B_d}\right), \tag{5.68}$$

$$S_{\psi\phi} = \sin\left(2\left|\beta_{B_s}\right| - 2\phi_{B_s}\right). \tag{5.69}$$

The contributions of a scalar S that induces FCNCs to the width differences $\Delta\Gamma_{B_q}/\Gamma_{B_q}$, q=d,s are shown in Fig. 5.5. The width difference $\Delta\Gamma_s/\Gamma_s$ is plotted against the phase difference $S_{\psi\phi}$ in Fig. 5.5a and the values differ by $\mathcal{O}\left(10^{-25}\right)$ relative to the SM value of $\Delta\Gamma_s/\Gamma_s = 0.12943$ [6]. The phase difference $S_{\psi K_s}$ that is defined in Eq. (5.68) is plotted against the width difference $\Delta\Gamma_d/\Gamma_d$ in Fig. 5.5b. The predicted contributions to the width difference $\Delta\Gamma_d/\Gamma_d$ is smaller compared to the SM value of $\Delta\Gamma_d/\Gamma_d = 0.13072$ [6] by a factor of $\mathcal{O}\left(10^{-22}\right)$. Another possibility to study CP–violating effects to NP is the decay from B mesons into a pair of leptons that is now investigated, because here the Wilson coefficients Eq. (5.10)–Eq. (5.12) are sensitive to fermion interactions. The fermion masses contribute at both vertices. Furthermore, decays into pairs of leptons are particularly interesting, because if the lepton mass vanishes in the BSM, it will also vanish in the SM.

5.6.2 $b \to s\mu^+\mu^-$

The decay of a B meson into two leptons is a test of the flavor change between the generations $\Delta F = 2$ observables that are sensitive on the position of the quark profile function along the extra dimension. CP violation in the B^0 meson system was detected in 2001 [273]. Their branching ratio is very well determined by experiment. The experimental result of the LHCb collaboration for $R_K = 0.745^{+0.090}_{-0.074}(\text{stat}) \pm 0.036(\text{syst})$ is in a 2.6 σ tension with the SM [274, 275]. The decay $b \to X_s\mu^+\mu^-$ delivers a two–side bound on the branching ratio, because its limit is close to the SM expectation and is a stringent bound on NP models that reach into the parameter space of BSM theories [127]. The contribution of the scalar particle to the branching ratios

$$\mathcal{B}r\left(B_d \to \mu\mu\right) = (1.8 \pm 3.1) \cdot 10^{-10}, \tag{5.70}$$

$$\mathcal{B}r\left(B_s \to \mu\mu\right) = \left(2.4^{+0.9}_{-0.7}\right) \cdot 10^{-9} \tag{5.71}$$

is smaller by a factor of 10^{-31} in case of the branching ratio of the decay $\mathcal{B}r\left(B_d \to \mu\mu\right)$, while the contribution of a flavor–changing particle S is smaller by a factor of 10^{-32} in the case of the branching ratio of the decay $\mathcal{B}r\left(B_d \to \mu\mu\right)$ compared to their experimental value. The contributions induced by a scalar S that induces FCNCs are shown as a comparison in Fig. 5.6.

The authors of [215] performed an analysis if there exist a flavor change that is induced by new heavy scalar particles at tree–level. They investigated four general scenarios. Furthermore, they assumed the flavor–changing coupling as a complex number that is bounded from above by the $\Delta F = 2$ transition. The authors argued that a contribution from a heavy scalar particle S would not interfere with the SM contribution, towards to the case if a pseudo–scalar particle is investigated [215]. The same result is found for this case.

The effective Hamiltonian for the SM contribution of the decay $b \to ql^+l^-$ with $q = s, d$ reads

$$\mathcal{H}_{\text{eff}} = \frac{4G_F^2}{\sqrt{2}} \frac{\alpha}{4\pi} V_{tb}V_{ts}^* \mathcal{C}_{10}\mathcal{O}_{10} \tag{5.72}$$

The Wilson coefficient $\mathcal{C}_{10}$ in Eq. (5.72) describes the contributions from the SM that conserves the lepton flavor and reads [278, 279]

$$\mathcal{C}_{10} = \frac{1}{s^2_{\theta_W}} \left(\frac{x}{4} \left[\frac{x/2-3}{(x-1)} + \frac{3x/2+1}{(x-1)^2} ln\left(x\right) \right] - \frac{1}{4} \left[\frac{x}{(x-1)} + \frac{x}{(x-1)^2} ln\left(x\right) \right] \right), \tag{5.73}$$

with $x = m_t/m_W$ and the operator reads $\mathcal{O}_{10} = \left(\bar{s}_L\gamma^\mu b_R\right)\left(\bar{l}\gamma_\mu\gamma_5 l\right)$. The first term in Eq. (5.73) stems from the diagram, in which a Z boson couples to the lepton pair and the second term stems from contributions from the W box graph [279]. These contribution are depicted in Fig. 5.6a and Fig. 5.6b, while the new physics contribution enters at tree–level and is depicted in Fig. 5.6c. If the branching ratio of the three diagrams is calculated, it turns out that there is no interference between the new physics contribution and the SM contribution. This is due to the fact that there is no axial coupling in the lepton sector, as it would be the case in theories with axion–like particles. The branching ratio reads (for $q = d, s$)

$$\mathcal{B}r\left(b \to q\mu^+\mu^-\right) = \frac{G_F^2}{16\pi} \left(\frac{\alpha}{\pi}\right)^2 m^2_{B_q} f^2_{B_q} \left|V_{ts}^* V_{tb}\right|^2 \left|\mathcal{C}_{10}\right|^2 m^2_\mu \sqrt{1 - \frac{4m^2_\mu}{m^2_{B_q}}}$$

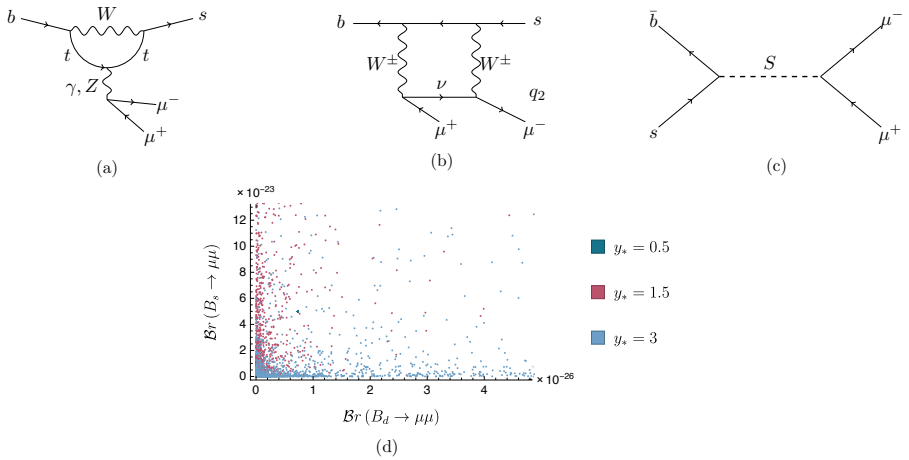

Figure 5.6: Contributions of a scalar S that induces FCNCs to the branching ratios of the decays $\mathcal{B}r\,(B_q \to \mu\mu)$ with $q = d, s$ are plotted against each other. The contribution of this scalar particle to the branching ratio $\mathcal{B}r\,(B_d \to \mu\mu)$ is smaller by a factor of 10^{-16} compared to the experimental value, which is $\mathcal{B}r\,(B_d \to \mu\mu) = (1.8 \pm 3.1) \cdot 10^{-10}$ [6]. The contribution of this scalar particle to the branching ratio $\mathcal{B}r\,(B_s \to \mu\mu)\,(2.4^{+0.9}_{-0.7}) \cdot 10^{-9}$ [6] is by a factor of 10^{-14} smaller. The contribution is obtained using Eq. (5.74). In Fig. 5.6a and Fig. 5.6b the SM contribution is depicted, while in Fig. 5.6c the new physics enters with a tree–level diagram.

$$+\frac{1}{32\pi}\frac{m_{B_q} f_{B_q}^2}{(m_b+m_s)^2}\left(\frac{m_{B_q}^2}{m_{B_q}^2-m_{\mathrm{sc}}^2}\right)^2 \Lambda_{\mu\mu}^2 |\Lambda_{bs}-\Lambda_{sb}^*|^2 \left(1-\frac{4m_\mu^2}{m_{B_q}^2}\right)^{3/2} \tag{5.74}$$

and the second line is identified with the new physics contribution. There is a contribution of a dimension 8 operator that is mainly responsible for the suppression. Considering only this part of the branching ratio yields values that are of $\mathcal{O}\left(10^{-23}\right)$. Therefore, only this contribution is shown in Fig. 5.6, because the SM contribution is of $\mathcal{O}\left(10^{-7}\right)$. The Feynman diagrams of the SM contribution are depicted in Fig. 5.6a and Fig. 5.6b.

5.6.3 K^0–$\overline{K}^0$ system

K^0–$\overline{K}^0$ mixing puts the most stringent constraints for new physics manifesting in flavor changing decays at tree level. CP violation was discovered and investigated in the neutral Kaon system putting even stronger bounds to new physics [3]. In the SM effective theory, K^0–$\overline{K}^0$ mixing is mediated *via* the $\Delta S = 2$ four quark operator $\mathcal{O}_1 = (s\gamma_\mu d)\,(s\gamma_\mu d)$. Furthermore, the observables Δm_K and ϵ_K are defined as

$$\epsilon_K = \frac{k_\epsilon e^{i\varphi_\epsilon}}{\sqrt{2}\Delta m_K^{\mathrm{exp}}} \mathrm{Im}\langle K^0|\mathcal{H}_{\mathrm{eff}}^{\Delta S=1}|\bar{K}^0\rangle, \qquad \Delta m_K = 2\left|\mathrm{Re}\langle K^0|\mathcal{H}_{\mathrm{eff}}^{\Delta S=1}|\bar{K}^0\rangle\right| \tag{5.75}$$

and depend on the long–distance contribution κ_ϵ. The long–distance contribution makes due to the experimental precision an exact theoretical estimation impossible. The best way to resolve this discrepancy is a division into a short–range and a long–range contribution and a comparison of the short–distance contributions with the experimental

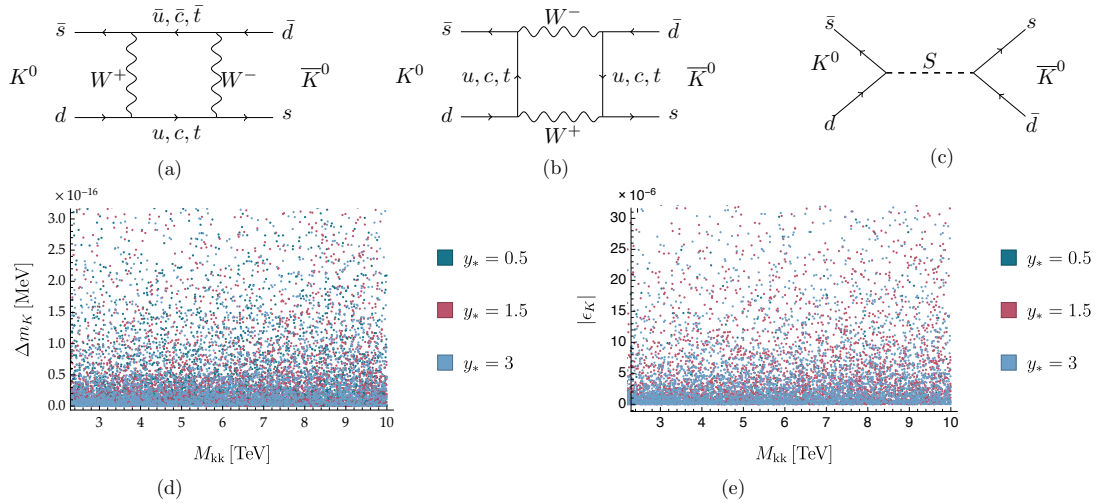

Figure 5.7: The first line contains the Feynman diagrams that contribute to neutral Kaon mixing. The first two diagrams describe the SM contribution, whereas the third diagram describes the new physics contribution. The contribution of the scalar S that induces FCNCs to Δm_K and ϵ_K are depicted in Fig. 5.7d and Fig. 5.7e in the second line. The mass difference in the neutral Kaon mixing Δm_K is plotted in MeV against the KK mass dependence $M_{\rm kk}$ in TeV in Fig. 5.7d. The experimental value for Δm_K is $(3.484 \pm 0.006) \cdot 10^{-12}$ MeV [6]. The values for the contribution of the scalar S to Δm_K differ by 10^{-4} compared to the experimental values. The contribution of the scalar S to the absolute value of ϵ_K is plotted against $M_{\rm kk}$ in TeV in Fig. 5.7e. The values for the contribution of the scalar S to $|\epsilon_K|$ differ by a factor of 10^{-3} compared to the SM value of ϵ_K, which is $(2.228 \pm 0.011)\, 10^{-3}$ [6].

results. Therefore it seems to be useful quoting both an upper limit and a lower limit that might explain discrepancies stemming from the experiment [127, 280]. The contributions are given by the Wilson coefficient in Eq. (5.31) and the RG running is given by Eq. (5.31) with the left–hand side of $C_i\,(2\text{GeV})$ that are the energy scale of both initial and final states of the Kaon. Both quantities Δm_K in MeV and ϵ_K are plotted in Fig. 5.7 against the KK mass in TeV. The predicted contribution to the mass difference in the neutral Kaon mixing Δm_K is for a scalar S that induces FCNCs of orders of magnitude smaller compared to the experimental value that is $(3.484 \pm 0.006) \cdot 10^{-12}$ MeV [6]. This can be seen in Fig. 5.7d. Furthermore, the contribution of a scalar S that induces FCNCs to Δm_K does not depend on the KK mass, because the points are distributed equally in Fig. 5.7d. The same behavior of the distribution of the simulated points is shown, whether the contribution of the scalar S that induces FCNCs to the absolute value of ϵ_K is considered. This contribution is smaller by a factor of 10^{-3} compared to the experimental value of ϵ_K, which is $(2.228 \pm 0.011)\, 10^{-3}$ [6]. This contribution is plotted against the KK mass in TeV. The contributions of the scalar S to Δm_K and ϵ_K have been calculated with Eq. (5.75). The corresponding Feynman diagrams of the SM model are depicted in Fig. 5.7a and Fig. 5.7b, whereas the new physics contribution in depicted in Fig. 5.7c.

5.7 Impact on electric dipole moments including a general bulk scalar S

Another diagnostic investigation is the comparison of the (chromo) electric dipole moment ([C]EDM) of the neutron including the Yukawa matrices. The investigation of EDMs of elementary systems may lead to a violation of time reversal if the experimental value of the EDM is unequal to zero. The vector of the EDM should be parallel to the particle spin that has an opposite symmetry. If the CPT symmetry is conserved, a violation of the T symmetry leads to CP violation, as well. Therefore, a non–zero value for EDMs is a sign for T violation [299, 300]. The measurement of the EDM is a complementary approach to search for New physics compared to the direct searches at the LHC, because the EDM is an indirect probe of NP [311]. The electric dipole moment is derived and the 5D matrices that induce a flavor–change are applied. Both CEDM and EDM impose bounds for new physics models from flavor–changing couplings stemming from direct measurements of tree–level decays, as well as indirect bounds stemming from the precision observables if they receive corrections from the couplings under consideration [3, 301]. The dominant BSM contribution to the neutron EDM stems from FCNC interactions to the scalar under consideration [301]. Usually, these couplings would be *e.g.* the coupling of the top quark to the Higgs boson and another quark [3, 301–309]. In the context of warped extra dimensions, the EDM of the neutron sets a lower bound to the KK mass around 10 TeV which is a very tough constraint [153, 154]. A detailed discussion on the impact of EDMs in various BSM scenarios is found *e*.g. in [310, 311] and a review of EDM of light nuclei is found *e*.g. in [312]. In the following, the results of the FCNC fermion coupling Λ_{ij} that has been derived in Sec. 5.2 with an arbitrary flavor–changing scalar S are compared to the recent measurements and the method follows [309].
The electric dipole moment is defined as

$$H_{\text{EDM}} = -\vec{d}_f \cdot \vec{E} \tag{5.76}$$

leading to the Lagrangian of a spin 1/2 field

$$\mathcal{L}_{\text{EDM}} = -\frac{1}{2} d_f \bar{\psi}_f \sigma^{\mu\nu} \gamma^5 \psi_f F_{\mu\nu} \tag{5.77}$$

with $\Gamma^\mu_Q\left(q^2\right) = \left[\frac{i\sigma^{\mu\nu}\gamma^5}{2m} q_\nu g_2\left(q^2\right)\right]$. An expression for $\vec{d}_f$ is obtained using

$$\begin{aligned} \vec{d}_f &= -\frac{q e g_2(0)}{2m_f}\vec{\sigma} \\ &= -\frac{q e g_2(0)}{2m_f}\vec{S} \end{aligned} \tag{5.78}$$

For the quarks, the Lagrangian of the chromo–electric dipole moment is defined in the same way to Eq. (5.77) [3]

$$\mathcal{L}_{\text{CEDM}} = -\frac{i}{2} d^c_r \bar{q}_f \sigma^{\mu\nu} \gamma^5 \frac{\lambda^i}{2} q_r G^i_{\mu\nu} \tag{5.79}$$

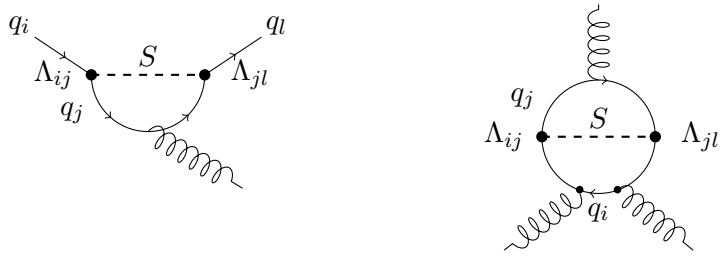

(a) (b)

Figure 5.8: Schematic drawing of one–loop and two–loop diagrams that contribute to the CEDM and the Weinberg operator. On the right hand side, Fig. 5.8a shows the contribution to the CEDM. The flavor change that is induced by the flavor–violating scalar S *via* the matrix Λ is marked with the dark dots.

For this analysis, both the top quark as well as the Higgs have been integrated out at $\mathcal{O}(m_t)$, resulting in the effective Lagrangian

$$\begin{aligned}\mathcal{L}_{\text{eff}} \ni & -d_q(\mu_t)\frac{i}{2}\bar{q}_f\sigma^{\mu\nu}\gamma_5 q F_{\mu\nu} - \tilde{d}_q(\mu_t)\frac{ig_s(\mu_t)}{2}\bar{q}_f\sigma^{\mu\nu}\gamma_5 q G^a_{\mu\nu} \\ & - w(\mu_t)\frac{1}{3}f^{abc}G^a_{\mu\sigma}G^{b,\sigma}_{\nu}\tilde{G}^{c,\mu\nu}\end{aligned} \tag{5.80}$$

with $q = u, d$, and the dual field strength tensor of QCD $\tilde{G}^{c,\mu\nu} = \frac{1}{2}\epsilon^{\mu\nu\alpha\beta}G^a_{\alpha\beta}$ with the Levi–Civita tensor $\epsilon^{0123} = 1$ containing the FCNC couplings under consideration [309].

5.7.0.1 Charm–top couplings

The dominant contribution to the CEDM stems from the penguin diagram in Fig. 5.8a at the scale μ_c and reads [313, 314]

$$\tilde{d}_c(\mu_t) = \frac{1}{32\pi^2}\frac{m_t}{m_s^2}f_1(x_{t,\text{sc}})\,\text{Im}(\Lambda_{tc}\Lambda_{ct}) \tag{5.81}$$

including

$$f_1(x_{1,2}) = \frac{x_{1,2}-3}{(x_{1,2}-1)^2} + \frac{2}{(x_{1,2}-1)^3}\ln(x_{1,2}), \quad x_{1,2} = \frac{m_1^2}{m_2^2}, \tag{5.82}$$

which is equivalent in the limit $x_{t,sc} \to 0$ and a charge replacement with the result obtained in [301, 308]. The dipole transition is provided *via* the enhancement of the top quark in Eq. (5.81).
The matching condition $w(\mu_t)$ for the Weinberg operator is only obtained *via* a two loop calculation of the diagram displayed in Fig. 5.8 and reads [309, 314–316]

$$w(\mu_t) = \frac{g_s^3(\mu_t)}{(32\pi^2)^2}\frac{1}{m_{sc}^2}f_2(x_{t,\text{sc}})\,\text{Im}(\Lambda_{tc}\Lambda_{ct}) \tag{5.83}$$

with

$$f_2(x_{1,2}) = -\frac{x_{1,2}^2 - 5x_{1,2} - 2}{3(x_{1,2}-1)^3} + \frac{2x_{1,2}}{(x_{1,2}-1)^4} \quad x_{1,2} = \frac{m_1^2}{m_2^2}. \tag{5.84}$$

The Weinberg operator $w(\mu_t)$ mixes under renormalization with both the quark EDM and CEDM, but not vice verse. Furthermore, the Weinberg operator $w(\mu_t)$ receives corrections from the CEDM at every heavy quark threshold reading at one loop level if the charm quark is integrated out [313, 319, 320]

$$\delta w(\mu_c) = \frac{g_s^3(\mu_c)}{(32\pi^2)^2} \frac{\tilde{d}_c(\mu_c)}{m_c}. \tag{5.85}$$

The shift $\delta w(\mu_c)$ as well as the RG evolution to the hadronic scale cause non–vanishing contributions of the top–quark and the down–quark that are considered, as well. In the discussion, the contributions from the Weinberg operator are negligible and set to zero.

5.7.0.2 Top–up couplings

The calculation of the up–quark EDM $d_u(\mu_t)$ is obtained *via* the diagram Fig. 5.8a in Fig. 5.8 *via* a replacement of the gluon by a photon. The calculation of both EDM and CEDM are easier as only the scalar boson S has to be integrated out. The result reads [301, 308, 309, 313, 314]

$$d_u(\mu_t) = \frac{Q_u e}{32\pi^2} \frac{m_t}{m_{\text{sc}}^2} f_1(x_{t,\text{sc}}) \operatorname{Im}(Y_{tu} Y_{ut}) \tag{5.86}$$

with the electric charge Q_u of the up quark as well as f_1 defined in Eq. (5.82). Analogously to Eq. (5.81), the results for the CEDM $\tilde{d}_u(\mu_t)$ and for the contribution of the Weinberg operator $w(\mu_t)$ are obtained. The only replacement which has to be done compared to Eq. (5.81) in order to obtain the expression for $\tilde{d}_u(\mu_t)$ is the change of $\Lambda_{ct} \to \Lambda_{ut}$ and $\Lambda_{tc} \to \Lambda_{tu}$, respectively.
The evolution of the EDM and the CEDM of the higher scale $\mu_t = 163.3\,\text{GeV}$ down to the lower scale μ_c is achieved by the evolution matrix $U(\mu, \Lambda)$, which obeys the renormalization group equation [253]

$$\begin{aligned} \frac{\mathrm{d}}{\mathrm{d}\ln(\mu)} U(\mu) &= \gamma^T(g)(\alpha_s) U(\mu, m) \\ &= T_g \exp\left(\int_{g(m)}^{g(\mu)} \mathrm{d}g' \frac{\gamma^T(g')}{\beta(g')} \right), \end{aligned} \tag{5.87}$$

with T_g being an ordering operator acting on the functions $\exp\left(\int_{g(m)}^{g(\mu)} \mathrm{d}g' \frac{\gamma^T(g')}{\beta(g')}\right)$. T_g achieves an ordering of the increasing coupling constants from the left to the right. This is not necessarily guaranteed as the anomalous dimension matrices do not commute.
In leading logarithmic approximation, the evolution matrix $U(\mu, \Lambda)$ is given by

$$U(\mu, \Lambda) = V \left(\frac{\alpha_s(\Lambda)}{\alpha_s(\mu)} \right)^{\frac{\vec{\gamma}^0}{2\beta_0}} V^{-1}, \tag{5.88}$$

where V is a matrix that diagonalizes γ^{0^T}. The vector $\vec{\gamma}^0$ in Eq. (5.88) contains the diagonal elements of the diagonal matrix [253]

$$\gamma_D^0 = V^{-1} \gamma^{0^T} V. \tag{5.89}$$

At the same time, the magic numbers a_i that are mentioned in Sec. 5.5 are obtained with the same equation using [317]

$$U(\mu, \Lambda) = V \left(\frac{\alpha_s(\Lambda)}{\alpha_s(\mu)} \right)^{a_i} V^{-1} \tag{5.90}$$

and

$$\begin{aligned} \gamma_D^0 &= \left(V^{-1} \gamma^{0^T} V \right)_{ij} \\ &= 2\beta_0 a_i \delta_{ij}. \end{aligned} \tag{5.91}$$

Performing an evolution from a higher scale leads to a negligible contribution [318]. Equipped with the necessary formulae, the neutron EDM results in [321, 322]

$$\begin{aligned} \frac{d_n}{e} = (1.0 \pm 0.5) \Bigg\{ 1.4 \left[\frac{d_d(\mu_t)}{e} - 0.25 \frac{d_u(\mu_t)}{e} \right] + 1.1 \left[\tilde{d}_d(\mu_t) + 0.5\, \tilde{d}_u(\mu_t) \right] \Bigg\} \\ + (22 \pm 10) \cdot 10^{-3} \mathrm{GeV} w(\mu_t), \end{aligned} \tag{5.92}$$

in which $d_d(\mu_t)$ and $\tilde{d}_d(\mu_t)$ are analogously defined as The present bound is obtained by ILL and reads [323]

$$\left| \frac{d_n}{e} \right| < 2.9 \cdot 10^{-26} \,\mathrm{cm}. \tag{5.93}$$

Other experiments as the nEDM and n2EDM experiment is expected to measure the neutron EDM in the near future [324]. After the nEDM experiment moderates spallation neutrons through heavy water, the measurement is re–executed using solid D_2 crystals [324, 311]. The SNS nEDM collaboration [325] will measure the neutron EDM using a ^{4}He moderator for the ultra–cold neutrons. They will also use ^{4}He to sustain a high electric field as a high voltage insulator [325, 326, 311]. Furthermore, polarized ^{3}He is used, because of its magnetic characteristics. It will be used for three tasks: to be a co–magnetometer, measuring the magnetic field, and as a superconducting magnetic shield [326, 311]. For the deuteron EDM, the following formula is obtained [309]

$$\begin{aligned} \left| \frac{d_D}{e} \right| = (0.5 \pm 0.3) \left[\frac{d_d(\mu_t)}{e} + \frac{d_u(\mu_t)}{e} \right] + \left[5^{+11}_{-3} + (0.6 \pm 0.3) \right] \left(\tilde{d}_d(\mu_t) - \tilde{d}_u(\mu_t) \right) \\ - (0.2 \pm 0.1) \left(\tilde{d}_d(\mu_t) + \tilde{d}_u(\mu_t) \right) + (22 \pm 10) \cdot 10^{-3} \mathrm{GeV} w(\mu_t), \end{aligned} \tag{5.94}$$

a present experimental limit does not yet exist at the moment. The deuteron EDM is expected to be measured in the future by the JEDI collaboration [327–329] and to a sensitivity to around $\mathcal{O}\left(10^{-29}\right)$ by the Storage Ring Electric Dipole Moment collaboration [331, 332]. While a in recent SM calculation it was shown that the EDM of the deuteron is $2.8 \cdot 10^{-31}\, e$ cm [333], the prediction for the RS model differs by a factor of $\mathcal{O}\left(10^5\right)$ from this value.

The contributions from a flavor–changing scalar particle to the neutron EDM and deuteron EDM are plotted against the KK gluon mass $M_g^{(1)}$ in Fig. 5.9. In case of the contributions of a flavor–changing scalar to the neutron EDM, there is a relative

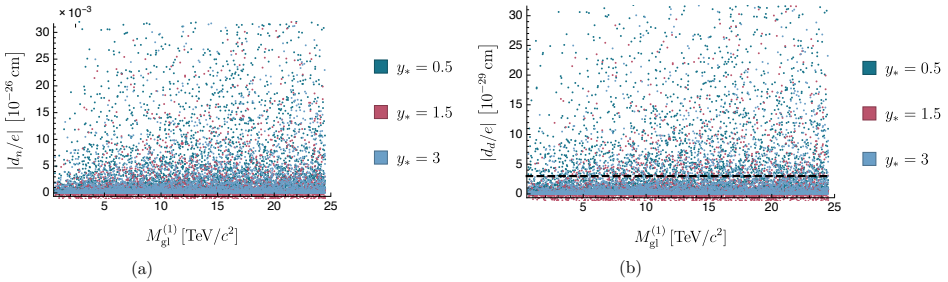

Figure 5.9: Contributions of the scalar S that induces FCNCs to the EDM of the neutron and the deuteron are plotted against the gluon mass $M_g^{(1)}$ in TeV. The contributions of the flavor–changing scalar S to the neutron are displayed in Fig. 5.9a and are not yet detectable. The contributions to the deuteron, however, are in reach if the desired precision of [331, 332] is available. The limit of $3 \cdot 10^{-29}\, e$ cm is displayed as dashed line in Fig. 5.9b.

deviation of $\mathcal{O}\left(10^{-3}\right)$ to the upper limit of Eq. (5.93) [323]. The obtained values from the contribution of the flavor–changing scalar particle have a relative deviation to the upper bound of the neutron EDM in the Storage ring EDM collaboration's prediction. The theoretical prediction of the contribution of a flavor–changing scalar particle to the upper bound of the deuteron EDM deviates relatively by a factor of $\mathcal{O}\left(10^{2}\right)$ to the desired sensitivity of $\mathcal{O}\left(10^{-29}\right)$. For $y^* = 0.5$, 78.4% of the generated data points are in agreement with the upper bound of the prediction, for $y^* = 1.5$ are 88.5% of the generated points are in agreement with the predicted sensitivity of the Storage Ring EDM collaboration. As a consequence, the hypothesis of extending the scalar sector of the RS model by a flavor–changing scalar with a mass of 750 GeV will be tested in the near future. This is displayed in Fig. 5.9b. The dashed line in Fig. 5.9b corresponds to the predicted sensitivity of the Storage Ring Electric Dipole Moment collaboration.

Conclusion

The SM is a well–proven and consistent model. However, the SM is unable to address yet open questions. This issue and the fact, that the LHC did not yet find any hint for new physics suggest a new physics model that is of order a higher energy scale, in which the SM is incorporated and regarded as an effective field theory. As an underlying theory, the Randall Sundrum model is considered in this thesis. The Randall Sundrum model extends the SM by one spatial extra–dimension that is curved. The particle fields propagate in the bulk of the extra dimension, except for the Higgs boson. Confining the Higgs boson on the IR brane leads to a geometrical solution of the hierarchy problem. In this thesis, the Higgs is considered both on the IR brane or close to the IR brane. It was shown earlier in [128, 131] that a smooth interpolation between the Higgs localizations does not exist. This observation that affects amplitudes, in which fermions are involved. This has been confirmed in Ch. 4, in which the impact of RS particles to the loop–induced Higgs decay into two photons were studied. The different localizations of the Higgs field are referred to as the *brane–localized Higgs* scenario, in which the Higgs field is confined on the IR brane. The other localization is referred to as the *narrow–bulk localized Higgs* scenario, in which the Higgs field is moved by a small amount into the bulk of the extra dimension. The two scenarios are identified by the width η of the Higgs field, and by the UV cutoff Λ_{TeV} of the theory. This turns into $\eta \ll v\,|Y_q|\,/\Lambda_{\text{TeV}}$ in case of the brane–localized Higgs scenario and by $v\,|Y_q|\,/\Lambda_{\text{TeV}} \ll \eta \ll v\,|Y_q|\,/M_{\text{kk}}$ in case of the narrow–bulk localized Higgs scenario. The diagrams that contribute to the $h \to \gamma\gamma$ decay are calculated using the 5D propagators derived in Ch. 3. They are valid to all orders in v^2/M_{kk}^2 and deliver an analytical closed expression. Furthermore, the KK description is avoided, in which the particles are considered as excitations with infinite sums. The amplitudes for the 5D contributions to the $h \to \gamma\gamma$ decay were calculated in the unitary gauge, because the full amplitude is gauge–independent. The full 5D amplitude contains expressions in terms of the 5D fermion propagator and of the W boson propagator. In the custodial RS model exists a larger contribution of the 5D fermion propagator that stems from the additional fermion fields in the loop–amplitude of the $h \to \gamma\gamma$ decay in the custodial RS model.
The impact on several flavor observables has been investigated if the scalar sector of the RS model is extended by a neutral heavy flavor–violating scalar that is a singlet under the RS gauge group. It turned out that there is a relative deviation to the SM values of $\mathcal{O}\left(10^{-5}\right)$ in case of Δm_{B_d}, $\mathcal{O}\left(10^{-8}\right)$ in case of Δm_{B_s}, $\mathcal{O}\left(10^{-4}\right)$ in case of Δm_K, and of $\mathcal{O}\left(10^{-2}\right)$ in case of Δm_D. A future detection of these contributions and therefore accepting or rejecting this hypothesis of the extended scalar sector is also the relative deviation to the upper bounds of the neutron EDM and the deuteron EDM in the SM. In case of the neutron EDM, the contributions are smaller by a factor up to $\mathcal{O}\left(10^{-3}\right)$, while in the case of the deuteron EDM the contributions are of the same and larger by a factor of $\mathcal{O}\left(10^{2}\right)$ compared to the estimates of the future sensitivity of the Storage Ring EDM collaboration [331]. As a consequence, the hypothesis of an extended scalar sector in the RS model with a scalar that has mass of 750 GeV will be tested in the near

future.
It has been shown in this thesis that it is possible to extend the scalar sector of the RS model. The predictions are not in conflict with current measurements. In the case of the contributions of a flavor–changing neutral scalar S to the deuteron EDM, the extension will be tested soon. If there exists a scalar particle, the contributions of this particle might be less, because the Wilson coefficients contribute with the inverse mass. Despite this fact, the coupling of the flavor–changing particle to fermions does not contain any term that depends explicitly on the mass of the scalar particle. The 750 GeV mass for the flavor–changing scalar particle therefore is considered as a possible upper bound.
Summarizing, the RS model is still a possible extension of the SM, because the predictions of the branching ratio of the decay $h \to \gamma\gamma$ does not show a large deviation relative to the SM values

A Appendix Ch.4

A.1 Feynman rules of the decay $h \to \gamma\gamma$ in the 4D effective theory

$$\mathcal{A}^{\{\phi^{\pm(n)}(p_\phi)h(p_h)W_\nu^{\mp(m)}\}} = \frac{\tilde{m}_W^2}{v m_n^W} 2\pi \chi_m^W(1)\,\chi_n^W(1)\,(p_\phi - p_h)_\nu\,, \tag{A.1}$$

$$\mathcal{A}^{\{W_\mu^{\pm(n)}hW_\nu^{\mp(m)}\}} = \frac{2i\tilde{m}_W^2}{v} 2\pi \chi_m^W(1)\,\chi_n^W(1)\,\eta_{\mu\nu}, \tag{A.2}$$

$$\mathcal{A}^{\{\phi^{\pm(n)}h\phi^{\mp(m)}\}} = -\frac{im_h^2}{v}\frac{\tilde{m}_W^2}{m_m^W m_n^W} 2\pi \chi_m^W(1)\,\chi_n^W(1)\,, \tag{A.3}$$

$$\mathcal{A}^{\{A_\mu^0\phi^{\pm(n)}W_\nu^{\mp(m)}\}} = \pm e m_n^W \eta_{\mu\nu}\delta_{mn}, \tag{A.4}$$

$$\mathcal{A}^{\{A_\mu^0\phi^{\pm(n)}(p_+)\phi^{\mp(m)}(p_-)\}} = \pm ie\,(p_+ - p_-)_\mu\,\delta_{nm}, \tag{A.5}$$

$$\mathcal{A}^{\{hA_\mu^0\phi^{\pm(n)}W_\nu^{\mp(m)}\}} = \pm e\frac{\tilde{m}_W^2}{v m_n^W} 2\pi \chi_m^W(1)\,\chi_n^W(1)\,, \tag{A.6}$$

$$\mathcal{A}^{\{c_\mu^{\pm(n)}hc_\nu^{\mp(m)}\}} = \frac{-\xi 2i\tilde{m}_W^2}{v} 2\pi \chi_m^W(1)\,\chi_n^W(1)\,, \tag{A.7}$$

$$\mathcal{A}^{\{c_\mu^{\pm(n)}A^0c_\nu^{\mp(m)}\}} = \pm iep_\mu\delta_{nm}, \tag{A.8}$$

$$\mathcal{A}^{\{A_\mu^0A_\nu^0\phi^{\pm(n)}\phi^{\mp(m)}\}} = \pm 2ie^2\eta_{\mu\nu}\delta_{mn}, \tag{A.9}$$

$$\tag{A.10}$$

$$\mathcal{A}^{\{W_\mu^{\pm(m)}A_\nu^{(0)}A_\sigma^{(0)}W_\rho^{\mp(n)}\}} = \\ -\left[2\eta_{\rho\sigma}\eta_{\mu\nu} - \eta_{\sigma\mu}\eta_{\rho\nu} - \eta_{\nu\sigma}\eta_{\rho\mu}\right] ie^2\delta_{nm}, \tag{A.11}$$

$$\mathcal{A}^{\{W_\beta^{\pm,(n)}(p)A_\alpha^{(0)}(q)W_\gamma^{\mp,(k)}(k)\}} = \\ ie_5\Big[\eta_{\alpha\beta}\,(q-p)_\gamma + \eta_{\beta\gamma}\,(p-k)_\alpha + \eta_{\gamma\alpha}\,(k-q)_\beta\Big]\,\delta_{nk}, \tag{A.12}$$

$$\tag{A.13}$$

A.2 Fit parameter

A.2.1 Brane, minimal RS model

$$f_{y_*=0.5}(x) = 1 + \frac{0.340696}{x^2} - \frac{4.15709\mathrm{sech}(2/x)\tanh(1/x)}{x}, \tag{A.14}$$

$$f_{y_*=1.5}(x) = 1 + \frac{11.2073}{x^2} - \frac{12.822\tanh(1/x)}{x}, \tag{A.15}$$

$$f_{y_*=3}(x) = 1 + \frac{200.865}{x^{2.01}} - \frac{212.376\tanh(1/x)}{x}. \tag{A.16}$$

$$\tag{A.17}$$

A.2.2 Bulk, minimal RS model

$$f_{y_*=0.5}(x) = 1 + \frac{11.242}{x^2} - \frac{11.2645\tanh(1/x)}{x}, \tag{A.18}$$

$$f_{y_*=1.5}(x) = 1 + \frac{61.6812}{x^2} - -\frac{51.8533\tanh(1/x)}{x}, \tag{A.19}$$

$$\begin{aligned} f_{y_*=3}(x) = \Bigg(& -1992.72 + \frac{1.26353 \cdot 10^{12}}{x^{13}} - \frac{3.85012 \cdot 10^{12}}{x^{12}} + \frac{5.2912 \cdot 10^{12}}{x^{11}} \\ & - \frac{4.33594 \cdot 10^{12}}{x^{10}} + \frac{2.36041 \cdot 10^{12}}{x^9} - \frac{9.00335 \cdot 10^{11}}{x^8} \\ & + \frac{2.47362 \cdot 10^{11}}{x^7} - \frac{4.95673 \cdot 10^{10}}{x^6} + \frac{7.25573 \cdot 10^9}{x^5} \\ & - \frac{7.69668 \cdot 10^8}{x^4} + \frac{5.80747 \cdot 10^7}{x^3} \\ & - \frac{3.01545 \cdot 10^6}{x^2} + \frac{101733.}{x} \Bigg) \tanh\left(\frac{1}{x}\right) + 18.1152. \end{aligned} \tag{A.20}$$

A.2.3 Brane, custodial RS model

$$f_{y_*=0.5}(x) = 1 + \frac{14.6376}{x^2} - \frac{17.6243\tanh\left(\frac{1}{x}\right)}{x}, \tag{A.21}$$

$$f_{y_*=1.5}(x) = 1 + \frac{738.951}{x^4} - \frac{2172.44}{x^2} + \frac{2159.75\tanh\left(\frac{1}{x}\right)}{x}, \tag{A.22}$$

$$f_{y_*=3}(x) = 1 + \frac{66098.7}{x^4} - \frac{198423.}{x^2} + \frac{198378.\tanh\left(\frac{1}{x}\right)}{x}. \tag{A.23}$$

A.2.4 Bulk, custodial RS model

$$f_{y_*=0.5}(x) = 1 - \frac{22.3381}{x^2} + \frac{21.6553\tanh\left(\frac{1}{x}\right)}{x}, \tag{A.24}$$

$$f_{y_*=1.5}(x) = 1 + \frac{4008.12}{x^2} - \frac{4087.17\tanh\left(\frac{1}{x}\right)}{x}, \tag{A.25}$$

$$f_{y_*=3}(x) = 1 + \frac{95347.9}{x^2} - \frac{95943.9\tanh\left(\frac{1}{x}\right)}{x}. \tag{A.26}$$

B Appendix Ch. 5

B.1 CP violation

As a lot of investigated observables discussed in this thesis are sensitive to CP violation and a summary of CP violation in the literature is given, mainly based on [243]. The milestones in the derivation of CP violation are marked, as well.
CP violation is the combination of the charge conjugation C and the parity P which interchanges the handedness of the particles. The charge conjugation C interchanges the quantum numbers of the particle. The physical meaning of this interchange is that particles are interchanged with their own antiparticles and vice verse. CP symmetry is only violated by the weak interaction which also breaks C and P separately. Therefore, CP is not an exact symmetry. In general, C and P are violated separately, but not CP [341, 342].
CP is violated in both K^0 and B meson decays. There exist CP violating decays which related to meson mixing and decays where the CP violation originates from decay amplitudes. The first experimental evidence of CP violation was found in the neutral Kaon decay $K^0 \to 2\pi$ by Christenson et al. [281, 282].
Further, CP violation is important for cosmology as an explanation for the inequivalent amount of both matter an antimatter, known as baryogenesis. The assumption is that in the beginning of the universe both antimatter and matter existed in the same amount while CP violation exists [343].
In the SM, CP violation happens in the mass basis *via* a complex phase in the 3×3 matrix assigning the couplings of the W to quarks. There exist three definitions of CP violation which can be later summarized into *direct* and *indirect* CP violation:

1. The decay amplitude A_f for a decay of both a meson M into a (multi-particle) final state f and its CP conjugate amplitude $\bar{A}_{\bar{f}}$ read

$$A_f = \langle f|H|M\rangle \qquad \bar{A}_{\bar{f}} = \langle \bar{f}|H|\bar{M}\rangle. \tag{B.1}$$

   In Eq. (B.1) the bars indicate the CP conjugate of the quantities. Further, H denotes the weak Hamiltonian, $M\left(\bar{M}\right)$ the (CP conjugate of the)meson and $f\left(\bar{f}\right)$ denotes the (CP conjugated) final state f under consideration. If there is no CP violation in the amplitudes, the absolute value of the ratio $\left|\bar{A}_{\bar{f}}/A_f\right| = 1$, otherwise

$$\left|\bar{A}_{\bar{f}}/A_f\right| \neq 1 \tag{B.2}$$

   indicates that there is CP violation. The detection of CP violation in charged decays is measured *via* the asymmetry

$$\frac{\left|\bar{A}_{\bar{f}^-}/A_{f^+}\right|^2 - 1}{\left|\bar{A}_{\bar{f}^-}/A_{f^+}\right|^2 + 1} \tag{B.3}$$

2. In the case of both semileptonic decays of mesons, $M \to lX$ and in neutral meson mixing, CP violation can be measured of the asymmetry of the time dependent rates

$$\mathcal{A}_{SL} = \frac{1 - |q/p|^4}{1 + |q/p|^4} \tag{B.4}$$

3. The third case occurring CP violation is in an interference of a decay without mixing an a decay stemming from a meson mixing. The decay product is a CP eigenstate. With the definition

$$\lambda_f = \frac{q}{p}\frac{\bar{A}_f}{A_f}, \tag{B.5}$$

the imaginary part of Eq. (B.5) is the only hint of CP violation, if the final state f is a CP eigenstate. Furthermore, if the additional condition $\bar{A}_{f_{CP}} = A_{f_{CP}}$ is fulfilled, then the source of CP violation can be found only in the asymmetry of the decays mentioned above.

In general there exist two phases which are CP violating. These phases are the so-called weak phase and strong phase. The words weak and strong may be misleading, as they are not related to the weak and strong interaction.
The weak phase originates from the complex couplings in the Lagrangian and the amplitudes A_f and $\bar{A}_{\bar{f}}$ should have opposite signs. The difference of the phases in the amplitudes is convention independent. Further, the weak phase ϕ manifests itself in the couplings of the W boson. On the contrary, should have A_f and $\bar{A}_{\bar{f}}$ the same sign as the strong phase δ stems from a CP invariant interaction. A possibility to exhibit the strong phase is the final state interaction of on-shell particles. The other possibility for the existence of the strong phase an even product with more than four γ matrices in combination with γ_5 as in

$$\gamma^\nu\gamma^\mu\gamma^\sigma\gamma^\rho\gamma_5 = -i\epsilon^{\nu\mu\sigma\rho} \tag{B.6}$$

The amplitudes in Eq. (B.1) can be rewritten in terms of the weak phase ϕ and the strong phase δ with some parameters a_i leading to

$$A_f = |a_1|e^{i(\delta_1+\phi_1)} + |a_2|e^{i(\delta_2+\phi_2)} \tag{B.7}$$

$$\bar{A}_{\bar{f}} = |a_1|e^{i(\delta_1-\phi_1)} + |a_2|e^{i(\delta_2-\phi_2)} \tag{B.8}$$

and the neutral mesons An explanation of the *direct* CP violation *via* ϕ as only reason is not possible, because in this case the strong phase δ and the parameters a_i contribute, as well. Both the difference of the strong phases as the fraction of the quantities a_i depend on hadronic parameters which are not easy to calculate, but can be determined by experiment. The case of *direct* CP violation corresponds to 1.
The so-called *indirect* CP violation appears, if only the weak phase of the investigated mesons $\phi_M \neq 0$, but both a_i and the strong phase δ are vanishing. Then, the asymmetry in Eq. (B.4) can be rewritten in terms of the decay rate and the matrix element

$$\mathcal{A}_{SL} = -\left|\frac{\Gamma_{12}}{M_{12}}\right| \sin\left(\phi_M - \phi_\Gamma\right). \tag{B.9}$$

The challenge is the extraction of $\phi_M - \phi_\Gamma$ in Eq. (B.9), as the ratio $\frac{\Gamma_{12}}{M_{12}}$ depends on long distance physics contributions.

Summarizing, CP violation happens both direct and indirect as CP violation is an explanation of the baryon asymmetry in the universe which is assumed to originated from an equal distributed matter-antimatter state [343]. At the same time the Sakharov conditions are fulfilled in the SM [343, 45–47].

B.2 Input parameter for Sec. 5.4

B.2.1 B^0–$\overline{B}^0$ mixing

The bag parameters are taken from [249] and the magic numbers are taken from [334] that read

$$
\begin{aligned}
a_i &= (0.286, -0.692, 0.787, -1.143, 0.143) \\
b_i^{(1,1)} &= (0.865, 0., 0., 0., 0.) & c_i^{(1,1)} &= (-0.017, 0., 0., 0., 0.) \\
b_i^{(2,2)} &= (0., 1.879, 0.012, 0., 0.) & c_i^{(2,2)} &= (0., -0.18, -0.003, 0., 0) \\
b_i^{(2,3)} &= (0., -0.493, 0.18, 0., 0.) & c_i^{(2,3)} &= (0., -0.014, 0.008, 0., 0.) \\
b_i^{(3,2)} &= (0., -0.044, 0.035, 0., 0.) & c_i^{(3,2)} &= (0., 0.005, -0.012, 0., 0.) \\
b_i^{(3,3)} &= (0., 0.011, 0.54, 0.) & c_i^{(3,3)} &= (0., 0., 0.028, 0., 0.) \\
b_i^{(4,4)} &= (0., 0., 0., 2.87, 0.) & c_i^{(4,4)} &= (0., 0., 0., -0.48, 0.005) \\
b_i^{(4,5)} &= (0., 0., 0., 0.961, -0.22) & c_i^{(4,5)} &= (0., 0., 0., -0.25, -0.006) \\
b_i^{(5,4)} &= (0., 0., 0., 0.09, 0.) & c_i^{(5,4)} &= (0., 0., 0., -0.013, -0.016) \\
b_i^{(5,5)} &= (0., 0., 0., 0.029, 0.863) & c_i^{(5,5)} &= (0., 0., 0., -0.007, 0.019) \\
B_i &= (0.88, 0.82, 1.02, 1.15, 1.99)
\end{aligned}
\tag{B.10}
$$

The masses have been evaluated at the bottom mass.

B.2.2 D^0–$\overline{D}^0$ mixing

The bag parameter for $D^0 - \bar{D}^0$ mixing are from [335] and the masses have been evaluated at 3 GeV.

$$
\begin{aligned}
a_i &= (0.286, -0.692, 0.787, -1.143, 0.143) \\
b_i^{(1,1)} &= (0.837, 0., 0., 0., 0.) & c_i^{(1,1)} &= (-0.016, 0., 0., 0., 0.) \\
b_i^{(2,2)} &= (0., 2.163, 0.012, 0., 0.) & c_i^{(2,2)} &= (0., -0.20, -0.002, 0., 0) \\
b_i^{(2,3)} &= (0., -0.567, 0.176, 0., 0.) & c_i^{(2,3)} &= (0., -0.016, 0.006, 0., 0.) \\
b_i^{(3,2)} &= (0., -0.032, 0.031, 0., 0.) & c_i^{(3,2)} &= (0., 0.004, -0.010, 0., 0.) \\
b_i^{(3,3)} &= (0., 0.008, 0.474, 0.) & c_i^{(3,3)} &= (0., 0., 0.025, 0., 0.) \\
b_i^{(4,4)} &= (0., 0., 0., 3.63, 0.) & c_i^{(4,4)} &= (0., 0., 0., -0.56, 0.006) \\
b_i^{(4,5)} &= (0., 0., 0., 1.21, -0.19) & c_i^{(4,5)} &= (0., 0., 0., -0.29, -0.006) \\
b_i^{(5,4)} &= (0., 0., 0., 0.14, 0.) & c_i^{(5,4)} &= (0., 0., 0., -0.019, -0.016) \\
b_i^{(5,5)} &= (0., 0., 0., 0.045, 0.839) & c_i^{(5,5)} &= (0., 0., 0., -0.009, 0.018) \\
B_i &= (0.75, 0.66, 0.96, 0.91, 1.10)
\end{aligned}
\tag{B.11}
$$

B.2.3 K^0–$\overline{K}^0$ mixing

With the application of Eq. (5.49) as well as the following magic numbers from [336]:

$$
\begin{aligned}
a_i &= (0.29, -0.69, 0.79, -1.1, 0.14) \\
b_i^{(1,1)} &= (0.82, 0., 0., 0., 0.) & c_i^{(1,1)} &= (-0.016, 0., 0., 0., 0.) \\
b_i^{(2,2)} &= (0., 2.4, 0.011, 0., 0.) & c_i^{(2,2)} &= (0., -0.23, -0.002, 0., 0) \\
b_i^{(2,3)} &= (0., -0.63, 0.17, 0., 0.) & c_i^{(2,3)} &= (0., -0.018, 0.0049, 0., 0.) \\
b_i^{(3,2)} &= (0., -0.019, 0.028, 0., 0.) & c_i^{(3,2)} &= (0., 0.0028, -0.0093, 0., 0.) \\
b_i^{(3,3)} &= (0., 0.0049, 0.43, 0.) & c_i^{(3,3)} &= (0., 0.00021, 0.023, 0., 0.) \\
b_i^{(4,4)} &= (0., 0., 0., 4.4, 0.) & c_i^{(4,4)} &= (0., 0., 0., -0.68, 0.0055) \\
b_i^{(4,5)} &= (0., 0., 0., 1.5, -0.17) & c_i^{(4,5)} &= (0., 0., 0., -0.35, -0.0062) \\
b_i^{(5,4)} &= (0., 0., 0., 0.18, 0.) & c_i^{(5,4)} &= (0., 0., 0., -0.026, -0.016) \\
b_i^{(5,5)} &= (0., 0., 0., 0.061, 0.82) & c_i^{(5,5)} &= (0., 0., 0., -0.013, 0.018) \\
B_i &= (0.6, 0.66, 1.05, 1.03, 0.73) \\
R_i &= (1, -12.9, 3.98, 20.8, 5.2)
\end{aligned}
\tag{B.12}
$$

have been used to obtain the mixing down to $\mu = 2$GeV.

Input parameter for Meson mixing

Parameter	Value	Reference
φ_ϵ	43.51°	[6]
κ_ϵ	0.94 ± 0.02	[337, 338]
f_{B_d}	$(186 \pm 11) \cdot 10^{-3}$ GeV	[339]
f_D	$201\pm \cdot 10^{-3}$ GeV	[249]
f_K	$156.2 \cdot 10^{-3}$ GeV	[340]
m_B	$(5279.63 \pm 0.15) \cdot 10^{-3}$ GeV	[6]
m_D	$(1864.83 \pm 0.005) \cdot 10^{-3}$ GeV	[6]
m_K	$(497.611 \pm 0.013) \cdot 10^{-3}$ GeV	[6]
Δm_K^{exp}	$(3.484 \pm 0.006) \cdot 10^{-15}$ GeV	[6]
m_{sc}	750 GeV	[211, 212]

Input parameter for the $B_{s/d}$ Meson decay		
Parameter	Value	Reference
G_F	$1.166 \cdot 10^{-5}$ GeV^{-2}	[6]
$\alpha(m_Z)$	1/127.9	[6]
$s^2_{\theta_W}$	0.231	[6]
f_{B_s}	$(222 \pm 11) \cdot 10^{-3}$ GeV	[339]
m_{B_s}	$(5366.89 \pm 0.16) \cdot 10^{-3}$ GeV	[6]
m_μ	$(105.6583745 \pm 0.0000024) \cdot 10^{-3}$ GeV	[6]

List of Figures

List of Tables

Acronyms

AdS Anti–de–Sitter

BC Boundary condition

BSM Beyond the Standard model

CFT Conformal field theory

CKM Cabibbo, Kobayashi, Maskawa

DD Dirichlet–Dirichlet

EFT Effective field theory

EOM Equation of motion

EWSB Electroweak symmetry breaking

FCNC Flavor changing neutral current

IR Infrared

KK Kaluza Klein

LHC Large Hadron Collider

NN Neumann–Neumann

QCD Quantum Chromodynamics

QFT Quantum field theory

RG Renormalization group

RGE Renormalization group equation

RS Randall Sundrum

SM Standard Model of particle physics

SSB Spontaneous symmetry breaking

UV Ultraviolet

VEV Vacuum expectation value

ZMA Zero mode approximation

Bibliography

[1] M. Neubert, "Effective field theory and heavy quark physics," hep-ph/0512222.

[2] M. E. Peskin and D. V. Schroeder, Reading, USA: Addison-Wesley (1995) 842 p

[3] P. Langacker, Boca Raton, USA: CRC Pr. (2010) 663 p

[4] M. Bohm, A. Denner and H. Joos, Stuttgart, Germany: Teubner (2001) 784 p

[5] S. Scherer and M. R. Schindler, hep-ph/0505265.

[6] C. Patrignani *et al.* [Particle Data Group], Chin. Phys. C **40**, no. 10, 100001 (2016). doi:10.1088/1674-1137/40/10/100001

[7] S. L. Glashow, Nucl. Phys. **22**, 579 (1961). doi:10.1016/0029-5582(61)90469-2

[8] S. Weinberg, Phys. Rev. Lett. **19**, 1264 (1967). doi:10.1103/PhysRevLett.19.1264

[9] A. Salam, "Weak and Electromagnetic Interactions," Conf. Proc. C **680519**, 367 (1968).

[10] G. Aad *et al.* [ATLAS Collaboration], "Observation of a new particle in the search for the Standard Model Higgs boson with the ATLAS detector at the LHC," Phys. Lett. B **716**, 1 (2012) [arXiv:1207.7214 [hep-ex]].

[11] S. Chatrchyan *et al.* [CMS Collaboration], "Observation of a new boson at a mass of 125 GeV with the CMS experiment at the LHC," Phys. Lett. B **716**, 30 (2012) [arXiv:1207.7235 [hep-ex]].

[12] G. 't Hooft and M. J. G. Veltman, "Regularization and Renormalization of Gauge Fields," Nucl. Phys. B **44**, 189 (1972).

[13] J. J. Aubert *et al.* [E598 Collaboration], Phys. Rev. Lett. **33**, 1404 (1974). doi:10.1103/PhysRevLett.33.1404

[14] J. E. Augustin *et al.* [SLAC-SP-017 Collaboration], Phys. Rev. Lett. **33**, 1406 (1974) [Adv. Exp. Phys. **5**, 141 (1976)]. doi:10.1103/PhysRevLett.33.1406

[15] S. L. Glashow, J. Iliopoulos and L. Maiani, Phys. Rev. D **2**, 1285 (1970). doi:10.1103/PhysRevD.2.1285

[16] H. Fritzsch, M. Gell-Mann and H. Leutwyler, Phys. Lett. **47B**, 365 (1973). doi:10.1016/0370-2693(73)90625-4

[17] G. Zweig, CERN-TH-401.

[18] D. J. Gross and F. Wilczek, Phys. Rev. Lett. **30**, 1343 (1973). doi:10.1103/PhysRevLett.30.1343

[19] D. J. Gross and F. Wilczek, Phys. Rev. D **8**, 3633 (1973). doi:10.1103/PhysRevD.8.3633

[20] D. J. Gross and F. Wilczek, Phys. Rev. D **9**, 980 (1974). doi:10.1103/PhysRevD.9.980

[21] M. L. Perl, E. R. Lee and D. Loomba, Mod. Phys. Lett. A **19**, 2595 (2004). doi:10.1142/S0217732304016019

[22] P.F. Smith, Ann. Rev. Nucl. and Part. Sci. **39**,73 (1989).

[23] L. Lyons, Phys. Rept. **129**, 225 (1985). doi:10.1016/0370-1573(85)90011-0

[24] M. Marinelli and G. Morpurgo, Phys. Rept. **85**, 161 (1982). doi:10.1016/0370-1573(82)90053-9

[25] G. Arnison *et al.* [UA1 Collaboration], Phys. Lett. **122B**, 103 (1983). doi:10.1016/0370-2693(83)91177-2

[26] M. Banner *et al.* [UA2 Collaboration], Phys. Lett. **122B**, 476 (1983). doi:10.1016/0370-2693(83)91605-2

[27] P. Bagnaia *et al.* [UA2 Collaboration], Phys. Lett. **129B**, 130 (1983). doi:10.1016/0370-2693(83)90744-X

[28] F. Abe *et al.* [CDF Collaboration], Phys. Rev. Lett. **74**, 2626 (1995) doi:10.1103/PhysRevLett.74.2626 [hep-ex/9503002].

[29] S. Abachi *et al.* [D0 Collaboration], Phys. Rev. Lett. **74**, 2632 (1995) doi:10.1103/PhysRevLett.74.2632 [hep-ex/9503003].

[30] M. Gell-Mann, Phys. Rev. **125**, 1067 (1962). doi:10.1103/PhysRev.125.1067

[31] G. 't Hooft, Nucl. Phys. B **35**, 167 (1971). doi:10.1016/0550-3213(71)90139-8

[32] K. Fujikawa, B. W. Lee and A. I. Sanda, Phys. Rev. D **6**, 2923 (1972). doi:10.1103/PhysRevD.6.2923

[33] Y. P. Yao, Phys. Rev. D **7**, 1647 (1973). doi:10.1103/PhysRevD.7.1647

[34] L. D. Faddeev and V. N. Popov, Phys. Lett. **25B**, 29 (1967). doi:10.1016/0370-2693(67)90067-6

[35] P. W. Higgs, "Broken Symmetries and the Masses of Gauge Bosons," Phys. Rev. Lett. **13**, 508 (1964).

[36] F. Englert and R. Brout, "Broken Symmetry and the Mass of Gauge Vector Mesons," Phys. Rev. Lett. **13**, 321 (1964).

[37] G. S. Guralnik, C. R. Hagen and T. W. B. Kibble, "Global Conservation Laws and Massless Particles," Phys. Rev. Lett. **13**, 585 (1964).

[38] P. W. Anderson, Phys. Rev. **130**, 439 (1963). doi:10.1103/PhysRev.130.439

[39] J. Goldstone, "Field Theories with Superconductor Solutions," Nuovo Cim. **19**, 154 (1961).

[40] N. Cabibbo, "Unitary Symmetry and Leptonic Decays," Phys. Rev. Lett. **10**, 531 (1963).

[41] M. Kobayashi and T. Maskawa, "CP Violation in the Renormalizable Theory of Weak Interaction," Prog. Theor. Phys. **49**, 652 (1973).

[42] L. Wolfenstein, "Parametrization of the Kobayashi-Maskawa Matrix," Phys. Rev. Lett. **51**, 1945 (1983).

[43] Y. Grossman, doi:10.5170/CERN-2010-002.111, 10.5170/CERN-2014-003.73 arXiv:1006.3534 [hep-ph].

[44] Y. Nir, CERN-2015-001, pp.123-156 doi:10.5170/CERN-2015-001.123 [arXiv:1605.00433 [hep-ph]].

[45] G. 't Hooft, Phys. Rev. Lett. **37**, 8 (1976). doi:10.1103/PhysRevLett.37.8

[46] V. A. Rubakov and M. E. Shaposhnikov, Usp. Fiz. Nauk **166**, 493 (1996) [Phys. Usp. **39**, 461 (1996)] doi:10.1070/PU1996v039n05ABEH000145 [hep-ph/9603208].

[47] V. A. Kuzmin, V. A. Rubakov and M. E. Shaposhnikov, Phys. Lett. **155B**, 36 (1985). doi:10.1016/0370-2693(85)91028-7

[48] Y. Fukuda *et al.* [Super-Kamiokande Collaboration], Phys. Rev. Lett. **81**, 1562 (1998) doi:10.1103/PhysRevLett.81.1562 [hep-ex/9807003].

[49] M. J. G. Veltman, Acta Phys. Polon. B **8**, 475 (1977).

[50] M. J. G. Veltman, Nucl. Phys. B **123**, 89 (1977). doi:10.1016/0550-3213(77)90342-X

[51] P. Sikivie, L. Susskind, M. B. Voloshin and V. I. Zakharov, Nucl. Phys. B **173**, 189 (1980). doi:10.1016/0550-3213(80)90214-X

[52] M. E. Peskin and T. Takeuchi, Phys. Rev. Lett. **65** (1990) 964. doi:10.1103/PhysRevLett.65.964

[53] M. E. Peskin and T. Takeuchi, Phys. Rev. D **46**, 381 (1992). doi:10.1103/PhysRevD.46.381

[54] W. Buchmuller and D. Wyler, Nucl. Phys. B **268**, 621 (1986). doi:10.1016/0550-3213(86)90262-2

[55] R. Alonso, E. E. Jenkins, A. V. Manohar and M. Trott, JHEP **1404**, 159 (2014) doi:10.1007/JHEP04(2014)159 [arXiv:1312.2014 [hep-ph]].

[56] S. Weinberg, Physica A **96**, 327 (1979). doi:10.1016/0378-4371(79)90223-1

[57] A. G. Riess *et al.* [Supernova Search Team], Astron. J. **116**, 1009 (1998) doi:10.1086/300499 [astro-ph/9805201].

[58] S. Perlmutter *et al.* [Supernova Cosmology Project Collaboration], Astrophys. J. **517**, 565 (1999) doi:10.1086/307221 [astro-ph/9812133].

[59] M. Trodden and S. M. Carroll, astro-ph/0401547.

[60] P. A. R. Ade *et al.* [Planck Collaboration], Astron. Astrophys. **571**, A16 (2014) doi:10.1051/0004-6361/201321591 [arXiv:1303.5076 [astro-ph.CO]].

[61] A. Pomarol and D. Tommasini, Nucl. Phys. B **466**, 3 (1996) doi:10.1016/0550-3213(96)00074-0 [hep-ph/9507462].

[62] R. Alonso, M. B. Gavela, L. Merlo and S. Rigolin, JHEP **1107**, 012 (2011) doi:10.1007/JHEP07(2011)012 [arXiv:1103.2915 [hep-ph]].

[63] R. S. Chivukula, H. Georgi and L. Randall, Nucl. Phys. B **292**, 93 (1987). doi:10.1016/0550-3213(87)90638-9

[64] G. D'Ambrosio, G. F. Giudice, G. Isidori and A. Strumia, Nucl. Phys. B **645**, 155 (2002) doi:10.1016/S0550-3213(02)00836-2 [hep-ph/0207036].

[65] N. Arkani-Hamed, L. J. Hall, D. Tucker-Smith and N. Weiner, Phys. Rev. D **61**, 116003 (2000) doi:10.1103/PhysRevD.61.116003 [hep-ph/9909326].

[66] C. D. Froggatt and H. B. Nielsen, Nucl. Phys. B **147** (1979) 277. doi:10.1016/0550-3213(79)90316-X

[67] A. E. Nelson and M. J. Strassler, JHEP **0009**, 030 (2000) doi:10.1088/1126-6708/2000/09/030 [hep-ph/0006251].

[68] K. S. Babu, arXiv:0910.2948 [hep-ph].

[69] B. Grinstein, M. Redi and G. Villadoro, JHEP **1011**, 067 (2010) doi:10.1007/JHEP11(2010)067 [arXiv:1009.2049 [hep-ph]].

[70] R. Slansky, Phys. Rept. **79**, 1 (1981). doi:10.1016/0370-1573(81)90092-2

[71] M. Gell-Mann, P. Ramond and R. Slansky, Rev. Mod. Phys. **50**, 721 (1978). doi:10.1103/RevModPhys.50.721

[72] G. F. Giudice, In *Kane, Gordon (ed.), Pierce, Aaron (ed.): Perspectives on LHC physics* 155-178 [arXiv:0801.2562 [hep-ph]].

[73] P. A. M. Dirac, Nature **139**, 323 (1937). doi:10.1038/139323a0

[74] P. A. M. Dirac, Proc. Roy. Soc. Lond. A **165**, 199 (1938). doi:10.1098/rspa.1938.0053

[75] G. 't Hooft, (ed.), C. Itzykson, (ed.), A. Jaffe, (ed.), H. Lehmann, (ed.), P. K. Mitter, (ed.), I. M. Singer, (ed.) and R. Stora, (ed.), "Recent Developments in Gauge Theories. Proceedings, Nato Advanced Study Institute, Cargese, France, August 26 - September 8, 1979," NATO Adv. Study Inst. Ser. B Phys. **59**, 1 (1980).

[76] D. Buttazzo, G. Degrassi, P. P. Giardino, G. F. Giudice, F. Sala, A. Salvio and A. Strumia, JHEP **1312**, 089 (2013) doi:10.1007/JHEP12(2013)089 [arXiv:1307.3536 [hep-ph]].

[77] G. Degrassi, S. Di Vita, J. Elias-Miro, J. R. Espinosa, G. F. Giudice, G. Isidori and A. Strumia, JHEP **1208**, 098 (2012) doi:10.1007/JHEP08(2012)098 [arXiv:1205.6497 [hep-ph]].

[78] W. A. Bardeen, A. J. Buras, D. W. Duke and T. Muta, Phys. Rev. D **18**, 3998 (1978). doi:10.1103/PhysRevD.18.3998

[79] G. F. Giudice and R. Rattazzi, Nucl. Phys. B **757**, 19 (2006) doi:10.1016/j.nuclphysb.2006.07.031 [hep-ph/0606105].

[80] D. B. Kaplan, H. Georgi and S. Dimopoulos, Phys. Lett. **136B**, 187 (1984). doi:10.1016/0370-2693(84)91178-X

[81] D. B. Kaplan and H. Georgi, Phys. Lett. **136B**, 183 (1984). doi:10.1016/0370-2693(84)91177-8

[82] H. Georgi, D. B. Kaplan and P. Galison, Phys. Lett. **143B**, 152 (1984). doi:10.1016/0370-2693(84)90823-2

[83] H. Georgi and D. B. Kaplan, Phys. Lett. **145B**, 216 (1984). doi:10.1016/0370-2693(84)90341-1

[84] M. J. Dugan, H. Georgi and D. B. Kaplan, Nucl. Phys. B **254**, 299 (1985). doi:10.1016/0550-3213(85)90221-4

[85] G. Panico and A. Wulzer, Lect. Notes Phys. **913**, pp.1 (2016) doi:10.1007/978-3-319-22617-0 [arXiv:1506.01961 [hep-ph]].

[86] K. Agashe, R. Contino and A. Pomarol, Nucl. Phys. B **719**, 165 (2005) doi:10.1016/j.nuclphysb.2005.04.035 [hep-ph/0412089].

[87] R. Contino, L. Da Rold and A. Pomarol, Phys. Rev. D **75**, 055014 (2007) doi:10.1103/PhysRevD.75.055014 [hep-ph/0612048].

[88] R. Contino, arXiv:1005.4269 [hep-ph].

[89] G. F. Giudice, C. Grojean, A. Pomarol and R. Rattazzi, JHEP **0706**, 045 (2007) doi:10.1088/1126-6708/2007/06/045 [hep-ph/0703164].

[90] D. B. Kaplan, Nucl. Phys. B **365**, 259 (1991). doi:10.1016/S0550-3213(05)80021-5

[91] K. A. Meissner and H. Nicolai, Phys. Lett. B **648**, 312 (2007) doi:10.1016/j.physletb.2007.03.023 [hep-th/0612165].

[92] T. Kaluza, "On the Problem of Unity in Physics," Sitzungsber. Preuss. Akad. Wiss. Berlin (Math. Phys.) **1921**, 966 (1921).

[93] O. Klein, "Quantum Theory and Five-Dimensional Theory of Relativity. (In German and English)," Z. Phys. **37**, 895 (1926) [Surveys High Energ. Phys. **5**, 241 (1986)].

[94] G. Nordstrom, "On the possibility of unifying the electromagnetic and the gravitational fields," Phys. Z. **15**, 504 (1914) [physics/0702221 [physics.gen-ph]].

[95] I. Antoniadis, Phys. Lett. B **246**, 377 (1990). doi:10.1016/0370-2693(90)90617-F

[96] N. Arkani-Hamed, S. Dimopoulos and G. R. Dvali, "The Hierarchy problem and new dimensions at a millimeter," Phys. Lett. B **429**, 263 (1998) [hep-ph/9803315].

[97] N. Arkani-Hamed and M. Schmaltz, "Hierarchies without symmetries from extra dimensions," Phys. Rev. D **61**, 033005 (2000) doi:10.1103/PhysRevD.61.033005 [hep-ph/9903417].

[98] L. Randall and R. Sundrum, "A Large mass hierarchy from a small extra dimension," Phys. Rev. Lett. **83**, 3370 (1999) [hep-ph/9905221].

[99] L. Randall and R. Sundrum, "An Alternative to compactification," Phys. Rev. Lett. **83**, 4690 (1999) [hep-th/9906064].

[100] D. E. Kaplan and T. M. P. Tait, JHEP **0111**, 051 (2001) doi:10.1088/1126-6708/2001/11/051 [hep-ph/0110126].

[101] C. Csaki, "TASI lectures on extra dimensions and branes," In *Shifman, M. (ed.) et al.: From fields to strings, vol. 2* 967-1060 [hep-ph/0404096].

[102] G. D. Kribs, "TASI 2004 lectures on the phenomenology of extra dimensions," hep-ph/0605325.

[103] T. Appelquist, H. C. Cheng and B. A. Dobrescu, Phys. Rev. D **64** (2001) 035002 doi:10.1103/PhysRevD.64.035002 [hep-ph/0012100].

[104] T. Appelquist and H. U. Yee, Phys. Rev. D **67**, 055002 (2003) doi:10.1103/PhysRevD.67.055002 [hep-ph/0211023].

[105] W. D. Goldberger and M. B. Wise, Phys. Rev. D **60**, 107505 (1999) doi:10.1103/PhysRevD.60.107505 [hep-ph/9907218].

[106] L. Randall and M. D. Schwartz, JHEP **0111**, 003 (2001) doi:10.1088/1126-6708/2001/11/003 [hep-th/0108114].

[107] A. Pomarol, Phys. Rev. Lett. **85**, 4004 (2000) doi:10.1103/PhysRevLett.85.4004 [hep-ph/0005293].

[108] K. w. Choi, H. D. Kim and I. W. Kim, JHEP **0211**, 033 (2002) doi:10.1088/1126-6708/2002/11/033 [hep-ph/0202257].

[109] W. D. Goldberger and I. Z. Rothstein, Phys. Rev. Lett. **89**, 131601 (2002) doi:10.1103/PhysRevLett.89.131601 [hep-th/0204160].

[110] K. Agashe, A. Delgado and R. Sundrum, Nucl. Phys. B **643**, 172 (2002) doi:10.1016/S0550-3213(02)00740-X [hep-ph/0206099].

[111] T. Gherghetta, arXiv:1008.2570 [hep-ph].

[112] K. Agashe, A. Falkowski, I. Low and G. Servant, JHEP **0804**, 027 (2008) doi:10.1088/1126-6708/2008/04/027 [arXiv:0712.2455 [hep-ph]].

[113] E. Ponton, "TASI 2011: Four Lectures on TeV Scale Extra Dimensions," arXiv:1207.3827 [hep-ph].

[114] K. Kong and K. T. Matchev, JHEP **0601**, 038 (2006) doi:10.1088/1126-6708/2006/01/038 [hep-ph/0509119].

[115] D. N. Spergel *et al.* [WMAP Collaboration], Astrophys. J. Suppl. **148**, 175 (2003) doi:10.1086/377226 [astro-ph/0302209].

[116] C. L. Bennett *et al.* [WMAP Collaboration], Astrophys. J. Suppl. **148**, 1 (2003) doi:10.1086/377253 [astro-ph/0302207]. [117]

[117] D. Hooper and S. Profumo, Phys. Rept. **453**, 29 (2007) doi:10.1016/j.physrep.2007.09.003 [hep-ph/0701197].

[118] A. J. Buras, A. Poschenrieder, M. Spranger and A. Weiler, Nucl. Phys. B **678**, 455 (2004) doi:10.1016/j.nuclphysb.2003.11.010 [hep-ph/0306158].

[119] H. C. Cheng, K. T. Matchev and M. Schmaltz, Phys. Rev. D **66**, 036005 (2002) doi:10.1103/PhysRevD.66.036005 [hep-ph/0204342].

[120] S. Casagrande, F. Goertz, U. Haisch, M. Neubert and T. Pfoh, "Flavor Physics in the Randall-Sundrum Model: I. Theoretical Setup and Electroweak Precision Tests," JHEP **0810**, 094 (2008) [arXiv:0807.4937 [hep-ph]].

[121] S. Casagrande, F. Goertz, U. Haisch, M. Neubert and T. Pfoh, "The Custodial Randall-Sundrum Model: From Precision Tests to Higgs Physics," JHEP **1009**, 014 (2010) [arXiv:1005.4315 [hep-ph]].

[122] H. Davoudiasl, J. L. Hewett and T. G. Rizzo, Phys. Lett. B **473**, 43 (2000) doi:10.1016/S0370-2693(99)01430-6 [hep-ph/9911262].

[123] A. Pomarol, Phys. Lett. B **486**, 153 (2000) doi:10.1016/S0370-2693(00)00737-1 [hep-ph/9911294].

[124] C. Csaki, C. Grojean, L. Pilo and J. Terning, Phys. Rev. Lett. **92**, 101802 (2004) doi:10.1103/PhysRevLett.92.101802 [hep-ph/0308038].

[125] Y. Grossman and M. Neubert, "Neutrino masses and mixings in nonfactorizable geometry," Phys. Lett. B **474**, 361 (2000) [hep-ph/9912408].

[126] F. Goertz, "Warped Extra Dimensions: Flavor, Precision Tests and Higgs Physics," arXiv:1112.6387 [hep-ph].

[127] M. Bauer "On the flavor problem in strongly coupled theories", PhD thesis, Mainz 2012

[128] K. Novotny, Diploma thesis, Mainz 2013

[129] Chr. Schmell, "Hunting for Warped Extra Dimensions via Loop-Induced Processes," PhD thesis, Mainz 2014

[130] R. Malm, " Five-dimensional Perspective on Higgs Physics and the $b \to s\gamma$ Transition in a Warped Extra Dimension," PhD thesis, Mainz 2016

[131] R. Malm, M. Neubert, K. Novotny and C. Schmell, "5D Perspective on Higgs Production at the Boundary of a Warped Extra Dimension," JHEP **1401**, 173 (2014) doi:10.1007/JHEP01(2014)173 [arXiv:1303.5702 [hep-ph]].

[132] R. Sundrum, "Tasi 2004 lectures: To the fifth dimension and back," hep-th/0508134.

[133] P. R. Archer, JHEP **1209**, 095 (2012) [arXiv:1204.4730 [hep-ph]].

[134] G. Cacciapaglia, C. Csaki, G. Marandella and J. Terning, "The Gaugephobic Higgs," JHEP **0702**, 036 (2007) doi:10.1088/1126-6708/2007/02/036 [hep-ph/0611358].

[135] R. Contino, Y. Nomura and A. Pomarol, Nucl. Phys. B **671**, 148 (2003) doi:10.1016/j.nuclphysb.2003.08.027 [hep-ph/0306259].

[136] B. Batell, T. Gherghetta and D. Sword, Phys. Rev. D **78**, 116011 (2008) doi:10.1103/PhysRevD.78.116011 [arXiv:0808.3977 [hep-ph]].

[137] J. A. Cabrer, G. von Gersdorff and M. Quiros, New J. Phys. **12**, 075012 (2010) doi:10.1088/1367-2630/12/7/075012 [arXiv:0907.5361 [hep-ph]].

[138] J. A. Cabrer, G. von Gersdorff and M. Quiros, Phys. Lett. B **697**, 208 (2011) doi:10.1016/j.physletb.2011.01.058 [arXiv:1011.2205 [hep-ph]].

[139] T. Gherghetta and A. Pomarol, "Bulk fields and supersymmetry in a slice of AdS," Nucl. Phys. B **586**, 141 (2000) doi:10.1016/S0550-3213(00)00392-8 [hep-ph/0003129].

[140] P. R. Archer, M. Carena, A. Carmona and M. Neubert, JHEP **1501**, 060 (2015) doi:10.1007/JHEP01(2015)060 [arXiv:1408.5406 [hep-ph]].

[141] M. Bauer, C. Hörner and M. Neubert, JHEP **1607**, 094 (2016) doi:10.1007/JHEP07(2016)094 [arXiv:1603.05978 [hep-ph]].

[142] P. Breitenlohner and D. Z. Freedman, "Stability in Gauged Extended Supergravity," Annals Phys. **144**, 249 (1982).

[143] B. Batell and T. Gherghetta, "Warped phenomenology in the holographic basis," Phys. Rev. D **77**, 045002 (2008) [arXiv:0710.1838 [hep-ph]].

[144] M. A. Luty and T. Okui, "Conformal technicolor," JHEP **0609**, 070 (2006) [hep-ph/0409274].

[145] C. Csaki, A. Falkowski and A. Weiler, "The Flavor of the Composite Pseudo-Goldstone Higgs," JHEP **0809**, 008 (2008) [arXiv:0804.1954 [hep-ph]].

[146] S. J. Huber, Nucl. Phys. B **666**, 269 (2003) doi:10.1016/S0550-3213(03)00502-9 [hep-ph/0303183].

[147] S. J. Huber and Q. Shafi, Phys. Lett. B **498**, 256 (2001) doi:10.1016/S0370-2693(00)01399-X [hep-ph/0010195].

[148] F. del Aguila and J. Santiago, Phys. Lett. B **493**, 175 (2000) doi:10.1016/S0370-2693(00)01110-2 [hep-ph/0008143].

[149] J. L. Hewett, F. J. Petriello and T. G. Rizzo, JHEP **0209**, 030 (2002) doi:10.1088/1126-6708/2002/09/030 [hep-ph/0203091].

[150] R. Barceló, S. Mitra and G. Moreau, Eur. Phys. J. C **75**, no. 11, 527 (2015) doi:10.1140/epjc/s10052-015-3756-3 [arXiv:1408.1852 [hep-ph]].

[151] C. Csaki, C. Grojean, J. Hubisz, Y. Shirman and J. Terning, Phys. Rev. D **70**, 015012 (2004) doi:10.1103/PhysRevD.70.015012 [hep-ph/0310355].

[152] J. A. Bagger, F. Feruglio and F. Zwirner, Phys. Rev. Lett. **88**, 101601 (2002) doi:10.1103/PhysRevLett.88.101601 [hep-th/0107128].

[153] K. Agashe, G. Perez and A. Soni, Phys. Rev. D **71**, 016002 (2005) doi:10.1103/PhysRevD.71.016002 [hep-ph/0408134].

[154] K. Agashe, G. Perez and A. Soni, Phys. Rev. Lett. **93**, 201804 (2004) doi:10.1103/PhysRevLett.93.201804 [hep-ph/0406101].

[155] K. Agashe, M. Papucci, G. Perez and D. Pirjol, hep-ph/0509117.

[156] K. Agashe, A. Delgado, M. J. May and R. Sundrum, JHEP **0308**, 050 (2003) doi:10.1088/1126-6708/2003/08/050 [hep-ph/0308036].

[157] K. Agashe, R. Contino, L. Da Rold and A. Pomarol, Phys. Lett. B **641** (2006) 62 doi:10.1016/j.physletb.2006.08.005 [hep-ph/0605341].

[158] M. Carena, E. Ponton, J. Santiago and C. E. M. Wagner, Nucl. Phys. B **759** (2006) 202 doi:10.1016/j.nuclphysb.2006.10.012 [hep-ph/0607106].

[159] G. Cacciapaglia, C. Csaki, G. Marandella and J. Terning, Phys. Rev. D **75**, 015003 (2007) doi:10.1103/PhysRevD.75.015003 [hep-ph/0607146].

[160] M. Carena, E. Ponton, J. Santiago and C. E. M. Wagner, Phys. Rev. D **76** (2007) 035006 doi:10.1103/PhysRevD.76.035006 [hep-ph/0701055].

[161] M. Blanke, A. J. Buras, B. Duling, S. Gori and A. Weiler, JHEP **0903**, 001 (2009) doi:10.1088/1126-6708/2009/03/001 [arXiv:0809.1073 [hep-ph]].

[162] M. E. Albrecht, M. Blanke, A. J. Buras, B. Duling and K. Gemmler, JHEP **0909**, 064 (2009) doi:10.1088/1126-6708/2009/09/064 [arXiv:0903.2415 [hep-ph]].

[163] G. Burdman and L. Da Rold, "Renormalization of the S Parameter in Holographic Models of Electroweak Symmetry Breaking," JHEP **0811**, 025 (2008) [arXiv:0809.4009 [hep-ph]].

[164] A. D. Medina, N. R. Shah and C. E. M. Wagner, Phys. Rev. D **76**, 095010 (2007) doi:10.1103/PhysRevD.76.095010 [arXiv:0706.1281 [hep-ph]].

[165] M. Bohm and H. Spiesberger, Nucl. Phys. B **294**, 1081 (1987). doi:10.1016/0550-3213(87)90624-9

[166] M. Baak *et al.* [Gfitter Group], Eur. Phys. J. C **74**, 3046 (2014) doi:10.1140/epjc/s10052-014-3046-5 [arXiv:1407.3792 [hep-ph]].

[167] G. Cacciapaglia, C. Csaki, C. Grojean and J. Terning, Phys. Rev. D **70**, 075014 (2004) doi:10.1103/PhysRevD.70.075014 [hep-ph/0401160].

[168] C. Csaki, J. Erlich and J. Terning, Phys. Rev. D **66** (2002) 064021 doi:10.1103/PhysRevD.66.064021 [hep-ph/0203034].

[169] G. Cacciapaglia, C. Csaki, C. Grojean and J. Terning, Phys. Rev. D **71** (2005) 035015 doi:10.1103/PhysRevD.71.035015 [hep-ph/0409126].

[170] H. Davoudiasl, G. Perez and A. Soni, "The Little Randall-Sundrum Model at the Large Hadron Collider," Phys. Lett. B **665**, 67 (2008) [arXiv:0802.0203 [hep-ph]].

[171] M. Bauer, S. Casagrande, L. Grunder, U. Haisch and M. Neubert, Phys. Rev. D **79**, 076001 (2009) doi:10.1103/PhysRevD.79.076001 [arXiv:0811.3678 [hep-ph]].

[172] S. Fichet and G. von Gersdorff, JHEP **1403**, 102 (2014) doi:10.1007/JHEP03(2014)102 [arXiv:1311.6815 [hep-ph]].

[173] V. Khachatryan *et al.* [CMS Collaboration], Phys. Lett. B **768**, 57 (2017) doi:10.1016/j.physletb.2017.02.010 [arXiv:1609.05391 [hep-ex]].

[174] G. Aad *et al.* [ATLAS Collaboration], JHEP **1508**, 148 (2015) doi:10.1007/JHEP08(2015)148 [arXiv:1505.07018 [hep-ex]].

[175] V. Khachatryan *et al.* [CMS Collaboration], Phys. Rev. D **93**, no. 1, 012001 (2016) doi:10.1103/PhysRevD.93.012001 [arXiv:1506.03062 [hep-ex]].

[176] A. M. Sirunyan *et al.* [CMS Collaboration], arXiv:1704.03366 [hep-ex].

[177] K. Agashe, H. Davoudiasl, G. Perez and A. Soni, Phys. Rev. D **76**, 036006 (2007) doi:10.1103/PhysRevD.76.036006 [hep-ph/0701186].

[178] K. Agashe *et al.*, arXiv:1309.7847 [hep-ph].

[179] M. Bauer, S. Casagrande, U. Haisch and M. Neubert, JHEP **1009**, 017 (2010) doi:10.1007/JHEP09(2010)017 [arXiv:0912.1625 [hep-ph]].

[180] Wolfram Research, Inc., Mathematica, Version 11.0, Champaign, IL (2016).

[181] Wolfram Research, Inc., Mathematica, Version 10.4, Champaign, IL (2016).

[182] S. Casagrande, Diploma thesis, Mainz 2008

[183] J. Charles *et al.*, Phys. Rev. D **91**, no. 7, 073007 (2015) doi:10.1103/PhysRevD.91.073007 [arXiv:1501.05013 [hep-ph]].

[184] G. Cowan, "Statistical data analysis," Oxford, UK: Clarendon (1998) 197 p

[185] M. Carena, A. Delgado, E. Ponton, T. M. P. Tait and C. E. M. Wagner, Phys. Rev. D **71**, 015010 (2005) doi:10.1103/PhysRevD.71.015010 [hep-ph/0410344].

[186] R. Contino and A. Pomarol, JHEP **0411**, 058 (2004) doi:10.1088/1126-6708/2004/11/058 [hep-th/0406257].

[187] M. Puchwein and Z. Kunszt, Annals Phys. **311**, 288 (2004) doi:10.1016/j.aop.2003.12.010 [hep-th/0309069].

[188] C. Csaki, Y. Grossman, P. Tanedo, Y. Tsai and , "Warped penguin diagrams," Phys. Rev. D **83**, 073002 (2011) [arXiv:1004.2037 [hep-ph]].

[189] J. M. Maldacena, Int. J. Theor. Phys. **38**, 1113 (1999) [Adv. Theor. Math. Phys. **2**, 231 (1998)] doi:10.1023/A:1026654312961 [hep-th/9711200].

[190] E. Witten, Adv. Theor. Math. Phys. **2**, 253 (1998) [hep-th/9802150].

[191] S. S. Gubser, I. R. Klebanov and A. M. Polyakov, Phys. Lett. B **428**, 105 (1998) doi:10.1016/S0370-2693(98)00377-3 [hep-th/9802109].

[192] E. Witten, Nucl. Phys. B **160**, 57 (1979). doi:10.1016/0550-3213(79)90232-3

[193] J. Hahn, C. Hörner, R. Malm, M. Neubert, K. Novotny and C. Schmell, "Higgs Decay into Two Photons at the Boundary of a Warped Extra Dimension," Eur. Phys. J. C **74**, no. 5, 2857 (2014) doi:10.1140/epjc/s10052-014-2857-8 [arXiv:1312.5731 [hep-ph]].

[194] M. Carena, S. Casagrande, F. Goertz, U. Haisch and M. Neubert, "Higgs Production in a Warped Extra Dimension," JHEP **1208**, 156 (2012) [arXiv:1204.0008 [hep-ph]].

[195] J. D. Wells, hep-ph/0512342.

[196] J. R. Ellis, M. K. Gaillard and D. V. Nanopoulos, "A Phenomenological Profile of the Higgs Boson," Nucl. Phys. B **106**, 292 (1976).

[197] M. A. Shifman, A. I. Vainshtein, M. B. Voloshin and V. I. Zakharov, "Low-Energy Theorems for Higgs Boson Couplings to Photons," Sov. J. Nucl. Phys. **30**, 711 (1979) [Yad. Fiz. **30**, 1368 (1979)].

[198] J. Hahn, " ", Diploma thesis, Mainz 2014

[199] C. Hörner, "Higgs Decay into Two Photons in a Small and Warped Extra Dimension," Master Thesis, Mainz 2014

[200] A. Azatov, M. Toharia and L. Zhu, "Higgs Production from Gluon Fusion in Warped Extra Dimensions," Phys. Rev. D **82**, 056004 (2010) [arXiv:1006.5939 [hep-ph]].

[201] G. Bhattacharyya and T. S. Ray, Phys. Lett. B **675**, 222 (2009) doi:10.1016/j.physletb.2009.03.069 [arXiv:0902.1893 [hep-ph]].

[202] C. Bouchart and G. Moreau, Phys. Rev. D **80**, 095022 (2009) doi:10.1103/PhysRevD.80.095022 [arXiv:0909.4812 [hep-ph]].

[203] G. Cacciapaglia, A. Deandrea and J. Llodra-Perez, "Higgs —¿ Gamma Gamma beyond the Standard Model," JHEP **0906**, 054 (2009) [arXiv:0901.0927 [hep-ph]].

[204] W. J. Marciano, C. Zhang and S. Willenbrock, Phys. Rev. D **85**, 013002 (2012) doi:10.1103/PhysRevD.85.013002 [arXiv:1109.5304 [hep-ph]].

[205] G. 't Hooft and M. J. G. Veltman, Nucl. Phys. B **153**, 365 (1979). doi:10.1016/0550-3213(79)90605-9

[206] G. Passarino and M. J. G. Veltman, Nucl. Phys. B **160**, 151 (1979). doi:10.1016/0550-3213(79)90234-7

[207] A. Azatov, M. Toharia and L. Zhu, "Higgs Mediated FCNC's in Warped Extra Dimensions," Phys. Rev. D **80**, 035016 (2009) [arXiv:0906.1990 [hep-ph]].

[208] M. Beneke and M. Neubert, Nucl. Phys. B **651**, 225 (2003) doi:10.1016/S0550-3213(02)01091-X [hep-ph/0210085].

[209] A. Djouadi, Phys. Rept. **459**, 1 (2008) doi:10.1016/j.physrep.2007.10.005 [hep-ph/0503173].

[210] G. Aad *et al.* [ATLAS and CMS Collaborations], JHEP **1608**, 045 (2016) doi:10.1007/JHEP08(2016)045 [arXiv:1606.02266 [hep-ex]].

[211] Tech. Rep. ATLAS-CONF-2015-081, CERN, Geneva (2015), URL http://cds.cern.ch/record/2114853.

[212] Tech. Rep. CMS-PAS-EXO-15-004, CERN, Geneva (2015), URL http://cds.cern.ch/record/2114808.

[213] L. D. Landau, Dokl. Akad. Nauk Ser. Fiz. **60** (1948) no.2, 207. doi:10.1016/B978-0-08-010586-4.50070-5

[214] C. N. Yang, Phys. Rev. **77**, 242 (1950). doi:10.1103/PhysRev.77.242

[215] A. J. Buras, F. De Fazio, J. Girrbach, R. Knegjens and M. Nagai, JHEP **1306**, 111 (2013) doi:10.1007/JHEP06(2013)111 [arXiv:1303.3723 [hep-ph]].

[216] S. Gori, H. E. Haber and E. Santos, JHEP **1706**, 110 (2017) doi:10.1007/JHEP06(2017)110 [arXiv:1703.05873 [hep-ph]].

[217] C. Cai, Z. H. Yu and H. H. Zhang, Phys. Rev. D **93**, no. 7, 075033 (2016) doi:10.1103/PhysRevD.93.075033 [arXiv:1512.08440 [hep-ph]].

[218] S. Abel and V. V. Khoze, JHEP **1605**, 063 (2016) doi:10.1007/JHEP05(2016)063 [arXiv:1601.07167 [hep-ph]].

[219] S. Fichet, G. von Gersdorff and C. Royon, Phys. Rev. D **93** (2016) no.7, 075031 doi:10.1103/PhysRevD.93.075031 [arXiv:1512.05751 [hep-ph]].

[220] C. Csáki, J. Hubisz and J. Terning, Phys. Rev. D **93**, no. 3, 035002 (2016) doi:10.1103/PhysRevD.93.035002 [arXiv:1512.05776 [hep-ph]].

[221] V. Khachatryan *et al.* [CMS Collaboration], Phys. Lett. B **768** (2017) 57 doi:10.1016/j.physletb.2017.02.010 [arXiv:1609.05391 [hep-ex]].

[222] M. T. Arun and P. Saha, arXiv:1512.06335 [hep-ph].

[223] C. Q. Geng and D. Huang, Phys. Rev. D **93**, no. 11, 115032 (2016) doi:10.1103/PhysRevD.93.115032 [arXiv:1601.07385 [hep-ph]].

[224] S. B. Giddings and H. Zhang, Phys. Rev. D **93**, no. 11, 115002 (2016) doi:10.1103/PhysRevD.93.115002 [arXiv:1602.02793 [hep-ph]].

[225] R. Rattazzi and A. Zaffaroni, JHEP **0104**, 021 (2001) doi:10.1088/1126-6708/2001/04/021 [hep-th/0012248].

[226] C. Csaki, M. L. Graesser and G. D. Kribs, Phys. Rev. D **63**, 065002 (2001) doi:10.1103/PhysRevD.63.065002 [hep-th/0008151].

[227] K. Agashe, A. Azatov and L. Zhu, Phys. Rev. D **79**, 056006 (2009) doi:10.1103/PhysRevD.79.056006 [arXiv:0810.1016 [hep-ph]].

[228] A. Ahmed, B. Grzadkowski, J. F. Gunion and Y. Jiang, Acta Phys. Polon. B **46**, no. 11, 2205 (2015) doi:10.5506/APhysPolB.46.2205 [arXiv:1510.04116 [hep-ph]].

[229] Z. Chacko, H. S. Goh and R. Harnik, Phys. Rev. Lett. **96**, 231802 (2006) doi:10.1103/PhysRevLett.96.231802 [hep-ph/0506256].

[230] I. P. Ivanov, Prog. Part. Nucl. Phys. **95**, 160 (2017) doi:10.1016/j.ppnp.2017.03.001 [arXiv:1702.03776 [hep-ph]].

[231] K. Assamagan *et al.*, arXiv:1604.05324 [hep-ph].

[232] E. E. Boos, V. E. Bunichev and I. P. Volobuev, J. Exp. Theor. Phys. **124**, no. 5, 722 (2017).

[233] E. E. Boos, V. E. Bunichev, M. A. Perfilov, M. N. Smolyakov and I. P. Volobuev, Phys. Rev. D **92**, no. 9, 095010 (2015) doi:10.1103/PhysRevD.92.095010 [arXiv:1505.05892 [hep-ph]].

[234] A. Ahmed, B. M. Dillon, B. Grzadkowski, J. F. Gunion and Y. Jiang, Phys. Rev. D **95**, no. 9, 095019 (2017) doi:10.1103/PhysRevD.95.095019 [arXiv:1512.05771 [hep-ph]].

[235] B. A. Dobrescu, D. Hooper, K. Kong and R. Mahbubani, JCAP **0710**, 012 (2007) doi:10.1088/1475-7516/2007/10/012 [arXiv:0706.3409 [hep-ph]].

[236] H. Melbeus, A. Merle and T. Ohlsson, Phys. Lett. B **715**, 164 (2012) doi:10.1016/j.physletb.2012.07.037 [arXiv:1204.5186 [hep-ph]].

[237] T. Flacke, D. W. Kang, K. Kong, G. Mohlabeng and S. C. Park, JHEP **1704**, 041 (2017) doi:10.1007/JHEP04(2017)041 [arXiv:1702.02949 [hep-ph]].

[238] H. C. Cheng, K. T. Matchev and M. Schmaltz, Phys. Rev. D **66**, 056006 (2002) doi:10.1103/PhysRevD.66.056006 [hep-ph/0205314].

[239] H. C. Cheng, J. L. Feng and K. T. Matchev, Phys. Rev. Lett. **89**, 211301 (2002) doi:10.1103/PhysRevLett.89.211301 [hep-ph/0207125].

[240] H. Melbéus, A. Merle and T. Ohlsson, Phys. Lett. B **706**, 329 (2012) Erratum: [Phys. Lett. B **713**, 350 (2012)] doi:10.1016/j.physletb.2012.05.059, 10.1016/j.physletb.2011.11.018 [arXiv:1109.0006 [hep-ph]].

[241] L. Bergstrom, T. Bringmann, M. Eriksson and M. Gustafsson, Phys. Rev. Lett. **94**, 131301 (2005) doi:10.1103/PhysRevLett.94.131301 [astro-ph/0410359].

[242] L. Bergstrom, T. Bringmann, M. Eriksson and M. Gustafsson, JCAP **0504**, 004 (2005) doi:10.1088/1475-7516/2005/04/004 [hep-ph/0412001].

[243] G. C. Branco, L. Lavoura and J. P. Silva, "CP Violation," Int. Ser. Monogr. Phys. **103**, 1 (1999).

[244] U. Nierste, "Three Lectures on Meson Mixing and CKM phenomenology," arXiv:0904.1869 [hep-ph].

[245] E. A. Paschos, "Electroweak theory,"

[246] A. Fridman, "Mixing And Cp Violation In The B System," CERN-EP-88-123.

[247] R. Waldi, "Flavour oscillation and CP violation of B mesons," Prog. Part. Nucl. Phys. **47**, 1 (2001).

[248] R. Waldi, "Flavour oscillation and CP violation of B mesons," Lect. Notes Phys. **591**, 43 (2002).

[249] M. Bona *et al.* [UTfit Collaboration], JHEP **0803**, 049 (2008) doi:10.1088/1126-6708/2008/03/049 [arXiv:0707.0636 [hep-ph]].

[250] I. I. Y. Bigi and A. I. Sanda, Camb. Monogr. Part. Phys. Nucl. Phys. Cosmol. **9**, 1 (2000).

[251] I. I. Y. Bigi and L. Moroni, Proc. Int. Sch. Phys. Fermi **137** (1998).

[252] A. Chodos, R. L. Jaffe, K. Johnson, C. B. Thorn and V. F. Weisskopf, Phys. Rev. D **9**, 3471 (1974). doi:10.1103/PhysRevD.9.3471

[253] G. Buchalla, A. J. Buras and M. E. Lautenbacher, Rev. Mod. Phys. **68**, 1125 (1996) [hep-ph/9512380].

[254] M. König and M. Neubert, JHEP **1508**, 012 (2015) doi:10.1007/JHEP08(2015)012 [arXiv:1505.03870 [hep-ph]].

[255] D. J. Broadhurst and A. G. Grozin, Phys. Rev. D **52**, 4082 (1995) doi:10.1103/PhysRevD.52.4082 [hep-ph/9410240].

[256] R. Tarrach, Nucl. Phys. B **183**, 384 (1981). doi:10.1016/0550-3213(81)90140-1

[257] M. Antonelli *et al.*, Phys. Rept. **494** (2010) 197 doi:10.1016/j.physrep.2010.05.003 [arXiv:0907.5386 [hep-ph]].

[258] Y. Amhis *et al.*, arXiv:1612.07233 [hep-ex].

[259] M. Staric *et al.* [Belle Collaboration], Phys. Rev. Lett. **98**, 211803 (2007) doi:10.1103/PhysRevLett.98.211803 [hep-ex/0703036].

[260] B. Aubert *et al.* [BaBar Collaboration], Phys. Rev. Lett. **98** (2007) 211802 doi:10.1103/PhysRevLett.98.211802 [hep-ex/0703020 [HEP-EX]].

[261] T. Aaltonen *et al.* [CDF Collaboration], Phys. Rev. Lett. **100**, 121802 (2008) doi:10.1103/PhysRevLett.100.121802 [arXiv:0712.1567 [hep-ex]].

[262] R. Aaij *et al.* [LHCb Collaboration], Phys. Rev. Lett. **111**, no. 25, 251801 (2013) doi:10.1103/PhysRevLett.111.251801 [arXiv:1309.6534 [hep-ex]].

[263] J. L. Diaz-Cruz and U. J. Saldaña-Salazar, Nucl. Phys. B **913**, 942 (2016) doi:10.1016/j.nuclphysb.2016.10.018 [arXiv:1405.0990 [hep-ph]].

[264] A. Abulencia *et al.* [CDF Collaboration], Phys. Rev. Lett. **97**, 242003 (2006) doi:10.1103/PhysRevLett.97.242003 [hep-ex/0609040].

[265] R. Aaij *et al.* [LHCb Collaboration], Phys. Lett. B **709**, 177 (2012) doi:10.1016/j.physletb.2012.02.031 [arXiv:1112.4311 [hep-ex]].

[266] R. Aaij *et al.* [LHCb Collaboration], New J. Phys. **15**, 053021 (2013) doi:10.1088/1367-2630/15/5/053021 [arXiv:1304.4741 [hep-ex]].

[267] R. Aaij *et al.* [LHCb Collaboration], Phys. Rev. Lett. **114**, no. 4, 041801 (2015) doi:10.1103/PhysRevLett.114.041801 [arXiv:1411.3104 [hep-ex]].

[268] R. Aaij *et al.* [LHCb Collaboration], Eur. Phys. J. C **73**, no. 12, 2655 (2013) doi:10.1140/epjc/s10052-013-2655-8 [arXiv:1308.1302 [hep-ex]].

[269] M. Bona *et al.* [UTfit Collaboration], JHEP **0603**, 080 (2006) doi:10.1088/1126-6708/2006/03/080 [hep-ph/0509219].

[270] M. Blanke, A. J. Buras, D. Guadagnoli and C. Tarantino, JHEP **0610**, 003 (2006) doi:10.1088/1126-6708/2006/10/003 [hep-ph/0604057].

[271] S. Chang, C. S. Kim and J. Song, Phys. Rev. D **77** (2008) 075001 doi:10.1103/PhysRevD.77.075001 [arXiv:0712.0207 [hep-ph]].

[272] M. Blanke, A. J. Buras, B. Duling, K. Gemmler and S. Gori, JHEP **0903**, 108 (2009) doi:10.1088/1126-6708/2009/03/108 [arXiv:0812.3803 [hep-ph]].

[273] B. Aubert *et al.* [BaBar Collaboration], "Observation of CP violation in the B^0 meson system," Phys. Rev. Lett. **87**, 091801 (2001) [hep-ex/0107013].

[274] S. Bifani [LHCb Collaboration], arXiv:1705.02693 [hep-ex].

[275] R. Aaij *et al.* [LHCb Collaboration], arXiv:1705.05802 [hep-ex].

[276] A. J. Buras, R. Fleischer, J. Girrbach and R. Knegjens, JHEP **1307**, 77 (2013) doi:10.1007/JHEP07(2013)077 [arXiv:1303.3820 [hep-ph]].

[277] D. Becirevic, N. Kosnik, F. Mescia and E. Schneider, Phys. Rev. D **86**, 034034 (2012) doi:10.1103/PhysRevD.86.034034 [arXiv:1205.5811 [hep-ph]].

[278] I. Doršner, S. Fajfer, A. Greljo, J. F. Kamenik and N. Košnik, Phys. Rept. **641**, 1 (2016) doi:10.1016/j.physrep.2016.06.001 [arXiv:1603.04993 [hep-ph]].

[279] B. Grinstein, M. J. Savage and M. B. Wise, Nucl. Phys. B **319**, 271 (1989). doi:10.1016/0550-3213(89)90078-3

[280] M. Blanke, arXiv:1704.03753 [hep-ph].

[281] J. H. Christenson, J. W. Cronin, V. L. Fitch and R. Turlay, "Evidence for the 2 pi Decay of the k(2)0 Meson," Phys. Rev. Lett. **13**, 138 (1964). doi:10.1103/PhysRevLett.13.138

[282] J. H. Christenson, J. W. Cronin, V. L. Fitch and R. Turlay, "Regeneration of K-10 Mesons and the K-10- K-20 Mass Difference," Phys. Rev. **140**, B74 (1965).

[283] M. Moulson [NA62-KLEVER Project Collaboration], J. Phys. Conf. Ser. **800**, no. 1, 012037 (2017) doi:10.1088/1742-6596/800/1/012037 [arXiv:1611.04864 [hep-ex]]. [284]

[284] F. Newson *et al.*, arXiv:1411.0109 [hep-ex].

[285] G. Buchalla, "Kaon and charm physics: Theory," hep-ph/0103166.

[286] A. J. Buras, M. Gorbahn, S. Jäger and M. Jamin, JHEP **1511**, 202 (2015) doi:10.1007/JHEP11(2015)202 [arXiv:1507.06345 [hep-ph]].

[287] B. Vallage [NA48 Collaboration], Nucl. Phys. A **721**, 439 (2003). doi:10.1016/S0375-9474(03)01094-7

[288] J. R. Batley *et al.* [NA48 Collaboration], Phys. Lett. B **544**, 97 (2002) doi:10.1016/S0370-2693(02)02476-0 [hep-ex/0208009].

[289] A. Alavi-Harati *et al.* [KTeV Collaboration], Phys. Rev. D **67**, 012005 (2003) Erratum: [Phys. Rev. D **70**, 079904 (2004)] doi:10.1103/PhysRevD.70.079904, 10.1103/PhysRevD.67.012005 [hep-ex/0208007].

[290] E. T. Worcester [KTeV Collaboration], arXiv:0909.2555 [hep-ex].

[291] J. Santiago, JHEP **0812**, 046 (2008) doi:10.1088/1126-6708/2008/12/046 [arXiv:0806.1230 [hep-ph]].

[292] C. Csaki, A. Falkowski and A. Weiler, Phys. Rev. D **80**, 016001 (2009) doi:10.1103/PhysRevD.80.016001 [arXiv:0806.3757 [hep-ph]].

[293] J. L. Chkareuli, JETP Lett. **32**, 671 (1980)

[294] C. Csaki, G. Perez, Z. Surujon and A. Weiler, Phys. Rev. D **81**, 075025 (2010) doi:10.1103/PhysRevD.81.075025 [arXiv:0907.0474 [hep-ph]].

[295] A. Crivellin, G. D'Ambrosio and J. Heeck, Phys. Rev. Lett. **114**, 151801 (2015) doi:10.1103/PhysRevLett.114.151801 [arXiv:1501.00993 [hep-ph]].

[296] R. Malm, "Mitigation of the ϵ_K Fine-tuning Problem in the Randall-Sundrum Model," Diploma Thesis, Mainz 2012

[297] M. Bauer, R. Malm and M. Neubert, "A Solution to the Flavor Problem of Warped Extra-Dimension Models," Phys. Rev. Lett. **108**, 081603 (2012) [arXiv:1110.0471 [hep-ph]].

[298] R. Malm, M. Neubert and C. Schmell, JHEP **1604**, 042 (2016) doi:10.1007/JHEP04(2016)042 [arXiv:1509.02539 [hep-ph]].

[299] M. S. Sozzi and I. Mannelli, Riv. Nuovo Cim. **26N3**, 1 (2003) [hep-ex/0312015].

[300] N. Yamanaka, B. K. Sahoo, N. Yoshinaga, T. Sato, K. Asahi and B. P. Das, Eur. Phys. J. A **53**, 54 (2017) doi:10.1140/epja/i2017-12237-2 [arXiv:1703.01570 [hep-ph]].

[301] R. Harnik, J. Kopp and J. Zupan, JHEP **1303**, 026 (2013) doi:10.1007/JHEP03(2013)026 [arXiv:1209.1397 [hep-ph]].

[302] CMS PAS SUS-13-002, http://cds.cern.ch/record/1599719/files/SUS-13-002-pas.pdf

[303] CMS PAS HIG-13-034, http://cds.cern.ch/record/1666526/files/HIG-13-034-pas.pdf

[304] G. Aad *et al.* [ATLAS Collaboration], JHEP **1406**, 008 (2014) doi:10.1007/JHEP06(2014)008 [arXiv:1403.6293 [hep-ex]].

[305] N. Craig, J. A. Evans, R. Gray, M. Park, S. Somalwar, S. Thomas and M. Walker, Phys. Rev. D **86**, 075002 (2012) doi:10.1103/PhysRevD.86.075002 [arXiv:1207.6794 [hep-ph]].

[306] A. Greljo, J. F. Kamenik and J. Kopp, JHEP **1407**, 046 (2014) doi:10.1007/JHEP07(2014)046 [arXiv:1404.1278 [hep-ph]].

[307] A. Goudelis, O. Lebedev and J. h. Park, Phys. Lett. B **707**, 369 (2012) doi:10.1016/j.physletb.2011.12.059 [arXiv:1111.1715 [hep-ph]].

[308] G. Blankenburg, J. Ellis and G. Isidori, Phys. Lett. B **712**, 386 (2012) doi:10.1016/j.physletb.2012.05.007 [arXiv:1202.5704 [hep-ph]].

[309] M. Gorbahn and U. Haisch, JHEP **1406**, 033 (2014) doi:10.1007/JHEP06(2014)033 [arXiv:1404.4873 [hep-ph]].

[310] J. Engel, M. J. Ramsey-Musolf and U. van Kolck, Prog. Part. Nucl. Phys. **71**, 21 (2013) doi:10.1016/j.ppnp.2013.03.003 [arXiv:1303.2371 [nucl-th]].

[311] P. Chang, K. F. Chen and W. S. Hou, Prog. Part. Nucl. Phys. **97**, 261 (2017) doi:10.1016/j.ppnp.2017.07.001 [arXiv:1708.03793 [hep-ph]].

[312] N. Yamanaka, Int. J. Mod. Phys. E **26**, no. 4, 1730002 (2017) doi:10.1142/S0218301317300028 [arXiv:1609.04759 [nucl-th]].

[313] G. Boyd, A. K. Gupta, S. P. Trivedi and M. B. Wise, Phys. Lett. B **241**, 584 (1990). doi:10.1016/0370-2693(90)91874-B

[314] M. Jung and A. Pich, JHEP **1404**, 076 (2014) doi:10.1007/JHEP04(2014)076 [arXiv:1308.6283 [hep-ph]].

[315] S. Weinberg, Phys. Rev. Lett. **63**, 2333 (1989). doi:10.1103/PhysRevLett.63.2333

[316] D. A. Dicus, Phys. Rev. D **41**, 999 (1990). doi:10.1103/PhysRevD.41.999

[317] M. Gorbahn,

[318] W. Dekens and J. de Vries, JHEP **1305**, 149 (2013) doi:10.1007/JHEP05(2013)149 [arXiv:1303.3156 [hep-ph]].

[319] E. Braaten, C. S. Li and T. C. Yuan, Phys. Rev. Lett. **64**, 1709 (1990). doi:10.1103/PhysRevLett.64.1709

[320] D. Chang, W. Y. Keung, C. S. Li and T. C. Yuan, Phys. Lett. B **241** (1990) 589. doi:10.1016/0370-2693(90)91875-C

[321] M. Pospelov and A. Ritz, Annals Phys. **318**, 119 (2005) doi:10.1016/j.aop.2005.04.002 [hep-ph/0504231].

[322] J. M. Pendlebury *et al.*, Phys. Rev. D **92**, no. 9, 092003 (2015) doi:10.1103/PhysRevD.92.092003 [arXiv:1509.04411 [hep-ex]].

[323] C. A. Baker *et al.*, Phys. Rev. Lett. **97**, 131801 (2006) doi:10.1103/PhysRevLett.97.131801 [hep-ex/0602020].

[324] https://www.psi.ch/nedm/.

[325] http://www.phy.ornl.gov/nedm/

[326] R. Golub and K. Lamoreaux, Phys. Rept. **237**, 1 (1994). doi:10.1016/0370-1573(94)90084-1

[327] http://collaborations.fz-juelich.de/ikp/jedi/

[328] Y. Senichev, A. Aksentyev, S. Andrianov, M. Berz, S. Chekmenev, A. Ivanov, J. r. Pretz and E. Valetov, doi:10.18429/JACoW-IPAC2017-TUPVA084

[329] J. Pretz [JEDI Collaboration], Hyperfine Interact. **214** (2013) no.1-3, 111 doi:10.1007/s10751-013-0799-4 [arXiv:1301.2937 [hep-ex]].

[330] O. Lebedev, K. A. Olive, M. Pospelov and A. Ritz, Phys. Rev. D **70**, 016003 (2004) doi:10.1103/PhysRevD.70.016003 [hep-ph/0402023].

[331] https : //www.bnl.gov/edm/files/pdf/deuteron$_{\rm p}$roposal$_0$80423$_{\rm f}$inal.pdf

[332] V. Anastassopoulos *et al.*, Rev. Sci. Instrum. **87** (2016) no.11, 115116 doi:10.1063/1.4967465 [arXiv:1502.04317 [physics.acc-ph]].

[333] N. Yamanaka and E. Hiyama, Nucl. Phys. A **963**, 33 (2017) doi:10.1016/j.nuclphysa.2017.04.015 [arXiv:1605.00161 [nucl-th]].

[334] D. Becirevic *et al.*, Nucl. Phys. B **634**, 105 (2002) [hep-ph/0112303].

[335] N. Carrasco *et al.*, Phys. Rev. D **90**, no. 1, 014502 (2014) doi:10.1103/PhysRevD.90.014502 [arXiv:1403.7302 [hep-lat]].

[336] M. Ciuchini *et al.*, JHEP **9810**, 008 (1998) [hep-ph/9808328].

[337] A. J. Buras and D. Guadagnoli, Phys. Rev. D **78**, 033005 (2008) doi:10.1103/PhysRevD.78.033005 [arXiv:0805.3887 [hep-ph]].

[338] A. J. Buras, D. Guadagnoli and G. Isidori, Phys. Lett. B **688**, 309 (2010) doi:10.1016/j.physletb.2010.04.017 [arXiv:1002.3612 [hep-ph]].

[339] M. J. Baker, J. Bordes, C. A. Dominguez, J. Penarrocha and K. Schilcher, JHEP **1407**, 032 (2014) doi:10.1007/JHEP07(2014)032 [arXiv:1310.0941 [hep-ph]].

[340] A. Bazavov *et al.* [MILC Collaboration], PoS CD **09**, 007 (2009) [arXiv:0910.2966 [hep-ph]].

[341] G. C. Wick, A. S. Wightman and E. P. Wigner, Phys. Rev. **88**, 101 (1952).

[342] L. D. Landau, "On the conservation laws for weak interactions," Nucl. Phys. **3**, 127 (1957).

[343] A. D. Sakharov, "Violation of CP Invariance, c Asymmetry, and Baryon Asymmetry of the Universe," Pisma Zh. Eksp. Teor. Fiz. **5**, 32 (1967) [JETP Lett. **5**, 24 (1967)] [Sov. Phys. Usp. **34**, 392 (1991)] [Usp. Fiz. Nauk **161**, 61 (1991)].

Own contribution

In this thesis, the first chapter and the second are based on books, articles, and other publications and therefore is not my own contribution. Except for the discussion of the Higgs–localisation that is a remainder of my diploma thesis. Another remainder of my diploma thesis is the derivation of the fermion propagator that is found in Ch.5. The derivation of the boson propagator was not first derived by me and is therefore not my own contribution. All work that contains the fourth chapter and a short discussion of the wave–function renormalization in Ch.3 belongs to the publication [A] is my own work, except for the showing the gauge invariance of the total amplitude. The content of Ch. 5 contains my own work, as well. Here, new physics contributions that are induced by a gauge singlet scalar that gives rise to fermion FCNCs are investigated to neutral meson mixing, to the rare decays of B mesons into two muons, $\mathcal{B}r\,(b \to q\mu^+\mu^-)$, q=d,s, and to the neutron EDM and deuteron EDM.
This thesis lead to the following publication:
[A] J.Hahn, C.Hörner, R.Malm, M.Neubert, K.Novotny and C.Schmell, Higgs Decay into Two Photons at the Boundary of a Warped Extra Dimension, Eur. Phys. J. C **74**, no. 5, 2857 (2014),doi:10.1140/epjc/s10052-014-2857-8, [arXiv:1312.5731 [hep-ph]].

Versicherung

für das Gesuch um Zulassung zur Promotion am Fachbereich 08

Hiermit versichere ich gemäß § 12 Abs. 3e der Promotionsordnung des Fachbereichs 08, Physik, Mathematik und Informatik der Johannes Gutenberg-Universität Mainz vom 02.12.2013:

a) Ich habe die jetzt als Dissertation vorgelegte Arbeit selbständig verfasst. Es wurden ausschließlich die angegebenen Quellen und Hilfsmittel verwendet. Von der Ordnung zur Sicherung guter wissenschaftlicher Praxis in Forschung und Lehre und vom Verfahren zum Umgang mit wissenschaftlichem Fehlverhalten habe ich Kenntnis genommen.

b) Ich habe oder hatte die jetzt als Dissertation vorgelegte Arbeit nicht schon als Prüfungsarbeit für eine andere Prüfung eingereicht *)

~~Ich hatte die jetzt als Dissertation vorgelegte Arbeit als Prüfungsarbeit für folgende Prüfung eingereicht: *)~~

(Bezeichnung der Prüfung)

(Bezeichnung und Ort der Prüfungsstelle)

c) Ich hatte weder die jetzt als Dissertation vorgelegte Arbeit noch Teile davon an einer anderen Stelle als Dissertation eingereicht *)

~~Ich hatte die folgende Abhandlung mit anstehendem Ergebnis als Dissertation eingereicht~~ *)

(Titel der Abhandlung)

(Fakultät bzw. Fachbereich und Hochschule)

(Ergebnis bzw. Beurteilung)

11.12.2017
(Datum)

Kristiane Novotny
(Unterschrift)

) Nichtzutreffendes bitte streichen